CONTROLS ON POROSITY AND PERMEABILITY HETEROGENEITY IN THE TOCITO SANDSTONE (UPPER CRETACEOUS), SAN JUAN BASIN, NEW MEXICO

Mark Raymond Lambert

Submitted in partial fulfillment
of the requirements for the degree
of Master of Science in Geology

Department of Geoscience
New Mexico Institute of Mining and Technology
Socorro, New Mexico
December 1993

ACKNOWLEDGEMENTS

I am indebted to my wife, Cathy, who sacrificed a good number of weekends to help measure outcrop permeabilities, proofread and edit thesis text, and spent many a night transforming my cut-and-paste figures into fabulous works of computerized art. I would also like to thank the New Mexico Petroleum Recovery Research Center for permitting Cathy to use their computer equipment while working on my thesis figures.

I am grateful to Rex Cole, Art Trevena, and Unocal Energy Resource Division in Brea, CA for their support, advice, data, mechanical field permeameter, and the manufacturing of petrographic thin sections; Richard Koch and the Navajo Nation Mineral Department for the loan of shallow subsurface Tocito Sandstone cores and access to Tocito outcrop; Richard Bottjer of Amoco Production Company in Denver, CO for the loan of Tocito thin sections and laboratory core data from San Juan Basin oil fields; Alan Emmendorfer of Giant Exploration and Production Company in Farmington, NM for the loan of Gallup core; and Mobil Oil in Dallas for the use of their petrographic microscope and reprographics facilities.

I thank Peter Mozley for his role as academic advisor, his assistance in developing the goals of this study, for guidance with petrography, cathodoluminescence, diagenesis, and porosity and permeability problems, and for numerous stages of editing; David Johnson for his advice on administrative issues and petrography, training me on the cathodoluminoscope, and on the shooting of photomicrographs, as well as writing techniques and editing; Andrew Campbell for his assistance and direction with the mass spectrometer, help in interpreting isotopic data, and editing thesis text; John Heller for his guidance in calibrating Unocal's mechanical field permeameter, the use of the instrument in the field, interpreting permeability data, editing thesis text, and the use of the computer-controlled minipermeameter that John and his colleagues developed at the New Mexico Petroleum Recovery Research Center; Neil Whitehead III for published literature and data on the Tocito Sandstone and the San Juan Basin, his thorough evaluation of the thesis manuscript, and numerous discussions on both my thesis work and on future employment; the Materials and Metallurgical Engineering Department at New Mexico Institute of Mining and Technology for the use of their scanning electron microscope; David Fritchman for analyzing an extracted oil sample with the chromatograph at the Petroleum Recovery Research Center; and Earl and Donna Lambert and John and Kay Almeida for their love and support.

For financial assistance, I thank Mobil Oil in Midland, TX (especially Joseph Jensen), the Society of Economic Paleontologists and Mineralogists/Rocky Mountain Section, the Society of Professional Well Log Analysis Foundation, the Richard Matuzeski Foundation, and Lamb-Fry Oil and Gas in Socorro, NM.

ABSTRACT

Lithofacies type is the controlling factor for porosity and permeability variation in the Upper Cretaceous Tocito Sandstone of the Mancos Shale in the San Juan Basin. The Tocito lentils are major oil reservoirs, but efforts at secondary recovery have been disappointing due to early water breakthrough. Results of this study suggest that the poor recoveries are primarily due to macroscopic-scale (well-to-well scale) heterogeneities between different lithofacies. The Tocito consists of the following four lithofacies (from bottom to top): muddy bioturbated sandstone; cross-bedded sandstone which interfingers with interbedded sandstone and shale; and ripple cross-laminated sandstone.

Cross-bedded sandstone lithofacies have the highest porosities (ϕ) and permeabilities (k) in outcrop (ave. ϕ = 22.0%, ave. k = 4.2 darcies) and deep subsurface core (ave. ϕ = 8.2%, ave. k = 101.8 millidarcies). Cross-bedded sandstone beds are fluid conduits and mudstone drapes, bioturbated muddy foresets, and contorted strata are fluid flow baffles and barriers. Permeability trends are often subparallel to foresets and permeabilities are usually greatest near the center of each sandstone bed.

Interbedded sandstone and shale lithofacies have moderate porosities and permeabilities in outcrop (ave. ϕ = 8.0%, ave. k = 1.6 darcies) and deep subsurface core (ave. ϕ = 3.5%, ave. k = 26.9 millidarcies), and have the most variable reservoir properties of the lithofacies studied. Shale interbeds effectively compartmentalize sandstone interbeds so that fluid may pass through some beds while bypassing adjacent beds.

Muddy bioturbated sandstone lithofacies and ripple cross-laminated sandstone lithofacies have the lowest porosities and permeabilities in outcrop (ave. ϕ = 2.5%, ave. k = 0.5 darcies) and deep subsurface core (ave. ϕ = 1.7%, ave. k = 4.1 millidarcies). High clay content makes this lithofacies a baffle and barrier to fluid migration.

There is a strong relationship between lithofacies type and diagenetic modification

of porosity and permeability in both outcrop and deep subsurface. Cross-bedded sandstone lithofacies experienced significant framework-grain dissolution and minor calcite cementation, whereas interbedded sandstone and shale lithofacies experienced abundant but spatially variable grain dissolution and calcite cementation. Muddy bioturbated sandstone lithofacies and ripple cross-laminated sandstone lithofacies are usually well cemented with calcite, but have experienced only minor grain dissolution.

A burial history plot demonstrates that burial of the Tocito Sandstone now cropping out in the Hogback oil field was great enough for smectite-illite transformation and oil generation in the underlying Mancos Shale. Water released from the shale during such reactions, as well as from compaction, may be responsible for framework-grain dissolution in the Tocito sandstones.

Oxygen and carbon isotopes and cathodoluminescence distinguishes two separate phases of calcite cementation in the Tocito Sandstone outcrop at the Hogback oil field. Isotopes indicate that calcite precipitated from trapped seawater mixed with ^{18}O- and ^{13}C-depleted meteoric water.

TABLE OF CONTENTS

ABSTRACT ii

LIST OF TABLES viii

LIST OF FIGURES viii

INTRODUCTION 1
Reservoir Heterogeneity and Hydrocarbon Recovery 1
Objectives 2
Previous Work 3
Past Studies on Controls of Porosity and Permeability Heterogeneity . . . 3
Past Studies of Porosity and Permeability Heterogeneities in the Tocito Sandstone 6

GEOLOGIC SETTING 6
The San Juan Basin and the Tocito Sandstone 6
Stratigraphy of the Tocito Sandstone 11
Lithology and Sedimentary Structures of the Tocito Sandstone 13
Depositional environment of the Tocito Sandstone 14
Provenance of Tocito Sandstone sediments 15
Thermal History of the Tocito Sandstone and the Mancos Shale 16

LITHOFACIES 16
Large-scale Cross-bedded Sandstone Lithofacies 18
Medium-scale Cross-bedded Sandstone Lithofacies 18
Interbedded Sandstone and Mudstone Lithofacies 19
Muddy, Bioturbated Sandstone Lithofacies 19
Ripple Cross-laminated Sandstone Lithofacies 20
Pebbly Sandstone Lithofacies 20

METHODS 20
Burial History Plot 20
Upper Cretaceous to Present Depositional and Tectonic Events 20
Petrography 21
Thin Section Petrography 21
Scanning Electron Microscope 21
Cathodoluminescence 22
Isotopic Analysis 22
Oil Extraction 23
Permeability Measurements 23
Tocito Sandstone Outcrop Measurements 26
Tocito Sandstone outcrops in the Hogback oil field 26
Tocito Sandstone outcrops along the Chaco River 28
Hand Specimen Measurements 28
Core Measurements 29
Shallow subsurface core 29
Deep subsurface reservoir core 30

RESULTS 31

TABLE OF CONTENTS, CONTINUED

Burial History Curve for Tocito Sandstone Outcrop 31
Petrology and Diagenetic History 33
Tocito Sandstone Composition and Texture 33
Diagenetic History 35
Glauconite 35
Pyrite 37
Compaction 42
Quartz overgrowths 42
Feldspar overgrowths 42
Calcite cements 47
Ferroan dolomite 50
Framework grain dissolution 50
Kaolinite 58
Fracturing 61
Oil emplacement 61
Hematite and gypsum 64
Isotopic Measurements 64
$\delta^{13}C$ Values 68
$\delta^{18}O$ Values 69
Permeability Measurements 72
Large-scale Permeability Grids at Hogback Oil Field Outcrop 72
Grid #1 72
Grid #2 72
Grid #3 72
Grid #4 76
Grid #5 76
Grid #6 76
Grid #7 80
Grid #8 80
Grid #9 83
Large-scale Permeability Grids Along the Chaco River Outcrop 83
Grids #10, #12 and #13 83
Grids #11 and #14 83
Grid #15 86
Grids #16 and #17 86
Grid #18 86
Grid #19 89
Grid #20 89
Grid #21 89
Macroscopic Permeability Profiles from Shallow Core Plugs and Outcrop 91
Mesoscopic HOF #2 Core Permeability Profile and Grids 91
Permeability Results from Reservoir Core 97

DISCUSSION 97
Effect of Sedimentary Structures on Porosity and Permeability 97
Reactivation Surfaces 97
Cross-bedding 100
Contorted Cross-Bedding 102

TABLE OF CONTENTS, CONTINUED

Bioturbated Sediments 102
Ripple Cross-laminated Sediments 103
Mudstone Layers 105
Effect of Diagenetic Alterations on Porosity and Permeability 106
Compaction 107
Quartz and Feldspar Overgrowths 107
Calcite Cementation 107
Framework-grain Dissolution 109
Kaolinite Precipitation 109
Additional Framework Grain Dissolution in Outcrop 109
Relationship of Lithofacies to Porosity and Permeability 111
Large-scale Cross-bedded Sandstones Lithofacies 111
Medium-scale Cross-bedded Sandstones Lithofacies 113
Interbedded Sandstone and Mudstone Lithofacies 113
Muddy, Bioturbated Sandstone Lithofacies 114
Ripple-laminated Sandstone Lithofacies 115
Extent to which Outcrop Sections Reflect Subsurface Conditions 115
Effect of Reservoir Geometry on Porosity and Permeability 116

APPLICATION TO HYDROCARBON RECOVERY 119

FUTURE WORK 121

CONCLUSIONS 122

REFERENCES CITED 124

APPENDICES 132

1. Method of construction for burial history plot. 132

2a. Well data used to establish average thicknesses of Cretaceous and Tertiary strata once overlying the Tocito Sandstone outcrop in the Hogback oil field. 134

2b. Published data used to construct the burial history plot. 135

3. Petrographic methods used in this study and the sources for thin sections used in diagenetic history of subsurface Tocito Sandstone. 136

4. Operation and calibration of the mechanical field permeameter and the computer-controlled scanning minipermeameter. 139

5. Core from Tocito Sandstone oil reservoirs used in permeability studies. . . . 146

6. Petrographic data for deep subsurface Tocito Sandstone in four oil fields in the central San Juan Basin. 147

7. Petrographic data for shallow subsurface cores through the Tocito Sandstone outcrop in the Hogback oil field, San Juan Basin. 148

8. Cathodoluminescence data for calcite cements in "upper" Tocito Sandstone cropping out in Hogback oil field and Chaco River. 149

TABLE OF CONTENTS, CONTINUED

9. Isotopic data for calcite cements in the Tocito Sandstone outcrop in the Hogback oil field, San Juan Basin, New Mexico. 151

10. Mesoscopic-macroscopic-scale permeability data for grids along Tocito Sandstone outcrop in Hogback oil field and Chaco River. 152

11. Geostatistics for outcrop permeability data. 159

12. Macroscopic-scale permeability data for HOF #2 and HOF #3 core plugs and the vertical outcrop traverse. 160

13. Mesoscopic-scale permeability data for HOF #2 core. 163

14. Lithologic data for HOF #2 core. 207

15. Permeability data for subsurface Tocito Sandstone reservoir core. 254

LIST OF TABLES

1. Petrographic parameters vs permeability and porosity. 106

LIST OF FIGURES

1. Scales of heterogeneity in a sandstone reservoir. 5

2. (A) Location of San Juan Basin. (B) Distribution of most of the Tocito Sandstone lentils in subsurface of the northwestern San Juan Basin, New Mexico. (C) Tocito Sandstone outcrop pattern within Hogback oil field and along the Chaco River of northwest New Mexico. 7

3. Chronostratigraphic chart of the Cretaceous and Tertiary section in the San Juan Basin, northwest New Mexico and southwest Colorado. 9

4. North-south and east-west cross-sections of Tocito Sandstone outcrop in the Hogback oil field. 17

5. A) The mechanical field permeameter and B) core frame module during the calibration process. 24

6. The mechanical field permeameter and hand-held probe as used in the field. 25

7. The computer-controlled scanning minipermeameter during calibration process. 25

8. Locations of permeability grids #1 through #9 on the Tocito Sandstone outcrop in the Hogback oil field, San Juan Basin, New Mexico. Also identified in the panorama is the location of the traverse made during outcrop permeability measurements. 27

9. Burial history curve for the Tocito Sandstone cropping out in the Hogback oil field, San Juan Basin, New Mexico. 32

10. Quartz-rock fragment-feldspar ternary diagram for samples from the shallow and deep subsurface cores. 34

11. Diagenetic history of the Tocito Sandstone cropping out in the Hogback oil field, as determined from petrographic, SEM and cathodoluminescence observations of outcrop and subsurface specimens. 36

12. Photomicrograph of glauconite. 39

13. Photomicrographs of pyrite framboids and octahedrons. 41

14. Photomicrographs of authigenic quartz overgrowths. 44

15. Photomicrograph of authigenic feldspar overgrowth. 46

LIST OF FIGURES CONTINUED

16. Photomicrographs of ferroan and nonferroan calcite cement. 49

17. Photomicrograph of authigenic and detrital ferroan dolomite. 52

18. Photomicrographs of framework grain dissolution. . . . . 55 & 57

19. Photomicrographs of authigenic kaolinite. 60

20. Photograph of oil stain in HOF #2 core. 63

21. Photomicrographs of hematite and gypsum in outcrop. 66

22. A) Plot of $\delta^{13}C$ calcite against proportion of nonferroan calcite (versus ferroan calcite) in the sample. B) Plot of $\delta^{18}O$ calcite against proportion of nonferroan calcite (versus ferroan calcite) in the sample. 67

23. Plot of $\delta^{18}O$ vs. precipitation temperatures for Fe-rich first-stage calcite cement and Fe-poor second-stage calcite cement from the "upper" Tocito Sandstone cropping out in the Hogback oil field. 70

24. Permeability grid #1 in an interbedded sandstone and mudstone unit of the "upper" Tocito Sandstone cropping out in the Hogback oil field, San Juan Basin, northwest New Mexico. 73

25. Permeability grid #2 in an interbedded sandstone and mudstone unit of the "upper" Tocito Sandstone cropping out in the Hogback oil field, San Juan Basin, northwest New Mexico. 74

26. Permeability grid #3 in muddy, bioturbated sandstone at the base of the "upper" Tocito Sandstone cropping out in the Hogback oil field, San Juan Basin, northwest New Mexico. 75

27. Permeability grid #4 in the phosphatic nodular mudstone sandwiched between the "upper" and "lower" Tocito Sandstones cropping out in the Hogback oil field, San Juan Basin, northwest New Mexico. 77

28. Permeability grid #5 in ripple cross-laminated sandstone near the top of the "lower" Tocito Sandstone cropping out in the Hogback oil field, San Juan Basin, northwest New Mexico. 78

29. Permeability grid #6 in the ripple cross-laminated sandstone of the "lower" Tocito Sandstone exposed in the Hogback oil field, San Juan Basin, northwest New Mexico. 79

30. Permeability grid #7 in the larger-scale cross-bedded sandstone unit of the "lower" Tocito Sandstone cropping out in the Hogback oil field, San Juan Basin, northwest New Mexico. 81

LIST OF FIGURES CONTINUED

31. Perspective view of grid #8 on a three-dimensional exposure of the large-scale cross-bedded sandstone lithofacies in the "lower" Tocito Sandstone cropping out in the Hogback oil field. 82

32. Permeability grid #9 in the large-scale cross-bedded sandstone unit of the "lower" Tocito Sandstone cropping out in the Hogback oil field, San Juan Basin, northwest New Mexico. 84

33. Permeability grids #10 through #14 on Tocito Sandstone cropping out along the Chaco River. 85

34. Permeability grids #15 through #17 on Tocito Sandstone cropping out along the Chaco River. 87

35. Permeability grids #18 and #19 on Tocito Sandstone cropping out along the Chaco River. Grid #19 is continued in Figure 36. 88

36. Permeability grids #19 through #21 on Tocito Sandstone cropping out along the Chaco River. Grid #19 is continued from Figure 35. 90

37. Permeability profiles from core plugs of the HOF #2 and HOF #3 cores and from hand samples of a vertical traverse of the "upper" Tocito Sandstone outcrop. 92

38. Mesoscopic-scale permeability profile from the computer-controlled minipermeameter of the HOF #2 core. 93

39. Permeability contour plots for large-scale cross-bedded sandstone lithofacies and medium-scale cross-bedded sandstone lithofacies. 95

40. Permeability contour plots for interbedded sandstone and shale lithofacies and muddy bioturbated sandstone lithofacies. 96

41. Permeability profile for Solar Petroleum Navajo Tribal F-151 in the Horseshoe oil field, San Juan Basin. 98

42. Permeability contour plots for interbedded sandstone and shale lithofacies and medium-scale cross-bedded sandstone lithofacies in the subsurface. . . . 99

43. Box plot of permeability values for sedimentary structures identified in the Tocito Sandstone outcrop (Hogback oil field) and in the HOF #2 core. . . 101

44. Enhancement of vertical permeability due to the penetration of impermeable mud drapes by sand-filled burrows. 104

45. Cross-plot of secondary porosity in feldspar and chert grains versus permeability, for the Navajo Tribal F-151 and the HOF #2 cores. 110

LIST OF FIGURES CONTINUED

46. Box plots of permeability values for sandstone lithofacies identified in A) the Tocito Sandstone outcrop in the Hogback oil field, and B) Tocito subsurface core from the Gallegos, Cha Cha, Totah and Horseshoe oil fields. 112

47. Permeability and porosity profiles for deep subsurface Tocito Sandstones. 117

A-1. Correlation between permeabilities measured on Tensleep Sandstone core plugs by the mechanical field permeameter and the Hassler Sleeve. 141

A-2. Plot of permeability vs. pressure drop time for estimating permeability of low-permeability rock, using the mechanical field permeameter 143

A-3. Correlation between permeabilities measured on Tensleep Sandstone core plugs by the PRRC minipermeameter and (A) the Hassler Sleeve and (B) the mechanical field permeameter. 145

INTRODUCTION

Reservoir Heterogeneity and Hydrocarbon Recovery

Oil recovery from sandstone reservoirs in the United States using current technology has averaged 34 percent of the original oil in place. This means that 330 out of 500 billion barrels of oil discovered so far nationwide remains unproduced (Tyler and Finley, 1991). Up to 70 percent of mobile oil is not recovered because it is prevented from migrating to the producing well by heterogeneities in laterally complex reservoirs and by facies and permeability stratification in vertically complex reservoirs. Fisher (1987) estimated that 100 billion barrels of unrecovered mobile oil awaits advanced-recovery applications.

There has recently been increased focus on understanding the distribution of sandstone fabrics and their controls on porosity, permeability, and migration of fluids through the sandstone (e.g., Jones et al., 1984; Weber, 1986; Sultan and Heller, 1989; Barton and Tyler, 1991; Cole and Mullen, 1992; Daws and Prosser, 1992; Dutton and Diggs, 1992; Jordan and Pryor, 1992). Each sandstone reservoir consists of individual facies with distinctive external geometries, sedimentary and biogenic structures, and lithologies (Miall, 1991). Superimposed on these features are diagenetic overprints that enhance or diminish the primary porosity and permeability of the sandstone. Communication between adjacent facies promotes reservoir drainage, whereas the lack of communication results in compartmentalized reservoirs and inefficient drainage.

The geometry of reservoir compartmentalization is a product of depositional processes and is therefore predictable (Tyler and Finley, 1991). If the characteristic locations of unrecovered oil can be related to lithofacies, and thus depositional systems, then oil production from that reservoir may also be predictable. The better we understand the relationship between facies architecture, diagenetic modification and

hydrocarbon migration, the more efficient our recovery programs will be, and the greater the volume of recoverable reserves will become.

Objectives

One of the primary oil reservoirs in New Mexico is the Tocito Sandstone in the San Juan Basin. As of January 1, 1990, 115 million barrels of oil (MMBO) and 409 billion cubic feet of gas (BCFG) have been produced in the San Juan Basin from the Tocito (Bottjer, 1992). This accounts for approximately 81% of the oil and less than 1% of the gas produced from the San Juan Basin (Rice, 1983). Estimates of undiscovered conventional oil and gas from the Tocito are 9.3 million barrels of oil and 46.6 billion cubic feet of gas (Powers, 1993).

Efforts at secondary recovery from Tocito Sandstone reservoirs have been disappointing due to early water breakthroughs (e.g., Bisti, Cha Cha, Horseshoe and Totah oil fields; Fassett et al., 1987). The Tocito is therefore a good candidate for studying lithologic and diagenetic variations that influence fluid migration. Controls on porosity and permeability in the Tocito (pronounced **TOE**-see-toe and meaning "warm springs" in Navajo) of northwest New Mexico were determined using well-exposed outcrops of a pair of stacked Tocito lentils in the Hogback oil field west of Farmington. The principal objectives were to determine: 1) the effect of facies architecture on porosity and permeability heterogeneity, 2) the effect of diagenesis on porosity and permeability heterogeneity, and 3) the extent to which outcrop sections reflect subsurface conditions.

Previous Work

Past Studies on Controls of Porosity and Permeability Heterogeneity

Bryant et al. (1988), Harris (1989), and Barton and Tyler (1991) found that porosity and permeability heterogeneities within most sandstones are strongly influenced by both primary facies architecture and diagenesis. However, they noted that permeability distributions and trends are most strongly related to facies architecture, composition, bedding type, and grain-size. Each facies and bedding type has statistically different permeability characteristics, and bounding surfaces between facies provide discontinuities in the permeability trends. Bryant et al. (1988) found that the sheetlike geometry of storm deposits in the Upper Lias Sands of Southern England resulted in laterally continuous cemented beds, and despite diagenetic alterations, the sandstone's reservoir properties are controlled by facies architecture. Cole and Mullen (1992) demonstrated that within the Tensleep Sandstone in Wyoming, eolian dune deposits act as conduits for oil, whereas interdune deposits are flow barriers and baffles.

Sedimentary structures have been found to have unique permeabilities. Trough cross-beds commonly have the highest permeabilities in many sandstones (Jones et al., 1984; Goggin et al., 1988a; Barton and Tyler, 1991; Dutton and Diggs, 1992). Soft sediment deformation and bioturbation usually reduced the permeability of cross-bedded sandstones (Jones et al., 1984; Barton and Tyler, 1991; Dutton and Diggs, 1992), and ripple cross-laminated sandstones generally had low permeabilities (Pettijohn et al., 1973; Jones et al., 1984; Goggin et al., 1988a; Cole and Mullen, 1992; Dutton and Diggs, 1992).

Current studies have also focused on the scales of permeability heterogeneity. Goggin et al. (1988a) distinguished two components of permeability variation. One is a structural component correlated to identifiable geologic processes, and the second is a

random component correlated to unexplained variations. However, at smaller scales of permeability measurement, even the random component possesses structure. Barton and Tyler (1991) documented permeability correlations in the Ferron Sandstone on several scales, ranging from 183 m (600 ft) to 6 m (20 ft). Daws and Prosser (1992) demonstrated with core-wireline log correlations that permeability heterogeneities in beach/foreshore sandstone facies and stacked tidal-channel sandstone facies of the Brent Group in the North Sea, could be placed within a five-fold hierarchy. The first four orders of heterogeneity are the result of depositional or syndepositional processes (strata type, facies transitions, bedding surfaces, laminations). The fifth-order heterogeneity is the product of diagenetic alterations. Jordon and Pryor (1992) recognized six hierarchical levels of permeability heterogeneity in the present day Mississippi River meanderbelt in southeastern Missouri. These scales range from oil field-size (high permeability sandy channels and low permeability muddy abandoned channels) down to individual laminae-size (grain-flow lenses, grain-fall sheets, mud drapes).

In order to apply the results of this study to hydrocarbon recovery, it is necessary to distinguish which scale (or scales) of heterogeneity has the greatest affect on oil storage and transfer. For this purpose, the following scales of heterogeneity are used: *Megascopic* heterogeneities are products of variability across depositional systems and are seen as variations across an oil field or between oil fields (on a scale greater than 1000 m or 3280 ft) (Tyler and Finley, 1991) (Fig. 1). Changes in permeability commonly occur along boundaries of different lithofacies, especially if there are significant differences in clay content, grain size, and sorting (Weber, 1986).

Macroscopic heterogeneities are defined by lithofacies type and diagenetic modification during burial. They are seen as well-to-well variations on a scale of meters to hundreds of meters (3-100s ft) (Tyler and Finley, 1991) (Fig. 1). Within individual lithofacies, there frequently is permeability zonation due to local variations in grain size

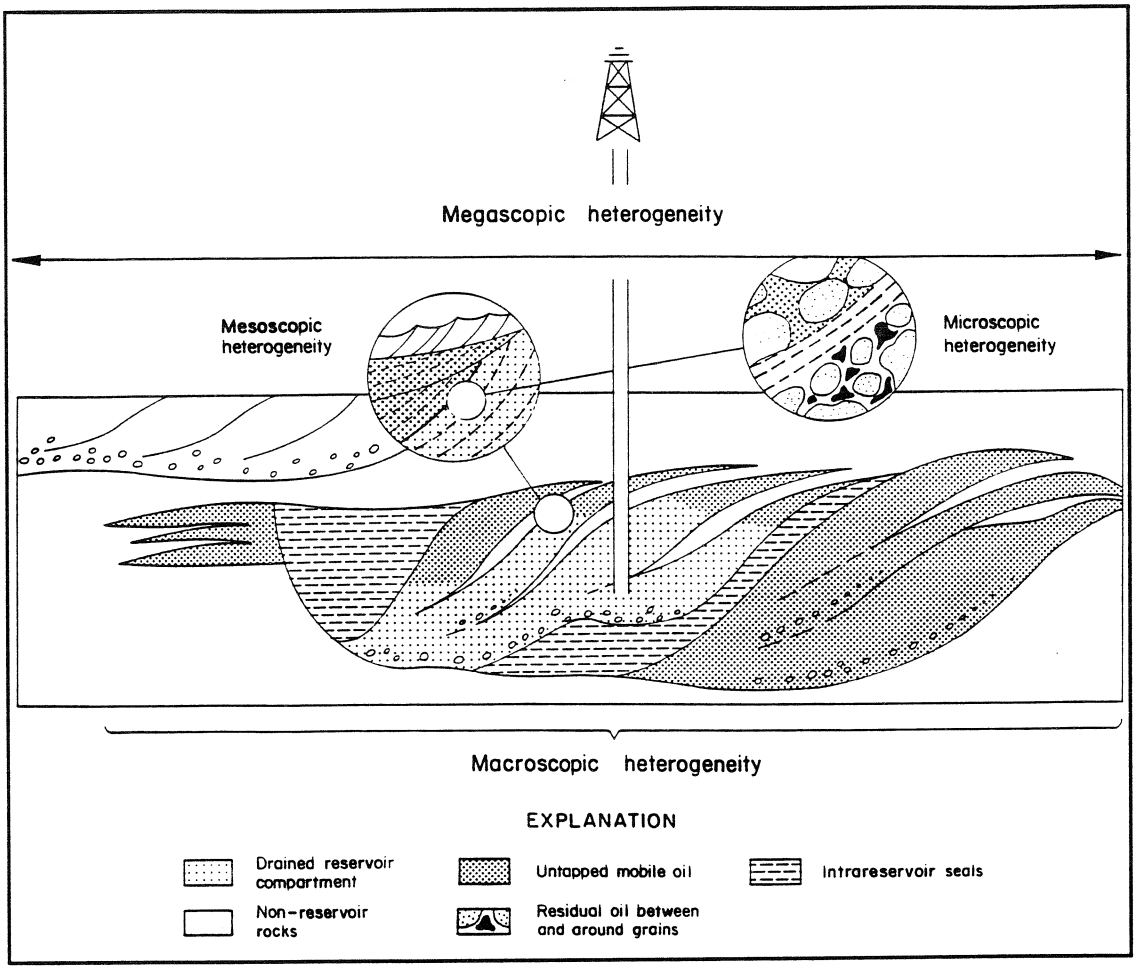

Figure 1 - Scales of heterogeneity in a sandstone reservoir. Note that heterogeneities at all scales (especially at the macroscopic scale) compartmentalize the reservoir and influence hydrocarbon drainage. From Tyler and Finley, 1991.

and sorting, clay content, compaction, cementation, and initial porosities and permeabilities (Weber, 1986).

Mesoscopic heterogeneities reflect variability at the ripple-laminae and cross-bed scale (scale of centimeters to meters or inches to feet) (Tyler and Finley, 1991) (Fig. 1). *Microscopic* heterogeneity is a function of variability at the pore or pore-throat scale (μm). Heterogeneities on the microscopic level are the result of cementation, framework-grain and cement dissolution, textural variations, mineralogy, and clay content.

Past Studies of Porosity and Permeability Heterogeneities in the Tocito Sandstone

There are no published reports that analyze the controls on porosity and permeability heterogeneities in the Tocito Sandstone. Sabins (1963) presented a detailed stratigraphic and petrographic analysis of Tocito core from the Bisti field and suggested that the depositional environment was the fundamental control on porosity and permeability.

GEOLOGIC SETTING

The San Juan Basin and the Tocito Sandstone

The San Juan Basin is a 160-240 km (100-150 mi) wide, roughly circular basin (Fig. 2A) that formed during the Late Cretaceous and early Tertiary Laramide orogeny (Nummedal and Riley, 1991). It is bound by steeply dipping monoclinal folds to the north, west, and east and by gently dipping strata to the south. The basin is structurally asymmetric, with the northern end of the basin being the deepest (Law, 1992). Basinward-directed early Tertiary thrust faults define the northern, western, and eastern margins of the San Juan Basin (Huffman and Taylor, 1989).

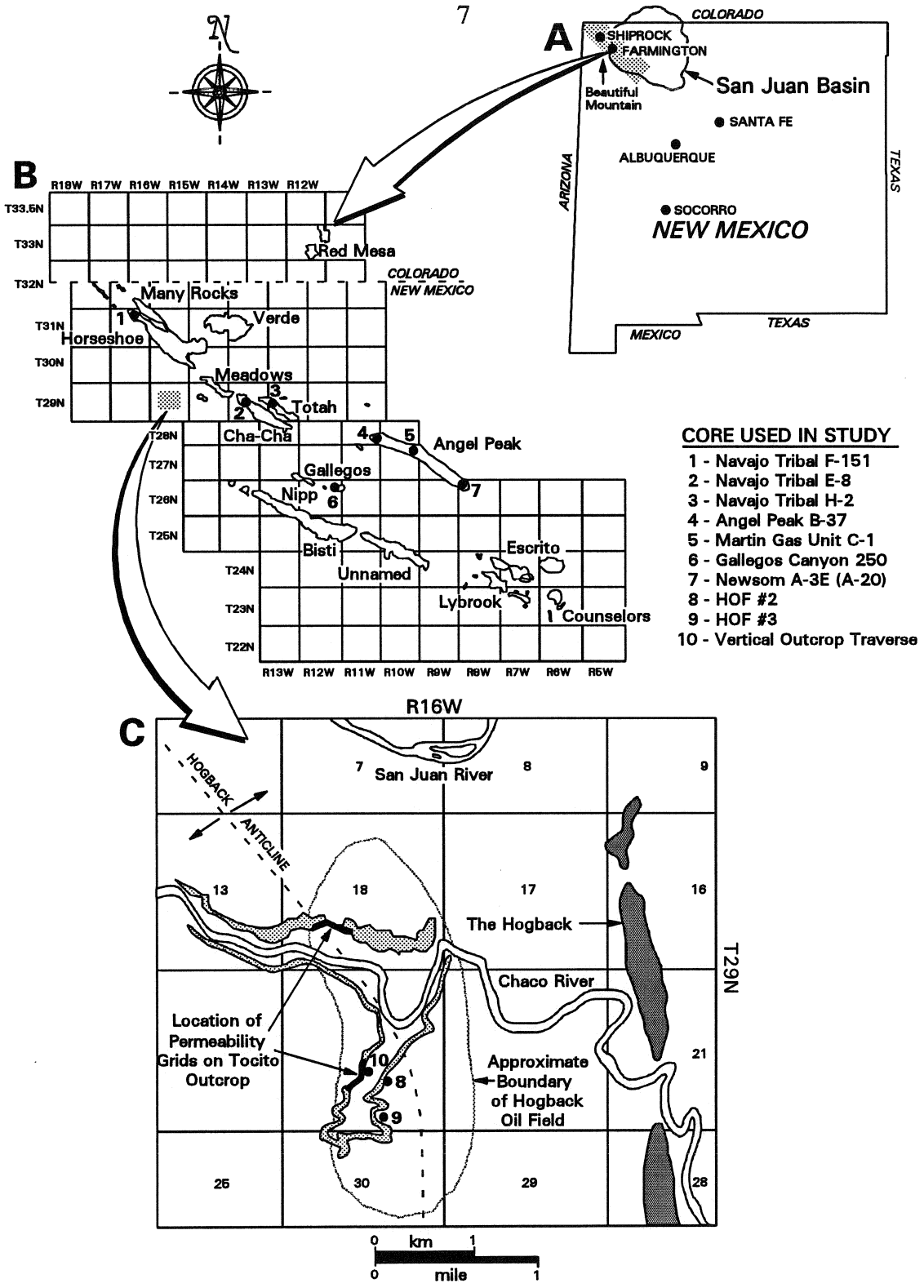

Figure 2 - (A) Location of San Juan Basin. (B) Distribution of most of the Tocito Sandstone lentils in subsurface of the northwestern San Juan Basin, New Mexico. (C) Tocito Sandstone outcrop pattern within Hogback oil field and along Chaco River of northwest New Mexico (modified from Cole, personal communication, 1985).

Of the 4600 m (15,100 ft) of sedimentary rocks that fill the deepest portion of the San Juan Basin, approximately 2700 m (8860 ft) are Cretaceous and younger sediments (Molenaar, 1988). The San Juan Basin underwent basin-wide uplift during the Laramide orogeny, which spanned the period from the latest Cretaceous to early Tertiary (Fassett, 1985). This resulted in the development of a regional unconformity at the Cretaceous-Tertiary boundary, which represents approximately an 11 m.y. hiatus in the southern portion of the basin and less than 11 m.y. hiatus in the northern San Juan Basin (Fassett, 1985).

Overlying the Cretaceous strata of the San Juan Basin are 1200 m (3936 ft) of Paleocene and Eocene sedimentary rocks (Molenaar, 1988) (Fig. 3). During Early to Middle Eocene, there was a brief period of uplift. Fassett (1985) believes that this minor uplift resulted only in erosion of the basin edges and that sedimentation continued unabated in the central parts of the basin.

Upper Eocene to Pliocene strata are not present in the San Juan Basin today. Using stratigraphic relationships of the Upper Eocene to Lower Oligocene Chuska Sandstone to underlying strata in the Lukachukai and Chuska Mountains west of the San Juan Basin, Fassett (1985) suggested that up to 760 m (2493 ft) of sedimentary rocks equivalent to the Chuska may have been deposited across the San Juan Basin.

The Tocito Sandstone is exposed along the northwest margin of the basin, outcropping in the Beautiful Mountain area, and in the Hogback oil field 30 km (18 mi) west of Farmington (Fig. 2). From the air, individual sandstone lentils exposed in outcrops are curvilinear and can be traced for tens of meters (Campbell, 1979; Tillman, 1985a). The orientation of the curvilinear ridges is constantly to the southeast (130-140°; Tillman, 1985a).

The Tocito Sandstone includes more than a dozen large individual elongate sand bodies that range from 20-50 km (12 to 31 mi) long, 5-10 km (3-6 mi) wide, and 10-

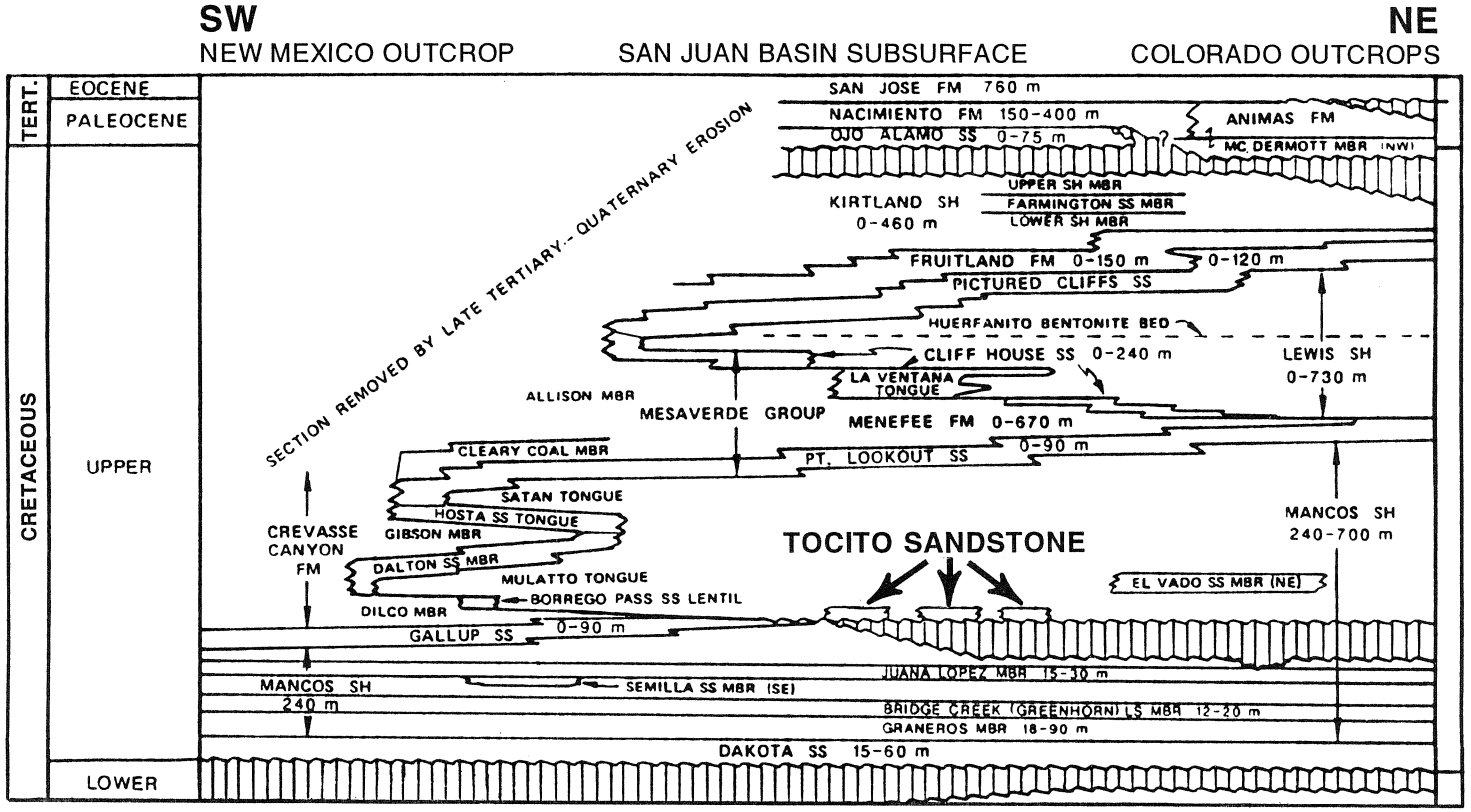

Figure 3 - Chronostratigraphic chart of the Cretaceous and Tertiary section in the San Juan Basin, northwest New Mexico and southwest Colorado. Strata removed by major unconformities are represented by vertical lines. Modified from Molenaar (1988).

20 m (33-66 ft) thick (Fig. 2B; Riley and Nummedal, 1989). These sandbodies, plus many smaller units, form a 30 km (19 mile) wide zone trending approximately N65W (Bergsohn, 1988), parallel to the regional paleoshoreline and seaward of the Gallup Sandstone pinch-out (Fig. 3). Dinoflagellates, spore, and pollen collected from outcrop and core from the Horseshoe oil field indicate a middle to late Coniacian age for the Tocito sediments (Jennette et al., 1991). Ammonites recovered from the Tocito include the early to late Coniacian *Cremnoceramus erectus, Cr. deformis, Forresteria* sp., and *Peroniceras westphalicum* (Nummedal and Riley, 1991).

The depositional setting of the Tocito Sandstone has been interpreted in different ways. McCubbin (1969) described the Tocito in the Horseshoe oil field as having been developed by shelf currents that moved clastic material from the northwest to the southeast several tens of miles offshore during a transgression or stillstand in the Cretaceous western interior seaway. Campbell's (1979) interpretation recognized two different depositional settings in the Bisti and Gallegos oil field and outcrop. Stratigraphically higher sandstone lentils were transgressive, deposited on wave cut terraces during short term stillstands. Stratigraphically lower sandstone ridges were deposited above multiple local unconformities and were time equivalent to the Gallup beach sandstones. Molenaar (1983a,b) suggested that the all Tocito lentils are post unconformity sandstones deposited contemporaneously with the Upper Mancos Shale. Tillman (1985a,b) described the Tocito in the Horseshoe oil field as inner middle shelf sand deposits affected by local tidal currents and storm currents. Riley and Nummedal (1992) interpreted the sandstone complex in the Hogback oil field as being tide-dominated prograding deltaic sandstones truncated and overlain by transgressive shelf sandbodies. Tidal currents were channelized and amplified on bathymetric highs caused by a regional uplift along basement faults associated with the Four Corners Lineament. Jennette et al. (1991) proposed that the Tocito was originally deposited during regressions as fluvial

sandstones within incised coastal valleys, and later reworked by tides as the valleys were inundated by following transgressions (Horseshoe, Bisti, Cha Cha, Verde, Many Rocks, Gallegos, South Waterflow, and Totah oil fields).

Stratigraphy of the Tocito Sandstone

Initially the Tocito Sandstone lentils were included within the Gallup Sandstone (Cretaceous) as offshore and beach sands (Sears, 1925). Subsequent stratigraphic work has convincingly demonstrated that the Tocito is stratigraphically younger than the Gallup (Lamb, 1968; Molenaar, 1973, 1983a,b; Tillman, 1985a,b; Jennette et al., 1991). Lamb (1968) and Molenaar (1973, 1983a,b) studied the microfauna in the Gallup and Tocito sandstones and concluded that a major unconformity separates the two formations (Fig. 3). In addition, they noted that bentonite time markers are truncated by a pre-Tocito unconformity in the Horseshoe, Many Rocks, Mesa, South Waterflow, and Verde oil fields. The name "Tocito" was first used for Upper Cretaceous sandstones in 1924 by Reeside.

The Tocito Sandstone lentils are enclosed entirely by Mancos Shale except for a few landward ridges which overlie continental sediments (e.g., Dilco Member of the Crevasse Canyon Formation; Fig. 3 herein; Jones et al., 1991). Some basal sequence boundaries are marked by the erosional truncation of underlying strata, predominately the Mancos Shale, the Torrivio Sandstone, and the Gallup Sandstone (Jennette et al., 1991). Where the Tocito is developed above an unconformity in the Horseshoe, Many Rocks, Mesa, South Waterflow, and Verde oil fields, there is a basal lag consisting of quartz clasts, carbonate and phosphate pebbles, and fragments of bone, shark teeth, and shell. The overlying sediments are commonly medium- to very-coarse-grained sandstones that are frequently stacked into coarsening-upwards packages. In other areas (e.g., Bisti and

Horseshoe oil fields) the basal contact of some Tocito lentils are more transitional, grading upwards from shale into medium- to coarse-grained sandstone (Sabins, 1972). Penttila (1964), Lamb (1968), McCubbin (1969), and Sabins (1972) believed that the distribution of the Tocito Sandstone is limited to local erosional lows and suggested that the Tocito lentils are strike-valley deposits separated by escarpments. Jennette et al. (1991) proposed that there are four major unconformities, each produced by a significant drop in relative sea-level that exposed marine shelf sediments to incision by rivers. They suggested that the Cretaceous drainage patterns were strongly influenced by subparallel faults. These faults would have redirected the rivers along a northwest-southeast trend, nearly perpendicular to the underlying Gallup Sandstone shoreline deposits. Fluvial sandstone accumulations became concentrated within these incised lows during regressions, and later when relative sea level rose again, tides reworked the fluvial sands and mixed them with marine components (glauconite, phosphate nodules, shell fragments). As relative sea level continued to rise, the region became inundated and the Tocito was overlain by open-marine shale and occasional thin-bedded, bioturbated sandstones (Jennette et al., 1991).

Nummedal and Riley (1991), however, point to the evidence of marine erosional processes throughout the basin and a lack of evidence for subaerial exposure. They note that most of the unconformities are located on broad structural highs rather than within incised lows. Such interpretations support shallow marine scouring of highs within storm base rather than fluvial incision of subaerially exposed marine shelf sediments. They further proposed that local uplift during the early Coniacian produced a regional high just seaward of the Gallup Sandstone. The uplift brought deep marine sediments up to storm wave base, causing scouring. This paleo-high was uplifted after Gallup deposition and subsided throughout Tocito Sandstone deposition (Nummedal and Riley, 1991; R. Bottjer, oral communication, 1992;). During Tocito time, tectonic uplift in the source area

(possibly the Mogollon highlands) provided coarse sand and gravel to the shoreline. Embayments, straits (?) or estuaries, possibly associated with the structural high, may have enhanced the tidal currents which collected medium- to coarse-grained sand from river mouths and redeposited the sand within tide-dominated deltas and shelf sand ridges. The Tocito outcrop in the Hogback oil field consists of two stacked sandstone lentils. Riley and Nummedal (1992) interpret the underlying lentil as progradational, deltaic sands that were scoured and truncated by the onset of a localized tectonically-enhanced transgression. As the transgression proceeded, phosphatic muddy sands and muds were deposited above the lower sands at the Hogback field and in turn were overlain by a transgressive, tidal, Tocito sand ridge.

Supporting an onlap history for the Tocito Sandstone, Pasley et al. (1989) demonstrated increasing degradation and hydrogen content of organic matter in the underlying Mancos Shale, upwards through the Tocito and into the overlying Mancos Shale. The nature of the phytoclasts indicates predominantly terrestrial organic matter in the underlying Mancos Shale changing to increasingly marine organic matter up through the Tocito and the overlying Mancos. This trend is consistent with characteristics of phytoclasts found in transgressive shales in the North Atlantic, Colorado, and Alberta (Pasley et al., 1989).

Lithology and Sedimentary Structures of the Tocito Sandstone

The Tocito Sandstone consists mainly of buff to tan, arkosic to lithic arkosic, medium- to very coarse-grained sandstones characterized by coarsing-upward tidal sedimentary structures (e.g., tidal bundles, abundant bottomset beds, sand waves, compound cross-beds, reactivation surfaces, alternating angular and tangential foresets, and double mud drapes), planar cross-bedding, trough and sigmoidal cross-laminations,

ripple laminations, overturned and convoluted foresets, and rare to extensive bioturbation (personal communication, Nummedal and Cole, 1990; Jones et al., 1991). When glauconite exceeds 10%, the beds are green in the outcrop and core. Detailed descriptions are in the lithofacies section.

Depositional Environment of the Tocito Sandstone

Sabins (1963) described three individual Tocito Sandstone lentils within the Bisti field as classic examples of marine sand-bar type stratigraphic traps. The Marye, Huerfano, and Carson sands (informal rock-stratigraphic units) are all northwest-trending, ranging from 2 to 3 km (1-2 mi) wide, 9 to 12 m (30-40 ft) thick, and 14 to 48 km (9-30 mi) long. They were interpreted by Sabins as having a silty shale "fore-bar facies" on the seaward (northeastward) flank and a fine-grained sandstone "back-bar" facies on the landward flank. The "fore-bar facies" is characterized by *Inoceramus* (mollusca), collophane (fish bones and shark teeth), and planktonic foraminifera, which are all indicators of open marine settings. On the other hand, the "back-bar facies" is more characteristic of a restricted marine environment, having predominately benthonic foraminifera and occasional *Inoceramus* and collophane debris. In the Bisti field, glauconite rarely exceeds 10% in both facies and is rare in the shales (Sabins, 1963). Sabins (1963) postulated that when the sand bars were deposited in an agitated, shallow-marine environment, the agitation concentrated fecal pellets from the adjacent sandy and silty clay areas and redeposited them in the sand bars. Glauconite later replaced the pellets and rare biotite grains. His sole evidence for this is that some clay pellets show incipient glauconitization in a few "bar" and "back-bar" thin sections. The absence of glauconite in the Gallup and Torrivio sandstones indicates that the glauconite was not reworked from older strata (Sabins, 1963).

Lateral and vertical lithofacies architecture in the Hogback oil field area is from the down-current migration of linear sand ridges by tidal currents producing an overall coarsening-upwards sequence (personal communication, Nummedal and Cole, 1990; Riley and Nummedal, 1992). In addition, burrows (*Ophiomorpha nodosa, Thalassinoides suevicus, Thalassinoides paradoxicus, Trichichnus linearis, Skolithos* sp., *Asterosoma, Teichichnus, Planolites, Cylindrichnus*, and rare *Terebellina*) are indicative of shallow inner-shelf or nearshore open marine environments (Kofron, 1987).

Provenance of Tocito Sandstone Sediments

The source area for Tocito Sandstone clastics may have been the Mogollon highlands in Arizona (Nummedal and Riley, 1991). How the clastics reached the San Juan Basin is not certain. The fine- to coarse-grained sediments that make up the Tocito could not have come from Gallup beach and shoreface deposits, which are almost all fine-grained. The most likely candidate is the Torrivio Member of the Gallup Sandstone Formation, a coarse-grained, fluvial, braided-channel sandstone complex that may be time-equivalent or slightly older than the Tocito (Nummedal, 1988; Nummedal and Riley, 1991). The Torrivio in outcrops on the flank of the Beautiful Mountain area (Fig. 2), is an angular to sub-angular, medium- to very coarse-grained feldspathic sandstone that truncates Gallup sediments. At the "Sanostee East" outcrop (Sec. 27, T26N, R19W) near Beautiful Mountain, the Tocito rests unconformably upon Torrivio sediments (Nummedal et al., 1989). On the flank of Beautiful Mountain, a thin interval of the Dilco Member of the Crevasse Canyon Formation (Fig. 3) separates the Torrivio from the overlying Tocito (Jones et al., 1991). Pebbles of polycrystalline quartz, chert, feldspar, and carbonaceous material found in the Tocito may have been reworked from the Dilco.

Thermal History of the Tocito Sandstone and the Mancos Shale

Rice (1983), Bond (1984), Huffman (1987), Meissner (1987), and Law (1992), have used vitrinite-reflectance (R_o), coal rank, chemical and isotopic compositions of produced natural gases, time-temperature and kinetic modeling of R_o profiles, and burial/temperature/maturity geohistory plots to determine thermal maturity throughout the San Juan Basin. They all concluded that the thermal gradient was the greatest in the northern part due to its proximity to the San Juan Mountains, a major source of volcanism-related heat. The geothermal gradient is thought to have been relatively constant up to the end of the Cretaceous. At that time, the temperature may have steadily increased until it peaked during Late Oligocene volcanism. Law (1992) suggests that the thermal maturity pattern is due to either: 1) convective heat transfer associated with a deeply buried heat source located directly below the northern part of the San Juan Basin, or 2) the introduction of relatively hot fluids into the basin from a heat source north of the basin located near the San Juan Mountains.

LITHOFACIES

Six discrete lithofacies in the Tocito Sandstone are recognized by Riley (1993) in outcrop and in core at the Hogback oil field. Riley's (1993) cross-sections of the lithofacies present in the Hogback oil field (Figs. 2, 4) were used in this study as a framework in which permeability grids were located. Therefore, Riley's (1993) lithofacies classification was used rather than those of Sabins (1963), Campbell (1979), or Tillman (1985a,b).

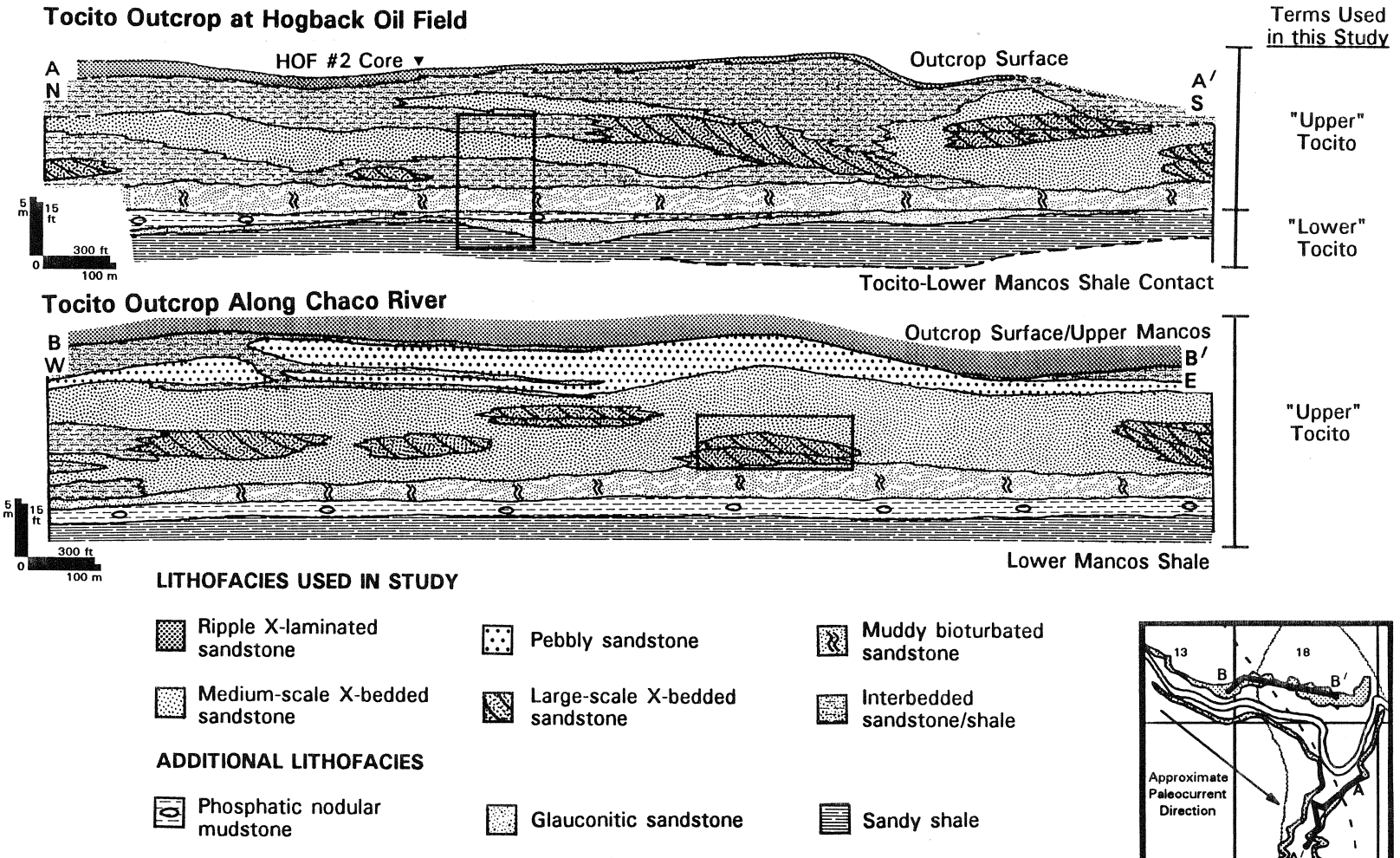

Figure 4 - North-south and east-west cross sections of the Tocito Sandstone lentil within the Hogback oil field (modified from Riley, 1993). The box in cross-section A-A′ is the approximate location of the panorama in Fig. 8, though on the opposite side of the valley. The locations of permeability grids are indicated in Figs. 2 and 8. The box in cross-section B-B′ is the approximate location of grids 10 through 21.

Large-scale Cross-bedded Sandstone Lithofacies

The large-scale cross-bedded sandstone lithofacies is made up of medium- to coarse-sized quartz and feldspar grains, with quartz and chert granules and pebbles commonly present on foresets and the tops of cross-bed sets. Structures include cross-strata exceeding 100 cm (39 inches) in thickness, common soft-sediment deformation (water-escape structures, recumbent folding, contorted stratification), and common reactivation surfaces (with mud drapes). Packages of cross-strata are traceable down-current for over 200m (656 feet) with their foreset orientations and types changing down-current. Locally, cross-bed sets form distinct tidal bundles and bundle sequences. Burrows are rare.

Medium-scale Cross-bedded Sandstone Lithofacies

The medium-scale cross-bedded sandstone lithofacies is made up of medium- to coarse-sized quartz and feldspar grains with occasional quartz granules, locally abundant intrabasinal phosphate, glauconite, mud rip-up clasts, sand-filled burrow intraclasts, and minor extrabasinal chert pebbles. Sedimentary structures include well-stratified 30-100 cm (12-39 inches) thick bed sets dominated by tabular cross-stratification. Rare wide trough-shaped sets may reach two meters in thickness. Foresets are tangential or planar and variable in length. Toesets are occasionally rippled and interbedded with thin drapes of laminated clay. Bed sets pinch-out or are terminated by low-angle truncations. They are frequently separated by thin, horizontally laminated sandstones with wispy mud drapes. Paleocurrent directions measured in separate outcrops are consistently to the southeast. Bioturbation is minor and includes the vertical and subvertical trace fossils, *Rosselia, Ophiomorpha*, and *Skolithos*. Minor burrowing within the toesets consists of the horizontal varieties *Thallassinoides* and *Planolites*.

Interbedded Sandstone and Mudstone Lithofacies

The interbedded sandstone and mudstone lithofacies is made up of medium-sized quartz and feldspar grains with rare mud rip-up clasts, shell fragments, glauconite, and lithoclasts. Sedimentary structures include low-angle cross-bedding, ripple laminations, and rare high-angle tabular cross-bedding. Foresets commonly thicken and steepen in an up-current direction. Burrows are *Ophiomorpha, Rosselia, Thallassinoides*, and *Skolithos*. The sandstone beds are interbedded with thinner (less than 5 cm thick) muddy sandstones and mudstones. Sedimentary structures in the mudstones include ripple cross-lamination, horizontal lamination, and lenticular, wavy and rare flaser bedding. Burrows in the mudstone are *Planolites* and *Trichichnus*.

Muddy Bioturbated Sandstone Lithofacies

The muddy bioturbated sandstone lithofacies is made up of medium-sized quartz and feldspar grains with common to locally abundant detrital mud and trace to minor glauconite. Basal pebble lags consist primarily of phosphate nodules and sandy casts of burrows. Sedimentary structures include low-angle stratification, tabular-tangential and tabular-planar cross-stratification, and rare trough cross-stratification. Cross-bed sets are commonly separated by thin, heavily burrowed, muddy sandstone interbeds. Where not destroyed by bioturbation, the interspersed muddy sandstone has horizontal and/or lenticular ripple-laminations. Locally, there are thin bioturbated calcareous mudstone lenses. This facies generally occurs near the base of the Tocito Sandstone and is differentiated from other lithofacies by its abundance of biological versus physical sedimentary structures. Burrows include *Planolites, Thallasinoides, Teichichnus, Skolithos, Trichichnus, Ophiomorpha,* and rare *Terebellina*.

Ripple Cross-laminated Sandstone Lithofacies

The ripple cross-laminated sandstone lithofacies is made up of fine quartz and feldspar grains and detrital mudstone with locally abundant shell fragments, and scattered phosphate nodules and mud rip-up clasts. Sedimentary structures are wave and combined-flow ripple cross-laminations, and thin bioturbated sandstone and mudstone interbeds. Local thin medium-grained sets are trough cross-stratified. Patchy burrowing consists of *Thallasinoides, Skolithos*, and *Ophiomorpha*.

Pebbly Sandstone Lithofacies

The pebbly sandstone lithofacies is made up of medium- to coarse-sized quartz and feldspar grains with abundant quartz, chert and phosphate granules and pebbles, and abundant shell fragments. Sedimentary structures include low-angle stratification and planar and trough cross-bedding. Sets form amalgamated co-sets that are typically one meter thick. Bioturbation is patchy and limited to locally high concentrations of vertical burrows. These lithofacies are generally found at the top of the Tocito Sandstone overlying a scour surface that can commonly be traced for several hundreds of meters and slightly truncates underlying units.

METHODS

Burial History Plot

Upper Cretaceous to Present Depositional and Tectonic Events

Burial history plays a major role in determining the post-burial alterations of sediments. A burial history curve was constructed to establish the timing and depth of maximum burial, the maximum burial temperature encountered, and if that temperature

was high enough to initiate temperature dependent reactions (e.g., illite-smectite transformation or hydrocarbon generation). In addition, the curve illustrates periods of uplift in which meteoric waters could have passed through the formations and affected the chemical balance between framework-grains, detrital clays, and authigenic minerals. The method and data used for constructing the burial history plot are given in Appendices 1 and 2.

Petrography

Thin Section Petrography

Petrographic techniques were used to quantify mineral abundances (grains and cements) and porosity, and document diagenetic textures (especially compaction, cementation, and dissolution). Thin sections from Tocito Sandstone outcrop, shallow-subsurface cores that were drilled through the outcrop, and Horseshoe oil field core were provided by Unocal Corporation in Brea, CA. Amoco Production Company in Denver, CO provided thin sections from cores obtained in the Gallegos, Cha Cha and Totah oil fields. Additional thin sections, sampled from the permeability grids in the Hogback oil field outcrops, were prepared by Unocal Corporation. Listed in Appendix 3 are the methods and well locations for cores used in this study.

Scanning Electron Microscope

A Hitachi High-Scan HHS-2R scanning electron microscope (SEM), operated by the Materials and Metallurgical Engineering Department at New Mexico Tech, was used to confirm the presence of kaolinite, gypsum, and framboidal pyrite. In addition, the geometries of pores were studied, focusing on relationships between pore throats, quartz

overgrowths, and detrital and authigenic clays. Details on methodology are given in Appendix 3.

Cathodoluminescence

Cathodoluminescence was used to differentiate and quantify potassium and plagioclase feldspars and compositional zonation in calcite cement. Because the calcite cement distributed throughout the Tocito Sandstone has a poikilotopic texture, it is impossible to distinguish more than one cement phase without using stains or cathodoluminescence. Details on the methodology are given in Appendix 3.

Isotopic Analysis

Stable isotope analyses ($\delta^{18}O$ and $\delta^{13}C$) of carbonate cements were performed on a Finnigan MAT Delta E gas-source mass spectrometer operated by the Geoscience Department at New Mexico Tech. The mass spectrometer is connected to a Compaq 386/20e computer and a Kipp & Zonen BD-40 recorder.

All framework-grains, overgrowths, and detrital and authegenic clays in the Tocito Sandstone are silicates. Since calcite cement was the only constituent that would react with phosphoric acid, it was possible to extract CO_2 from the calcite cement by reacting powdered bulk-rock samples with 100% phosphoric acid. The process was carried out under a vacuum so as not to contaminate the CO_2 sample with atmospheric CO_2. The fractionation factor of the acid was determined earlier by reacting it with a Mexican Calcite standard, a Solenhofen Limestone standard, and a Toilet Seat Limestone standard.

Each CO_2 sample was run through the mass spectrometer twice to check the precision of the instrument. Values for $\delta^{18}O$ were corrected for fractionation that occurred during reaction with the phosphoric acid.

Oil Extraction

During the Late Oligocene or Early Miocene, oil may have migrated into the Tocito Sandstone that now crops out in the Hogback oil field. The majority of the oil has long since been lost (escaped when sandstone was exhumed?) or biodegraded, and possible staining of framework-grains is the only indicator of oil. To confirm that oil was once present, core sections of cross-bedded sandstone, each 10-15 cm (4-6 in) in length, were placed in large glass beakers of toluene for two days. The specimens are not contaminated with an oil-based drilling fluid because gel-based fluids were used during the coring (Schlumberger electric log header). The solvents were then decanted and distilled. The remaining sludge was analyzed by a chromatograph at the New Mexico Petroleum Recovery Research Center, a division of the New Mexico Institute of Mining and Technology.

Permeability Measurements

Tocito Sandstone outcrop and core plug permeabilities were measured on a macroscopic-scale with a mechanical field permeameter (built by Edinburgh Services Limited) loaned by Unocal Corporation (Figs. 5, 6). A computer-controlled scanning minipermeameter (Fig. 7), designed and operated at the New Mexico Petroleum Recovery Research Center, was used to produce mesoscopic-scale permeability grids on a slabbed shallow subsurface core. Details on the operation and calibration of the minipermeameters are given in Appendix 4.

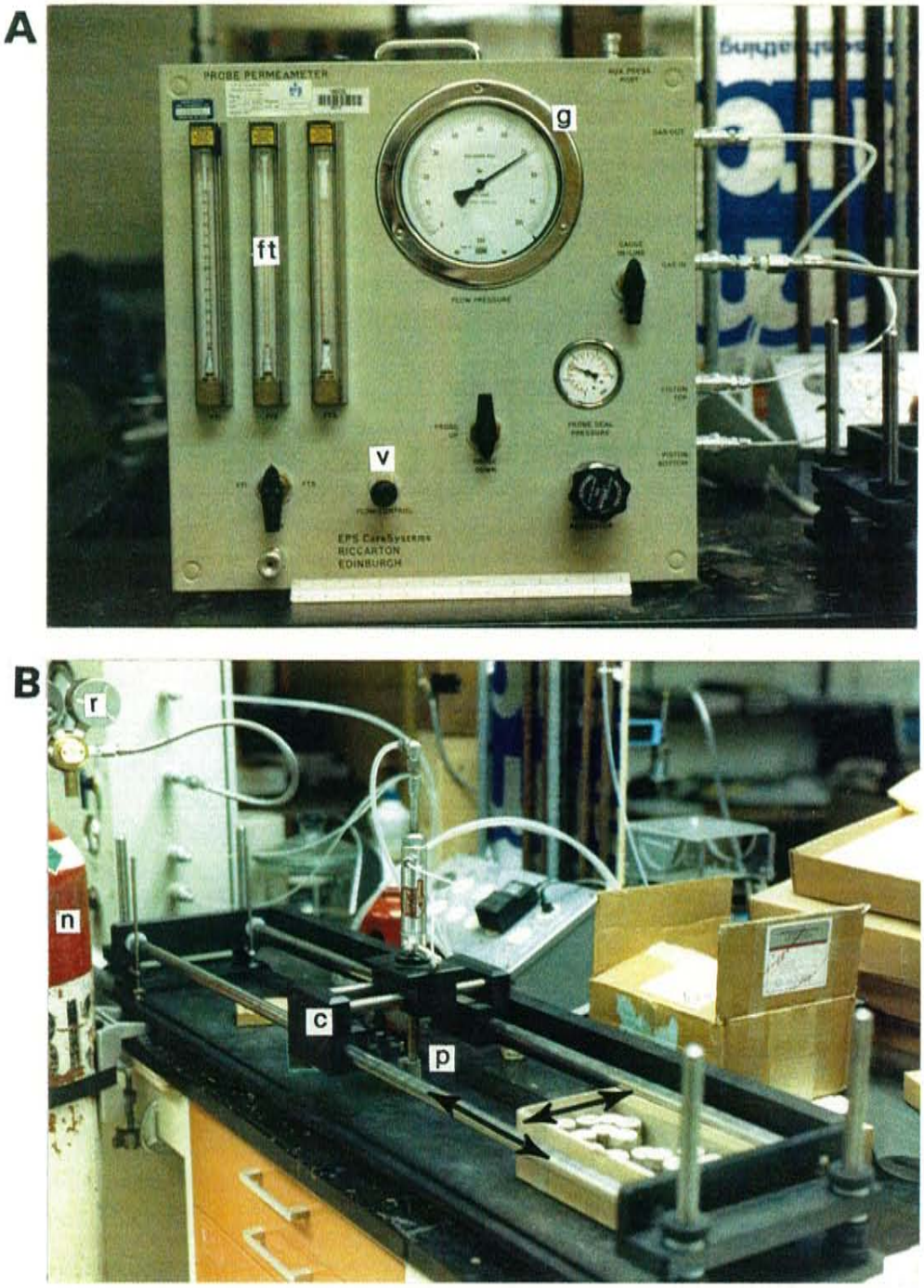

Figure 5 - A) The mechanical field permeameter and B) core frame module during the calibration process. Gas flow is generated by a compressed nitrogen gas cylinder (n) controlled by a two-stage regulator (r). Gas flux is measured by three different flow tubes (ft), each calibrated by the manufacturer for different rates of gas flow. Gas flow and pressure is adjusted with a needle valve (v). A pressure gauge (g) downstream of the flow tubes monitors flow pressure at the point where probe tip (p) touches the rock's surface. Probe is attached to a carriage plate (c) which moves longitudinally and laterally (arrows) on guide rails. White scale is 12.5 inches long.

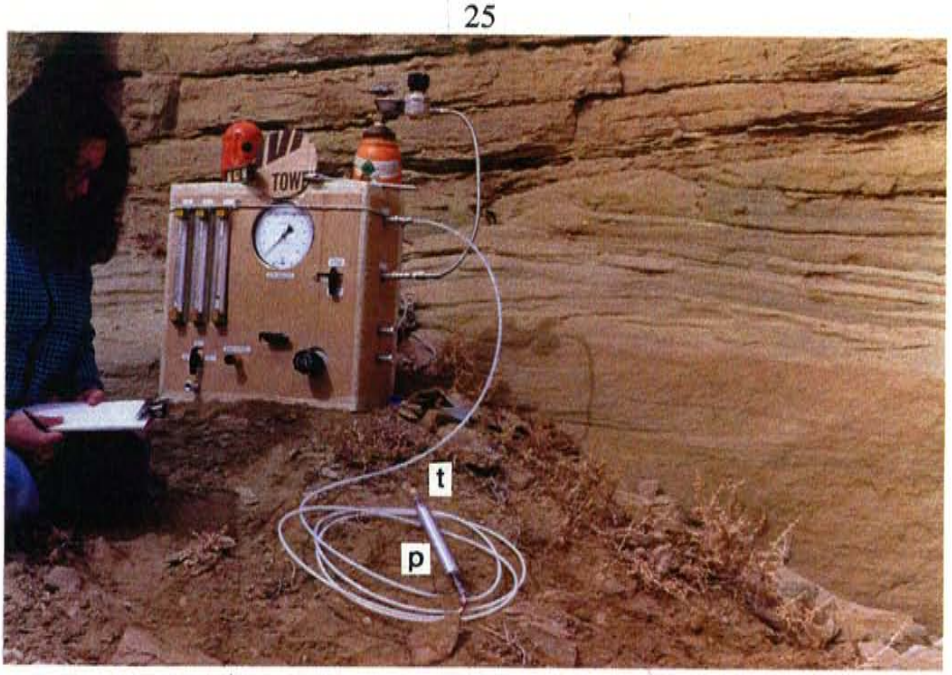

Figure 6 - The mechanical field permeameter and hand-held probe (p) as used in the field. The permeameter is encased in protective cardboard. One person presses the probe's yellow silicone rubber tip (t) against the outcrop as a second person operates the permeameter and records gas flow rates and pressures.

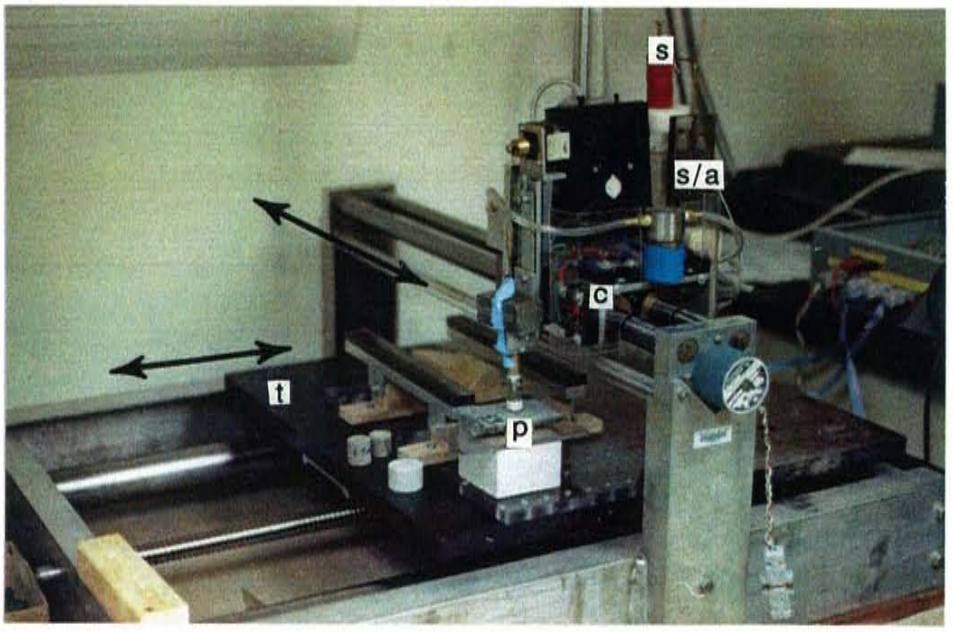

Figure 7 - The computer-controlled scanning minipermeameter during calibration process. Consists of a syringe (s) for constant pressure air supply, computer-controlled sensors and actuators (s/a) to measure air flow, and a white silicon rubber probe tip (p). They are all mounted on a computer-controlled traveling carriage (c) which scans (arrows) the desired length of a core. The table (t) upon which the core rests moves (arrows) in a direction at right angles to the direction in which the instrument carriage moves.

Tocito Sandstone Outcrop Measurements

Tocito Sandstone outcrops in the Hogback oil field

At the Hogback oil field, representative lithofacies were selected from both the "lower" and "upper" Tocito Sandstone bodies and the phosphatic nodular mudstone unit between them. For this study, the term "upper" Tocito is assigned to the sandstone units above the uppermost horizontal black line drawn in Fig. 8 and contains grids #1 through #3. "Lower" Tocito refers to the sandstone units below the lowermost horizontal black line and contains grids #6 through #9.

Permeability measurements were conducted on seven square grids (Grids 1-5, 7, 9) with measurement intervals of 10-30 cm (4-12 in) horizontally and vertically irrespective of sedimentary structures. In a separate grid (Grid 8), each row of permeability measurements followed the individual lines of intersection between the plane of the foresets and the surface of the outcrop. An additional grid (Grid 6) with 100 cm (39 in) horizontal spacings, went along the "lower" Tocito Sandstone pinchout. Surfaces of the outcrop were chipped away to remove the weathered material. It was occasionally necessary to dig 5-8 cm (2-3 in) into the outcrop to reach probable unweathered rock. Strong blasts of nitrogen gas were used to clear out any remaining dust and loose grains that might plug pore throats during the permeability measurements. At times it was difficult to distinguish weathered outcrop from unweathered rock in which cement and feldspars were leached during burial. In addition, the medium- to coarse-grained nature of the Tocito frequently made it difficult to acquire a tight seal around the probe tip.

Permeability measurements were made with the probe tip pressed against the outcrop by one person, while a second person operated the MFP and recorded the raw gas-flow data. The injection pressure was 5 psi and the probe tip's internal radius was 0.13 cm (0.05 in) for all outcrop permeability measurements.

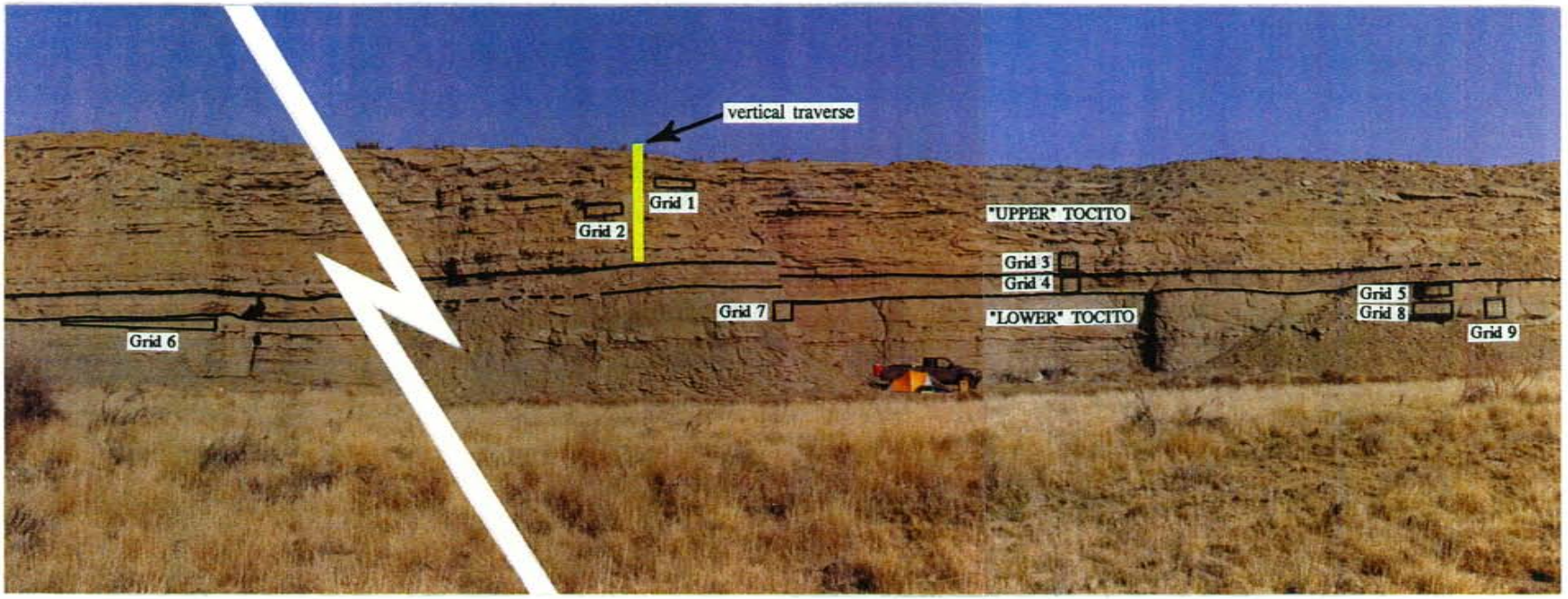

Figure 8 - Locations of permeability grids #1 through #9 on the Tocito Sandstone outcrop in the Hogback oil field, San Juan Basin, New Mexico. The location of this panorama with respect to the Tocito outcrop is indicated in Figure 4. The gap in the photo represents the removal of approximately 33 m (109 ft) of outcrop. For this study, the term "upper" Tocito is assigned to the sandstone units above the uppermost horizontal black line and contains grids #1 through #3. "Lower" Tocito refers to the sandstone units below the lowermost horizontal black line and contains grids #6 through #9. The "phosphatic nodular mudstone" is bounded by the two horizontal black lines and contains grid #4. Also identified in the panorama is the location of the traverse made during outcrop permeability measurements.

Tocito Sandstone outcrops along the Chaco River

In the Hogback oil field, the "upper" Tocito Sandstone rests unconformably upon the "lower" Tocito. One of the results of the unconformity is to truncate the "lower" Tocito so that only the "upper" Tocito crops out along the Chaco River, northwest of the field. Due to its overhanging profile, the outcrop along the Chaco River provided minimally-weathered sandstone surfaces in which to conduct permeability studies. Nine permeability grids (Grids 10-14, 16-18, and 20-21) had spacings between permeability measurements of 30 cm (1 ft) horizontally and 15-30 cm (6-12 in) vertically. Five of these nine grids paralleled foresets (Grids 10, 12-13, and 18-19). Grid 19 had a 150 cm (59 in) horizontal and 100 cm (39 in) vertical spacing so as to detect any large scale trends in permeability along a single cross-bedded sandstone unit. A separate grid (Grid 15), located within a highly contorted cross-bedded sandstone unit, had measurement sites strategically placed throughout the area. Grids were focused within representative lithofacies and sedimentary structures. The gas injection pressure was 5 psi and the probe tip's internal radius was 0.13 cm (0.05 in). Dense vegetation in front of the outcrop prevented the recording of grids on an outcrop-scale photo panorama, as was done in the Hogback oil field.

Hand Specimen Measurements

Hand specimens were collected along a vertical traverse of the "upper" Tocito Sandstone cropping out in the Hogback oil field (Fig. 8). Vertical sampling intervals ranged from 15-25 cm (6-10 in), and occasionally as much as 1 m (3 ft), when the outcrop was buried under talus.

Well-cemented hand samples were slabbed using a water-based lubricant. The poorly cemented sandstone samples were slabbed without lubricant, as they quickly deteriorated when wet. The slabbed surfaces were brushed and air-blown clean prior to

permeability measurements using the mechanical field permeameter. Billets were cut from the same samples and sent to Unocal Corporation in Brea, CA to be impregnated with blue-dyed epoxy and cut into thin sections. Permeabilities were then compared to petrographic observations and permeabilities measured from the HOF cores.

Core Measurements

Shallow subsurface core

Permeability measurements were conducted with the mechanical field permeameter on Tocito Sandstone core plugs provided by Unocal. The plugs had been cut from the HOF #1, #2, and #3 near-surface cores (Sec. 19, T29N, R16W and Sec. 13 T29N R17W) from the vicinity of the Hogback oil field. The cores are 20 to 32 m (67-107 ft) long and penetrated the entire Tocito. Plugs had been cut from the cores approximately every 0.3 m (1 ft). Six permeability measurements per core-plug were taken with the mechanical field permeameter using an injection pressure of 5 psi and a probe tip internal radius of 0.13 cm (0.05 in). The permeability measurements were averaged for each core-plug and plotted in order to compare the results with core descriptions provided by Rex Cole of Unocal Corporation in Brea, CA.

Permeability measurements were made on the HOF #2 core obtained from the Navajo Nation Mineral Department. The core was originally split three ways with equal portions going to the Navajo Nation, Louisiana State University, and Mobil Oil. The dimensions of the Navajo Nation's portion of the core are approximately 6 cm (2.3 in) wide and 21 m (69 ft) long. Permeability measurements using the computer-controlled scanning minipermeameter were conducted on grids 3.75 cm (1.5 in) wide down the length of the core. The spacing between permeability measurements was 0.625 cm (0.25 in) in rows perpendicular to the length of the core and in rows parallel to the length of the core. Contour plots were made for many of the grids and average permeabilities

were plotted with respect to depth to illustrate the trends in heterogeneity along the length of the core. By comparing each permeability measurement to the specific rock type in which the measurement was made, average permeabilities were assigned to lithofacies type and sedimentary structures.

Deep subsurface reservoir core

Four Tocito Sandstone reservoir cores (Appendix 5) were measured with the mechanical field permeameter. The most complete study was done on the Solar Petroleum Navajo Tribal F-151 core, stored at the United States Geologic Survey core warehouse in Denver, Colorado. Studies containing fewer measurements focused on specific sedimentary textures in the Pan American Martin Gas Unit C-1, the Union Texas Angel Peak B-37, and the Union Texas Newsom A-3E cores, all stored at Amoco's Denver core warehouse. Locations for each well are given in Appendix 5 and Fig. 2B.

Permeability grids were measured on portions of the Navajo Tribal F-151 core that were representative of lithofacies found in the Tocito Sandstone outcrop and HOF cores. Grids were commonly 2.5-3.8 cm (1-1.5 in) wide and 7.6-10.2 cm (3-4 in) long, with 1.27 cm (0.5 in) horizontal intervals and 2.5 cm (1 in) vertical intervals. Permeabilities were estimated for the remaining portions of the core in order to produce a permeability profile. However, *only* the measured data were used for statistical analysis and for comparisons with the outcrop and shallow subsurface cores.

For the Martin Gas Unit C-1, Angel Peak B-37, and Newsom A-3E core, permeability measurements were made with the mechanical field permeameter on lithofacies similar to those identified in outcrop and shallow subsurface core. Measurements were taken along the center of the core, usually with 2.5 cm (1 in) vertical spacing.

Permeability and porosity data were acquired from Richard Bottjer of Amoco for Pan American Petroleum wells Navajo Tribal E-8, Navajo Tribal H-2, and Gallegos Canyon #250. Locations of these wells are given in Appendix 3 and in Fig. 2B.

RESULTS

Burial History Curve for Tocito Sandstone Outcrop

The Tocito Sandstone outcrop at the Hogback oil field underwent relatively continuous rapid burial [66 meters/million years (m/m.y.)] throughout the Late Cretaceous (Fig. 9). During the Maastrichtian the Tocito outcrop was uplifted at a rate of 65 m/m.y., but was never exposed at the surface. This was followed by a period of relatively slow burial (30 m/m.y.), a second episode of uplift (16 m/m.y.), and a final period of rapid burial (51 m/m.y.). A maximum burial depth of 2042 meters (6700 ft) was reached during the Middle to Late Eocene [44 million years ago (m.y.a.)].

During the Late Eocene and throughout the Oligocene, the Tocito Sandstone was slowly uplifted at a rate of 3.4 m/m.y. to a depth of 1981 meters (6500 ft). At that point, the rate of uplift greatly increased (76.2 m/m.y.) and the Tocito became exhumed in the Hogback oil field.

The Tocito Sandstone outcrop experienced a maximum burial temperature of approximately 96°C (205°F) at a depth near 1981 meters (6500 ft) during the Late Oligocene (26 m.y.a.). Note that this does not correspond with maximum burial (2042m at 44 m.y.a.) during which the Tocito experienced a temperature of approximately 89°C (192°F). This was the result of a volcanism-influenced paleogeothermal gradient that increased more rapidly than the on-going uplift. Refer to the burial history construction in Appendices 1 and 2 for additional information.

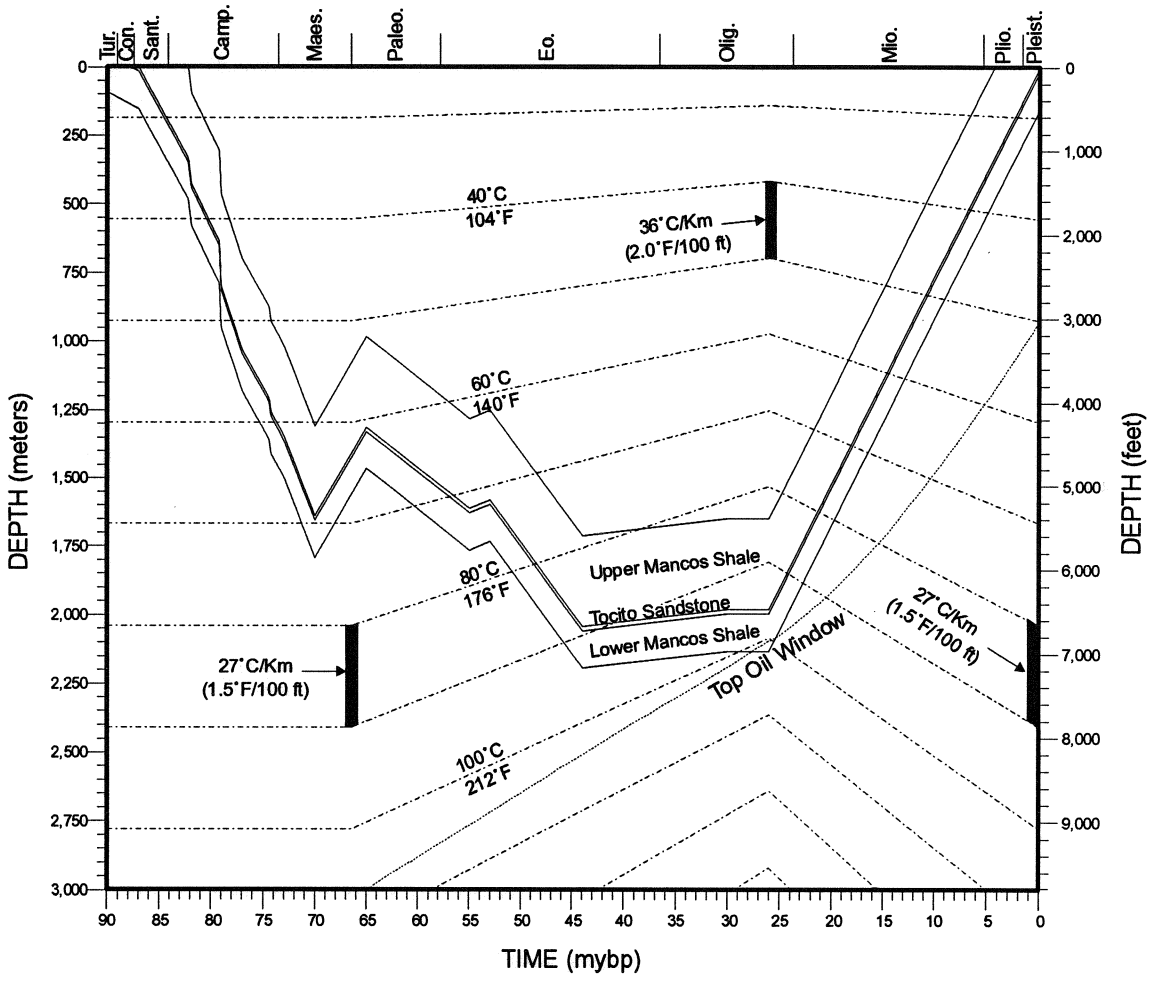

Figure 9 - Burial history curve for the Tocito Sandstone cropping out in the Hogback oil field (secs. 17-20 and 29-30, T29N, R16W), San Juan Basin, New Mexico. Geothermal gradients and orientation of the oil window are from Huffman (1987). Estimates for timing of deposition and erosion, and the thickness of strata deposited or eroded, are from Steven (1975), Bond (1984), Huffman (1987), Molenaar (1988), Ward (1990), Jennette et al. (1991), Hunt and Lucas (1992), Law (1992), and Williamson and Lucas (1992).

The organic-rich lower Mancos Shale entered the "oil window" during the end of the Oligocene for 2-3 m.y., perhaps longer if the paleogeothermal gradient was higher. Maturation of the organics was later retarded by Late Oligocene to Neogene uplift.

An important observation of the burial history curve is temperatures were high enough (> 50°C or 122°F) in the Mancos Shale for conversion of smectite to illite. This conversion would have released absorbed water (Siebert et al., 1984), which may have be responsible for framework-grain dissolution in the Tocito Sandstone (to be discussed later).

The burial history curve illustrated in Fig. 9 differs from the burial curves for the Tocito Sandstone oil reservoirs only because the Tocito outcrop was not buried as deep and is now exposed at the surface. Otherwise, the general pattern of burial and uplift should be similar for all Tocito lentils.

Petrology and Diagenetic History

Tocito Sandstone Composition and Texture

Tocito sandstones in the Cha Cha, Horseshoe, Totah, and Hogback oil fields are classified as arkoses, subarkoses, and sublitharenites (Folk's classification, 1968; Fig. 10). This spectrum appears to be the result of feldspar dissolution rather than absolute increases in quartz, as will be discussed later. Grain compositions found in the shallow HOF #3 core differ in that they form a relatively tight cluster of points within the arkose field of the quartz-rock fragment-feldspar ternary diagram. Sandstones in the four oil fields are moderately sorted and fine- to coarse-grained. Primary framework grains are quartz (ave. = 38%), microcline (ave. = 15%), plagioclase (ave. = 1%), and rock fragments (primarily chert and mudstone clasts; ave. = 2%). Where present, the matrix is detrital clay (ave. = 9%) and glauconite pseudomatrix (ave. = 3%). Additional

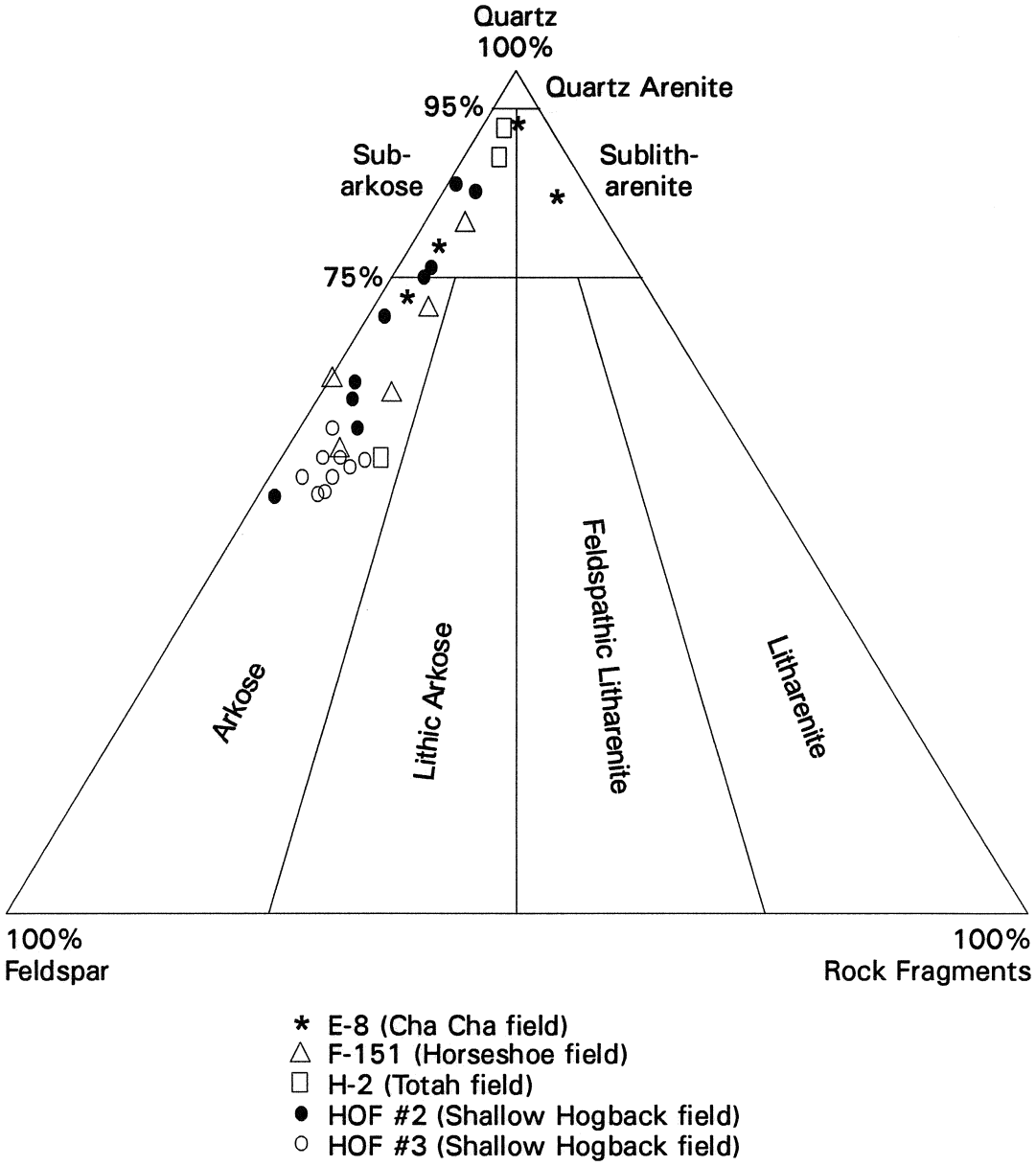

Figure 10 - Quartz-rock fragment-feldspar ternary diagram (Folk, 1968) for samples from shallow and deep subsurface cores. Note how HOF #3 is characterized by a cluster of points, whereas the other wells have a spectrum of compositions. Petrographic data are listed in Appendices 6 and 7.

minerals include nodular phosphate (ave. = 2%), pyrite (ave. = 1%), kaolinite (ave. = 1%), and carbonate cement (ave. = 10%). Petrographic data for thin sections from core are tabulated in Appendices 6 and 7.

Diagenetic History

The diagenetic history of the Tocito Sandstone cropping out in the Hogback oil field is summarized in Fig. 11. The sequence of important events (determined from petrographic, scanning electron microscope, and cathodoluminescence observations) are listed below.

Glauconite

Glauconite in the Tocito Sandstone consists mainly of sand- to pebble-sized, deep green to brownish-green particles that exhibit a microcrystalline or "scaly" birefringence under cross-polars (Fig. 12). When not plastically deformed into pseudomatrix, glauconite commonly has subrounded or rosette-like morphologies. Shrinkage fractures and/or fine ferroan dolomite rhombs are common in the particles. Glauconite is randomly scattered throughout bioturbated sediments, but is frequently concentrated in the coarse-grained foresets of cross-bedded sandstone units. The glauconite may have replaced detrital grains, such as fecal pellets or biotite after the detrital grains were concentrated by tidal currents. Pryor (1975) found that present day filter-feeding organisms produce significant quantities of argillaceous fecal pellets that are firm and resistant to abrasion. The pellets are transported and deposited with fine to medium sand-size quartz grains. Pryor (1975) also noted that the decay of organic matter in the pellets created microreducing conditions that promoted glauconitization of the pellet. Sandstone core from the Cha Cha and Horseshoe oil fields have 2.0 to 15.1% glauconite,

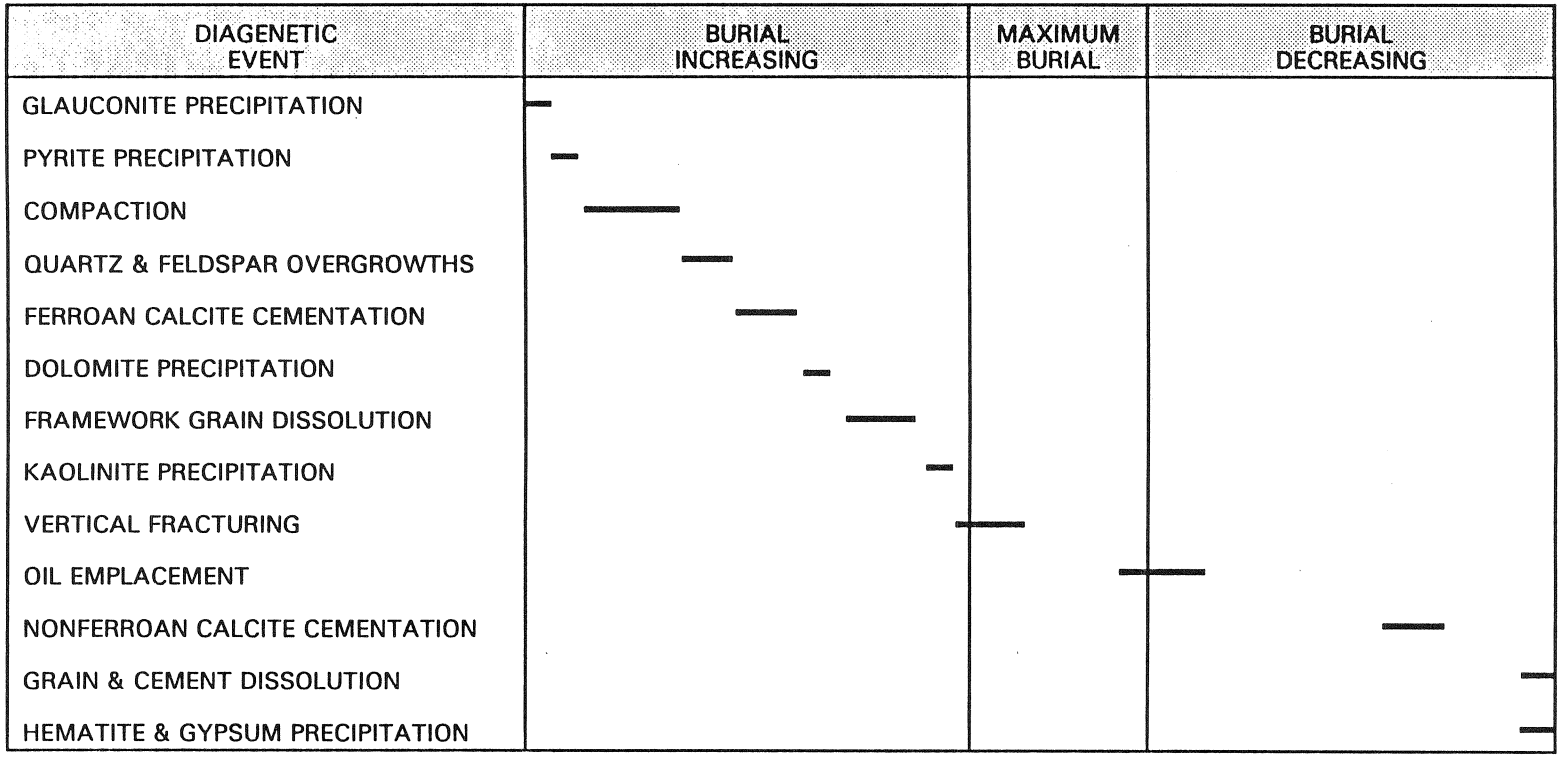

Figure 11 - Diagenetic history of the Tocito Sandstone outcropping in the Hogback oil field as determined from petrographic, SEM and cathodoluminesence observations of outcrop and subsurface specimens.

whereas the core from the Totah oil field and the Hogback oil field outcrop contains trace to 9.4% (Appendices 6 and 7).

Glauconite also exists as thin films coating the surfaces and internal fractures of framework-grains (Fig. 12). Some glauconite is laminated and is probably the result of complete replacement of detrital biotite by glauconite.

Glauconite is an early-forming mineral in modern environments where sedimentation rates are very low and the bottom waters are suboxic and moderately alkaline (pH = 7-8) (Odin and Matter, 1981). Compaction into pseudomatrix indicates that glauconite precipitation in the Tocito Sandstone occurred prior to compaction.

Pyrite

Pyrite is present in most Tocito Sandstones as framboids and discrete octahedrons (Figs. 13A,B) and is generally concentrated within mud lenses. These mud lenses are organic-rich, having plant-like and amorphous opaque material. The presence of organics is also cited by Pasley et al. (1989, 1991). Pyrite rarely exceeds 5% in the subsurface and averages 1% in the shallow nearsurface and outcrop (Appendices 6 and 7). The presence of very late-stage hematite and gypsum in the outcrop suggests that pyrite may have been oxidized by meteoric water in the outcrop.

There is little definitive petrographic evidence with which to determine the timing of pyrite precipitation. However, the framboid morphology is indicative of early diagenetic pyrite that precipitated as the sediment passed through the sulphate-reduction zone (Gautier, 1985) at burial depths of approximately 100 meters (328 ft) or less (Hesse, 1989). Euhedral octahedrons probably precipitated shortly afterwards as overgrowths on the pre-existing pyrite framboids (Gautier, 1985).

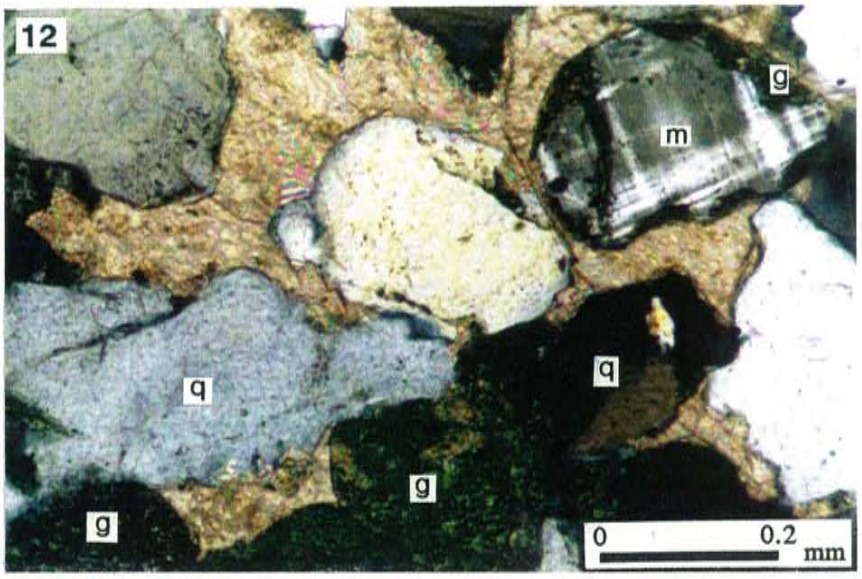
12
g
m
q
q
g
g
0
0.2
mm

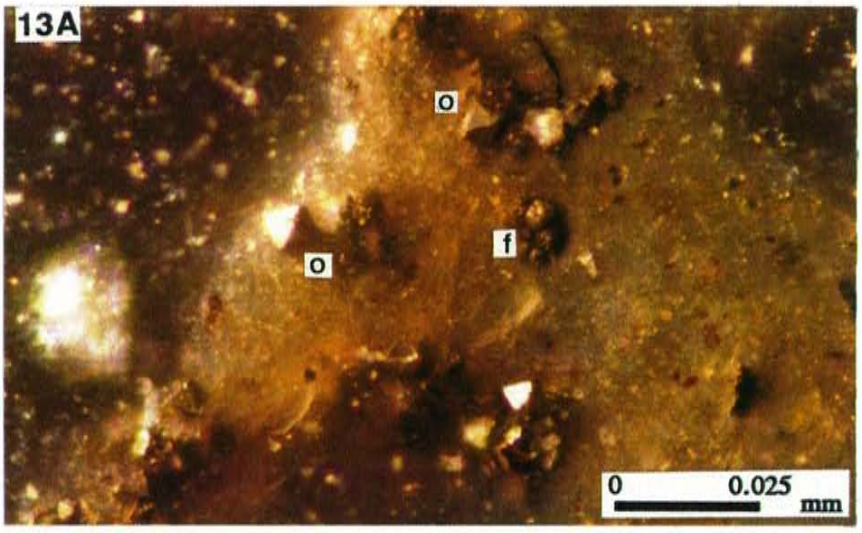
13A
o
o
f
0
0.025
mm

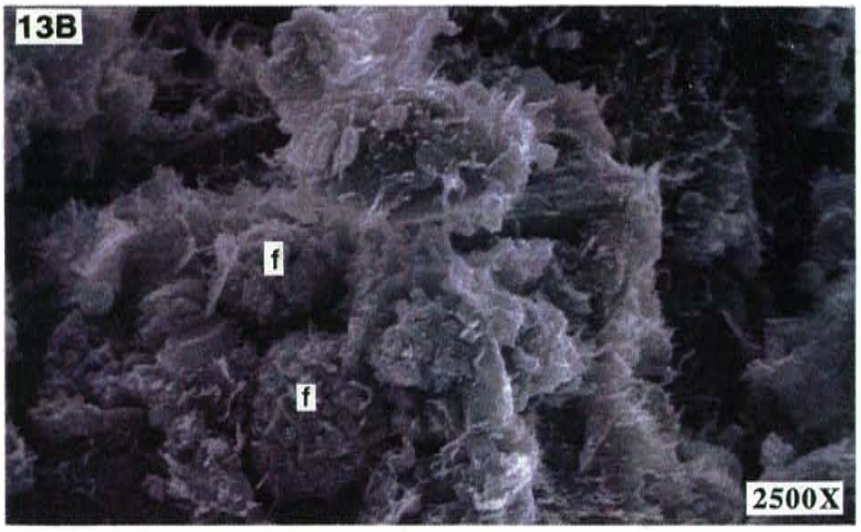
13B
f
f
2500X

Compaction

Grain-to-grain contacts are dominantly tangential (point) and long, with some grains "floating" in detrital clay matrix or phosphate and glauconite pseudomatrix. Concavo-convex contacts are very rare and sutured contacts were not observed. This suggests that the depth of burial was not great enough to induce pressure dissolution of framework-grains, or that quartz overgrowths or trapped connate waters provided adequate support to prevent pressure dissolution.

Mechanical compaction reoriented and fractured framework-grains, commonly feldspars (Fig. 12), cherts, micas, and some quartz grains. Glauconite and detrital clay clasts have been deformed plasticly into pseudomatrix (Fig. 12).

Quartz overgrowths

Quartz overgrowths are common between detrital quartz grains and have straight euhedral walls wherever they terminate within open pores (Figs. 14A,B). When viewed with an scanning electron microscope (Fig. 14B), these euhedral faces do not appear etched. As discussed earlier, the detrital quartz grains are almost never sutured or in concavo-convex contact with one another, so the likelihood of quartz overgrowth precipitation due to compaction-induced dissolution is small. Quartz overgrowths generally make up 2-5% of the total rock volume (Appendices 6 and 7).

Feldspar overgrowths

Rare feldspar overgrowths were observed in thin sections from the Navajo Tribal H-2 (5125'), Navajo Tribal F-151 (919.5'), and the HOF #3 (79.5') cores. They are rare and are distinguished primarily by their "fresh" euhedral appearance relative to the altered texture of their host feldspar grains (Fig. 15).

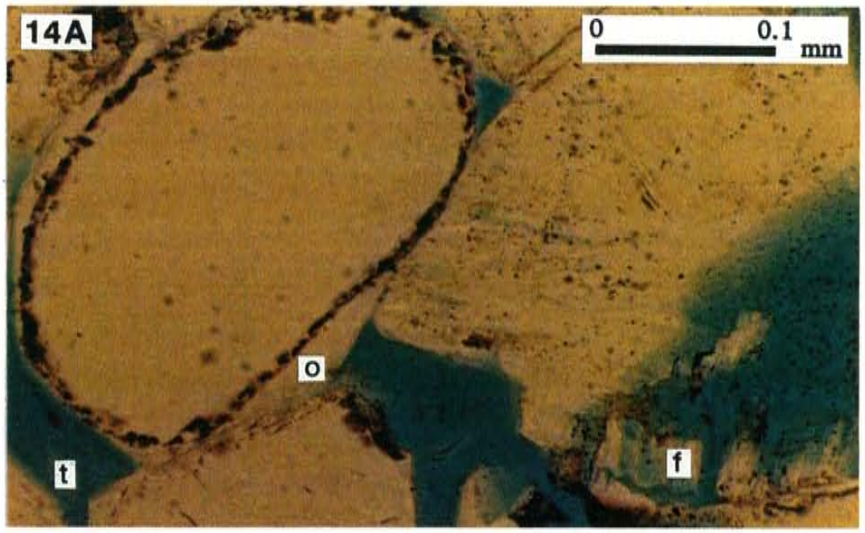
14A
0
0.1
mm
o
t
f

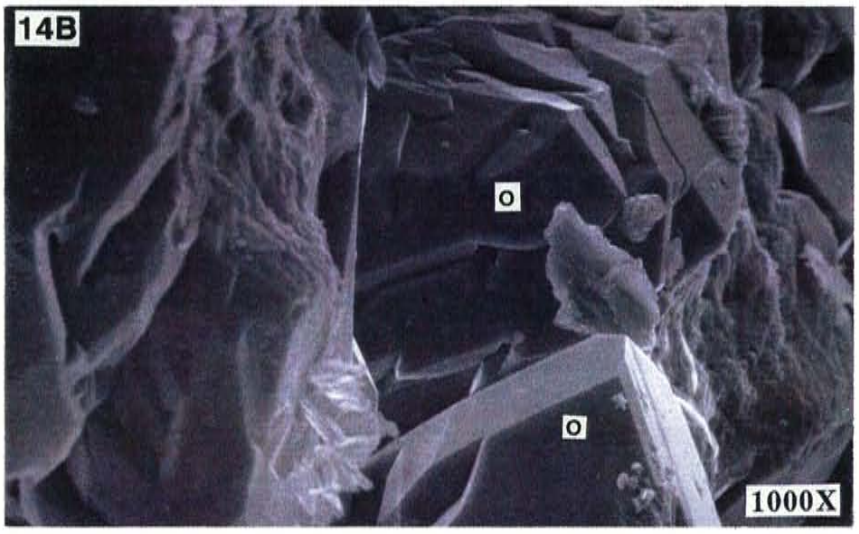
14B
o
o
1000X

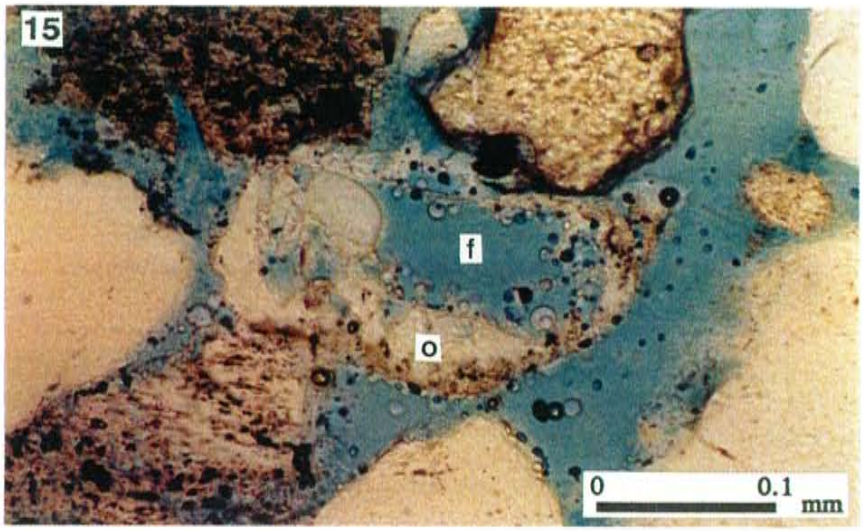
15
f
o
0
0.1
mm

Calcite cements

There are two distinct types of calcite cement in the Tocito Sandstone. One is poikilotopic (single crystals up to several centimeters across), stains blue (indicating that it is ferroan calcite), and has a dull brown luminescence when examined under a luminoscope (Fig. 12, 16A,B, Appendix 8). The second cement is a poikilotopic calcite which stains red (indicating that it is nonferroan) and has a bright orange luminescence (Fig. 16A,B, Appendix 8). Where calcite cement protrudes into open pores, it terminates as euhedral rhombs (Fig. 16C).

The contacts between the calcite cement and some of the framework-grains it surrounds are extremely ragged with grain relicts "floating" in calcite embayments within the grain (Fig. 16D). It appears that ferroan calcite has frequently replaced individual chert crystallites, polycrystalline quartz grains, and feldspar grains throughout the Tocito Sandstone. In Navajo Tribal H-2 (5122'), calcite replacement of framework-grains accounted for at least 6% of the total rock. Commonly the contacts between calcite cement and quartz overgrowth have no caries, embayments, relics, or ragged surfaces (Fig. 16C). Instead, the crystal faces of the quartz overgrowths remain euhedral, indicating that the fluids responsible for the calcite cementation were not corrosive to the quartz. In well-cemented sandstones there is occasional replacement of quartz grains and overgrowths by calcite. Such replacement and the apparent absence of calcite relics within quartz overgrowths suggest that calcite cementation occurred after quartz overgrowth precipitation.

Ferroan calcite is found in the shallow and deep subsurface core and in outcrop. However, the nonferroan calcite is found only in the outcrop and the shallow subsurface core, where it fills vertical fractures that cut the ferroan calcite cement and partially fills remaining primary and secondary porosity (Fig. 16A,B, Appendix 8). These observations indicate that ferroan calcite was precipitated before nonferroan calcite, and

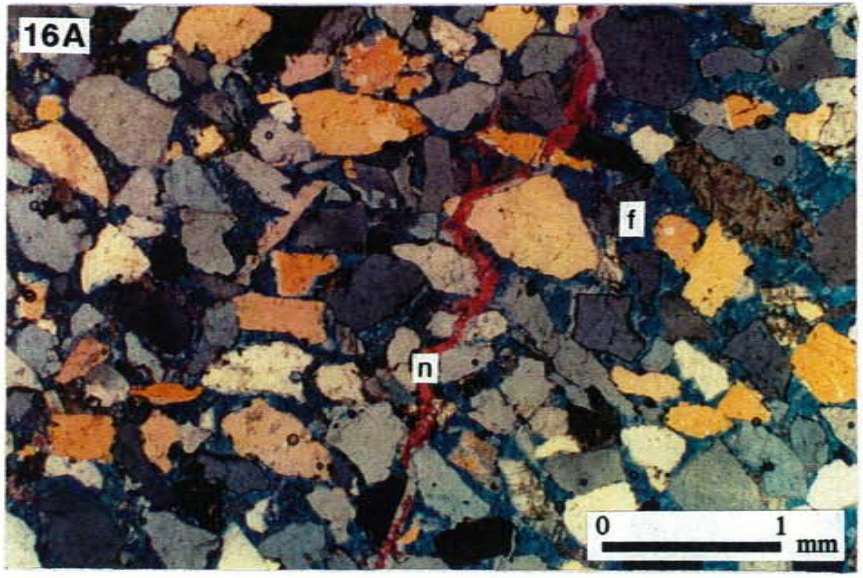
16A
f
n
0
1
mm

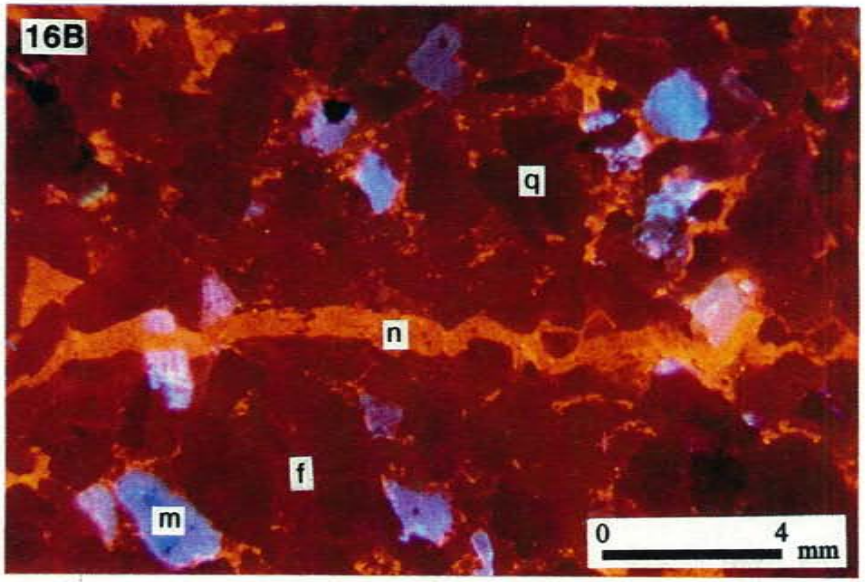
16B
q
n
f
m
0
4
mm

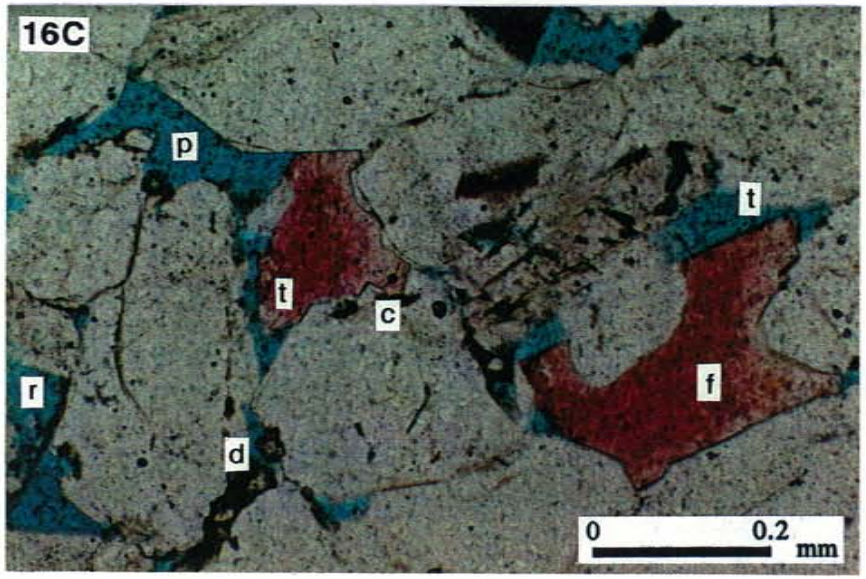
16C
p
t
t
c
f
r
d
0
0.2
mm

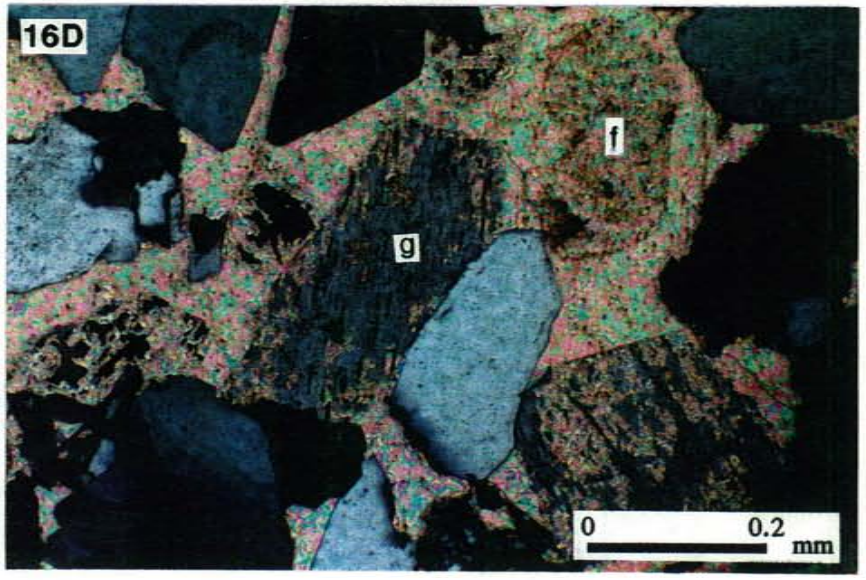
16D
f
g
0
0.2
mm

that fracturing occurred at some time between the two episodes of cementation. The irregular and gradational patterns observed under luminescence suggest that the nonferroan calcite may have replaced some of the ferroan calcite (Fig. 16B). Framework-grains in contact with nonferroan calcite have been dissolved in the outcrop. If this dissolution is due to leaching by meteoric waters, then the nonferroan calcite cement probably precipitated during the Miocene to Pleistocene uplift (Fig. 9) after the fracturing of the ferroan calcite and prior to outcrop exposure.

Ferroan dolomite

Dolomite occurs as isolated or clustered, fine (0.02-0.03 mm in diameter), euhedral rhombs floating almost exclusively in detrital clay and glauconite (Fig. 17). Fine dolomite rhombs are occasionally found within calcite cement and attached to the surfaces of framework-grains. Larger dolomite rhombs (0.10-0.15 mm in diameter) (Fig. 17) are rare and Sabins (1963) suggested that they may be detrital because their surfaces are often abraded and rounded in the Bisti oil field. Dolomite turns pale to deep turquoise when stained, indicating that the rhombs are ferroan. The volume of dolomite ranges from absent to 4.6% of the total rock (Appendices 6 and 7).

Ferroan dolomite rhombs have been noted "floating" in calcite cement and in the dissolution pores of detrital mudstone clasts and drapes. It is therefore probable that dolomite replaced pre-existing calcite cement, detrital mudstone, and glauconite. Like the calcite cement, the dolomite rhombs were not dissolved or etched by pore waters which caused grain dissolution. The dolomite rhombs, therefore, remained in the grain dissolution pores.

Framework-grain dissolution

Relic structures of plagioclase, microcline, chert fragments, mudstone clasts, and their residues are frequently observed in the Tocito Sandstone outcrop and subsurface

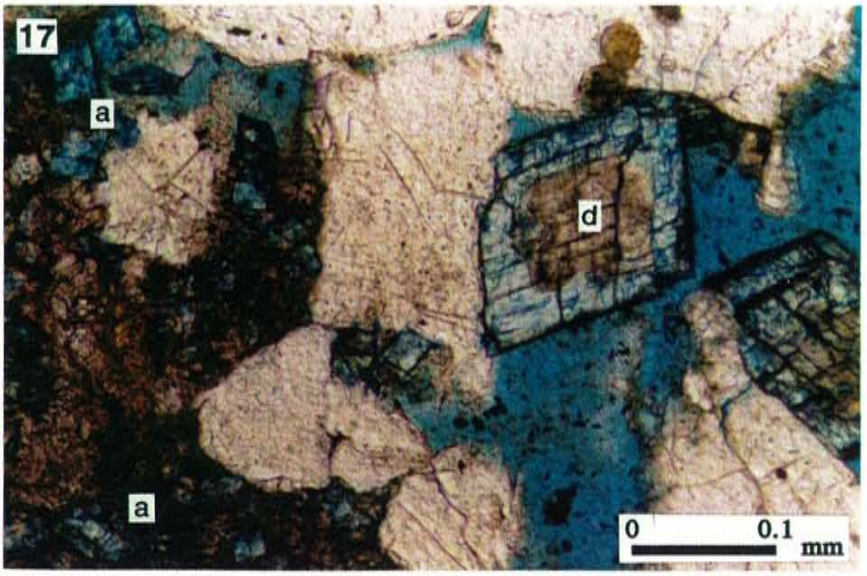
17
a
d
a
0
0.1
mm

samples (Figs. 14A, 15, 16C, 18A-F). Corroded feldspar and chert grains are found in direct contact with unaffected feldspar or chert grains. In porous sandstones, grain relics are generally found as very delicate, self-supporting features that rarely show signs of mechanical deformation or crushing (Fig. 18A). In calcite cemented sandstones, they occur as grain-sized and grain-shaped pores within the calcite cement and usually have a rim of insoluble residue along the pore walls (Fig. 18B). Elongate, oversized pores are abundant in the Tocito (Figs. 15, 17, 18A,C-E). Grain relics and elongate, oversized pores are characteristic of dissolution porosity (Schmidt and McDonald, 1979).

The preferred dissolution of feldspar, chert, and claystone fragments over quartz and glauconite (Fig. 18A,D,E), the occurrence of dissolved feldspars next to unaffected feldspars or feldspar overgrowths (Fig. 15), and the twin-controlled dissolution of plagioclase (Fig. 14A) all indicate that grain dissolution in the Tocito Sandstone was compositionally selective. Siebert et al. (1984) noted that a hierarchy of grain solubility existed in the Cretaceous Shannon Formation in Wyoming, the Oligocene Frio Formation in South Texas, and the Oligocene Nodosaria Sandstone in Louisiana. They concluded that the more calcic plagioclases were less stable and therefore more susceptible to dissolution. This may account for the notable imbalance between plagioclase grains (1-2% of total rock) and microcline grains (5-35% of total rock) observed in the Tocito thin sections. Chert, on the other hand, is more susceptible to dissolution than detrital quartz grains because of its extremely small grain size and correspondingly high surface area (Fig. 18E) (Blatt et al., 1972).

Relict structures found in the Tocito Sandstone did not form during the early stages of burial because they are too fragile to have survived the compaction and reorientation of framework-grains associated with burial. However, when compaction ceases, newly-formed relict structures do not experience mechanical deformation (Siebert et al.,1984). Therefore, grain dissolution must have occurred after significant burial.

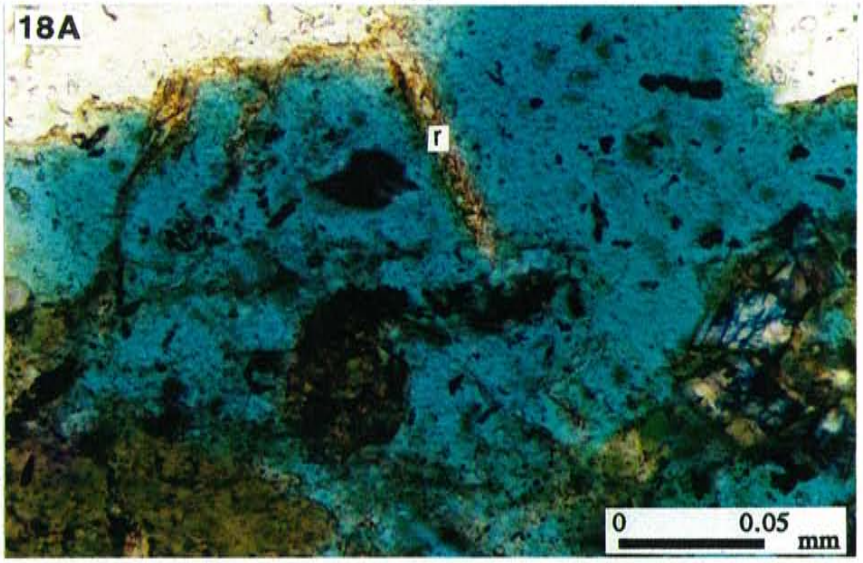
18A
r
0
0.05
mm

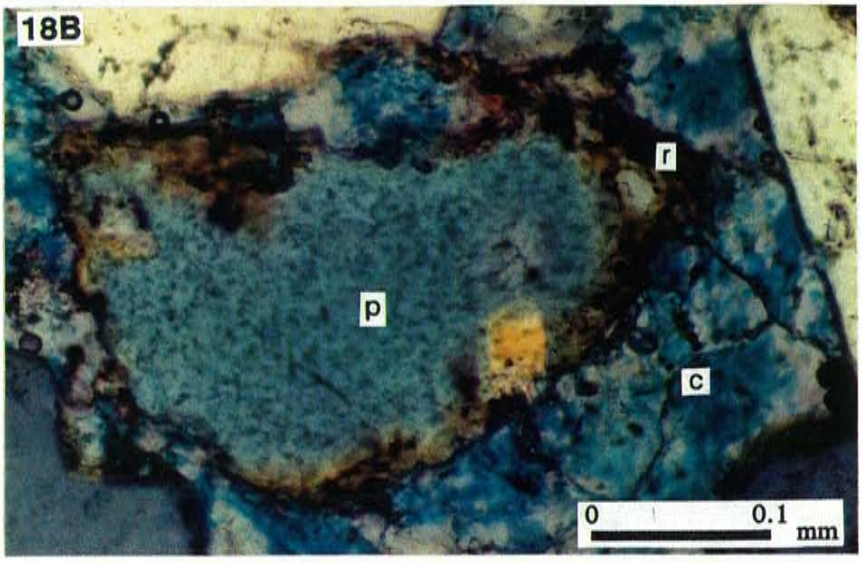
18B
r
p
c
0
0.1
mm

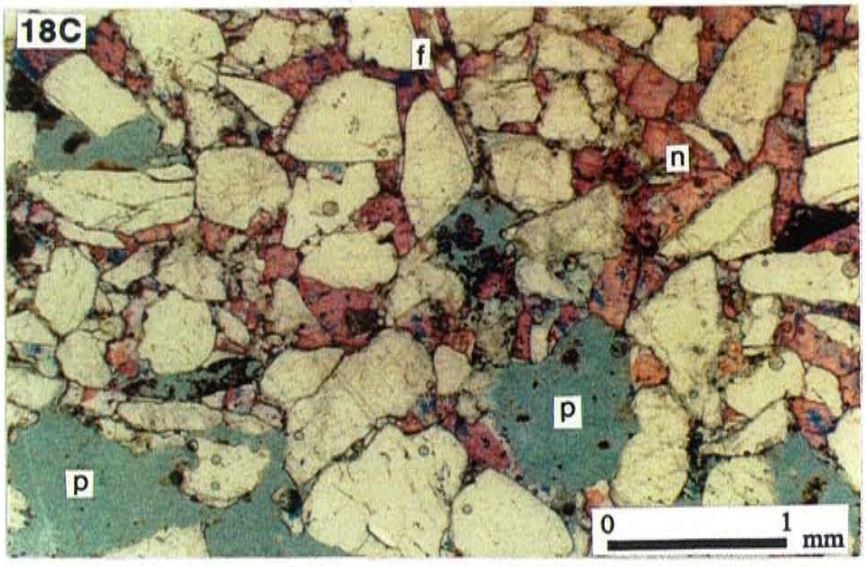
18C
f
n
p
p
0
1
mm

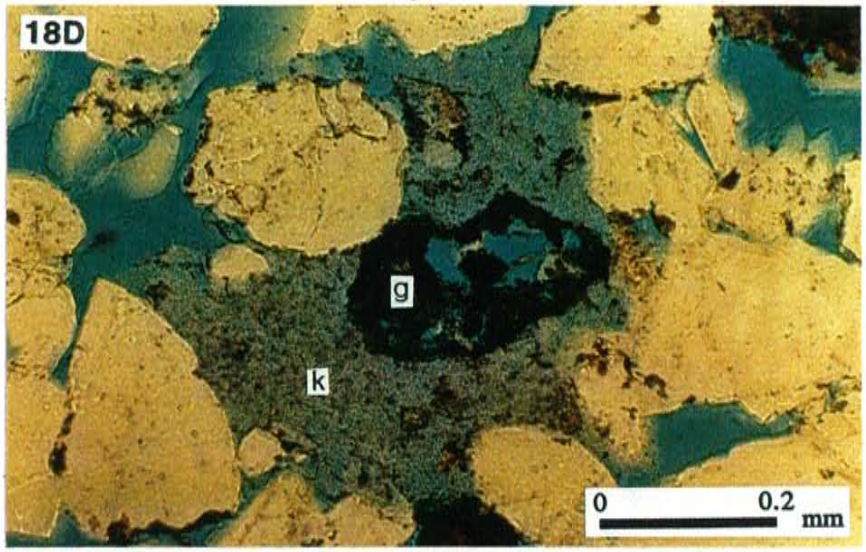
18D
g
k
0
0.2
mm

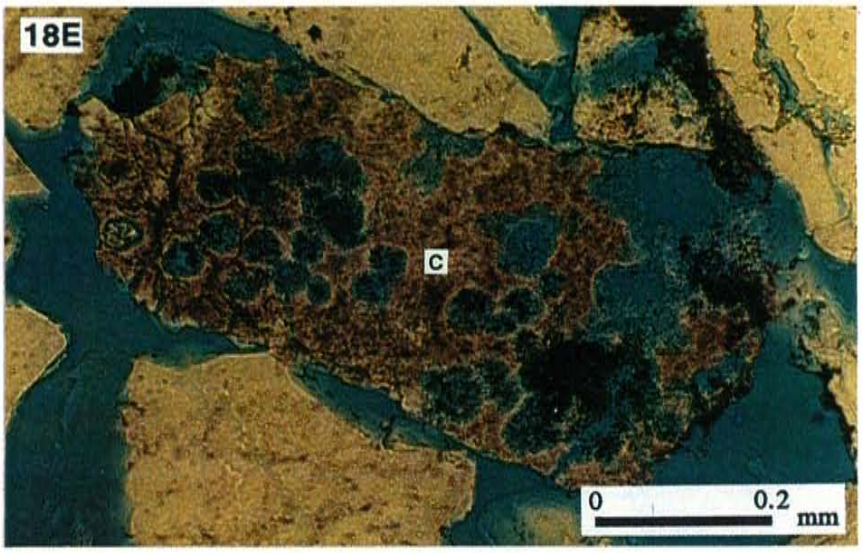
18E
c
0
0.2
mm

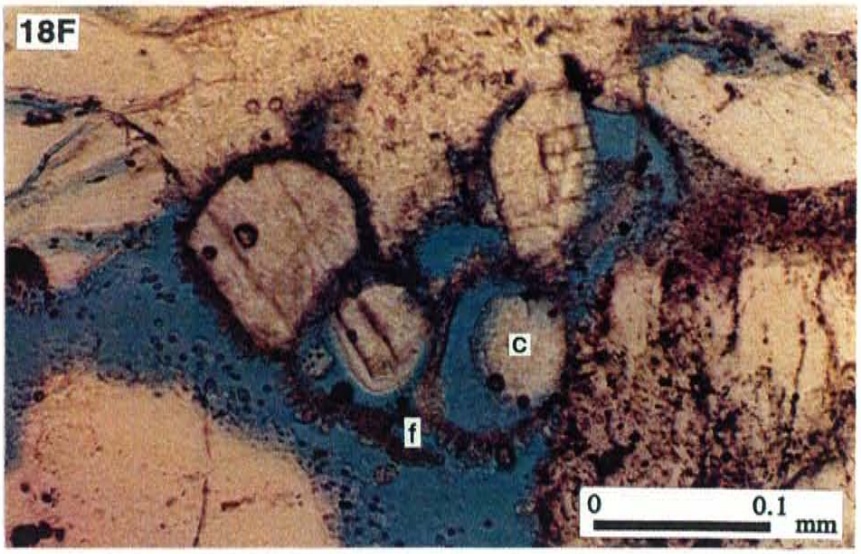
18F
c
f
0
0.1
mm

Grain dissolution has occurred in the outcrop as well, creating pores in contact with late-stage nonferroan calcite cement (Fig. 18C). Kaolinite has surrounded, but has not grown within, some dissolution pores, suggesting that some grain dissolution occurred after precipitation of kaolinite (Fig. 18D).

Pore waters responsible for dissolving framework-grains in the Tocito Sandstone may have been produced from the encasing Mancos Shale during the smectite-to-illite conversion and CO_2 generation (associated with Late Oligocene hydrocarbon generation). Petrographic evidence indicates that pore waters were not corrosive to the calcite cement. For example, rhombic terminations of calcite cement remained unetched in the subsurface (Figs. 16C, 18F), and grain-dissolution pores did not extend into the surrounding calcite cement (Fig. 18B). In addition, patches of poikilotopic calcite cement separated by pores have not been observed to be optically continuous. This suggests that the patches were not one larger cement crystal that has undergone dissolution. Finally, unetched and non-dissolved calcareous forams are found in elongate dissolution pores (Fig. 18F).

Siebert et al. (1984) proposed that during CO_2 generation from an organic-rich shale, the first gas generated is consumed during dissolution of any carbonate present in the shale and the formation of a calcium bicarbonate solution. If more calcite exists in the shale than can be dissolved by the CO_2, then the first waters expelled from the shales will contain calcium bicarbonate rather than CO_2 and will not dissolve calcite.

Kaolinite

Kaolinite occurs as highly porous to very dense, book-like aggregates filling dissolution and intergranular pores (Figs. 18D, 19A,B). Such a relationship not only indicates that kaolinite precipitated after grain dissolution, but also suggests that kaolinite may have incorporated aluminum and silica that was either released during grain dissolution or brought in with pore waters from the surrounding Mancos Shale.

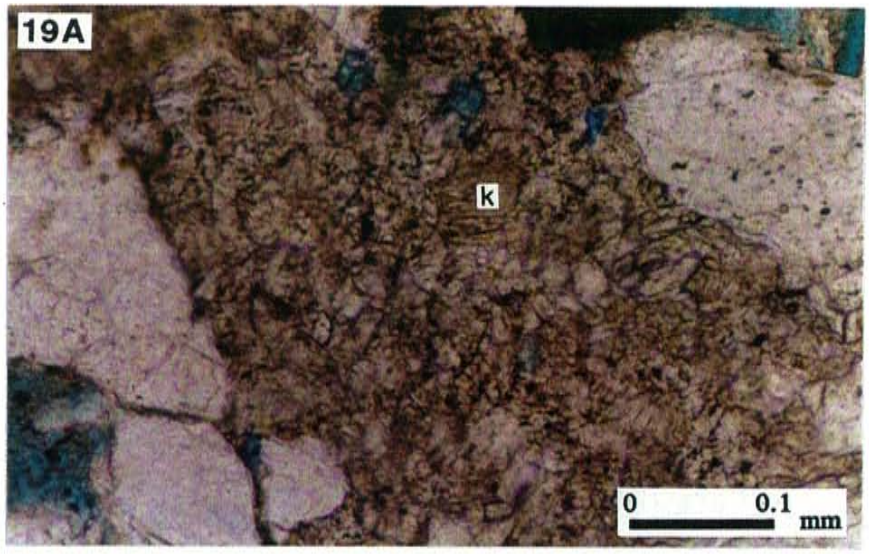
19A
k
0
0.1
mm

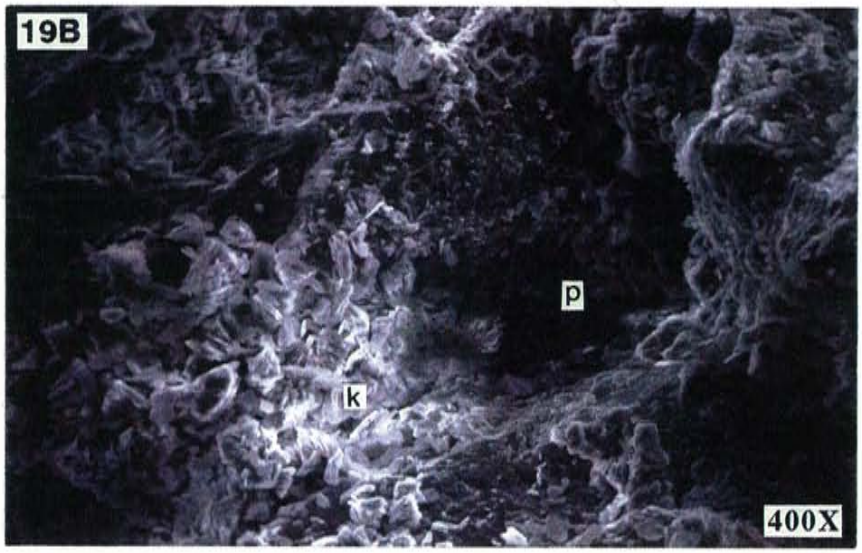
19B
p
k
400X

Occasionally kaolinite surrounds but does not fill dissolution pores within framework-grains (Fig. 18D).

Kaolinite ranges from absent to 3.5% (ave. = 0.6%) in the deep subsurface core and 0.1 to 7.1% (ave. = 1.7%) in shallow subsurface core (Appendices 6 and 7). The greater volume in the outcrop may be due to subsequent feldspar dissolution during outcrop weathering.

Fracturing

Vertical fractures cut through ferroan calcite cement, glauconite, mud drapes, and framework-grains and commonly span the entire length of thin sections (Figs. 16A,B). In the deep subsurface, these fractures have not been filled by authigenic minerals. In the Hogback oil field outcrop and shallow subsurface core, however, nonferroan calcite cement fills the fractures. This relationship brackets fracturing to a period after ferroan calcite cementation (which was probably before Late Oligocene oil generation) and before nonferroan calcite cementation (which occurred prior to outcrop exposure).

Oil emplacement

The timing for hydrocarbon migration into the Tocito Sandstone could not be determined petrographically. No oil was found in thin sections from the deep reservoir cores (Cha Cha, Horseshoe, Totah, and Gallegos). It is probable that solvent extractions were performed in a service company's lab, thus removing the oil prior to thin section preparation. Oil residue or staining was not positively identified in outcrop thin sections. It is likely that oil in the outcrop had volatilized or biodegraded. However, traces of bitumen were extracted from the shallow HOF #2 core using toluene (Fig. 20). The residue exceeded the measuring capability of the chromatograph (maximum limit of C_5).


20
22'
23'
32'

The organic-rich Lower Mancos Shale entered the "oil window" during the Late Oligocene (Fig. 9). Kerogen maturation in the shale and oil migration into the Tocito Sandstone reservoirs probably occurred during the Late Oligocene or Early Miocene.

Hematite and gypsum

Tocito Sandstone outcrops in the Hogback oil field and along the Chaco River contain hematite crystals (Fig. 21A) and localized hematite cement. Gypsum is common in mudstone units and in fractures and pores of interbedded sandstones (Figs. 21A,B).

There is an average of 2% pyrite in the Tocito Sandstone reservoirs and only 1% in the Tocito outcrop, whereas hematite exists only in outcrop. These observations suggest that hematite is the result of pre-existing pyrite reacting with oxygenated meteoric water during outcrop weathering. Sulfate released during pyrite oxidation may have been consumed during gypsum precipitation.

Isotopic Measurements

The two calcite cements identified in the Tocito Sandstone outcrop and shallow core have different isotopic values (Fig. 22, Appendix 9). Cements dominated by ferroan calcite (estimated 75% ferroan) have $\delta^{13}C$ values that range from -3.9 to -3.5‰ PDB ("Peedee belemnite" isotope standard) and $\delta^{18}O$ values that range from -15.6 to -14.8‰ PDB [14.8 to 15.5‰ SMOW (Standard Mean Ocean Water)]. Cements rich in nonferroan calcite (estimated 75-100% nonferroan) have $\delta^{13}C$ values ranging from -5.1 to -4.1‰ PDB and $\delta^{18}O$ values ranging from -14.0 to -10.1‰ PDB (16.5 to 20.5‰ SMOW). Minor differences in isotopic values for ferroan calcite-rich cements may be due to inaccuracies in visually-estimated ferroan-nonferroan calcite ratios or minor zonations in the cement due to variability in the isotopic composition of the pore waters. Estimates of $\delta^{13}C$ endmember compositions are -3.3‰ PDB for ferroan calcite and -

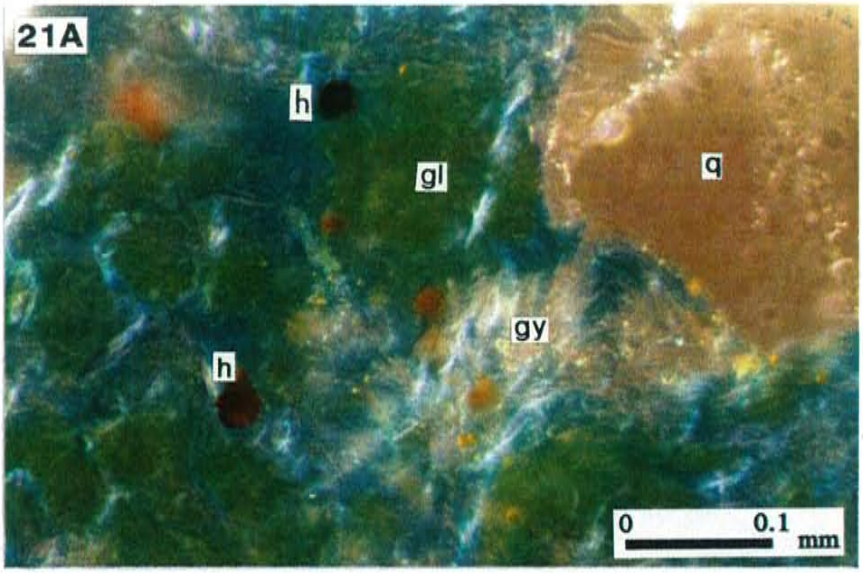
21A
h
gl
q
gy
h
0
0.1
mm


21B
g
o
f
1200X

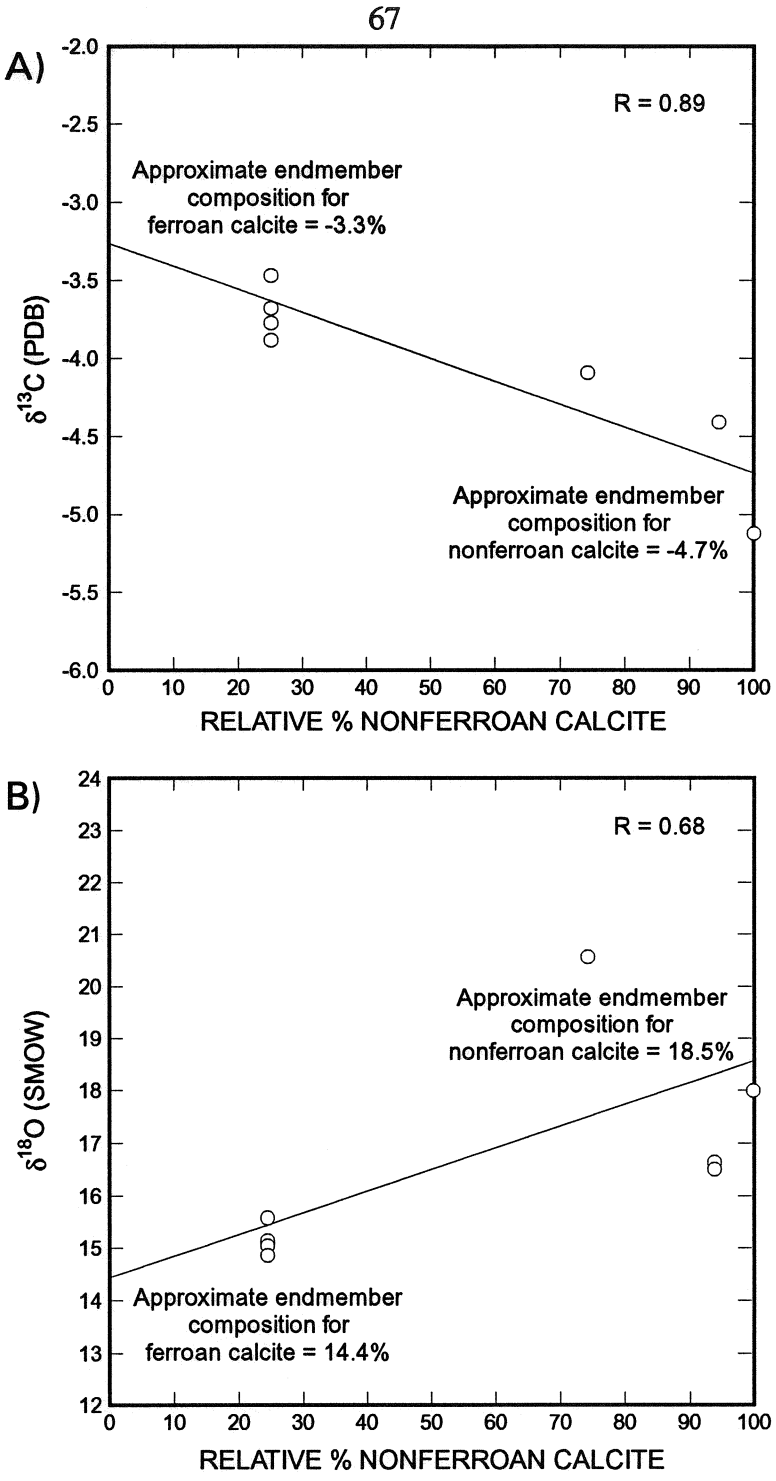

Figure 22 - A) Plot of $\delta^{13}C$ calcite against proportion of nonferroan calcite (versus ferroan calcite) in the sample. B) Plot of $\delta^{18}O$ calcite against proportion of nonferroan calcite (versus ferroan calcite) in the sample. Approximate percentages of ferroan and nonferroan calcite were estimated with calcite stain and cathodoluminescence (Appendix 8). Isotopic data from Appendix 9.

4.7‰ PDB for nonferroan calcite (Fig. 22A). Estimates of $\delta^{18}O$ endmember compositions are 14.4‰ SMOW for ferroan calcite and 18.5‰ SMOW for nonferroan calcite (Fig. 22B).

$\delta^{13}C$ values

The $\delta^{13}C$ values for ferroan calcite-rich cements (Fig. 22A) are slightly depleted in $\delta^{13}C$ with respect to seawater. This implies that the water from which the calcite precipitated had a contribution of carbon derived either from microbial decomposition of organic material at depths less than 150 meters, or from thermocatalytic decarboxylation of organic matter at depths exceeding 500 meters (Hennessy and Knauth, 1985). Ferroan calcite precipitated after pyrite (Fig. 11), so the cement probably did not precipitate while the sediments were in the sulfate reduction zone (commonly < 100 m depth). The earliest the cement could have formed was when the sediment passed through the upper portion of the microbial methane production zone (100-150 meters depth), because lower in the methane production zone the carbon is isotopically heavy (Hennessy and Knauth, 1985).

Nonferroan calcite-rich cements are ^{13}C-depleted with respect to ferroan calcite-rich cements (Fig. 22A). This indicates that the nonferroan calcite precipitated from pore waters that had become increasingly ^{13}C-depleted over time. The shift in isotopic composition of the waters may have been achieved by mixing the original formation water with expelled shale waters that have $\delta^{13}C$-depleted carbon from thermocatalytic decarboxylation of organic matter at greater depths, or meteoric waters with $\delta^{13}C$-depleted carbon from microbial oxidation and sulfate reduction at shallower depths.

$\delta^{18}O$ values

The $\delta^{18}O$ values for cements dominated by ferroan calcite form a relatively tight cluster of points that are isotopically lighter than the scattered $\delta^{18}O$ values of nonferroan calcite-rich cements (Fig. 22B). The fact that $\delta^{18}O$ values for ferroan calcite-rich cement are significantly more clustered than those of nonferroan calcite-rich cements suggests that either precipitation temperatures fluctuated during nonferroan calcite precipitation or isotopic conditions in the pore waters evolved over time from a relatively homogeneous fluid to an isotopically heterogeneous brine.

Petrographic evidence indicates that ferroan calcite precipitated during moderate to deep burial of the Tocito Sandstone (Fig. 11). To determine the isotopic composition of the pore waters during calcite precipitation, $\delta^{18}O$ values for pore waters were plotted against the range of temperatures in which calcite may have precipitated (Fig. 23). If ferroan calcite precipitated from unaltered seawater trapped during deposition, unrealistically high precipitation temperatures (exceeding 100°C) are required (Fig. 23); even assuming a pre-glacial Cretaceous seawater value of -1.2‰ (Shackleton and Kennett, 1975). If ferroan calcite precipitated at 80° to 100°C, then the pore water had to have a $\delta^{18}O$ value of -4.9 to -2.7‰ SMOW.

There are several possible causes of the observed low isotopic values: 1) mixing between original marine water and intruding ^{18}O-depleted meteoric water (Hudson, 1978; Boles et al., 1985; Bjørlykke, 1988; Mozley and Burns, 1993), 2) water/sediment interaction and the precipitation of volumetrically significant minerals such as glauconite, ankerite, and siderite, which may lower the pore-water oxygen values through a Rayleigh fractionation process (Lawrence and Gieskes, 1981; Mozley and Carothers, 1992; Mozley and Burns, 1993), and 3) calcite recrystallization at higher temperatures (Mozley and Carothers, 1992; Mozley and Burns, 1993). Although it is difficult to rule out any

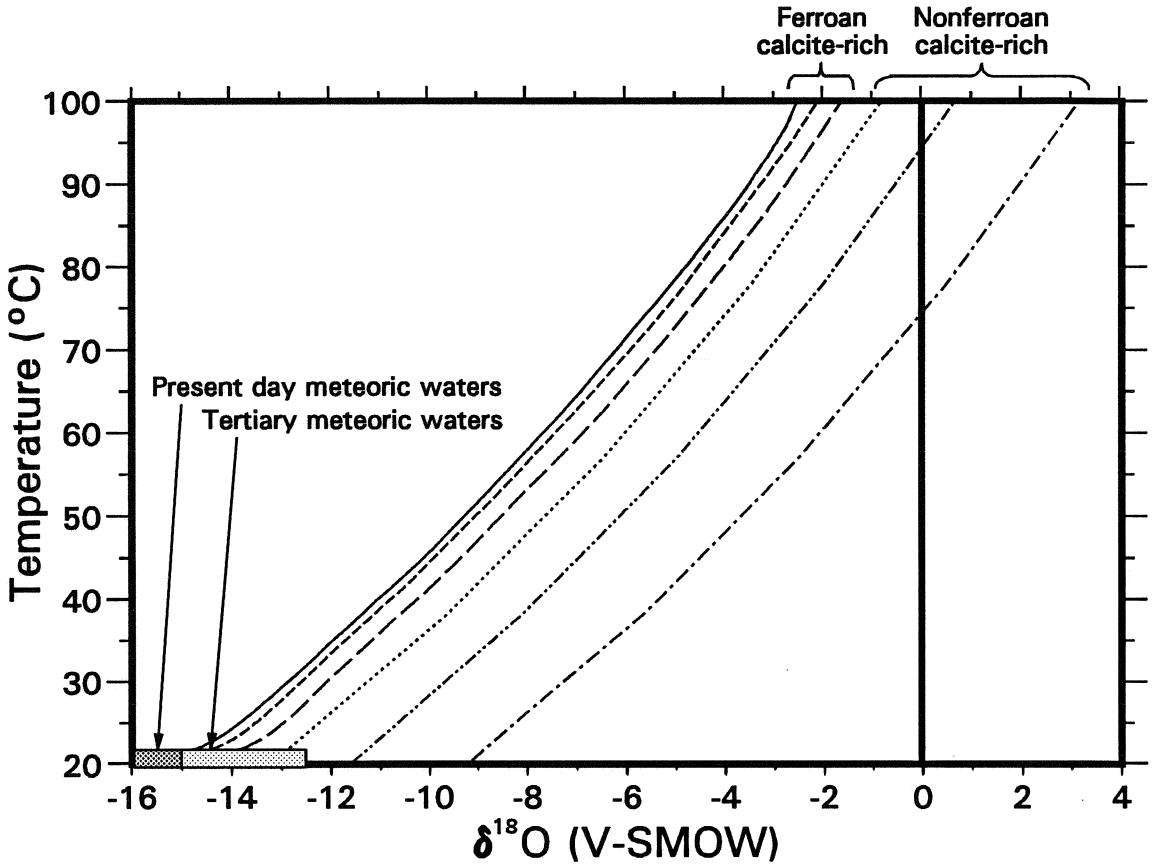

Ferroan Calcite Cement	Nonferroan Calcite Cement
Tocito #3D – – – – – – – – – – –	Tocito #2D ·····-·····-·····
Tocito #15 ————————	Tocito #11 -·-·-·-·-·-·-·-·-·-
Tocito #18 ----------	Tocito #30 ·····

Figure 23 - Plot of $\delta^{18}O$ vs. precipitation temperatures for ferroan calcite-rich cement and nonferroan calcite-rich cement from the "upper" Tocito Sandstone cropping out in the Hogback oil field. Calcite $\delta^{18}O$ values were calculated using the calcite-water fractionation of Friedman and O'Neill (1977). A maximum possible precipitation temperature of 100°C was obtained from the burial history curve (Fig. 9) and a minimum temperature of 10° C is representative of average marine bottom waters. Isotopic values for Tertiary and present day meteoric waters were calculated from Sheppard's (1986) generalized δD (deuterium) contour maps for North America ($\delta D = 8\delta^{18}O + 10$; Sheppard, 1986).

of the above causes, the simplest explanation is the mixing of the original marine formation water with ^{18}O-depleted meteoric water.

Nonferroan calcite-rich cements are isotopically heavier than cements dominated by ferroan calcite (Fig. 22B). Such a shift in isotopic composition may be due to nonferroan calcite precipitation from the same pore waters at lower temperatures, from ^{18}O-enriched waters at anomalously high temperatures, or from ^{18}O-depleted waters at very low temperatures (Fig. 23). Because nonferroan calcite is present only in outcrop, and petrographic evidence suggests it was a late diagenetic phase (Fig. 11), nonferroan calcite is believed to have precipitated during regional uplift. The burial history curve (Fig. 9) demonstrates that formation temperatures decreased during uplift, so it is likely that the relative ^{18}O enrichment of the nonferroan calcite is the result of precipitation at lower temperatures.

If during regional uplift, non-ferroan calcite precipitated at lower temperatures around 20° to 40°C (Fig. 9), then $\delta^{18}O$ values of the pore water would be -13.0 to -5.5‰ SMOW. Longstaffe (1984) suggested that calcite cement ($\delta^{18}O$ = 19.3‰ SMOW) in the Cretaceous Milk River Gas Pool, Alberta, precipitated at 15-20°C from a mixture of evolved sea water and meteoric water. Such water mixtures are typical for other Cretaceous oil and gas fields in the Alberta Basin (Longstaffe, 1984).

In summary, ferroan calcite precipitated during burial under relatively invariant water chemistries and temperature. The formation water was a mixture of trapped seawater and ^{18}O-depleted meteoric water that had incorporated isotopically-light carbon from organic matter degradation. Nonferroan calcite precipitated at lower temperatures during regional uplift. The water from which it precipitated may have been mixed with additional ^{18}O- and ^{13}C-depleted meteoric water.

Permeability Measurements

Large-scale Permeability Grids at Hogback Oil Field Outcrop

Grid #1

Permeability grid #1 (Fig. 24, Appendices 10 and 11) is a 1.2 m (2.7 ft) by 0.6 m (2.0 ft) grid (25 permeability measurements) in interbedded sandstone and mudstone lithofacies in the "upper" Tocito Sandstone outcrop, Hogback oil field (Fig. 8). The overall permeability trend shows three horizontal zones with average permeabilities increasing towards the base. The first row of measurements has permeability values less than 0.5 darcies for most of the hard, weathering-resistant sandstone. Rows two and three have moderate permeabilities (ave. = 3.2 darcies) among thin (up to 3 cm thick), moderately friable sandstone and mudstone interbeds. In the last two rows of data, high permeabilities (ave. = 4.5 darcies) were measured for sandstone beds that are equally as friable, but thicker (up to 10 cm) than those in the center of the grid.

Grid #2

Permeability grid #2 (Fig. 25, Appendices 10 and 11) is a 1.2 m (2.7 ft) by 0.3 m (1.0 ft) grid (15 permeability measurements) in interbedded sandstone and shale lithofacies, "upper" Tocito Sandstone outcrop at Hogback oil field (Fig. 8). A central row of moderate permeabilities (ave. = 1.8 darcies) contains thinly (<5 cm) interbedded sandstone and mudstone layers. Permeability values from the central row are sandwiched between upper and lower rows with permeabilities averaging 3.9 darcies. These higher permeabilities correspond with thicker (>10 cm) sandstone beds.

Grid #3

Permeability grid #3 (Fig. 26, Appendices 10 and 11) is a 1.2 m (2.7 ft) by 0.75 m (2.5 ft) grid (30 measurements) in muddy bioturbated sandstone lithofacies in the

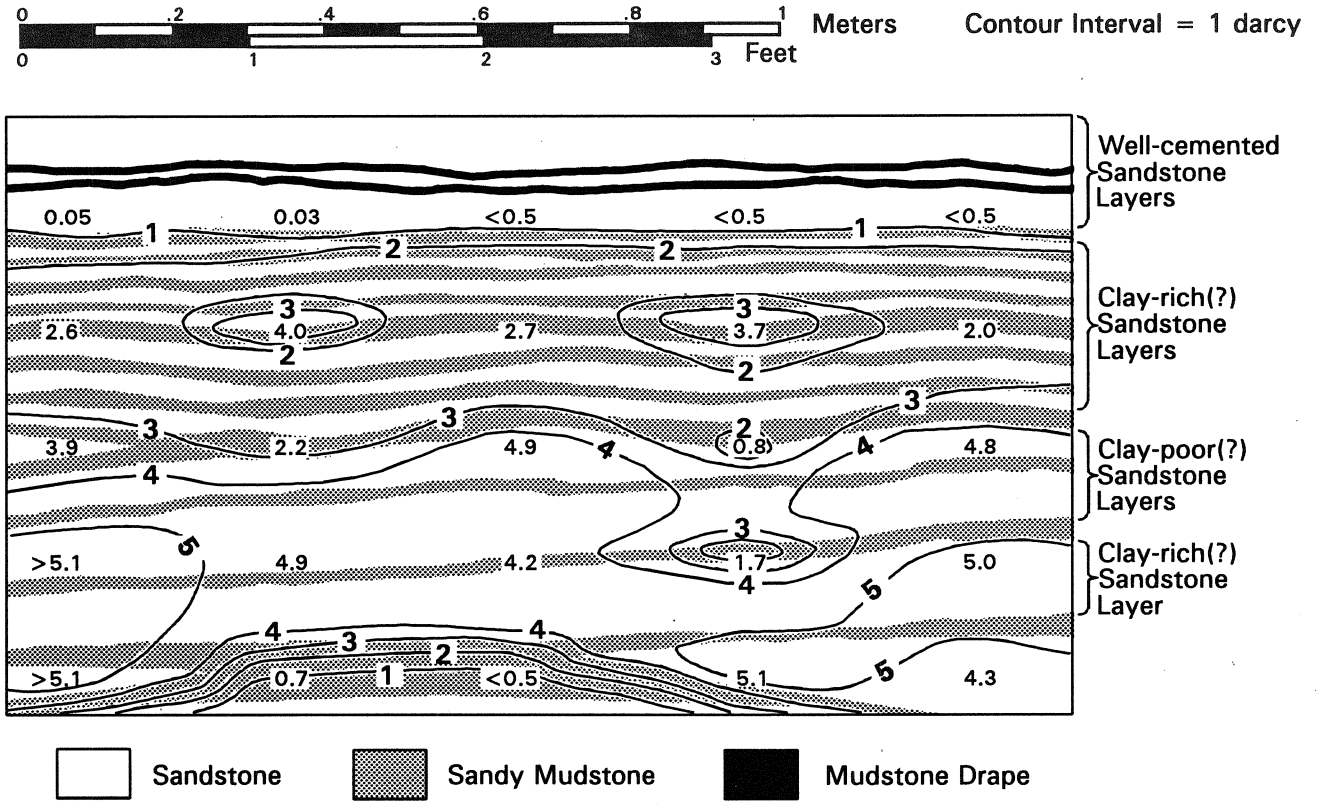

Figure 24 - Permeability grid #1 in an interbedded sandstone and mudstone unit of the "upper" Tocito Sandstone cropping out in the Hogback oil field, San Juan Basin, northwest New Mexico. Location of measurement is the permeability value's decimal point. Grid is approximately perpendicular to the paleocurrent direction. Geostatistics given in Appendix 11.

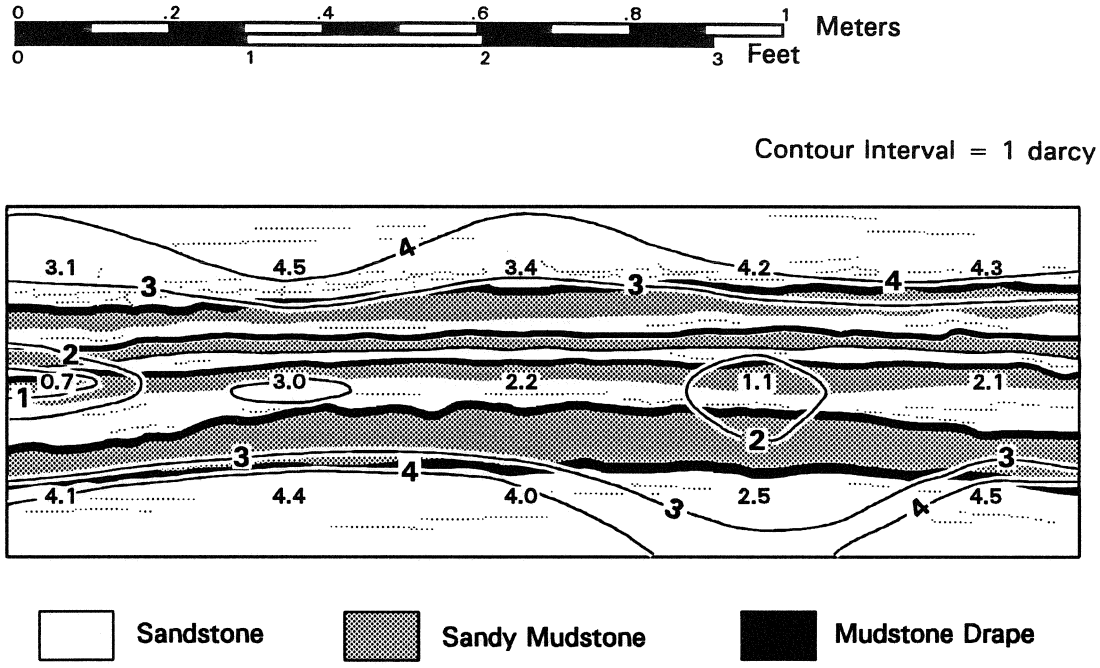

Figure 25 - Permeability grid #2 in an interbedded sandstone and mudstone unit of the "upper" Tocito Sandstone cropping out in the Hogback oil field, San Juan Basin, northwest New Mexico. Location of measurement is the permeability value's decimal point. Grid is approximately perpendicular to paleocurrent flow direction. Geostatistics given in Appendix 11.

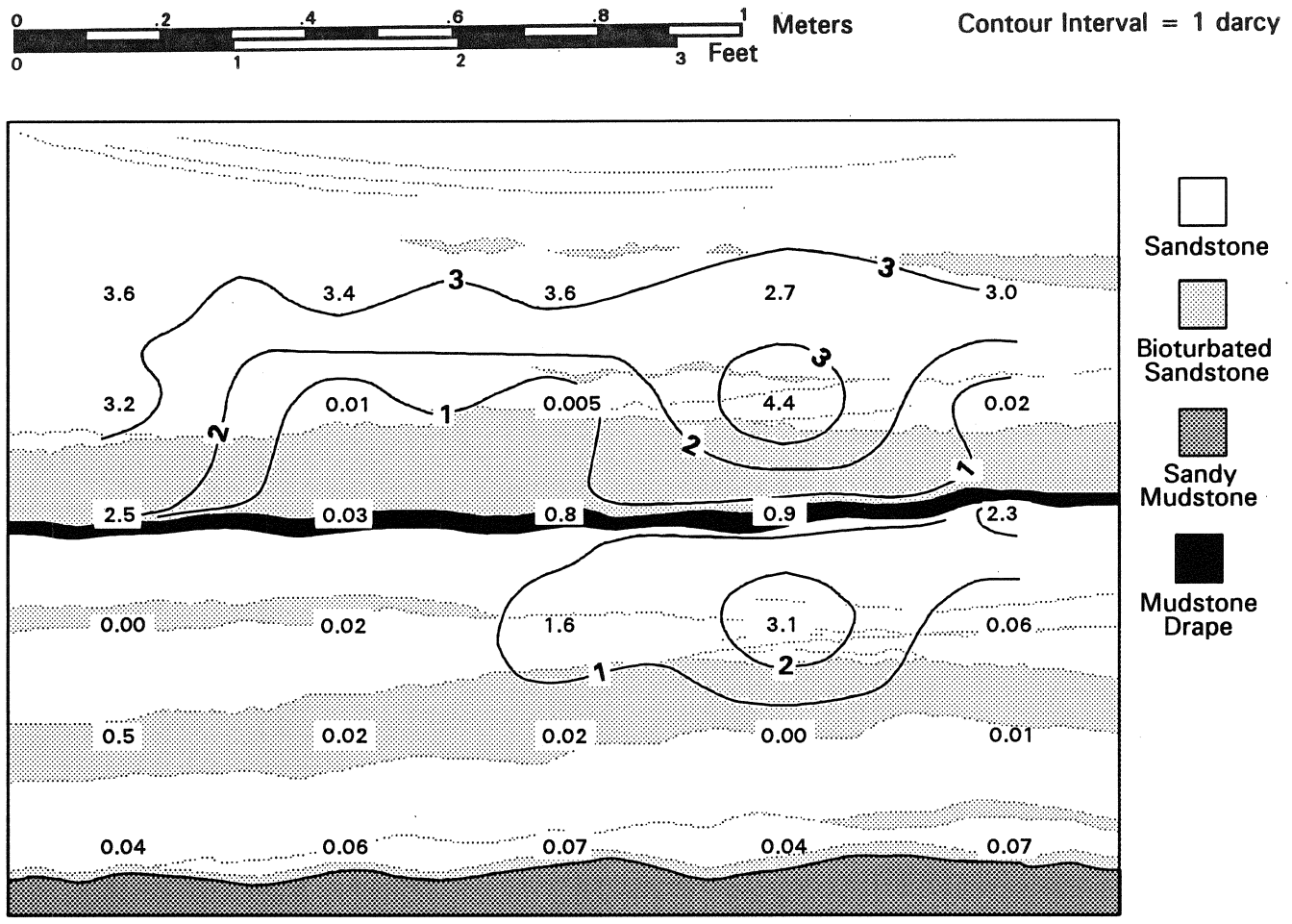

Figure 26 - Permeability grid #3 in muddy, bioturbated sandstone at the base of the "upper" Tocito outcropping in the Hogback oil field, San Juan Basin, northwest New Mexico. Measurement location is the permeability value's decimal point. Grid is approximately perpendicular to the paleocurrent flow direction. Geostatistics given in Appendix 11.

"upper" Tocito Sandstone (Fig. 8). The overall trend is one of sandstone permeability increasing upward. A mudstone drape splits the grid into an upper and lower half. The lower half is characterized by low permeability (ave. = 0.07 darcies), but has a localized lens of moderate permeability (ave. = 2.3 darcies). The upper half of the grid has an average permeability that increases from 1.3 darcies just above the mudstone drape to 3.3 darcies near the top of the grid.

Grid #4

Permeability grid #4 (Fig. 27, Appendices 10 and 11) is a 1.2 m (2.7 ft) by 0.6 m (2.0 ft) grid (25 measurements) in the phosphatic nodular mudstone unit between the "upper" and "lower" Tocito Sandstones at Hogback field (Fig. 8). Permeability values for the mudstone average 0.05 darcies. Siltstone stringers and silt-filled burrows within mudstone average 0.5 darcies, but the siltstone stringers are commonly only a few tens of centimeters long and the burrows are no longer than 10 cm.

Grid #5

Permeability grid #5 (Fig. 28, Appendices 10 and 11) is a 1.2 m (2.7 ft) by 0.3 m (1.0 ft) grid (18 measurements) in ripple cross-laminated sandstone in the "lower" Tocito Sandstone (Fig. 8). Overall sandstone permeability increases downward. However, the sandstone was highly weathered and the permeability trends reflected in the grid may not be representative of unweathered ripple cross-laminated sandstones.

Grid #6

Permeability grid #6 (Fig. 29, Appendices 10 and 11) is a 10m (33 ft) by 0.3 m (1.0 ft) grid (14 measurements) in ripple cross-laminated sandstone lithofacies in the "lower" Tocito Sandstone outcrop (Fig. 8). Permeability values are generally low, averaging 0.6 darcies and ranging from 0.01 to 1.2 darcies. The overall permeability pattern appears

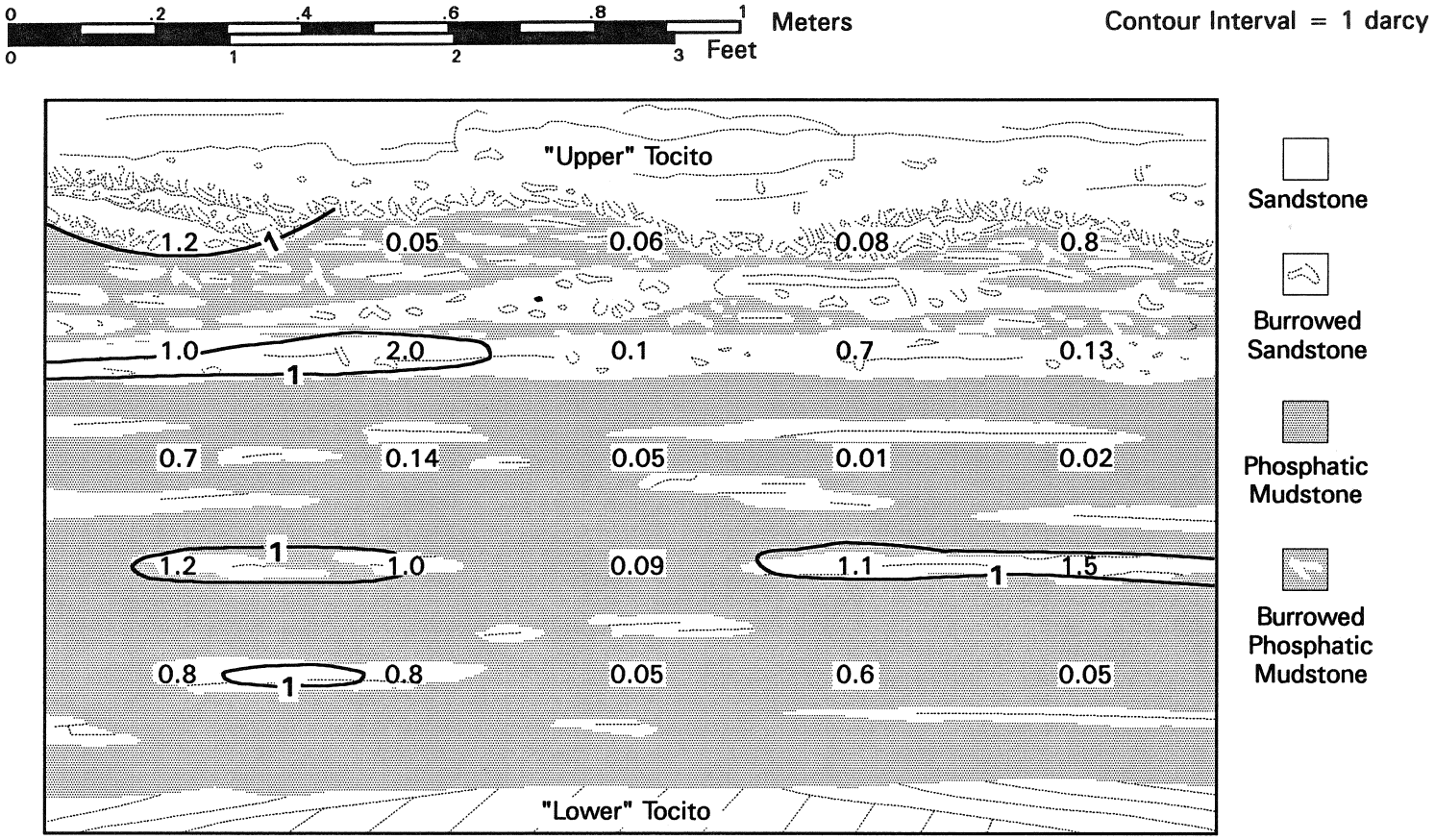

Figure 27 - Permeability grid #4 in the phosphatic nodular mudstone sandwiched between the "upper" and "lower" Tocito Sandstones cropping out in the Hogback oil field, San Juan Basin, northwest New Mexico. Measurement location is the permeability value's decimal point. Grid is approximately perpendicular to the paleocurrent flow direction. Geostatistics given in Appendix 11.

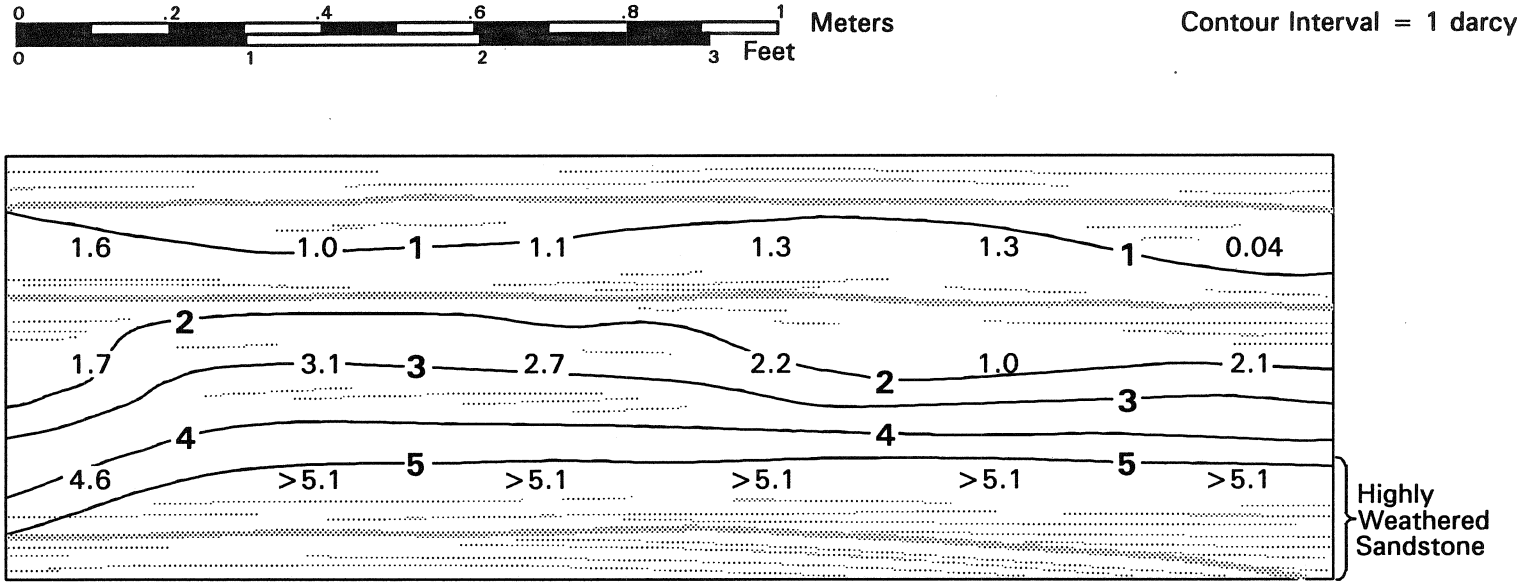

Figure 28 - Permeability grid #5 in ripple cross-laminated sandstone near the top of the "lower" Tocito Sandstone cropping out in the Hogback oil field, San Juan Basin, northwest New Mexico. Measurement location is the permeability value's decimal point. Grid is approximately perpendicular to the paleocurrent flow direction. Geostatistics given in Appendix 11.

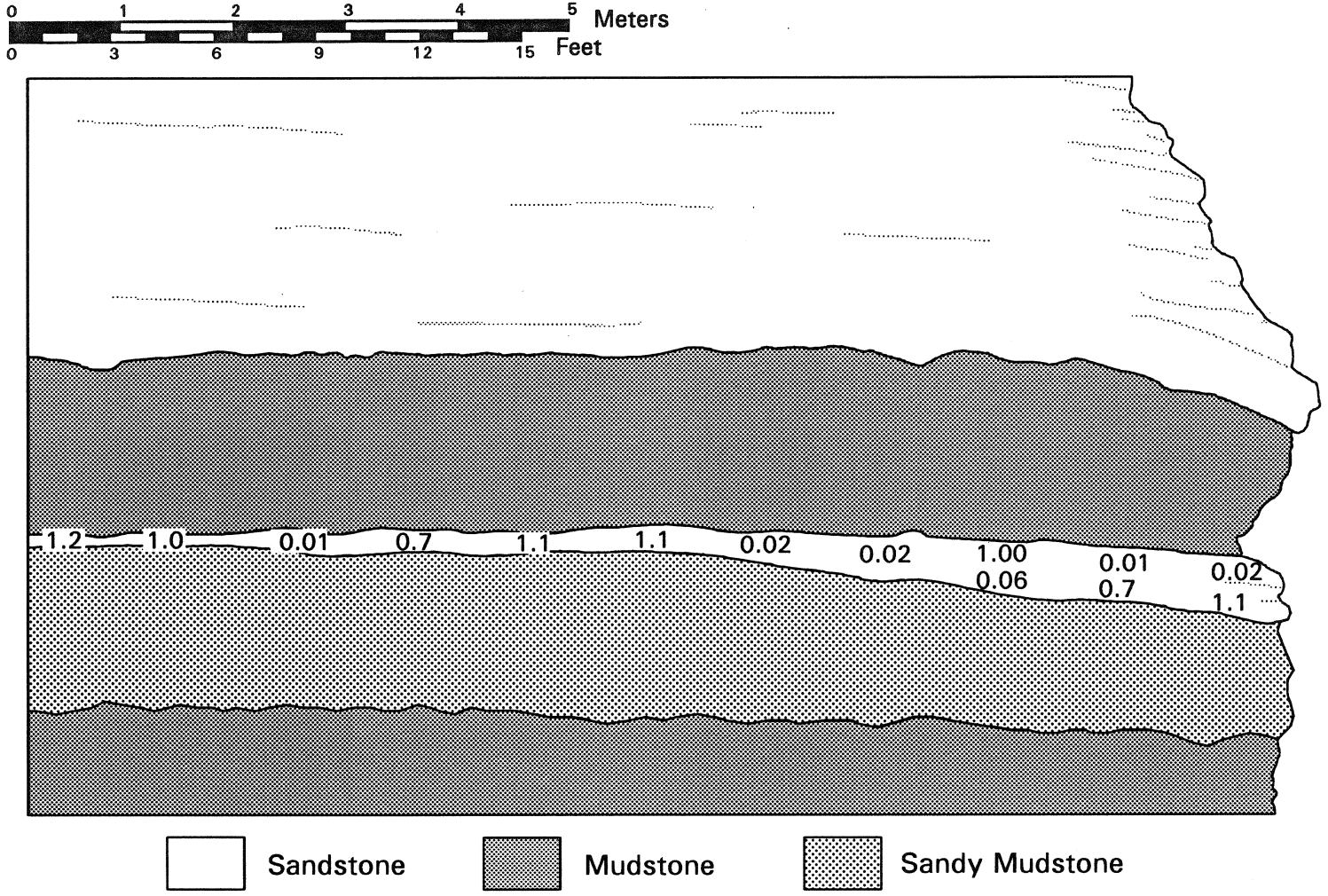

Figure 29 - Permeability grid #6 in the ripple cross-laminated sandstone of the "lower" Tocito exposed in the Hogback oil field, San Juan Basin, northwest New Mexico. Permeability measurements are in darcies. Measurement location is the permeability value's decimal point. Grid is approximately perpendicular to the paleocurrent flow direction. Geostatistics given in Appendix 11.

random at this scale of measurement. The entire sandstone unit is resistant to weathering.

Grid #7

Permeability grid #7 (Fig. 30, Appendices 10 and 11) is a 0.9 m (2.9 ft) by 1.0 m (3.3 ft) grid (100 measurements) from a large-scale cross-bedded sandstone lithofacies in the "lower" Tocito Sandstone (Fig. 8). The grid is oriented approximately parallel with the southeast-trending (about 120-140° azimuth; Nummedal et al., 1989) paleocurrent. Two relatively impermeable mudstone drapes divide the grid into three sandstone sections. Below the sandstone interval is a thinly interbedded sandstone and mudstone section. The middle sandstone section has a bull's-eye-like contour pattern in which permeability increases toward the center. The lower (and thickest) sandstone section is characterized by low permeabilities (1.0 darcies) near the base, high permeabilities (>5 darcies) in the center, and moderately high permeabilities (4.0 darcies) at the top. The thinly interbedded sandstone and mudstone section has an overall permeability of 1.2 darcies. The thin sandstone layers have low permeabilities and are resistant to weathering.

Grid #8

Permeability grid #8 (Fig. 31, Appendices 10 and 11) is approximately 3.3 m (10.8 ft) by 0.6 m (2.0 ft) (56 measurements) and wraps around a three-dimensional exposure of the large-scale cross-bedded sandstone lithofacies from the "lower" Tocito Sandstone outcrop (Fig. 8). The rows of permeability measurements are parallel to cross-strata foresets (more specifically, the line of intersection between the plane of the foresets and the outcrop surface). The average permeability is 3.2 darcies and generally increases upward from 1.5 darcies to 4.3 darcies. There is a weak trend in which permeability

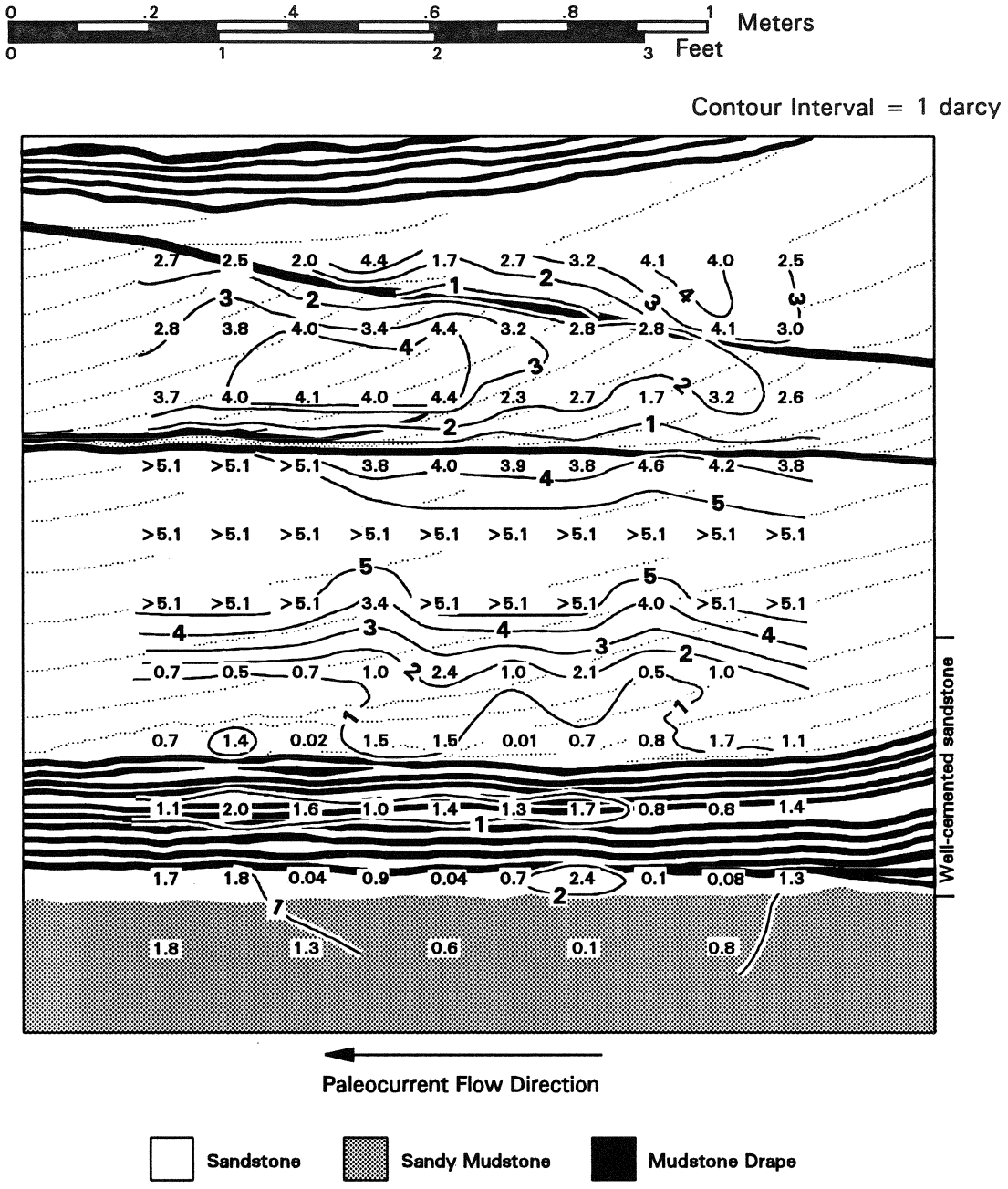

Figure 30 - Permeability grid #7 in the larger-scale cross-bedded sandstone unit of the "lower" Tocito Sandstone cropping out in the Hogback oil field, San Juan Basin, northwest New Mexico. Grid is oriented approximately parallel with the paleocurrent flow direction. Measurement location is the permeability value's decimal point. Geostatistics given in Appendix 11.

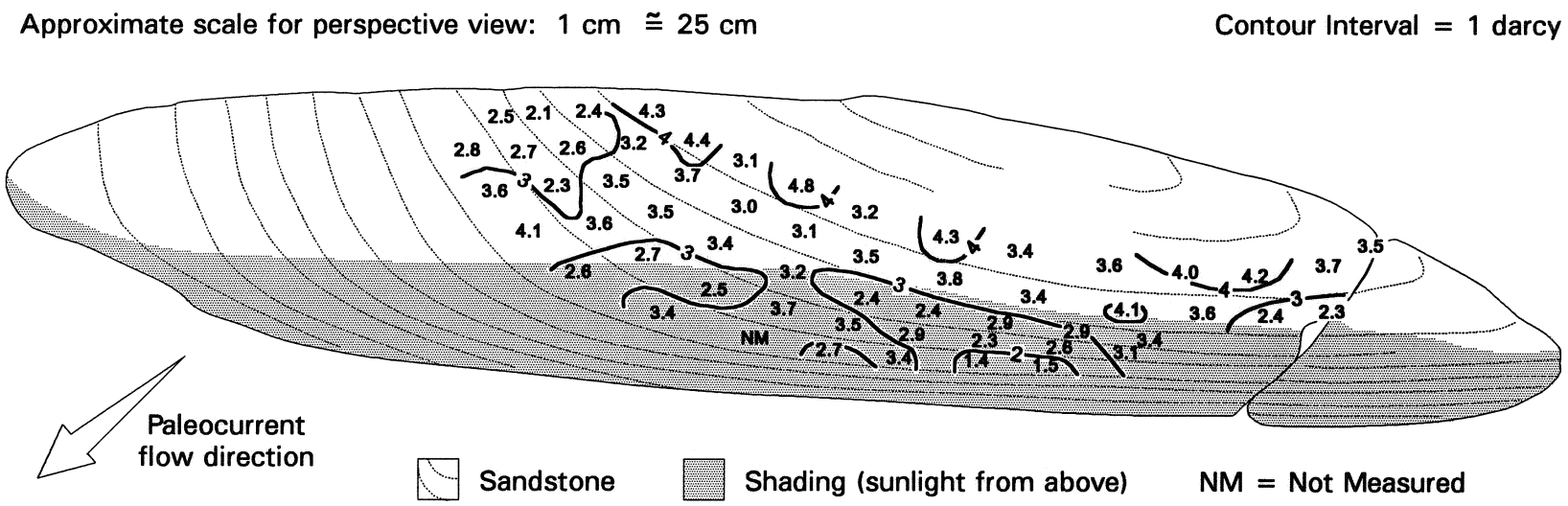

Figure 31 - Perspective view of Grid #8 on a three-dimensional exposure of the large-scale cross-bedded sandstone lithofacies in the "lower" Tocito Sandstone cropping out in the Hogback oil field. Shading has been added to distinguish those measurement sites that are on the underside of the outcrop. Rows of permeability measurements follow the trace of the foresets along the surface of the outcrop (traces are approximately perpendicular to the plane of the foresets). Spacing between measurements was 30 cm parallel to foresets and 15 cm perpendicular to foresets. Location of measurement is the permeability value's decimal point. Geostatistics given in Appendix 11.

contours are subparallel to the foresets. The sandstone unit is moderately friable and somewhat resistant to weathering.

Grid #9

Permeability grid #9 (Fig. 32, Appendices 10 and 11) is a 1.5 m (4.9 ft) by 1.2 m (3.9 ft) grid (113 measurements) in the large-scale cross-bedded sandstone lithofacies from the "lower" Tocito Sandstone (Fig. 8). The grid is oriented approximately perpendicular to the southeast-trending (120-140° azimuth; Nummedal et al., 1989) paleocurrent. Permeability increases upward from 3.2 darcies to 4.7 darcies and is reduced to 1 darcy directly below the thick mudstone drape at the top of the grid. Permeability contours frequently cross foresets and locally form bull's-eye-like patterns.

Large-scale Permeability Grids Along the Chaco River Outcrop

Grids #10, #12 and #13

Permeability grids #10, #12, and #13 (Fig. 33, Appendices 10 and 11) are 1.2 m (3.9 ft) by 1.5 (4.9 ft) grids (33, 43, and 28 measurements respectively) with rows of measurements parallel to foresets of large-scale cross-bedded sandstone lithofacies or (in the case of grid #12) reactivation surfaces. The general trend in the three grids is that permeability contours follow the foreset inclination. In addition, permeabilities in grids #10 and #13 tend to be lower at the base of the sandstone bed (1.3 darcies) and higher near the top (3.6 darcies). In grid #12, a zone of high permeability (4.0-5.0+ darcies) exists in the center of the unit, parallel to the reactivation surfaces.

Grids #11 and #14

Permeability grid #11 (Fig. 33, Appendices 10 and 11) is a horizontal 2.7 m (8.9 ft) by 0.3 m (1.0 ft) grid (20 measurements) on a moderately friable, thin, tabular sandstone bed with very thin muddy laminae and local burrows. Permeability is

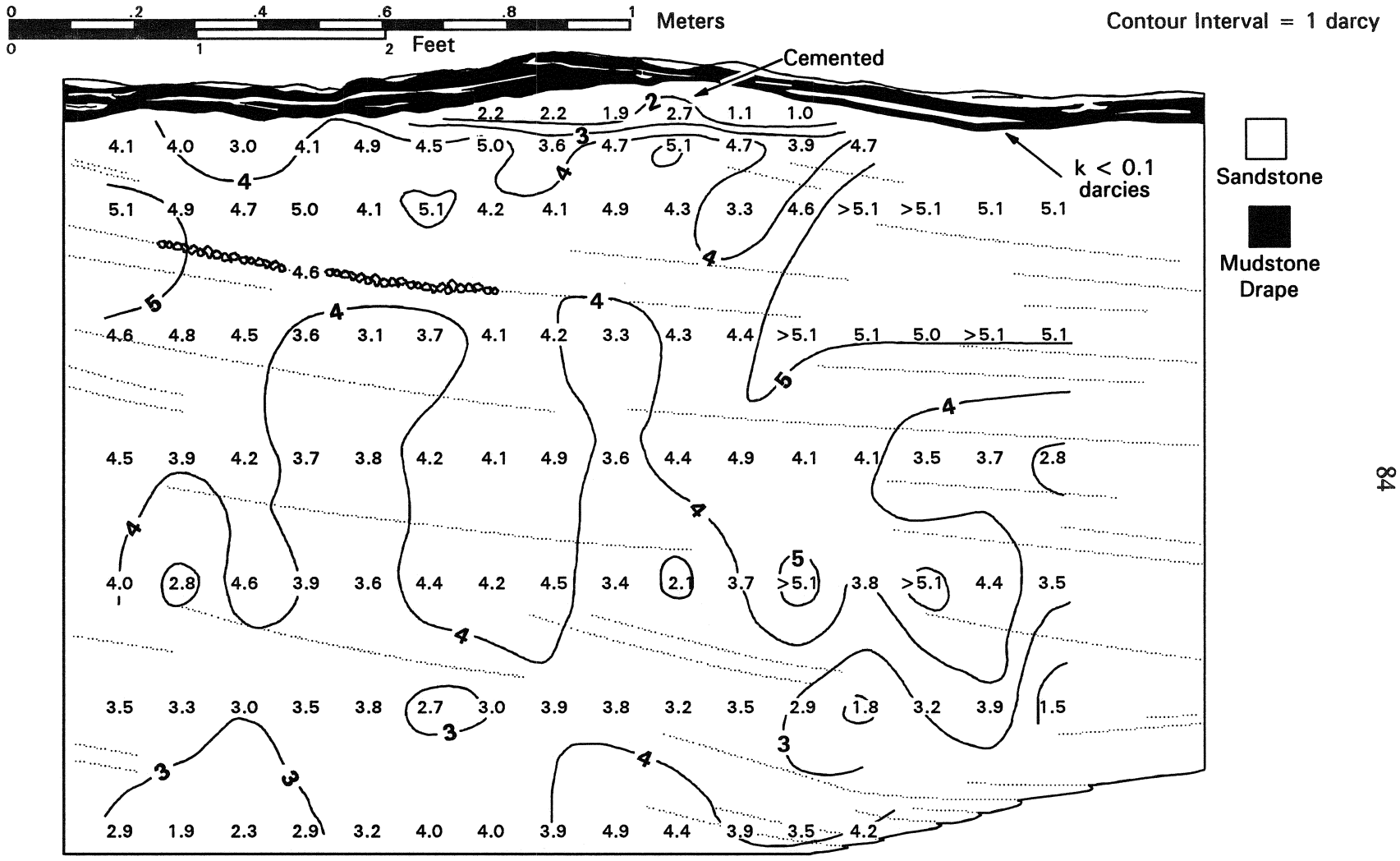

Figure 32 - Permeability grid # 9 in the large-scale cross-bedded sandstone unit of the "lower" Tocito Sandstone cropping out in the Hogback oil field, San Juan Basin, northwest New Mexico. Orientation of grid is oblique to the paleocurrent flow direction. Measurement location is the permeability value's decimal point. Geostatistics given in Appendix 11.

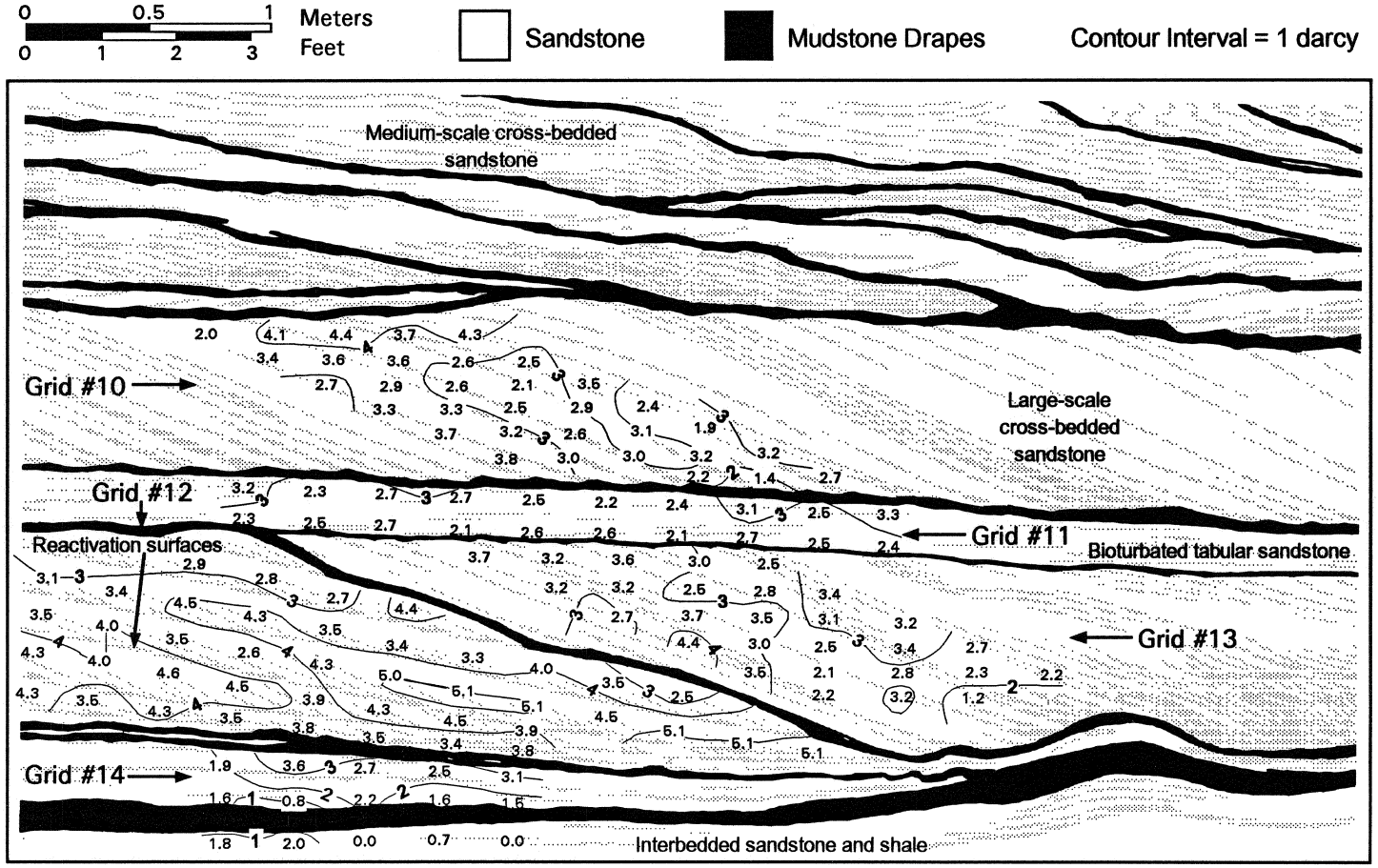

Figure 33 - Permeability grids #10 through #14 on Tocito Sandstone cropping out along the Chaco River. Location of measurement is the permeability value's decimal point. Geostatistics given in Appendix 11.

generally homogeneous (ave. = 2.6 darcies), with relatively higher values near the top of the grid.

Permeability grid #14 (Fig. 33, Appendices 10 and 11) is a 1.2 m (3.9 ft) by 0.4 m (1.3 ft) grid (15 measurements) in interbedded sandstone and mudstone lithofacies directly below the sandstone unit with the reactivation surfaces. It is characterized by horizontal zones of permeability that increase upward from <1 darcy to 3.6 darcies.

Grid #15

Grid #15 (Fig. 34, Appendices 10 and 11) contains a set of 20 measurements on large-scale overturned foresets in cross-bedded sandstone lithofacies. Average permeability is 4.0 darcies. The overall trend consists of a high permeability zone (>4 darcies) that encircles a lower permeability zone (<4 darcies) that bends in much the same way the foresets have deformed by overturning.

Grids #16 and #17

Grids #16 and #17 (Fig. 34, Appendices 10 and 11) are 0.6 m (2.0 ft) by 0.6 m (2.0 ft) grids (9 measurements each) positioned on large-scale cross-bedded sandstone lithofacies outcrop. The primary purpose for these grids was to compare their permeability values to those of the same beds shown in Fig. 33. Average permeability values are significantly greater in grid #16 (3.5 darcies) than in grid #10 (3.0 darcies); whereas the average permeability is notably less in grid #17 (2.6 darcies) than in grid #13 (3.0 darcies).

Grid #18

Permeability grid #18 (Fig. 35, Appendices 10 and 11) is a 1.2 m (3.9 ft) by 2.3 m (7.4 ft) grid (79 measurements) inclined so that its rows are parallel with the foresets of cross-bedded sandstone lithofacies. Average permeability for the grid is 3.41 darcies.

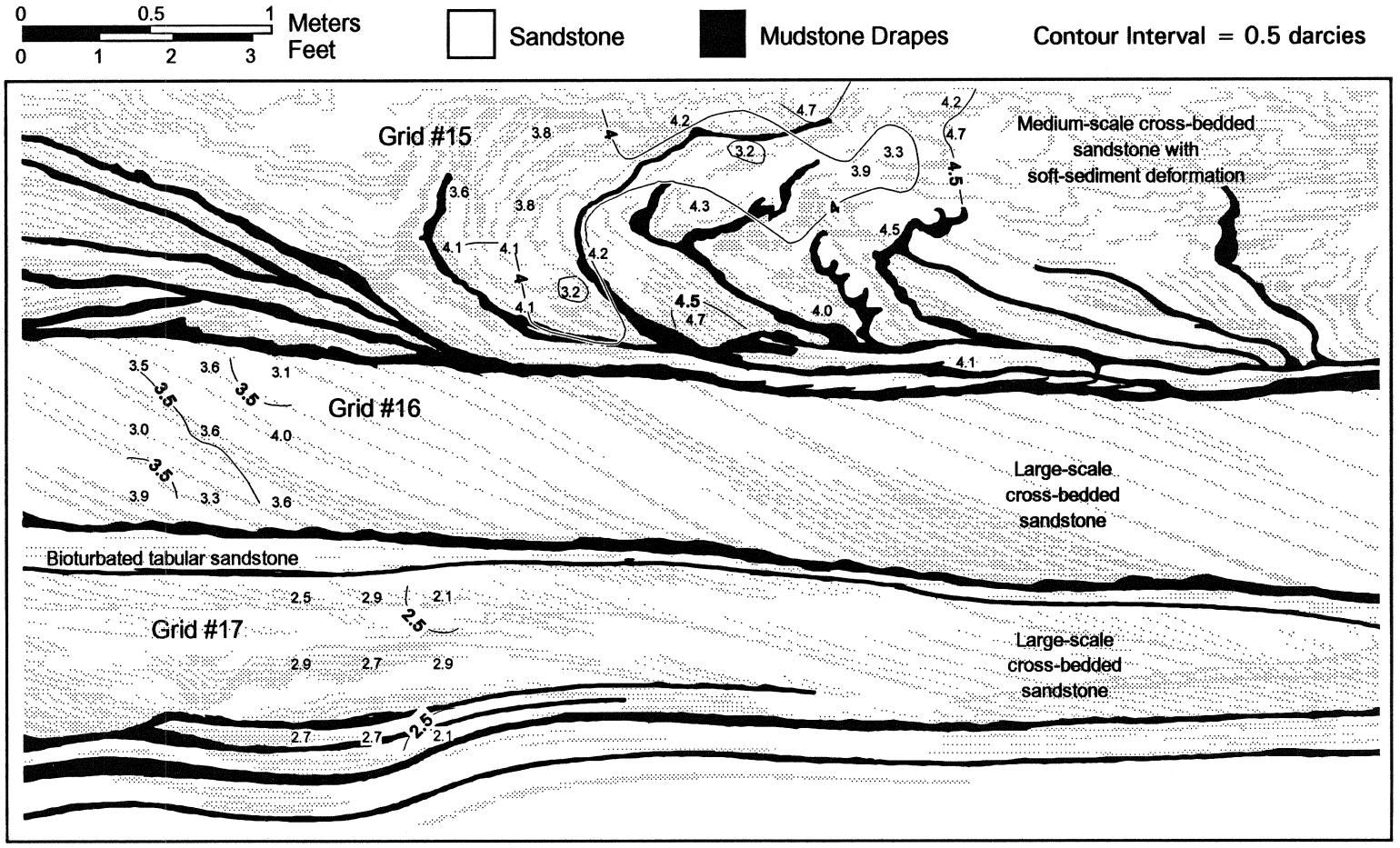

Figure 34 - Permeability grids #15 through #17 on Tocito Sandstone cropping out along the Chaco River. Measurement locations are the permeability value's decimal point. Geostatistics given in Appendix 11.

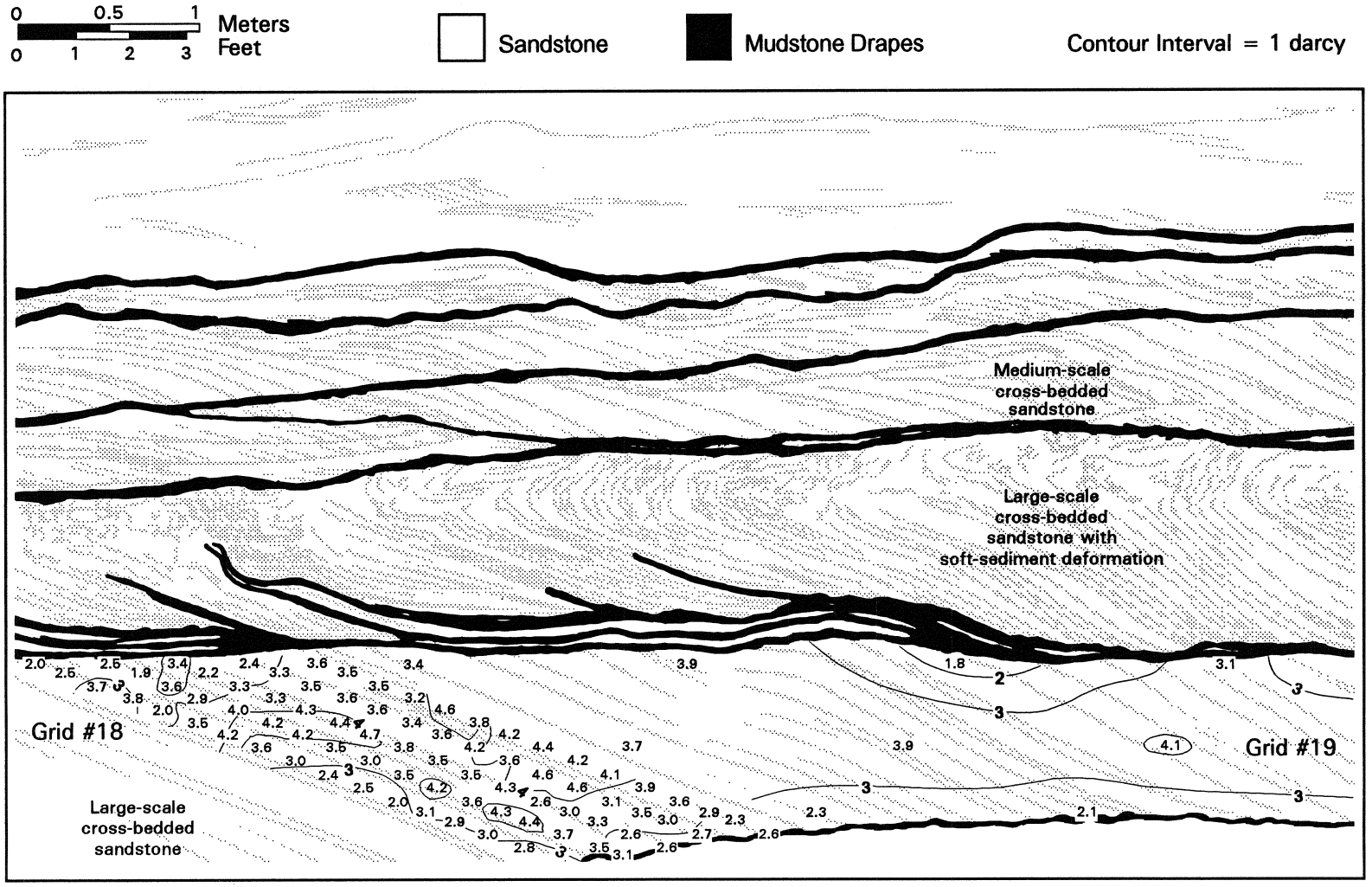

Figure 35 - Permeability grids #18 and #19 on Tocito Sandstone cropping out along the Chaco River. Grid #19 is continued in Figure 36. Measurement location is the permeability value's decimal point. Geostatistics given in Appendix 11.

Relatively lower permeabilities (<3 darcies) exist at the top and base of the sandstone bed, whereas the higher permeabilities (>4 darcies) occur near the center of the bed. Permeability contours locally follow foresets.

Grid #19

Grid #19 (Figs. 35-36, Appendices 10 and 11) is 7.5 m (24.6 ft) long by 2.3m (7.4 ft) high (18 measurements) and is a continuation of grid #18, but with greater horizontal and vertical spacing between permeability measurements (1.5 m and 1.0 m respectively, compared to grid #18's 0.3 m and 0.15 m spacings). The purpose of grid #19 was to see if permeability values and trends observed in grid #18 extended horizontally for a significant distance. Grid #19 has an average permeability value of 2.7 darcies, which is significantly lower than grid #18's average of 3.4 darcies. However, the relatively low permeabilities again are near the top and bottom of the sandstone bed and the higher permeabilities are near the center.

Grid #20

Grid #20 (Fig. 36, Appendices 10 and 11) is a 0.9 m (3.0 ft) by 0.9 m (3.0 ft) square grid (16 measurements) set on the contorted foresets of cross-bedded sandstone lithofacies. Average permeability is 2.5 darcies, but there exists a pattern of low (<2 darcies) and high (>3 darcies) permeability zones that appear unrelated or unaffected by the overturned foresets. There are fewer contorted mudstone drapes in grid #20 than in grid #15.

Grid #21

Grid #21 (Fig. 36, Appendices 10 and 11) is approximately 0.9 m (3.0 ft) wide and 0.9 m (3.0 ft) high (28 measurements) and was placed on medium-scale cross-bedded sandstone lithofacies. The average permeability value for grid #21 is 3.7 darcies.

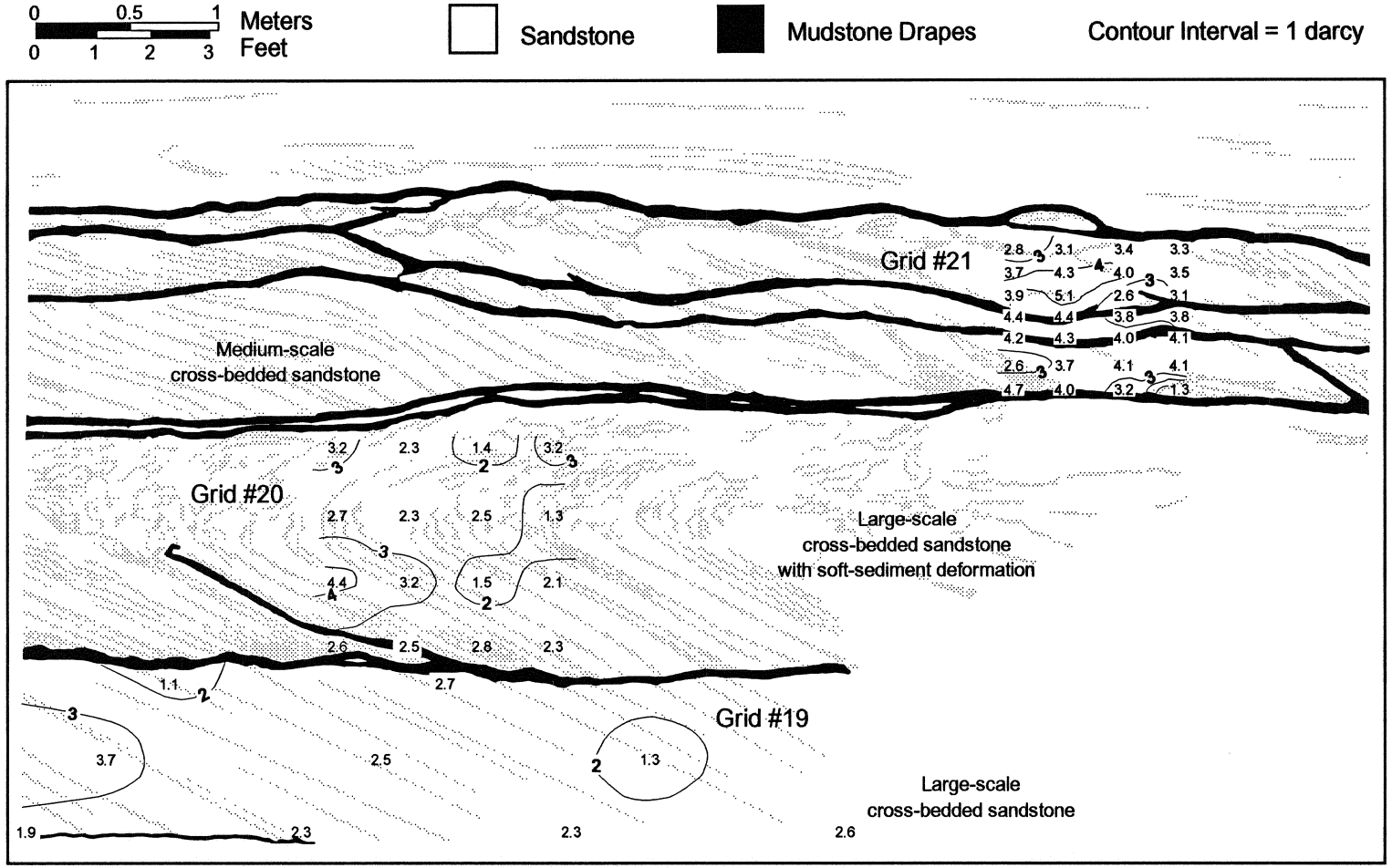

Figure 36 - Permeability grids #19 through #21 on Tocito Sandstone cropping out along Chaco River. Grid #19 is continued from Figure 35. Measurement location is the permeability value's decimal point. Geostatistics given in Appendix 11.

Impermeable mudstone drapes partition the grid into three vertically-stacked sandstone beds. The top bed has relatively low permeabilities (<3 darcies) at its top and base, and higher permeabilities (>4 darcies) near its center. The middle bed is relatively thin and permeable (ave. = 4.1 darcies). The lower bed has low permeabilities (<3 darcies) at its base and top, and moderately high permeability (ave. 4.1 darcies) along the center of the bed.

Macroscopic-scale Permeability Profiles from Shallow Core Plugs and Outcrop

Permeability measurements with the mechanical field permeameter of forty-one HOF #2 core plugs and fifty-three HOF #3 core plugs suggest blocky permeability profiles, in which thick segments of high permeability strata (2.0 to 4.4 darcies) are separated by thin zones of low-permeability strata (0.0 to 1.0 darcies; Fig. 37). Permeability data are given in Appendix 12. Permeability measurements made in a vertical traverse of the Hogback oil field outcrop (Appendix 12) are more closely spaced than those in the HOF cores and thus a greater degree of heterogeneity is revealed. The thick blocks in the HOF cores can probably be subdivided into thinner blocks, as in the outcrop permeability profile. Note that the maximum permeability values in the shallow core and outcrop are similar. The lack of very low permeability values in the outcrop traverse is due to sampling bias (weathered mudstones were difficult to measure due to leaking of nitrogen into exfoliation cleavage) and the leaching of clays and cements by meteoric water, giving the mudstones uncharacteristically high permeabilities.

Mesoscopic-scale HOF #2 Core Permeability Profile and Grids

The computer-controlled scanning minipermeameter was used to study the affects of lithology, percent cement (silica and calcite), percent mudstone, percent bioturbation, and interpreted lithofacies on permeability heterogeneity (Fig. 38). The percentages of

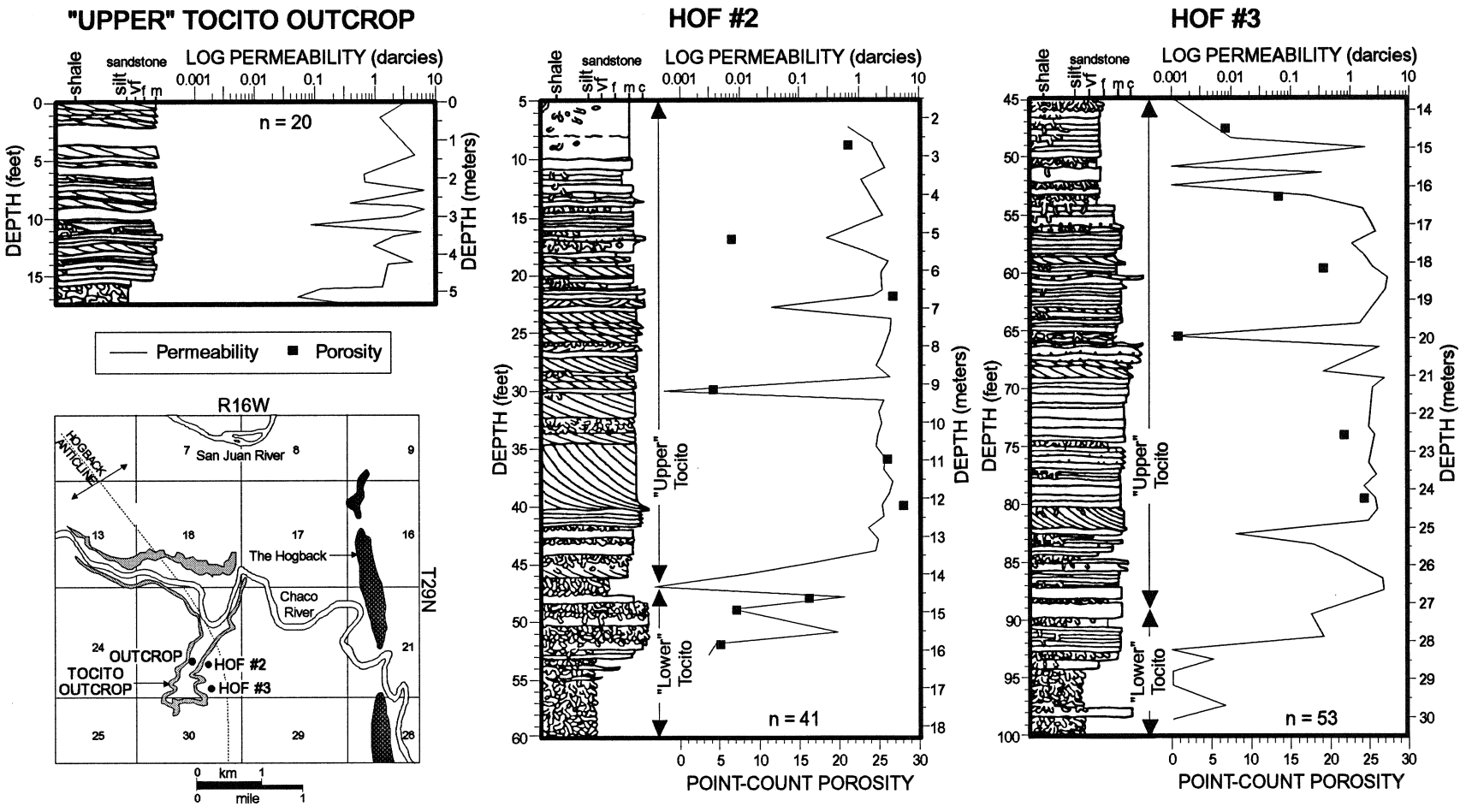

Figure 37 - Permeability profiles from core plugs of the HOF #2 and HOF #3 cores and from hand samples of a vertical traverse of the "upper" Tocito Sandstone outcrop. Sampling density of core plugs is approximately every 0.3 meters. Permeability measurements were obtained with the mechanical field permeameter and porosities were calculated from petrographic point-count data. Location of cores and outcrop traverse are shown on the inset map. Core descriptions were modified from R. Cole of Unocal Corporation, Brea, CA. Permeability values are listed in Appendix 12. Sedimentary structures defined in Figures 38 and 41.

total cement and mudstone are visual estimations that were "calibrated" with point-count percentages from available thin sections. Bioturbation intensity was visually estimated from the core. Gaps in the data are due to missing core or not sampling the highly fragmented or rubblized core. Permeability data used to construct Fig. 38 are given in Appendix 13. Lithologic data are listed in Appendix 14.

In general, thicker sandstone units have higher permeabilities than thinner units [Fig. 38, core depths 7-8 m (23-26 ft)]. Mudstone drapes segment all of the lithofacies except the large-scale cross-bedded sandstone lithofacies [Fig. 38, 10.2-12.2 m (33.5-40 ft)]. Mudstone drapes are most abundant in the interbedded sandstone and mudstone lithofacies and tend to be disrupted and mixed in the muddy bioturbated lithofacies. From 13.4 m (44 ft) to 16 m (53 ft), there is a significant decrease in permeability due to bioturbation.

Large-scale cross-bedded sandstone core intervals are broken up into thick permeable units by bedding surfaces and occasional mudstone drapes (Fig. 39). Permeability contours are subparallel to the foresets. Permeability values are highest in this lithofacies (up to 9.0 darcies). In the medium-scale cross-bedded sandstone lithofacies (Fig. 39), permeability values are lower (3.0 to 6.0 darcies) and mudstone intercalations are impermeable enough (<1.0 darcy) to isolate sandstone beds. Permeability contours are subparallel to foresets.

Interbedded sandstones and mudstones appear as subparallel bands of high and low permeability (Fig. 40). Mudstone beds with permeabilities of <1.0 darcy effectively isolate sandstone beds with permeabilities between 2.0 and 5.0 darcies.

Muddy bioturbated sandstone lithofacies have irregular permeability contours (Fig. 40) in which individual burrows appear as small "islands" of low permeable sediment in amongst impermeable mudstone and shale. Ripple-laminated sandstone lithofacies are

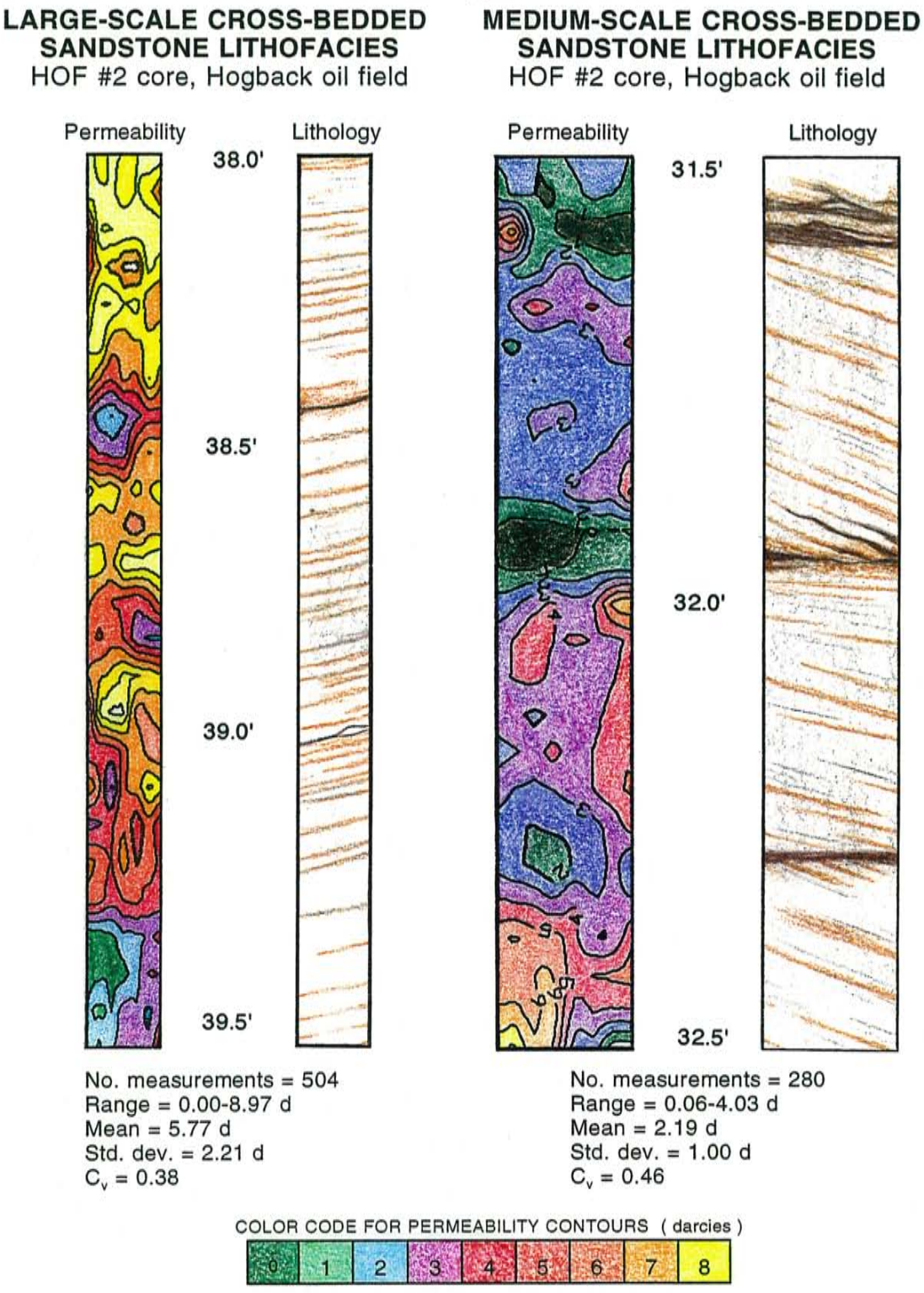

Figure 39 - Permeability contour plots for large-scale cross-bedded sandstone lithofacies and medium-scale cross-bedded sandstone lithofacies. Permeability measurements were made on the HOF #2 core using the computer-controlled minipermeameter. Contour interval is 1 darcy. C_v is the coefficient of variation.

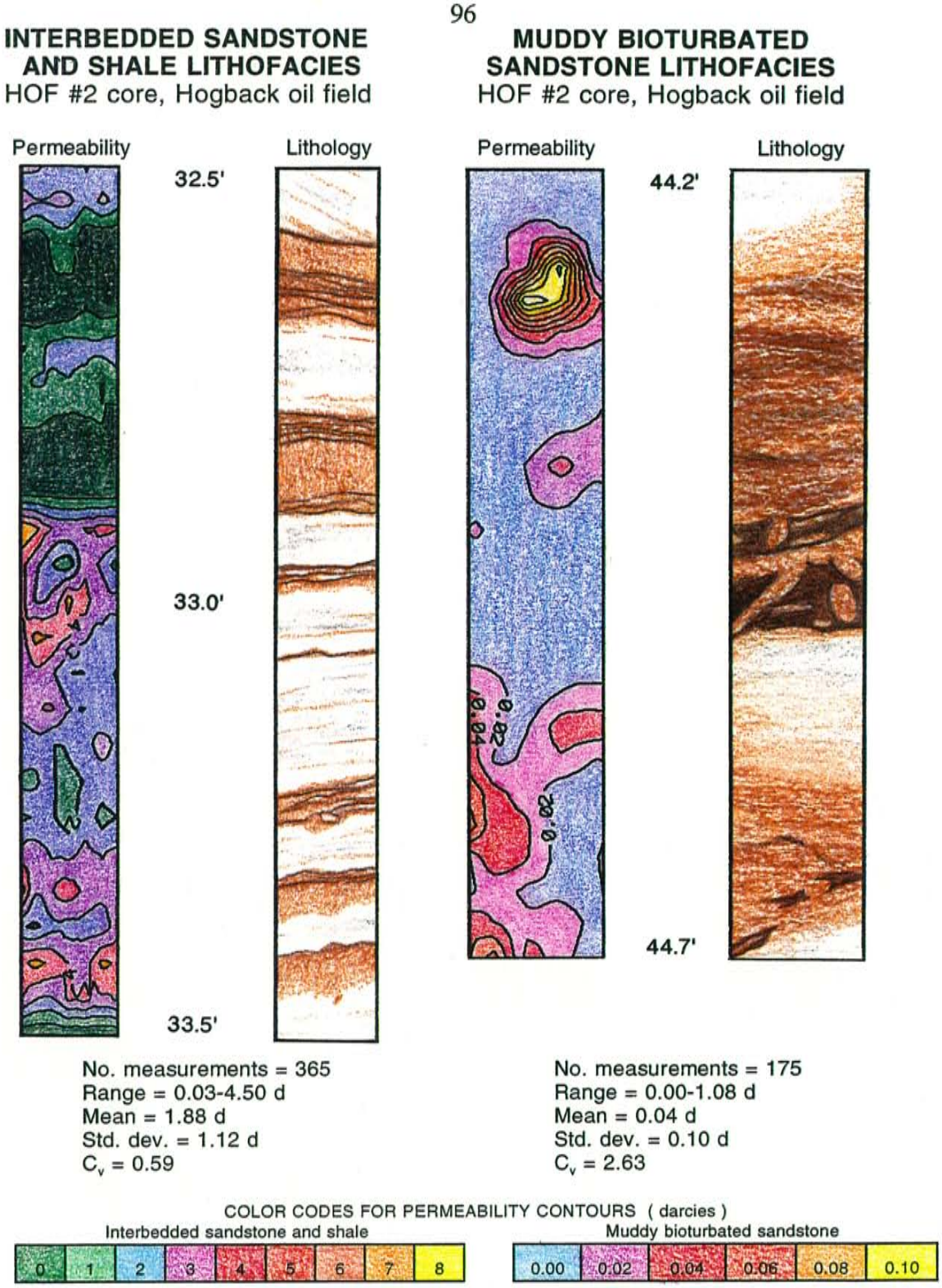

Figure 40 - Permeability contour plots for interbedded sandstone and shale lithofacies and muddy bioturbated sandstone lithofacies. Permeability measurements were made on the HOF #2 core using the computer-controlled minipermeameter. Contour interval is 1 darcy. C_v is the coefficient of variation.

fairly homogeneous and permeability contours are subparallel to the ripple laminations. Permeabilities range from 0.01 to 0.10 darcies.

Permeability Results from Reservoir Core

The permeability profile for the Solar Petroleum Navajo Tribal F-151 core (Fig. 41) shows distinct 0.3-0.6 m (1-2 ft) thick permeable zones separated by 0.3-0.6 m (1-2 ft) thick impermeable zones. The average permeability was 99.8 md for the cross-bedded sandstone lithofacies, 26.9 md for the interbedded sandstone and shale lithofacies, 27.1 md for the muddy bioturbated sandstone lithofacies, and 1.0 md for the ripple cross-laminated sandstone lithofacies. Permeability data for the reservoir core are given in Appendix 15.

The permeability trend observed in interbedded sandstones and shales (Fig. 42, 922-927') is one of horizontal, subparallel zones of moderate (0.027-0.120 darcies in poorly- to moderately-cemented sandstones) and low (0.0004-0.027 darcies in mudstones and well-cemented sandstones) permeabilities. Permeability trends are similar for the cross-bedded sandstones near the base of the core (Fig. 42, 940-944.5').

Permeabilities are low (<0.050 darcies) throughout the Martin Gas Unit C-1, the Angel Peak B-37, and the Newsom A-3E cores. The Martin Gas Unit C-1 has significant sandstone, but the other two cores are clay-rich and have few sandstone beds.

DISCUSSION

Effect of Sedimentary Structures on Porosity and Permeability

Reactivation Surfaces

Reactivation deposits in the Tocito Sandstone outcrop (Fig. 33) have the highest permeabilities of all structures measured. The permeability values range from 2.6 to 5.2

Solar Petr. Navajo Tribal F-151
Sec. 10 T31N R17W, Horseshoe Oil Field

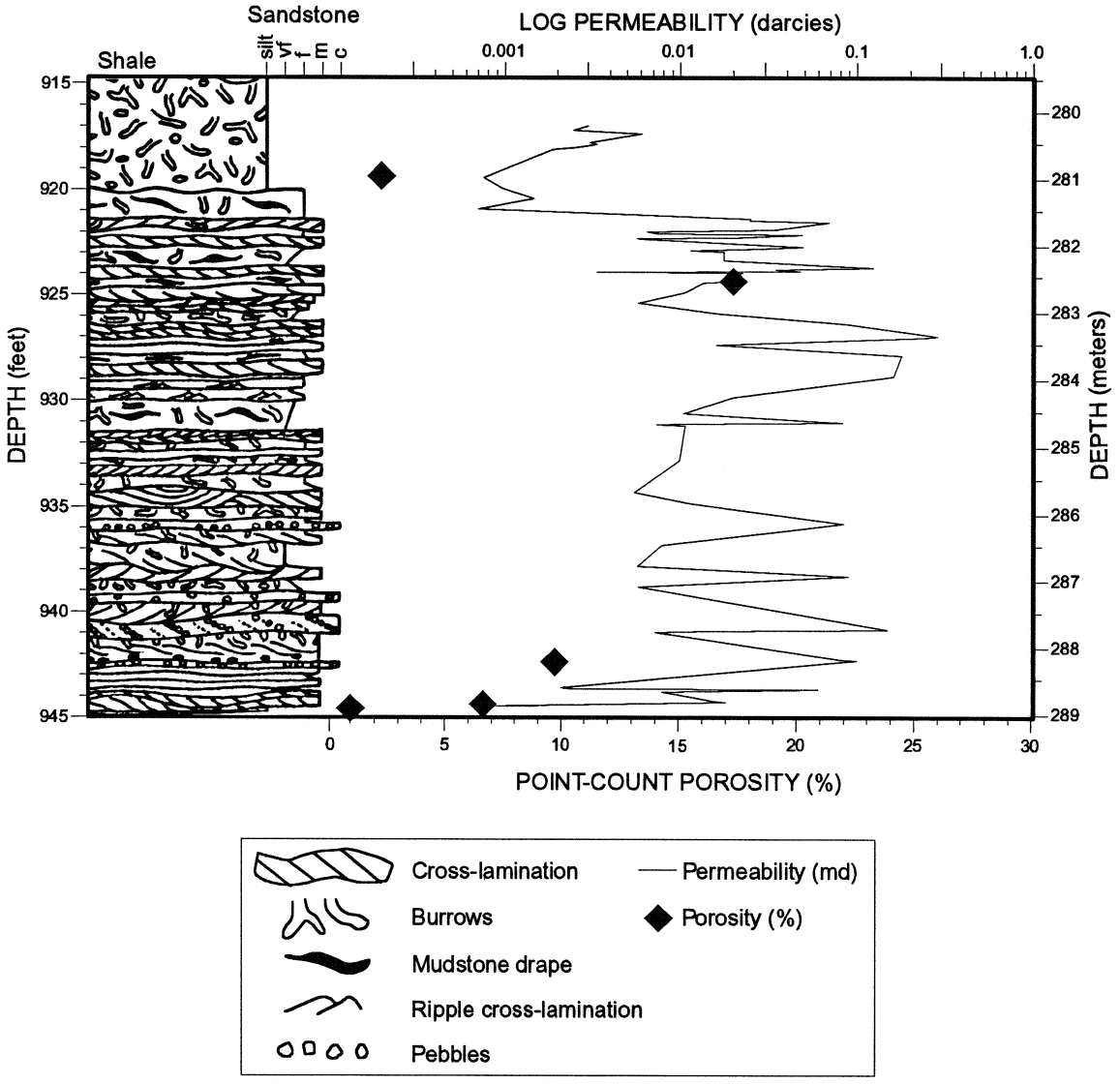

Figure 41 - Permeability profile for Solar Petroleum Navajo Tribal F-151 in the Horseshoe oil field, San Juan Basin. Permeability measurements were obtained with the mechanical field permeameter and are listed in Appendix 15. Porosities were calculated from petrographic point-count data.

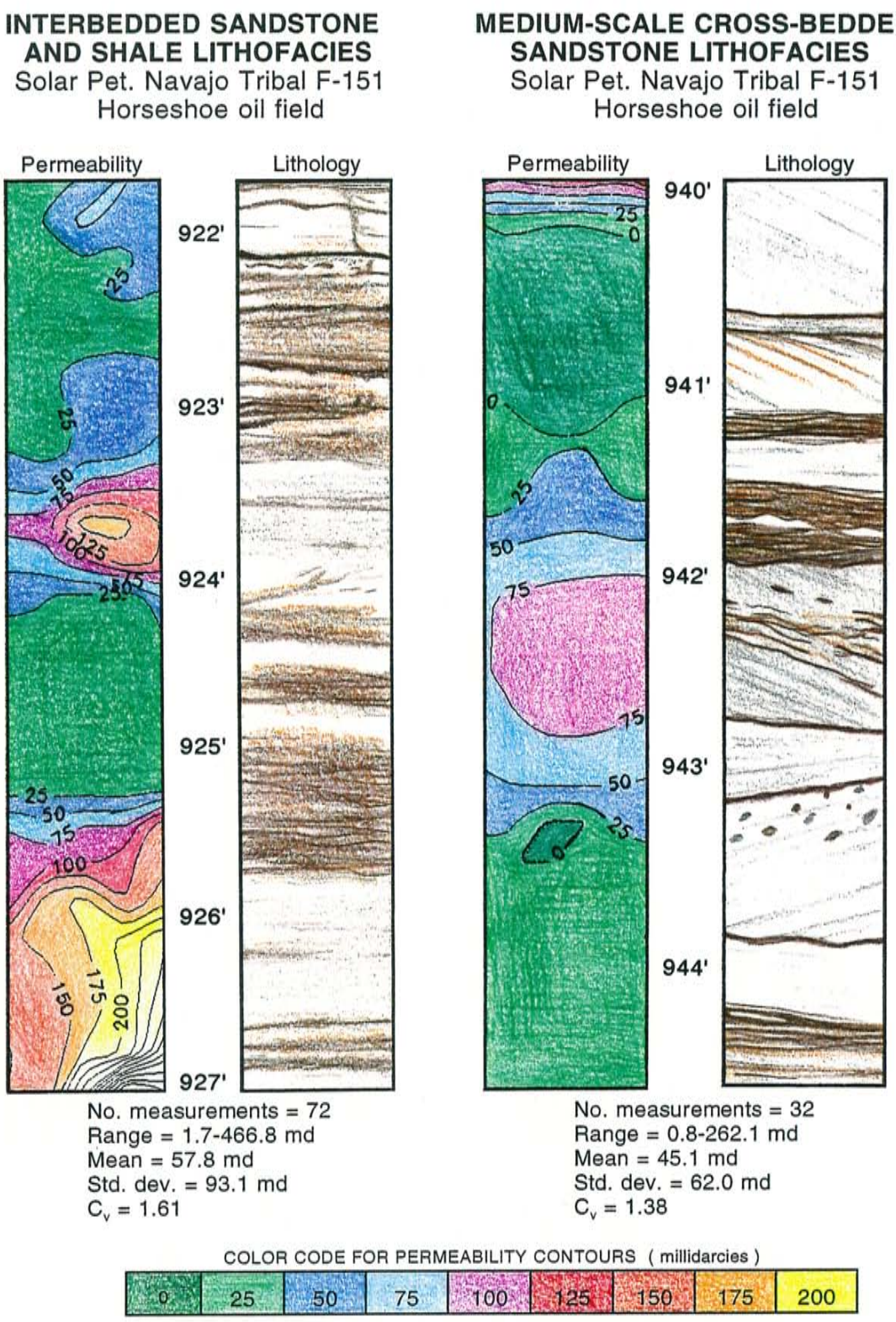

Figure 42 - Permeability contour plots for interbedded sandstone and shale lithofacies and medium-scale cross-bedded sandstone lithofacies in the subsurface. Permeability measurements were made on the F-151 core using the mechanical field permeameter. Contour interval is 25 md. C_v is the coefficient of variation.

darcies with a mean of 3.9 darcies (Fig. 43, Appendix 11). Permeability contours appear to parallel reactivation surfaces more closely than the cross-bed foresets the reactivation surfaces truncate.

Cross-bedding

Cross-bedded sandstone in the Tocito Sandstone outcrops and shallow subsurface core has a mean permeability of 3.6 darcies and a range of 0.01 to 9.0 darcies (Fig. 43, Appendix 11). Cross-beds cause porosity and permeability heterogeneity in the Tocito, primarily due to contrasts in grain-size. For example, in the shallow subsurface HOF #2 core, a sandstone unit at 36' to 38' (Fig. 38) has an average grain-size of 2.0ϕ (upper fine- to lower medium-grained), but has foresets with average grain-sizes of 1.5ϕ (upper medium-grained) and 4.0ϕ (lower very-fine-grained or silt-sized). The 2.0ϕ sandstone has average permeabilities of about 4.0 darcies, whereas the coarse-grained foresets may reach permeabilities of 7.0 or 8.0 darcies and the fine-grained foresets may have permeabilities of only 1.0 to 2.0 darcies. Jones et al. (1984), Goggin et al. (1988a), Barton and Tyler (1991), and Dutton and Diggs (1992) also found that the permeability of cross-bedded sandstones in other formations was significantly greater than that of other sedimentary structures.

Permeability contours in the Tocito Sandstone are generally parallel to the direction of cross-bedding inclination and the southeast-trending paleocurrent direction (Figs. 31, 33, and 35). Studies on other sandstones had results that indicated a similar trend (Pettijohn et al., 1973, p. 525). Foresets in the Tocito cross-bedded sandstone are significantly more permeable (or less permeable if covered by a mudstone drape) than the remainder of the sandstone, so fluid flow should be more pronounced parallel to the foresets than perpendicular to the foresets. Emmett et al. (1971) found that permeability

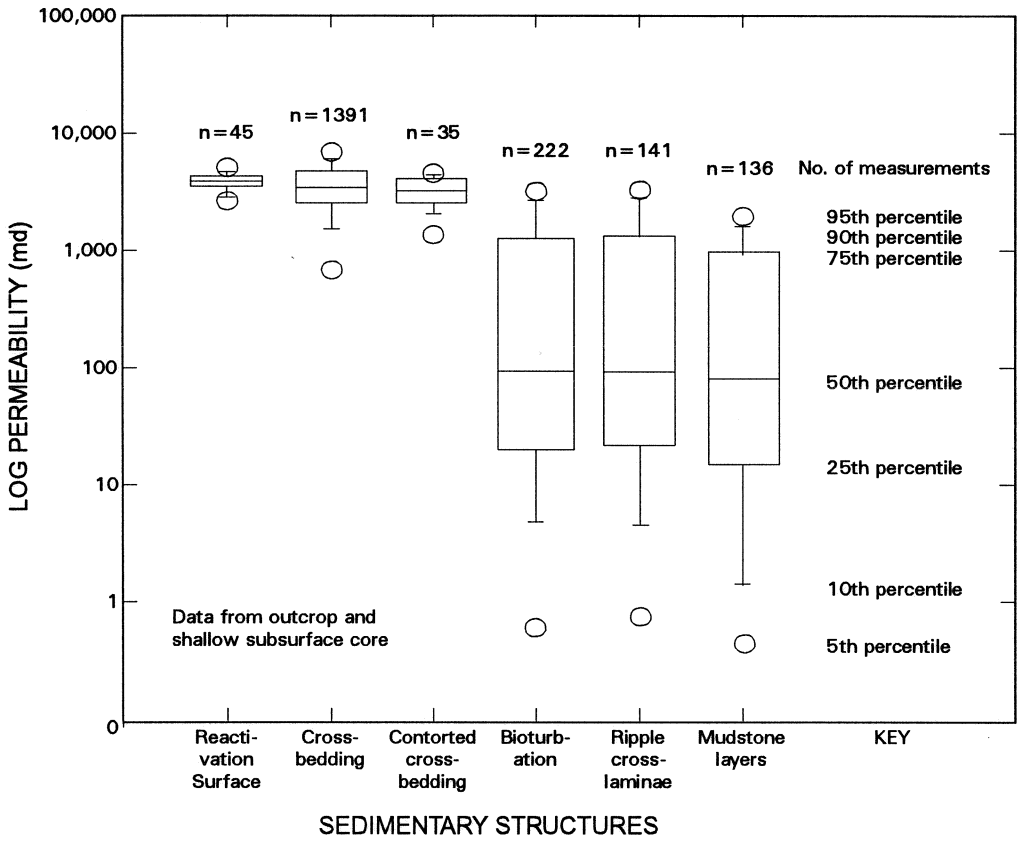

Figure 43 - Box plot of permeability values for sedimentary structures identified in the Tocito Sandstone outcrop (Hogback oil field) and in the HOF #2 core. Permeability values were obtained with both the mechanical field permeameter and the computer-controlled minipermeameter. Permeability values are listed in Appendices 10, 12, and 13.

parallel to the cross-bedding laminae was approximately four times greater than permeability perpendicular to the laminae in the Tensleep Sandstone of Wyoming.

Contorted Cross-bedding

Sandstone with contorted cross-bedding, measured in two grids on the Tocito Sandstone outcrop, has a mean permeability value of 3.3 darcies and a range of 1.3 to 4.7 darcies (Fig. 43, Appendix 11). Maximum and minimum permeability values of the contorted sandstone are less extreme than those of noncontorted cross-bedded sandstone. The mean permeability is also slightly lower in the contorted sandstone (3.3 darcies versus 3.6 darcies in noncontorted cross-bedded sandstone). As discussed, intercalated mudstone drapes retard both vertical and horizontal permeabilities when they separate permeable cross-bedded sandstone units. When foresets are overturned during soft sediment deformation, these shale intercalations became intermixed with the sandstones producing sediments with lower overall permeability. However, the new sediment mixture is more permeable than the original mud drapes. Similar trends were documented in the Mesaverde Sandstone (Jones et al., 1984), Travis Peak Formation (Dutton and Diggs, 1992), and Ferron Sandstone (Barton and Tyler, 1991).

Bioturbated Sediments

Bioturbated sediments in the Tocito Sandstone outcrop and shallow subsurface core have a permeability range of <0.01 to 4.6 darcies and a permeability mean of 0.8 darcies (Fig. 43, Appendix 11). Bioturbation greatly reduced the original porosity and permeability very soon after deposition and was influential in later diagenetic processes. Burrowing reduced the porosity and permeability by introducing silt and mud into the pores. Intense bioturbation resulted in relatively homogeneous sediment with low porosity and permeability. In the shallow subsurface core, HOF #2 (Fig. 38), the

average grain size in the interval 8-10 m (27-32 ft) and 13-15 m (44-48 ft) is about 2.0ϕ (upper fine- to lower medium-grained). Both intervals have mud drapes and thin shale layers, however, burrowing in the 13-15 m (44-48 ft) interval has churned the sediments into muddy sandstones that are much less permeable (<0.01 - 3.6 darcies) than non-burrowed sandstones in the 8-10 m (27-32 ft) interval (2.0 - 8.9 darcies).

Burrowing increased vertical communication of fluids in the Tocito Sandstone by piercing impermeable mud drapes and becoming backfilled with sandstone (Fig. 44). Observed concentrations of calcite cement near and in burrows that penetrate mud drapes suggest that such burrows were conduits for the vertical movement of pore-cementing fluids.

Ripple Cross-laminated Sediments

Ripple cross-laminated sandstone in the Tocito Sandstone outcrop and shallow core has a mean permeability of 0.8 darcies and a range of 0.01 to 4.4 darcies (Fig. 43, Appendix 11). These sandstones have an average grain size of 2.5ϕ [e.g., HOF #2 core, 7.83-7.85 m (25.7-25.75 ft)] compared to an average of 2.0ϕ in the Tocito as a whole. They also tend to have detrital clay and frequent thin mudstone laminations. Because their permeabilities are significantly lower than those of cross-bedded sandstones, ripple cross-laminated sandstones are probably barriers to vertical fluid flow in the Tocito reservoirs. Ripple cross-laminated sandstones have the lowest permeabilities in the Mesaverde Sandstone (Jones et al., 1984), Page Sandstone (Goggin et al., 1988a), Tensleep Sandstone (Cole and Mullen, 1992), and Travis Peak Sandstone (Dutton and Diggs, 1992). Pettijohn et al. (1973) suggest that the fine grain size and the abundant laminations combine to give ripple cross-laminated zones their low porosities and permeabilities. This is likely the case in the ripple cross-laminated sandstones of the Tocito.

Solar Petr. Navajo F-151, 921.5′ to 921.67′

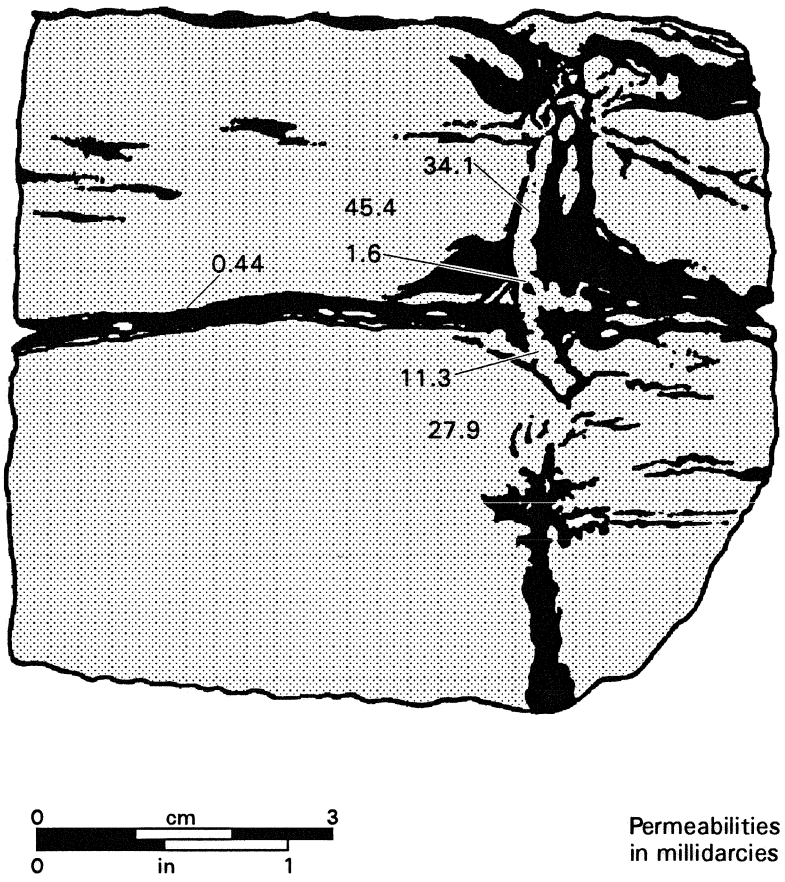

Figure 44 - Enhancement of vertical permeability due to the penetration of impermeable mud drapes by sand-filled burrows. In many cases, this was the only means for vertical fluid migration and such burrows often received higher quantities of calcite cement than did the surrounding sandstone.

Mudstone Layers

Mudstone layers measured in the Tocito Sandstone outcrop and core have a mean permeability value of 0.5 darcies (Fig. 43, Appendix 11). They range in permeability from <0.01 to 3.2 darcies and are the least permeable sedimentary structures studied. Mudstone drapes and thin shale layers blanket most Tocito sandstone beds and separate them from overlying sandstone beds (Figs. 33-36). The overall effect is the formation of long, tabular zones of moderate to high permeability separated by thin zones of low to very low permeability, with little or no vertical communication between zones (Figs. 25, 30, 33-38, 39, 40, 41). During oil extraction, the sandstone core interval 32.0-32.7 ft was stained with oil whereas the sandstone interval 22.0-23.5 ft was not (Fig. 20). This suggests that the dense claystone drapes that are present at the ends of the core compartmentalized the sandstone, either preventing oil from entering the 22.0-23.5 ft core interval or retarding the drainage of oil from the 32.0-32.7 ft interval.

The plane of the mud drapes is frequently subparallel to the plane of the sandstone foresets and inclined to the average bedding-plane direction (Figs. 30, 33-36). Thus, not only do they impede vertical fluid flow in the Tocito Sandstone reservoirs (Figs. 39, 40), but retard horizontal flow as well (Figs. 30, 33, 36). Horizontal flow would take the path of least resistance and would therefore travel parallel to the plane of the mud drape and perpendicular to the paleocurrent direction, similar to permeability trends found in the Tensleep Sandstone of the South Casper Creek field in Wyoming (Cole and Mullen, 1992). Jones et al. (1984) determined that mud-draped ripples would prevent fluid from migrating between sets of higher permeability ripples in the Mesaverde Sandstone.

Effect of Diagenetic Alterations on Porosity and Permeability

Excluding primary porosity still present in the Tocito Sandstone, cementation and framework-grain dissolution are most likely responsible for the permeabilities and porosities observed in the Tocito today. Statistical correlations exist between present permeability, the volumes of quartz overgrowths and calcite cement, and secondary porosity (Table 1). Similar correlations exist with total thin section porosity. There is no significant correlation with pyrite, kaolinite, detrital clay, fractures, gypsum, glauconite, dolomite, and phosphate nodules.

Table 1. Correlations between petrographic parameters and the permeabilities and porosities that are currently present in shallow and deep subsurface Tocito Sandstone core.

PARAMETER	PERMEABILITY CORRELATION COEFFICIENT	POROSITY CORRELATION COEFFICIENT
Quartz overgrowth (%)	0.59	0.71
Calcite cement (%)	0.51	0.72
Pyrite (%)	0.37	0.19
Kaolinite (%)	0.36	0.44
Detrital clay (%)	0.32	0.53
Gypsum (%)	0.18	0.23
Glauconite (%)	0.11	0.11
Dolomite (%)	0.07	0.16
Phosphate (%)	0.06	0.04
Intragranular ϕ / Fspr + Chert	0.95	0.81
Feldspar ϕ / Total ϕ	0.71	
Grain dissolution ϕ / Total ϕ	0.48	

Compaction

Framework-grains in the Tocito Sandstone have tangential (point) and long contacts. Concavo-convex contacts are not common except where ductile grains like glauconite and mica are plastically deformed around rigid grains. Although usually constituting only a few percent of the Tocito, glauconite is frequently concentrated along foresets [up to 30% glauconite in cross-bed laminations observed at 1851 m (6073 ft) in Pan American's Martin-1], where it is compressed into pseudomatrix during burial. Sutured contacts between framework-grains are rare in the Tocito. These textural observations suggest that mechanical compaction rather than chemical compaction (intergranular pressure solution) reduced original porosity and permeability by reorienting and repacking competent grains, fracturing brittle grains, and plastically deforming ductile grains.

Quartz and Feldspar Overgrowths

Although quartz and feldspar overgrowths make up only a few percent of the rock, they are ubiquitous, reducing porosity by 2-5% (volume of overgrowths from thin section point counts) and diminishing permeability (Table 1) by constricting and sealing pore throats (Figs. 14A,B, 15).

Calcite Cementation

Calcite cementation ranges from minor to complete occlusion of the pores, though cementation is usually incomplete, leaving some primary porosity (Figs. 16C, 18F). Calcite precipitation affects the reservoir properties (Table 1) in three general ways: by reducing originally low porosities and permeabilities in muddy, poorly sorted sandstones; by reducing porosity and permeability in sandstones directly below vertical flow barriers (such as thick mud drapes or shaly beds); and by occluding burrows that originally increased the vertical permeability through mud drapes.

Muddy, poorly sorted sandstones are commonly well cemented in Tocito Sandstone outcrop (Figs. 24, 26, 29, 30, grid 14 in Fig. 33, Figs. 40, 42). The muddy sediments and mudstone drapes are frequently organic-rich. When the organic matter decays, alkaline microenvironments are developed within the mudstone. High alkalinity favors the precipitation of calcite, and thus cementation tends to be concentrated in and near shale beds and mudstone drapes between sandstone beds.

Another example of how neighboring sandstone beds were affected differently during calcite cementation is grid 1 (Fig. 24). Row 1 of the grid measured the permeability of a very tightly cemented sandstone bed, whereas rows 2 and 3 measured low to moderately permeable beds directly beneath. It is possible that the interbedded mudstones in rows 2 and 3 had low total organic contents and therefore did not produce the local alkaline microenvironments necessary for carbonate precipitation. On the other hand, note that the more permeable sandstone layers pinch-out (Fig. 24, center of left margin of grid, also approximately 1 inch from center of right margin of grid). If the well-cemented sandstone unit is more laterally continuous than the compartmentalized permeable sandstone units, perhaps a greater volume of ion-bearing pore water passed through the continuous sandstone bed.

The third method in which calcite precipitation affects Tocito Sandstone reservoir quality is by cementing burrows. When a burrow penetrates a low-permeability mudstone layer, it offers pore waters a conduit with less resistance to vertical fluid flow. A relatively high volume of ion-bearing pore water will pass through the burrow, which frequently contains significant quantities of decaying organic matter and, therefore, a higher alkalinity. Eventually the burrow and surrounding sandstone becomes cemented with calcite. The porosity and permeability may become greatly reduced, but may still be higher than that of the original mudstone layer.

Replacement of framework-grains by calcite has no effect on porosity and permeability. Such replacement will only affect porosity and permeability when the strata is subjected to outcrop weathering. Then calcite dissolution will remove both calcite cement and calcite that has replaced framework-grains.

Framework-Grain Dissolution

There is a statistically significant correlation between permeability and framework-grain dissolution (Table 1, Fig. 45). Grain dissolution accounts for up to 6% (possibly even 16%) of the total porosity in the Tocito Sandstone, and is commonly the only form of porosity in well-cemented sandstones (Figs. 18B-C).

Kaolinite Precipitation

Kaolinite occurs as trace localized highly porous to dense aggregates and intergranular pore-fillings. Only in a few specimens is the kaolinite abundant enough and the booklets large enough to become lodged in pore throats during high flow velocities (i.e., during hydrocarbon recovery efforts). Such blockage would have a significant negative impact on permeability. This was a primary concern when injecting nitrogen into the outcrop and core during permeability measurements, until numerous petrographic examinations indicated that kaolinite was generally not abundant enough to become a factor.

Additional Framework-Grain Dissolution in Outcrop

The presence of grain dissolution pores in direct contact with the late-stage nonferroan calcite cement (Fig. 18C) suggests that additional framework-grains were leached during outcrop weathering. Dissolution of framework-grains and calcite cement in outcrop has increased porosity and permeability.

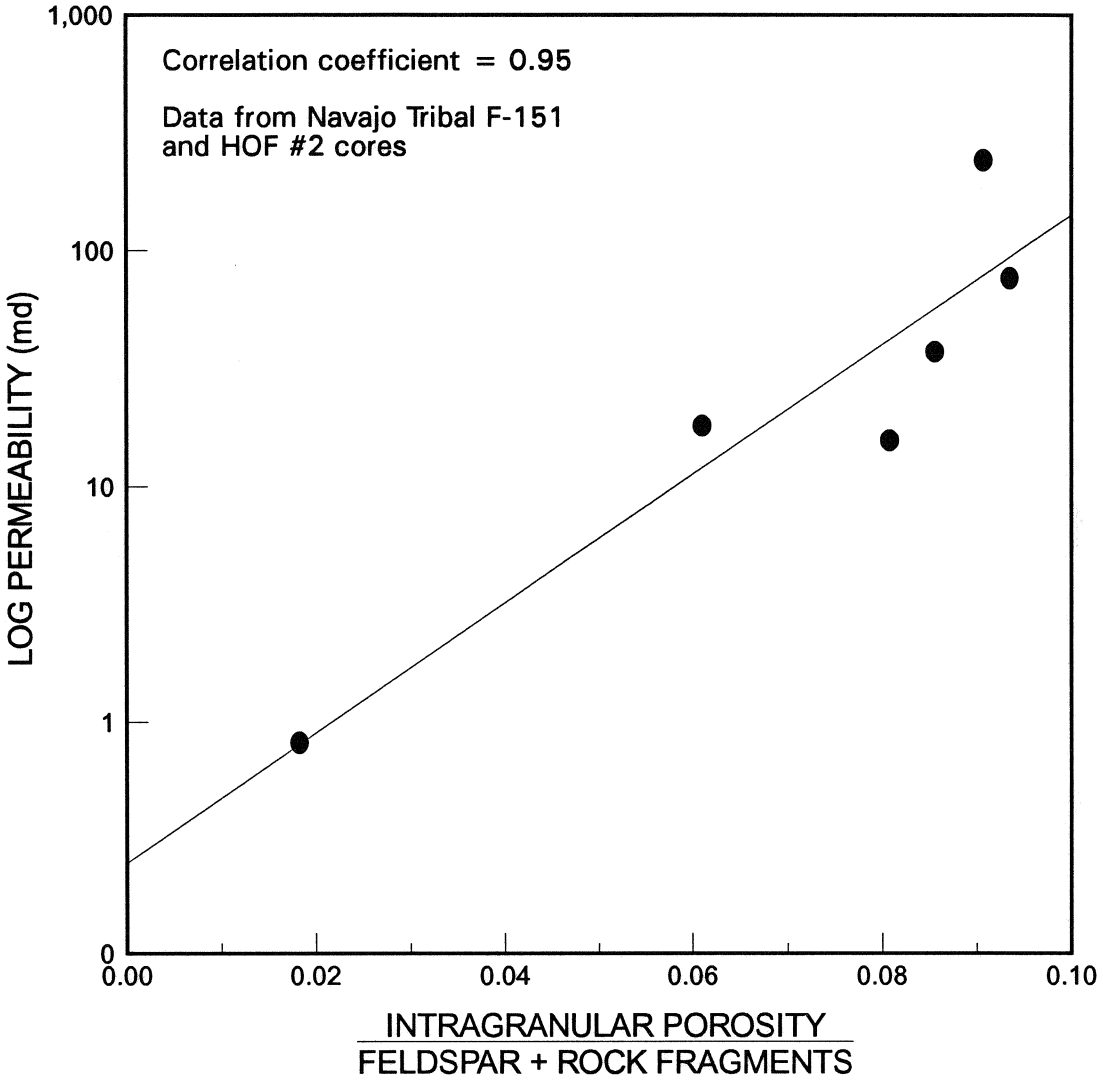

Figure 45 - Cross-plot of secondary porosity in feldspar and chert grains versus permeability for the Navajo Tribal F-151 and the HOF #2 cores. Secondary porosity was determined from petrographic point-count data. (Appendices 6 and 7) Permeability values were obtained with both the mechanical field permeameter and the computer-controlled scanning minipermeameter (Appendices 13 and 15).

Relationship of Lithofacies to Porosity and Permeability

Large-scale Cross-bedded Sandstone Lithofacies

Large-scale cross-bedded sandstone intervals are characterized by a mean permeability of 3.2 darcies and a range of 0.01 to 5.1 darcies in the outcrop (Appendix 11). In the shallow subsurface (HOF #2 and HOF #3 cores) they have a mean permeability of 5.0 darcies and a range of 0.9 to 8.6 darcies (Fig. 46A). The differences in the maximum and average permeabilities between outcrop and shallow subsurface core are due to the maximum limits of the mechanical field permeameter used in the outcrop and the computer-controlled minipermeameter used on the core. The large-scale cross-bedded sandstone's enhanced bed thicknesses (>100 cm or >39 in), common coarse-grained foresets, and their relative lack of thick mud drapes, interstitial detrital clay, and burrowing all contribute to their high original porosities and permeabilities. Pore waters were able to pass through the sandstone, induce framework-grain dissolution, and remove liberated ions from dissolution sites. Calcite cement is commonly low in these thick units, perhaps due to the lack of an alkaline microenvironment or because the large-scale cross-bedded sandstone lithofacies is limited in areal extent and may be sealed off from the other sandstones by impermeable mudstone drapes (Figs. 4, 30, 32-36).

The cross-bedded sandstone lithofacies was susceptible to soft sediment deformation; however there are few mudstone drapes on the foresets and thus intermixing of sand with minor amounts of detrital clay had minimal effect on permeability. In fact, both horizontal and vertical permeability may have locally been enhanced by removal of an impermeable mud drape while mixing it with abundant sand.

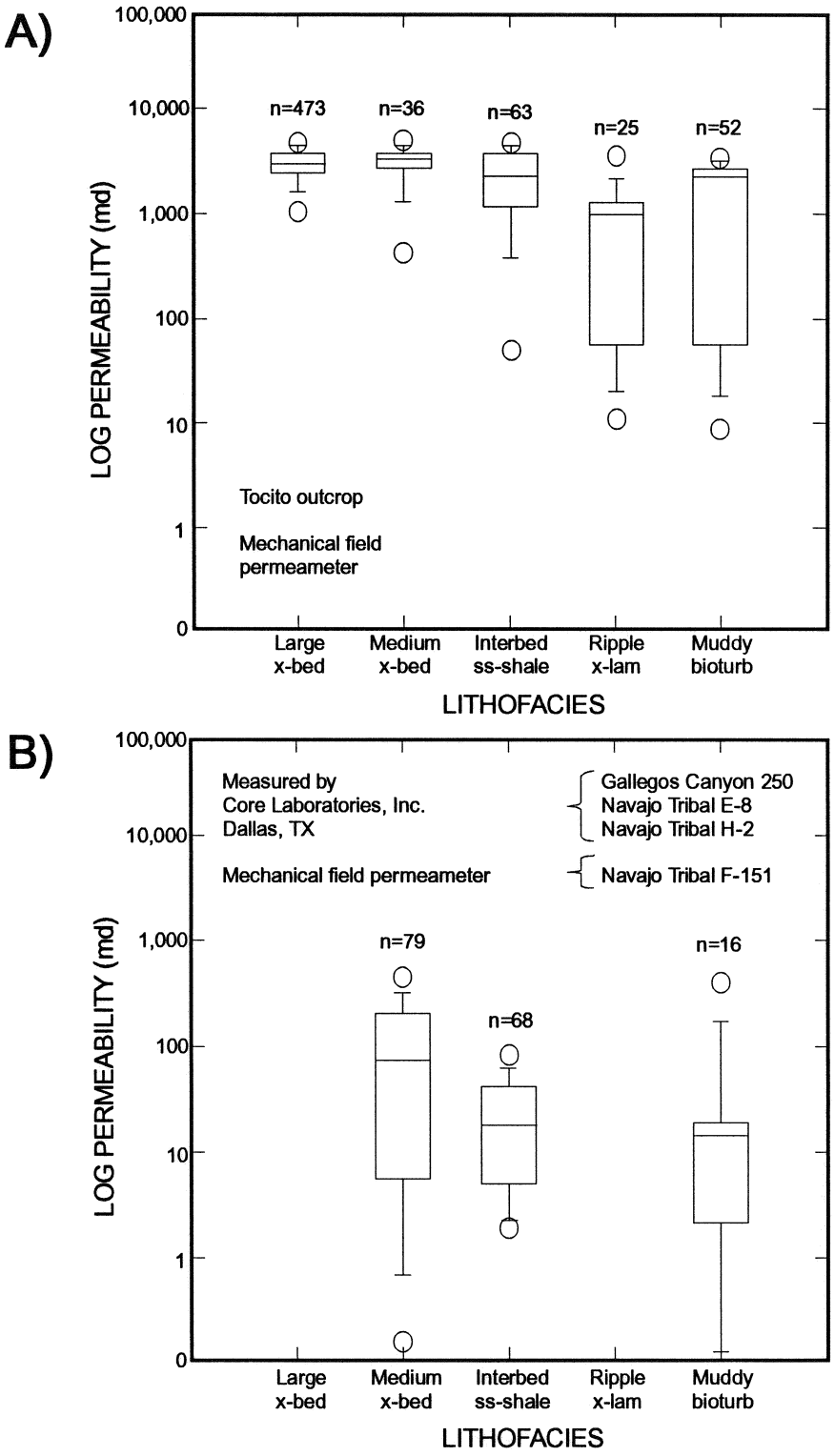

Figure 46 - Box plots of permeability values for sandstone lithofacies identified in A) the Tocito Sandstone outcrop in the Hogback oil field, and B) Tocito subsurface core from the Gallegos, Cha Cha, Totah, and Horseshoe oil fields. Refer to Figure 43 for an explanation of the box-and-whiskers symbols. Permeability values are given in Appendices 10 and 15.

Medium-scale Cross-bedded Sandstone Lithofacies

Medium-scale cross-bedded sandstones have a mean permeability value of 3.7 darcies in the outcrop and 3.4 darcies in the shallow subsurface (Fig. 46A, Appendix 11). In outcrop, the permeability range is 2.9 to 5.2 darcies and in the shallow subsurface it is 0.01 to 8.9 darcies. Again, the differences in mean permeabilities are due to the limits of the different permeameters used. This lithofacies has characteristics similar to those of the large-scale cross-bedded sandstones, but the beds are thinner (30-100 cm or 12-39 in) and commonly separated by 2-5 mm (0.08-0.20 in) thick mudstone layers. These layers act as barriers to horizontal and vertical flow of pore fluids (Figs. 33-36) and induce local cementation. Tops of individual sandstone beds may be locally bioturbated as well, and thus have diminished original porosity and permeability values. Soft sediment deformation occurs in the medium-scale cross-bedded sandstone lithofacies, thereby locally mixing mud drapes with sand. Although this reduces horizontal permeability, it may enhance vertical permeability by destroying the mud drapes.

Interbedded Sandstone and Shale Lithofacies

The interbedded lithofacies has a permeability range of <0.01 to 4.6 darcies and a mean value of 1.1 darcies in the outcrop (Fig. 46A, Appendix 11). In the shallow subsurface, the mean and range are 1.6 darcies and <0.01 to 6.0 darcies, respectively. Interbedded sandstones and mudstones are silty and locally bioturbated. Thin sandstone beds frequently pinch-out (Fig. 24) and thus may have no communication of pore waters with neighboring sandstones. Authigenic clay and calcite cement preferentially precipitated in the bioturbated sandstones and mudstones, further reducing porosity and permeability, and further compartmentalizing the interbeds.

The thicker the sandstone beds are in this lithofacies, the higher their permeabilities tend to be (Figs. 24, 25). In outcrop, sandstone beds more than 10 cm thick, not

extensively burrowed, and relatively clay-free, have permeabilities exceeding 5 darcies, whereas thinner (<5 cm), muddier, bioturbated sandstone layers have permeabilities of 1 to 2 darcies.

Although the reservoir quality of the interbedded lithofacies is poorer than that of the cross-bedded sandstone lithofacies, the interbedded sandstones do produce significant hydrocarbons (J. Hornbeck, personal communication, 1992). Cross-bedded sandstones may be absent in some Tocito Sandstone reservoirs, and the oil production is suspected to come from the interbedded sandstone and shale lithofacies (J. Hornbeck, personal communication, 1992).

Muddy Bioturbated Sandstone Lithofacies

The muddy bioturbated sandstone lithofacies in outcrop has a mean permeability of 0.6 darcies and a range from <0.01 to 2.0 darcies (Fig. 46A, Appendix 11). In the shallow subsurface, the mean permeability is 0.2 darcies and the range is <0.01 to 1.5 darcies. Thinly-bedded sandstone and mudstone layers were intermixed by extensive burrowing (50-75%), producing relatively homogeneous sediments with porosities and permeabilities much lower than those of the original sandstone. Fluid flow through this "homogenized" sediment is by burrows, which eventually become occluded by calcite cement. The reduced permeability later prohibits large quantities of pore fluids from percolating through the sediment, so framework-grain dissolution is minimal.

Relative to the higher permeabilities of the cross-bedded and interbedded lithofacies, the muddy bioturbated lithofacies is a barrier to vertical fluid flow through the Tocito Sandstone reservoir. However, since this lithofacies is commonly present near the base of the Tocito, the detrimental effects to reservoir communication are probably minor.

Ripple-laminated Sandstone Lithofacies

The ripple-laminated sandstone lithofacies has a mean outcrop permeability of 1.7 darcies and a range of <0.01 to 4.4 darcies (Fig. 46A, Appendix 11). In the shallow subsurface, the mean is 0.7 darcies and the range is from <0.01 to 3.0 darcies. This lithofacies is characterized by thin locally bioturbated sandstone and mudstone interbeds with ripple laminations. Bioturbation not only diminished porosity and permeability of the sand interbeds, but decaying organic matter in the mudstone interbeds provided an alkaline environment suitable for calcite cementation (Fig. 29). With the permeability reduced, later pore waters may have been unable to dissolve significant amounts of framework-grains. Relative to the high porosities and permeabilities of the cross-bedded sandstone lithofacies and the interbedded sandstone and shale lithofacies, the ripple-laminated sandstone lithofacies is probably a barrier to vertical flow in the Tocito Sandstone reservoir.

Extent to which Outcrop Sections Reflect Subsurface Conditions

Studies have shown that outcrop observations and trends are portable to the subsurface (Stalkup and Ebanks, 1986; Goggin et al. 1988a; Chandler et al., 1989; Kittridge et al., 1990), although actual outcrop permeability values are not portable. However, distribution type, coefficient of variation, and correlation measures are portable between outcrop and subsurface (Barton and Tyler, 1991).

The same lithofacies exist in the Tocito Sandstone outcrop (Hogback oil field), the Tocito reservoirs of the Cha Cha field (Navajo Tribal E-8 well), the Horseshoe field (Navajo Tribal F-151), the Totah field (Navajo Tribal H-2), and the Gallegos field (Gallegos Canyon Unit #250). Only the large-scale cross-bedded sandstone lithofacies was not identified in the subsurface.

In both outcrop and subsurface, the lithofacies have a similar hierarchy of relative permeabilities. The cross-bedded sandstone units always have the highest porosities and permeabilities, and are followed by the interbedded sandstone lithofacies (Figs. 46B, 47). Permeabilities of the ripple cross-laminated sandstone and the muddy bioturbated sandstone lithofacies are usually much lower than those of the cross-bedded and interbedded sandstone lithofacies.

Permeabilities measured in the Tocito Sandstone outcrop and shallow subsurface core are several orders of magnitude higher than those measured from deep subsurface core (Fig. 46A,B). Calcite cement and framework-grains have been dissolved in the outcrop and shallow subsurface, however the amount of dissolution is not significant (excluding the outcrop surface). Thomas and Ward (1971), Kilmer et al. (1987), and Dutton and Diggs (1992) found that sandstone core permeability decreases with increasing simulated overburden pressure. Thomas and Ward (1971) demonstrated that permeability decreased by 70-75% at 3000 psi and by 80-90% at 6000 psi. When water saturation was increased in the pressurized core, the permeability fell by 95%. Permeability in dry cores with microfractures decreased by about 95% at 3000 psi. Even so, Thomas and Ward (1971) noted that *relative* permeability between sandstone textures did not change significantly with overburden pressure. Thus it is probable that the porosities and permeabilities measured in the Tocito outcrop and shallow subsurface core are higher than those in the deep subsurface core primarily because of decompression by removal of overburden during uplift.

Effect of Reservoir Geometry on Porosity and Permeability

The Tocito Sandstone cropping out in the Hogback oil field provides a good analog for modeling the Tocito oil reservoirs. The Tocito outcrop (Fig. 4) consists of pods of

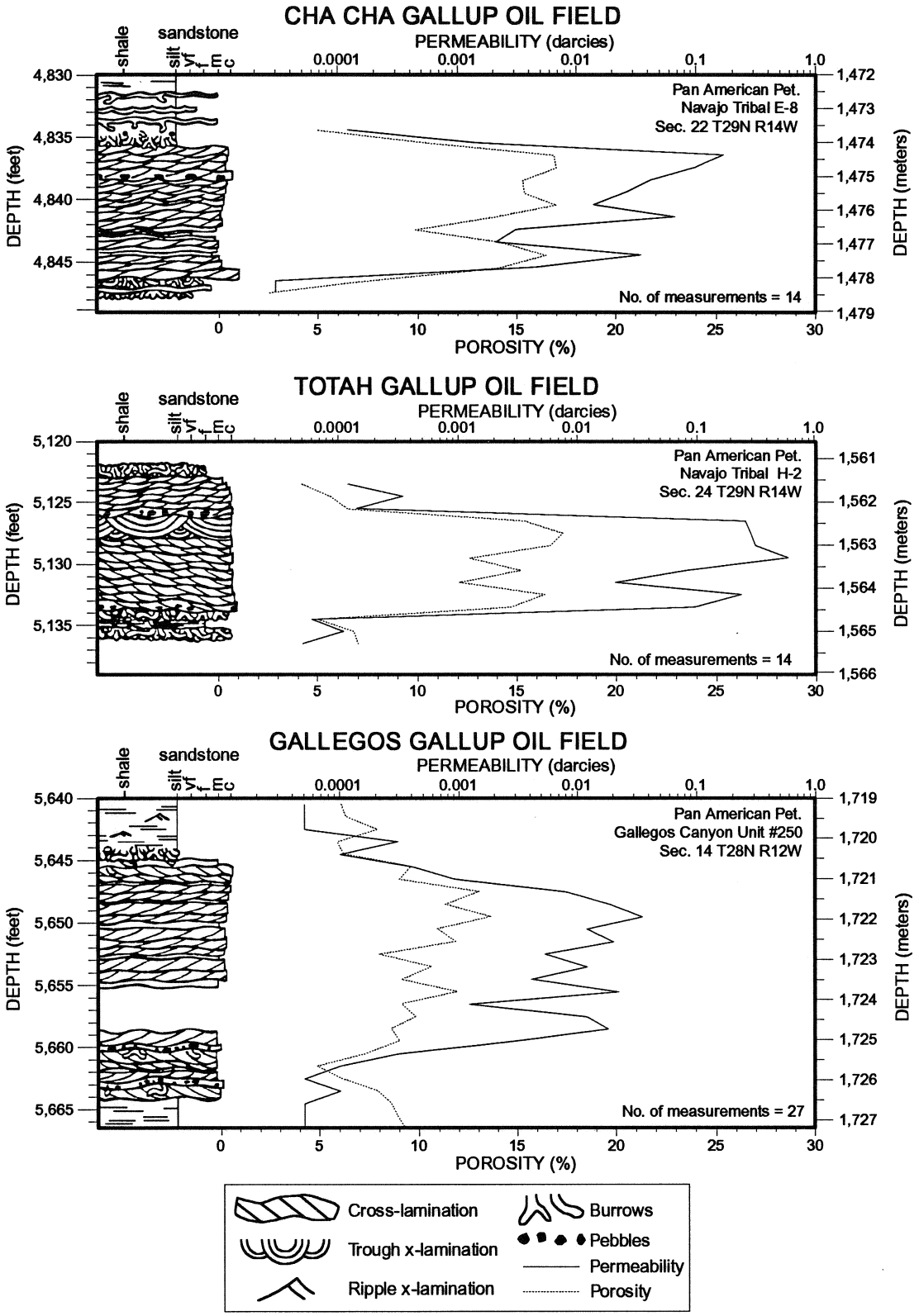

Figure 47 - Permeability and porosity profiles for deep subsurface Tocito Sandstones. Permeability and porosity measurements conducted by Core Laboratories, Inc., Dallas, TX, (Appendix 15) and core descriptions modified from R. Bottjer of Amoco in Denver, CO.

large-scale cross-bedded sandstone lithofacies surrounded by medium-scale cross-bedded sandstone lithofacies. The medium-scale cross-bedded sandstones commonly rest upon muddy bioturbated sandstone lithofacies, or interfinger with and are encased by interbedded sandstone and mudstone lithofacies. Ripple cross-laminated sandstones cap the interbedded sandstone and mudstone lithofacies. This entire package of sandstones and mudstones is then encased in the Mancos Shale. Viewed as a whole, the combined suite of lithofacies generates a permeability trend which increases towards the center of the sandstone body.

Quartz overgrowths, though rarely exceeding 5%, are most abundant in mudstone-poor lithologies (Appendices 6 and 7), suggesting that the mud-poor sediments were conduits for silica-bearing pore fluids. The small volume, but ubiquitous nature, of the overgrowths suggests a pervasive presence of limited quantities of silica ions.

When carbonate-bearing pore waters were expelled from the Mancos Shale and entered the Tocito Sandstone, they first passed through the muddy bioturbated and ripple cross-laminated sandstones, where alkaline conditions existed due to the decay of organic material. Alkaline conditions favored calcite cementation in these outer sandstone lithofacies, which significantly reduced permeability (Fig. 29). As the pore waters continue to migrate and enter the interbedded lithofacies, they were channelized through the sandstone interbeds by the mudstone interbeds, both of which may penetrate deep into the sandstone body (Fig. 4). Because these mudstone interbeds were organic-rich, calcite cementation occurred, further depleting the pore waters of carbonate ions. Not all sandstone interbeds are in communication with the Mancos Shale, however. Many sandstone beds pinch out and have mudstone drapes sealing them from surrounding sandstone beds (Figs. 24, 42). Such beds received minor volumes of pore water and thus experienced little cementation.

By the time pore waters percolated into the medium- and large-scale cross-bedded sandstone lithofacies, the ion concentration was probably low. Even if a large volume of pore water passed through the highly permeable cross-bedded sandstone lithofacies, the ion concentrations may have been naturally depleted. Any cementation that occurred existed near the organic-rich mudstone drapes along the toesets or the top of the cross-bedded sandstones (Figs. 30, 33, 35).

There is an inverse relationship between quartz overgrowths and calcite cement (Appendices 6 and 7), suggesting that the restriction of pore throats by overgrowths may have significantly reduced the flux of ion-bearing fluids through some sandstone beds, and therefore limited calcite cementation.

APPLICATION TO HYDROCARBON RECOVERY

Only a few of the Tocito Sandstone oil reservoirs have undergone secondary recovery programs. These have generally been unsuccessful or have had limited success. The estimated initial recovery for the Bisti Carson Unit was 16% of the original oil in place (6,015,000 barrels of oil) (Collins, 1987). A waterflood was initiated in an attempt to repressurize the reservoir and drive an oil bank from the injection wells to the producing wells. The waterflood was unsuccessful, the poor performance was attributed to rapid water breakthrough due to fractures and/or differential permeabilities parallel to the length of the reservoir. Oil retained in the lower permeability intervals was bypassed as water flowed through the more permeable zones. The Cha Cha, Horseshoe and Totah oil fields had similar problems (Matheny, 1987a, 1987b; McEachin and Royce, 1987). The Blanco Tocito South oil field is a notable exception. The field's estimated primary recovery was 12% of the original oil in place (1,680,000 barrels of oil) and the estimated

ultimate recovery after waterflooding was 40% (5,600,000 barrels of oil; Fassett and Jentgen, 1987).

From observations made in this study, there are at least four scales of permeability heterogeneity within the Tocito Sandstone that account for the poor waterflood results. On a megascopic-scale (oil field-wide scale), the Tocito is characterized by interwoven lithofacies with very different porosities and permeabilities. Lithofacies of very high permeability (cross-bedded sandstone) lie among lithofacies with highly variable permeabilities (interbedded sandstones and shales). At the base of the Tocito is the low-permeability muddy bioturbated sandstone lithofacies and capping the Tocito is the low-permeability ripple cross-laminated sandstone lithofacies. Water injected into a Tocito reservoir would take the path of least resistance, sweeping oil through the cross-bedded sandstone lithofacies and portions of the interbedded lithofacies and bypassing oil retained in the lower permeability lithofacies.

Macroscopic-scale (well-to-well scale) heterogeneities have the most influence on hydrocarbon production in the Tocito Sandstone. In particular, mudstone drapes effectively compartmentalize the medium-scale cross-bedded sandstone lithofacies and separate it from large-scale cross-bedded sandstone lenses. A well that penetrates and drains three or four stacked sandstone compartments will not drain adjacent compartments. If converted to an injection well, water or steam will not sweep the adjacent compartments. Shale beds within the interbedded sandstone and shale lithofacies have also compartmentalized the intercalated sandstone units, so that well-cemented sandstone intervals are adjacent to poorly-cemented sandstone intervals. Because of the extremes in permeability, water injected into such lithofacies would sweep the poorly-cemented sandstone beds and bypass oil in less permeable sandstone intervals.

Heterogeneities on the mesoscopic scale (lamination and cross-bed scale) will locally influence hydrocarbon recovery due to thin mudstone drapes on foresets, bioturbation,

and local cementation. Overall, however, this influence is negligible on a well-to-well or field-wide scale. Microscopic-scale heterogeneities govern the nature of oil saturation and the retention of residual oil in the Tocito Sandstone, but also have negligible controls on a well-to-well basis.

As seen in both the outcrop and subsurface core (HOF #2, Solar Petr. Navajo Tribal F-151), sandstone beds in the interbedded sandstone and shale lithofacies may be well cemented although adjacent sandstones beds are porous and permeable. Since injected water tends to follow the easiest path of flow, the effectiveness of water injection decreases with time when dealing with adjacent intervals with contrasting permeabilities. Using geologic and geophysical information, bypass zones (those beds with high permeabilities) can be delineated so that less permeable intervals are perforated for water or chemical injection. This may be coupled with introducing polymers that help seal the high permeability zones. In addition, stacked cross-bedded sandstone units all dip in the same direction (downcurrent, Figs. 4, 33-36), so a horizontal well may penetrate more compartments than a vertical well, thus increasing the drainage area per well and reducing the number of wells needed to drain the reservoir.

FUTURE WORK

This study has developed a data base which allows development of a field-scale model on sandstone facies distributions and their influence on diagenetic alterations and the migration and drainage of oil from a sandstone lentil reservoir. Complete vertical transects through the Tocito Sandstone outcrop in the Hogback oil field and lateral transects through each lithofacies at a well-to-well lateral scale are needed. With a larger data set that includes measurements taken at a well-to-well scale, a more comprehensive geostatistical evaluation of permeability structure within the Tocito outcrop can be made.

CONCLUSIONS

The mechanical field permeameter and the computer-controlled scanning minipermeameter provide reliable data from both outcrop and core. They are an inexpensive, nondestructive, and rapid means of acquiring permeability measurements on a scale much finer than commonly made with core plugs.

Lithofacies are the fundamental control on porosity and permeability heterogeneity in the Tocito Sandstone. Medium- to large-scale cross-bedded sandstone lithofacies have the highest porosities and permeabilities, interbedded sandstone and mudstone lithofacies have intermediate values, and muddy bioturbated sandstone and ripple cross-laminated sandstone lithofacies have the lowest porosities and permeabilities.

Mudstone drapes and shale beds compartmentalize sandstone reservoirs, channelize pore fluids, and encourage cementation by developing locally alkaline conditions during decay of organic material. Burrows initially increased vertical permeability by piercing the impermeable mudstone drapes. The burrows then became conduits for pore fluids which precipitated cement in the organic-rich burrows.

Isotopic measurements of calcite cements in the Tocito Sandstone outcrop, Hogback oil field, indicate that the cements precipitated from trapped seawater mixed with meteoric water. The later-stage cement is more enriched in $\delta^{18}O$ than the early-stage cement and precipitated at lower temperatures during regional uplift.

Porosity and permeability trends observed in outcrop reflect subsurface conditions. Both the Tocito Sandstone outcrops and the subsurface cores have similar suites of lithofacies, similar hierarchies in relative permeability, and similar permeability trends. Present porosity in the sandstones is a combination of primary (incomplete calcite cementation), and secondary (feldspar and chert dissolution, vertical fracturing) porosity. The Tocito outcrop has experienced two episodes of calcite cementation, whereas the

subsurface has experienced only one episode. In addition, Tocito outcrop samples and shallow subsurface core samples have significantly higher porosities and permeabilities than the subsurface Tocito samples, due to decompression during uplift and overburden removal and the additional leaching of framework-grains by meteoric water.

REFERENCES CITED

Ali, M., 1993, Small scale heterogeneities in permeability: A correlative study of permeability and corresponding pore morphologies using minipermeameter and petrographic analysis, M. Sc. thesis: New Mexico Institute of Mining and Technology, Socorro, New Mexico, 135 p.

Barton, M.D., and N. Tyler, 1991, Quantification of permeability structure in distributary-channel deposits, Ferron Sandstone, Utah, *in* T.C. Chidsey Jr., ed., Geology of East-Central Utah, 1991 field symposium: Utah Geological Association, publication 19, p. 273-281.

Bergsohn, I., and D. Nummedal, 1988, Facies architecture of Tocito shelf sandstone, northwest New Mexico: American Association of Petroleum Geologists Bulletin, v. 72, p. 161.

Bjϕrlykke, K., 1988, Sandstone diagenesis in relation to preservation, destruction and creation of porosity, *in* G.V. Chilingarian and K.H. Wolf, eds., Diagenesis I. Developments in Sedimentology 41: New York, Elsevier, p. 531-565.

Blatt, H., G.V. Middleton, and R.C. Murray, 1972, Origin of sedimentary rocks: Prentice-Hall, Englewood Cliffs, N.J., 634 p.

Boles, J.R., C.A. Landis, and P. Dale, 1985, The Moeraki boulders - anatomy of some septarian concretions: Journal of Sedimentary Petrology, v. 55, p. 398-406.

Bond, W.A., 1984, Application of Lopatin's method to determine burial history, evolution of the geothermal gradient, and timing of hydrocarbon generation in Cretaceous source rocks in the San Juan Basin, northwestern New Mexico and southwestern Colorado, *in* Woodward, J., F.F. Meissner, and J.L. Clayton, eds., Hydrocarbon source rocks of the Greater Rocky Mountain Region: Rocky Mountain Association of Geologists, Denver, CO, p. 433-447.

Bottjer, R.J., 1992, Multiple submarine erosion surfaces and the origin of the Tocito Sandstone, San Juan Basin, New Mexico, Society of Economic Paleontologists and Mineralogists, Mesozoic of the Western Interior Ft. Collins, Colorado, August 1992, Abstracts, p. 14.

Bryant I.D., J.D. Kantorowicz and C.F. Love, 1988, Depositional and diagenetic models to explain origin of laterally continuous carbonate cemented layers, upper Lias sands, southern England: American Association of Petroleum Geologists Bulletin, v. 72, p. 166.

Campbell, C.V., 1979, Model for beach shoreline of Gallup Sandstone (Upper Cretaceous) of northwestern New Mexico: New Mexico Bureau of Mines and Mineral Resources Circular 164, 25 p.

Chandler, M.A., D.J. Goggin, and L.W. Lake, 1989, A mechanical field permeameter for making rapid, non-destructive, permeability measurements: Journal of Sedimentary Petrology, v. 59, no. 4, p. 613-635.

Cole, R.D., and C.E. Mullen, 1992, Sedimentologic reservoir characterization of Tensleep Sandstone, South Casper Creek field, Wyoming, *in* Wyoming Geological Association 43rd field conference guidebook, p. 121-137.

Collins, C.O., 1987, Bisti Carson Unit Gallup, *in* J.E. Fassett, N.D. Thomaidis, M.L. Matheny, and R.A. Ullrich, eds., Oil and Gas Fields of the Four Corners Area, volume 1: Four Corners Geological Society, p. 209-212.

Daws, J.A. and D.J. Prosser, 1992, Scales of permeability heterogeneity within the Brent Group: Journal of Petroleum Geology, v. 15, no. 4, p. 397-418.

Dickson, J.A.D., 1966, Carbonate identification and genesis as revealed by staining: Journal of Sedimentary Petrology, v. 36, p. 491-505.

Dutton, S.P., and T.N. Diggs, 1992, Evolution of porosity and permeability in the Lower Cretaceous Travis Peak Formation, East Texas: American Association of Petroleum Geologists Bulletin, v. 76, no. 2, p. 252-269.

Emmett, W.R., K.W. Beaver, and J.A. McCaleb, 1971, Little Buffalo Basin Tensleep heterogeneity - Its influence on infill drilling and secondary recovery: Journal of Petroleum Technology, Feb. 1971, p. 161-168.

Fassett, J.E., 1985, Early Tertiary paleogeography and paleotectonics of the San Juan Basin area, New Mexico and Colorado, *in* Flores, R.M., and Kaplin, S.S., eds., Cenozoic paleogeography of the west-central United States: Society of Economic Paleontologists and Mineralogists, Rocky Mountain Section, p. 317-334.

Fassett, J.E., and R.W. Jentgen, 1987, Blanco Tocito, South, *in* J.E. Fassett, N.D. Thomaidis, M.L. Matheny, and R.A. Ullrich, eds., Oil and Gas Fields of the Four Corners Area, volume 1: Four Corners Geological Society, p. 233-240.

Fassett, J.E., N.D. Thomaidis, M.L. Matheny, and R.A. Ullrich, 1987, Oil and Gas Fields of the Four Corners Area, v. 1 and 2: Four Corners Geological Society, 727 p.

Fisher, W.L., 1987, Can the U.S. oil and gas resource base support sustained production?: Science, v. 236, p. 1631-1636.

Folk, R.L., 1968, Petrology of sedimentary rocks: Austin, Texas, Hemphill's Book Store, 170 p.

Friedman, I., and J.R. O'Neil, 1977, Compilation of stable isotope fractionation factors of geochemical interest (Data of Geochemistry, Sixth Edition, Chapter KK): United States Geological Survey Professional Paper 440-KK, 12 p.

Gautier, D.L., 1985, Interpretation of early diagenesis in ancient marine sediments, *in* Gautier, D.L., Y.K. Kharaka and R.C. Surdam, eds., Relationship of Organic Matter and Mineral Diagenesis, short course no. 17: Society of Economic Paleontologists and Mineralogists, p. 6-72.

Goggin, D.J., M.A. Chandler, G. Kocurek, and L.W. Lake, 1988a, Patterns of permeability in eolian deposits: Page Sandstone (Jurassic), northeastern Arizona: Society of Petroleum Engineers Formation Evaluation, p. 297-306.

Goggin, D.J., R.L. Thrasher, and L.W. Lake, 1988b, A theoretical and experimental analysis of minipermeameter response including gas slippage and high velocity flow effects: In Situ, v. 12, no. 1 & 2, p. 79-116.

Harris, N.B., 1989, Reservoir geology of Fangst Group (Middle Jurassic), Heidrun Field, offshore mid-Norway: American Association of Petroleum Geologists Bulletin, v. 73, p. 1415-1435.

Heller, J.P., 1992, The PRRC Automatic Scanning Minipermeameter: New Mexico Petroleum Recovery Research Center Paper 92-20.

Hennessy, J., and L.P. Knauth, 1985, Isotopic variations in dolomite concretions from the Monterey Formation, California: Journal of Sedimentary Petrology, v. 55, p.120-130.

Hesse, R., 1989, Early diagenetic pore water/sediment interaction, modern offshore basins, *in* I.A. Mclireath and D.W. Morrow, eds., Diagenesis: Geoscience Canada reprint series 4, p. 277-315.

Hudson, J.D., 1978, Concretions, isotopes, and the diagenetic history of the Oxford Clay (Jurassic) of central England: Sedimentology, v. 25, p. 339-370.

Huffman, A.C. Jr., 1987, Petroleum geology and hydrocarbon plays of the San Juan Basin petroleum province: United States Geological Survey Open-File Report #87-450 B, 67 p.

Huffman, A.C. Jr., and D.J. Taylor, 1989, San Juan Basin faulting - More than meets the eye (abs.): American Association of Petroleum Geologists, Bulletin, v. 73, p. 1161.

Hunt, A.P., and S.G. Lucas, 1992, Stratigraphy, paleontology and age of the Fruitland and Kirtland Formations (Upper Cretaceous), San Juan Basin, New Mexico, *in* S.G. Lucas, B.S. Kues, T.E. Williamson, and A.P. Hunt, eds., San Juan Basin IV: New Mexico Geological Society 43rd annual field conference, September 30-October 3, 1992, p. 217-239.

Jennette, D.C., Jones, C.R., van Wagoner, J.C., and Larsen, J.E., 1991, High-resolution sequence stratigraphy of the Upper Cretaceous Tocito Sandstone: The relationship between incised valleys and hydrocarbon accumulation, San Juan Basin, New Mexico, *in* J.C. Van Wagoner, C.R. Jones, D.R. Taylor, D. Nummedal, D.C. Jennette, and G.W. Riley, eds., Sequence stratigraphy applications to shelf sandstone reservoirs; Outcrop to subsurface examples: American Association of Petroleum Geologists Field Conference September 21-28, 1991, p.7-24 to 7-62.

Jones, C.R., J.C. Van Wagoner, D.C. Jennette, D. Nummedal, and G.W. Riley, 1991, Road log, day six: Sequence stratigraphy and facies architecture of the Torrivio and Tocito Sandstones near Beautiful Mountain, Four Corners Platform, northwestern

New Mexico, *in* J.C. Van Wagoner, C.R. Jones, D.R. Taylor, D. Nummedal, D.C. Jennette, and G.W. Riley, eds., Sequence stratigraphy applications to shelf sandstone reservoirs; Outcrop to subsurface examples: American Association of Petroleum Geologists Field Conference September 21-28, 1991, p.6-1 to 6-11.

Jones, J.R., A.J. Scott, and L.W. Lake, 1984, Reservoir characterization for numerical simulation of Mesaverde Meanderbelt Sandstone, northwestern Colorado: Society of Petroleum Engineers Paper 13052, 14 p.

Jordan, D.W., and W.A. Pryor, 1992, Hierarchical levels of heterogeneity in a Mississippi River meander belt and application to reservoir systems: American Association of Petroleum Geologists Bulletin, v. 76, no. 10, p. 1601-1624.

Kilmer, N.H., N.R. Morrow, and J.K. Pitman, 1987, Pressure sensitivity of low permeability sandstones: Journal of Petroleum Science and Engineering, v. 1, Elsevier Science Publishers B.V., Amsterdam, p. 65-81.

Kittridge, M.G., L.W. Lake, F.J. Lucia, and G.E. Fogg, 1990, Outcrop/subsurface comparisons of heterogeneity in the San Andres Formation: Society of Petroleum Engineers Formation Evaluation, p. 233-240.

Kofron, B.M., 1987, Facies characteristics of the Upper Cretaceous Tocito Sandstone, San Juan Basin, New Mexico, M.S. thesis: Louisiana State University, Baton Rouge, 104 p.

Lamb, G.M., 1968, Stratigraphy of the Lower Mancos Shales in the San Juan Basin: Geological Society of America Bulletin, v. 79, p.827-854.

Law, B.E., 1992, Thermal maturity patterns of Cretaceous and Tertiary rocks, San Juan Basin, Colorado and New Mexico: Geological Society of America Bulletin, v. 104, p. 192-207.

Lawrence, J.R., and J.M. Gieskes, 1981, Constraints on water transport and alteration in the oceanic crust from isotopic composition of pore water: Journal of Geophysical Research, v. 86, p. 7924-7934.

Longstaffe, F.J., 1984, The role of meteoric water in diagenesis of shallow sandstones: Stable isotope studies of the Milk River Aquifer and Gas Pool, southeastern Alberta, *in* D.A. McDonald and R.C. Surdam, eds., Clastic diagenesis: American Association of Petroleum Geologists Memoir 37, p. 81-98.

Matheny, M.L., and J.P. Matheny, 1987, Cha Cha Gallup, *in* J.E. Fassett, N.D. Thomaidis, M.L. Matheny, and R.A. Ullrich, eds., Oil and Gas Fields of the Four Corners Area, volume 1: Four Corners Geological Society, p. 256-259.

Matheny, M.L., and J.P. Matheny, 1987, Totah Gallup, *in* J.E. Fassett, N.D. Thomaidis, M.L. Matheny, and R.A. Ullrich, eds., Oil and Gas Fields of the Four Corners Area, volume 2: Four Corners Geological Society, p. 535-537.

McCubbin, D.G., 1969, Cretaceous strike valley sandstone reservoirs, northwestern New Mexico: American Association of Petroleum Geologists, v. 53, p. 2114-2140.

McEachin, W.D., and Royce, R.M., 1987, Horseshoe Gallup, *in* J.E. Fassett, N.D. Thomaidis, M.L. Matheny, and R.A. Ullrich, eds., Oil and Gas Fields of the Four Corners Area, volume 2: Four Corners Geological Society, p. 335-337.

Meissner, F.F., 1987, Mechanisms and patterns of gas generation, storage, expulsion-migration, and accumulation associated with coal measures, Green River and San Juan Basins, Rocky Mountain Region, USA, *in* B. Doligez, ed., Migration of Hydrocarbons in Sedimentary Basins, Inst. Fr. Pet., Rueil-Malmaison, France, p. 79-112.

Miall, A.D., 1991, Hierarchies of architectural units in terrigenous clastic rocks, and their relationship to sedimentation rate, *in* A.D. Miall and N. Tyler, eds., The three-dimensional facies architecture of terrigenous clastic sediments and its implications for hydrocarbon discovery and recovery, Concepts in Sedimentology and Paleontology, v. 3: Society of Economic Paleontologists and Mineralogists, p. 6-12.

Molenaar, C.M., 1973, Sedimentary facies and correlation of the Gallup Sandstone and associated formations, northwestern New Mexico: Four Corners Geological Society, p. 85-110.

Molenaar, C.M., 1983a, Major depositional cycles and regional correlations of Upper Cretaceous rocks, southern Colorado Plateau, *in* N.W. Reynolds and E.D. Dolly (eds.), Mesozoic Paleogeography of West Central United States: Rocky Mountain Section of SEPM Symposium, No. 2, p. 201-224.

Molenaar, C.M., 1983b, Principal reference section and correlation of Gallup Sandstone, northwestern New Mexico, *in* Contributions to Mid-Cretaceous Paleontology and Stratigraphy of New Mexico, Part II: New Mexico Bureau of Mines and Mineral Resources Circular, v. 185, p. 29-40.

Molenaar, C.M., 1988, Cretaceous and Tertiary rocks of the San Juan Basin, *in* Barrs, D.L., Chapter 8, Basins of the Rocky Mountain region, *in* L.L. Sloss, ed., Sedimentary cover - North American craton, U.S.; Boulder, Colorado, Geological Society of America, The Geology of North America, v. D-2, p. 129-134.

Mozley, P.S., and S.J. Burns, 1993, Oxygen and carbon isotopic composition of marine carbonate concretions: An overview: Journal of Sedimentary Petrography, v. 63, no. 1, p. 73-83.

Mozley, P.S., and W.W. Carothers, 1992, Elemental and isotopic composition of siderite in the Kuparuk Formation, Alaska: Effect of microbial activity and water/sediment interaction on early pore-water chemistry: Journal of Sedimentary Petrology, v. 62, no. 4, p. 681-692.

Nummedal, D., 1988, Sequence stratigraphic analysis of Upper Turonian and Coniacian strata in the San Juan Basin, New Mexico, USA, *in* R.N. Ginsburg and B. Beaudoin, eds., Cretaceous resources, events, and rhythms; background and plans for research: NATO Advanced Study Institutes Series, series C, Mathematical and Physical Sciences. 304. p. 33-46.

Nummedal, D., and G.W. Riley, 1991, Origin of late Turonian and Coniacian unconformities in the San Juan Basin, *in* J.C. Van Wagoner, C.R. Jones, D.R. Taylor, D. Nummedal, D.C. Jennette, and G.W. Riley, eds., Sequence stratigraphy applications to shelf sandstone reservoirs; Outcrop to subsurface examples: American Association of Petroleum Geologists Field Conference September 21-28, 1991, p.7-63 to 7-74.

Nummedal, D., R. Wright, D.J.P. Swift, R.W. Tillman, and R.W. Wolter, 1989, Depositional systems architecture of shallow marine sequences, *in* D. Nummedal and R. Wright, eds., Cretaceous Shelf Sandstones and Shelf Depositional Sequences, 28th International Geological Congress Field Trip, p. 35-73.

Nummedal D., and R. Wright, 1989, Cretaceous shelf sandstones and shelf depositional sequences, western interior basin, Utah, Colorado and New Mexico: American Geophysical Union field trip guidebook T119.

Odin, G.S., and A. Matter, 1981, De glauconiarum origine: Sedimentology, v. 28, p. 611-641.

Pasley, M.A., W.A. Gregory, and G.F. Hart, 1991, Organic matter variations in transgressive and regressive shales: Organic Geochemistry, v. 17, no. 4, p. 483-509.

Pasley, M.A., G.W. Riley and D. Nummedal, 1989, Stratigraphic significance of organic matter variations; example from Mancos Shale and Tocito Sandstone, San Juan Basin, New Mexico: American Association of Petroleum Geologists Bulletin, v. 73, p. 1169-1170.

Penttila, A.G., 1964, Evidence for the pre-Niobrara unconformity in the northwestern part of the San Juan Basin: Mountain Geologist, v. 1, p. 3-14.

Pettijohn, F.J., P.E. Potter, and R. Siever, 1973, Sand and Sandstone: Springer-Verlag Berlin, Heidelberg, 618 p.

Powers, R.B., 1993, Petroleum exploration plays and resource estimates, 1989, onshore United States; Region 3, Colorado Plateau and Basin and Range: United States Geological Survey Open-File Report #93-248, 111 p.

Pryor, W.A., 1975, Biogenic sedimentation and alteration of argillaceous sediments in shallow marine environments: Geological Society of America Bulletin, v. 86, p. 1244-1254.

Reeside, J.B., Jr., 1924, Upper Cretaceous and Tertiary formation of the western part of the San Juan Basin, Colorado and New Mexico: United States Geological Survey Bulletin 767, 53 p.

Rice, D.D., 1983, Relation of natural gas composition to thermal maturity and source rock type in San Juan Basin, northwestern New Mexico and southwestern Colorado: American Association of Petroleum Geologists Bulletin, v. 67, no. 8, p. 1199-1218.

Riley, G.W., 1993, Origin of a coarse-grained shallow marine sandstone complex: Coniacian Tocito Sandstone, Northwestern New Mexico, PhD. dissertation: Louisiana State University, Baton Rouge, LA, 251 p.

Riley, G.W., and D. Nummedal, 1989, Facies architecture of tidal shelf sandstone ridge: Tocito Sandstone: American Association of Petroleum Geologists Bulletin, v. 73, p. 1172.

Riley, G.W., and D. Nummedal, 1992, The Tocito Sandstone; a tectonically-induced tide-dominated delta and transgressive shelf sandstone complex: Mesozoic of the Western Interior, SEPM 1992 theme meeting abstracts, p. 56.

Sabins, F.F. Jr., 1963, Anatomy of a stratigraphic trap, Bisti field, New Mexico: American Association of Petroleum Geologists Bulletin, v. 47, p. 193-228.

Sabins, F.F. Jr., 1972, Comparison of Bisti and Horseshoe Canyon Stratigraphic Traps, San Juan Basin, New Mexico, *in* R.E. King, ed., Stratigraphic oil and gas fields - classification, exploration methods, and case histories: American Association of Petroleum Geologists Memoir 16 and Society of Exploration Geophysicists Special Publication No. 10, p. 610-622.

Schmidt, V., and D.A. McDonald, 1979, Secondary reservoir porosity in the course of sandstone diagenesis, Education course note series no. 12, American Association of Petroleum Geologists, 125 p.

Sears, J.D., 1925, Geology and fuel resources of the Gallup-Zuni basin, New Mexico, U.S.G.S. Bulletin 767, 53 p.

Siebert, R.M., G.K. Moncure, and R.W. Lahann, 1984, A theory of framework-grain dissolution in sandstones, *in* D.A. McDonald and R.C. Surdam, eds., Clastic diagenesis: American Association of Petroleum Geologists Memoir 37, p. 163-175.

Shackleton, N.J., and J.P. Kennett, 1975, Late Cenozoic oxygen and carbon isotopic changes at DSDP site 284: implications for glacial history of the Northern Hemisphere, *in* J.P. Kennett, R.E. Houtz, et al., eds., Initial reports of the Deep Sea Drilling Project, v. 29: United States Government Printing Office, p. 801-807.

Sheppard, S.M.F., 1986, Characterization and isotopic variations in natural waters, *in* J.W. Valley, H.P. Taylor, Jr., and J.R. O'Neil, eds., Stable isotopes in high temperature geological processes: Mineralogical Society of America, Reviews in Mineralogy v. 16, p. 165-183.

Stalkup, F.I., and W.J. Ebanks Jr., 1986, Permeability variation in a sandstone barrier island-tidal delta complex, Ferron Sandstone (Lower Cretaceous), central Utah: Society of Petroleum Engineers Paper 15532, p. 1-8.

Steven, T.A., 1975, Middle Tertiary volcanic field in the southern Rocky Mountains, *in* B.F. Curtis, ed., Cenozoic history of the southern Rocky Mountains: Geological Society of America Memoir 144, p. 75-94.

Sultan, A.J., and J.P. Heller, 1989, Rock heterogeneity and geostatistical methods: New Mexico Petroleum Recovery Research Center Paper 89-9, 43 p.

Thomas, R.D., and D.C. Ward, 1971, Effect of overburden pressure and water saturation on gas permeability of tight sandstone cores: Society of Petroleum Engineers Journal of Petroleum Technology, p. 120-124.

Tillman, R.W., 1985a, The Tocito and Gallup Sandstones, New Mexico, a comparison, *in* R.W. Tillman, D.J.P. Swift, and R.G. Walker, eds., Shelf Sands and Sandstone Reservoirs, short course notes 13: Society of Economic Paleontologist and Mineralogists, p. 403-463.

Tillman, R.W., 1985b, Tocito Sandstone core, Horseshoe field, San Juan county, New Mexico, *in* R.W. Tillman, D.J.P. Swift, and R.G. Walker, eds., Shelf Sands and Sandstone Reservoirs, short course notes 13: Society of Economic Paleontologist and Mineralogists, p. 559-576.

Tyler, N., and R.J. Finley, 1991, Architectural controls on the recovery of hydrocarbons from sandstone reservoirs, *in* A.D. Miall and N. Tyler, eds., The Three-Dimensional Facies Architecture of Terrigenous Clastic Sediments and its Implications for Hydrocarbon Discovery and Recovery, Concepts in Sedimentology and Paleontology, Volume 3: Society of Economic Paleontologist and Mineralogists, p. 1-5.

Ward, A.W., 1990, Geologic map emphasizing the surficial deposits of the Farmington 30' X 60' quadrangle, New Mexico and Colorado: U.S. Geological Survey Miscellaneous Investigations Series, Map I-1978, 1 sheet [scale 1:100,000].

Williamson, T.E., and S.G. Lucas, 1992, Stratigraphy and mammalian biostratigraphy of the Paleocene Nacimiento Formation, southern San Juan Basin, New Mexico, *in* S.G. Lucas, B.S. Kues, T.E. Williamson, and A.P. Hunt, eds., San Juan Basin IV: New Mexico Geological Society 43rd annual field conference, September 30-October 3, 1992, p. 265-296.

Weber, K.J., 1986, How heterogeneity affects oil recovery, *in* Lake, L.W., and Carroll, H.B.J., eds., Reservoir Characterization: Academic Press, New York, p. 487-544.

APPENDICES

Appendix 1. Method of construction of burial history plot.

Thickness of overlying strata

Because the Tocito Sandstone crops out in the Hogback oil field, there is no way of directly measuring the thickness of strata that had once overlain the sandbodies. An estimation, however, was made from "scout cards" by recording depths at which each post-Tocito formation was encountered in twenty boreholes of nearby and basinward wells. Well data used to construct the burial history plot are listed in Appendix 2a. Since all of the Tertiary sediments have been removed by uplift and erosion, the speculated average thicknesses of Paleocene to Pleistocene sediments were obtained from Steven (1975), Rice (1983), Bond (1984), Huffman (1987), Meissner (1987), Molenaar (1988), Ward (1990), Jennette et al. (1991), Hunt and Lucas (1992), Law (1992), and Williamson and Lucas (1992). Published data used to construct the burial curve are given in the Appendix 2b.

The burial history curve was then constructed by orienting the Tocito Sandstone at a point in which "TIME" is 87 million years ago (m.y.a.) and DEPTH is zero meters (deposition at the sediment/water interface). Burial of the Tocito through time is then represented by sequentially adding the thickness of increasingly younger strata during their corresponding "TIME" of deposition. The net result is a falling burial profile line. When uplift and erosion remove sediment, then an estimated thickness is subtracted from the overburden and the result is a climbing burial profile line.

Paleogeothermal gradients

The thermal maturity pattern is well known throughout much of the San Juan Basin as many authors (e.g., Rice, 1983; Bond, 1984; Huffman, 1987; Meissner, 1987; Law, 1992) have acquired vitrinite-reflectance (R_0) and coal rank data from the Dakota and

Fruitland Formations. However, no geochemical data has been gathered from the region near the Hogback oil field. Pasley et al. (1991) acquired pyrolysis data from the Tocito Sandstone outcrop, but the organic material collected was adversely affected by outcrop weathering. Bond (1984) and Law (1992) have plots of vitrinite reflectance (R_0) gathered from the Fruitland Formation and the Dakota Sandstone for much of the central to northern San Juan Basin. Trends of the plotted data demonstrate a decrease in thermal maturity radially away from the San Juan Mountains. If this trend is projected to the Hogback oil field, then the thermal maturity of the Tocito outcrop will be similar to that of the Cretaceous strata used in Huffman's (1987) burial diagram for the south-central San Juan Basin (Sec. 12, T23N, R9W). With the assumption that the two locations experienced similar paleogeothermal gradients, the values used by Huffman were adopted. A gradient of 27°C/km (1.5°F/100 ft) was relatively constant up to the end of the Maastrichtian, when it began to steadily increase. The geothermal gradient reached its peak of 36°C/km (2.0°F/100 ft) during the Late Oligocene volcanism. Bond (1984) suggested that the paleogeothermal gradient was higher near the San Juan Mountains, possibly as high as 49° to 80°C/km (2.7° to 4.4°F/100 ft). Since the end of the Oligocene, the thermal gradient is assumed to have steadily decreased to its present value of approximately 27°C/km (1.5°F/100 ft; Huffman, 1987).

Paleogeothermal isotherms were plotted on the burial history curve by calculating the depth at which each would occur prior to the end of the Maestrichtian, during the Late Oligocene volcanism, and at the present time. The orientation of the top of the "oil window" was also adopted from Huffman (1987).

Appendix 2a. Well data used to establish average thicknesses of Cretaceous and Tertiary strata once overlying the Tocito Sandstone outcrop in the Hogback oil field. Measured thicknesses (in feet) for each unit are listed under the appropriate formation name. Well completion card data is from the New Mexico Library of Subsurface Data, New Mexico Bureau of Mines and Mineral Resources, Socorro, New Mexico.

LOCATION (Sec,Tns,Rge)	OPERATOR	WELL NAME	OJO ALAMO	KIRT-LAND	FRUIT-LAND	PICTURED CLIFFS	LEWIS	CLIFF HOUSE	MENEFEE	POINT LOOKOUT	UPPER MANCOS	TOCITO	LOWER MANCOS
13-29N-11W	H.L. Harvey	3 Jones		720 ft									
13-29N-11W	Manana Gas	1-M Ransom	388 ft	784 ft	210 ft								
1-29N-12W	Meridian Oil Inc.	2 Cornell	110 ft	950 ft	287 ft								
1-29N-12W	Tenneco Oil Company	1-E Allen "A"	157 ft	985 ft	237 ft	115 ft	1468 ft	190 ft	574 ft	356 ft	910 ft		
6-29N-12W	Amoco Production Co.	1-E Hutton Gas Com.	110 ft		255 ft	220 ft	1350 ft	415 ft	305 ft	305 ft	1040 ft		
1-29N-14W	Sunray Mid-Continent	2 NM Fed. "I"				200 ft	1345 ft	465 ft	465 ft	320 ft	1000 ft		800 ft
2-29N-14W	Compass Exploration	1 Southwest Mounds				120 ft	878 ft	635 ft	535 ft	613 ft	1024 ft		800 ft
3-29N-14W	Southland Royalty	1 Locke			320 ft	130 ft	1410 ft	477 ft	478 ft	300 ft	935 ft		
6-29N-14W	Sunray Mid-Continent	1 NM Fed "K"			330 ft	203 ft	1344 ft	500 ft	501 ft	223 ft	984 ft		
10-29N-14W	Southland Royalty	1 McWhorter-Duncan			262 ft	170 ft	1339 ft	561 ft	561 ft	300 ft	802 ft		
2-29N-16W	Dan M. Lockie	1 Miller							843 ft	477 ft	1040 ft	108 ft	
3-29N-16W	Erroc Assoc & Martin	1 Stampfel-Martin						629 ft	700 ft	359 ft	942 ft		
4-29N-16W	Stephen H. Kinney	1 Mabel L.									1183 ft	175 ft	
6-29N-16W	Walter Duncan	4 North Hogback "6"										98 ft	481 ft
7-29N-16W	Tiffany Gas	53 USG Section 18											509 ft
10-29N-16W	Zoller & Danneberg	1 Navajo 2025						825 ft	825 ft	238 ft	1332 ft	92 ft	
18-29N-16W	W.C. IMBT	2 Navajo 18											507 ft
23-29N-16W	Zoller & Danneberg	1 Navajo 2024						883 ft	883 ft	226 ft	1333 ft	85 ft	
24-29N-16W	Pure Oil	2 Pure-Sun Navajo 120						554 ft	554 ft	292 ft	1293 ft	64 ft	

Appendix 2b. Published data used to construct the burial history plot.

DEPOSITION		EROSION		BURIAL DEPTH OF TOCITO		END OF EVENT	DURATION	FORMATION NAME	BURIAL TEMPERATURE		SOURCE OF DATA
Feet	Meters	Feet	Meters	Feet	Meters	m.y.b.p.	period/epoch		°F/100 ft	°C/km	see below
				0	0	87.0	mid-late Coniacian	Tocito Sandstone	77	25	6,10
1086	331			-1086	-331	82.2	Santonian	Upper Mancos Sh	93	34	4,10
308	93			-1394	-425	81.9	early Campanian	Point Lookout Ss	98	36	4,10
696	212			-2090	-637	79.2	early Campanian	Menefee Fm	108	42	4,10
524	160			-2614	-797	79.0	middle Campanian	Cliff House Ss	116	47	4,10
771	235			-3385	-1032	77.0	middle Campanian	Chacra	128	53	10
573	175			-3958	-1206	74.4	mid-late Campanian	Lewis Shale	136	58	4,10
173	53			-4131	-1259	74.2	late Campanian	Pictured Cliffs Ss	139	59	4,10
286	87			-4417	-1346	73	late Campanian	Fruitland Fm	143	61	7,10
968	295			-5385	-1641	70	early Maastrichtian	Kirtland Fm	158	69	3,7,8,10
		1073	327	-4312	-1314	65	L. Cretaceous-E. Tertiary		142	60	3,8,10
189	58			-4501	-1372	63	Early Paleocene	Ojo Alamo Ss	145	63	9,10
787	240			-5288	-1612	55	Early-Late Paleocene	Nacimiento Fm	163	72	2,3,5,8,9
		100	30	-5188	-1581	53	L. Paleocene-M. Eocene		163	72	2,3,8
1512	461			-6700	-2042	44	Late Eocene	San Jose Fm	195	90	2,3,5,8
		200	61	-6500	-1981	30	L. Eocene-E. Oligocene		202	95	2,3
0	0			-6500	-1981	26	Late Oligocene	Volcanics	205	96	1,2,3
		6500	1981	0	0	0	Miocene-Recent		77	25	2

SOURCE OF DATA (Detailed listings given in References Cited section):

1) Steven, 1975
2) Bond, 1984
3) Huffman, 1987
4) Molenaar, 1988
5) Ward, 1990
6) Jennette et al., 1991
7) Hunt and Lucas, 1992
8) Law, 1992
9) Williamson and Lucas, 1992
10) Well completion card data

Appendix 3. Petrographic methods used in this study and the sources for thin sections used in diagenetic history of subsurface Tocito Sandstone.

Petrography

Thin sections were impregnated with blue epoxy to differentiate between true porosity and apparent porosity created during thin section preparation. Many of the thin sections provided by Unocal were half stained for potassium feldspar. The author used cathodoluminescence to detect and differentiate potassium feldspar and plagioclase (See section on luminescence). Carbonate cements in selected thin sections were stained with potassium ferrocyanide and alizarin red-s (Dickson, 1966) to identify calcite, dolomite, ferroan calcite, or ferroan dolomite cement.

A Swift automated point-counting device mounted on the stage of a Nikon Optiphot-Pol polarizing microscope was used to study 31 thin sections. Point counts were made on thin sections from the Horseshoe, Cha Cha and Totah oil fields and the HOF #2 and HOF #3 cores. Only observations were made on the thin sections from the Gallegos Canyon #250, Martin Gas Unit #C-1 and the HOF #1 core. For each thin section 300 to 350 point counts were made to quantify the grain types, cement types, matrix and total porosity. One hundred point counts were then made to quantify the different pore types. Microporosity within authigenic and detrital clays was determined by visually estimating the amount of porosity versus the amount of clay within the pore or detrital grain at 40X magnification. For example, if a cluster of kaolinite grains was so dense that no blue epoxy could be detected, the microporosity was estimated as being from 0 to 5%. On the other hand, if kaolinite appeared as patchy swaths of pale grey-white color within blue epoxy, microporosity was estimated at 75%. Such estimations were more easily done on partially dissolved framework-grains, such as chert. Observations were made on approximately 50 additional thin sections made from hand specimens sampled from

permeability grids in the outcrop. Photomicrographs were taken of representative textures and grains using a Nikon Microflex AFX photomicrograph attachment.

Scanning Electron Microscope

A Hitachi High-Scan HHS-2R scanning electron microscope (SEM), operated by the Materials and Metallurgical Engineering Department at New Mexico Tech, was used in this study. A total of six small chips, approximately 64 mm^3 in size, were sampled from shallow core (HOF #2, 53.0'; HOF #3, 53.4'; and HOF #3, 79.5') and from outcrops (hand specimens Tocito #2, Tocito #17 and Tocito #18) within the Hogback oil field. They were mounted on metal stubs and coated with a very thin layer (approximately 25Å thick) of gold and palladium.

Cathodoluminescence

Well-cemented outcrop samples were first stained with potassium ferrocyanide and alizarin red-s to determine the presence or absence of Fe^{2+} or Fe^{3+} (a common "cathodoluminescence-quencher") within the calcite cement. Once the type of cement was identified, 41 unstained and partially-stained billets and thin sections were selected from the tested samples and analyzed with a Nuclide ELM-3R series cathodoluminoscope hooked to an Olympus BH-2 polarizing microscope. Samples were placed in a vacuum chamber under a 60-80 millitorr vacuum and struck with a 0.5 Ma, 12-15 Kv cathode beam. The luminoscope also proved useful in determining the quantity and distribution of kaolinite, calcite-replacement of framework-grains, and dissolution textures of framework-grains.

Appendix 3 continued. Sources of thin sections

WELL NAME	ORIGINAL OPERATOR	WELL LOCATION	FIELD NAME	NO. OF SAMPLES	CURRENT REPOSITORY LOCATION
Navajo #F-151	Solar Petr. Inc.	Sec.10 T31N R17W	Horseshoe Gallup	5	USGS Core Research Center, Mail Stop 975, Box 25046, Denver Federal Center, Denver, Colorado 80225-0046 Telephone: (303) 236-1930
Navajo Tribal #E-8	Pan American Petr.	Sec.22 T29N R14W	Cha Cha Gallup	7	Amoco Core Facility Houston, Texas
Navajo Tribal #H-2	Pan American Petr.	Sec.24 T29N R14W	Totah Gallup	4	
Gallegos Canyon #250	Pan American Petr.	Sec.14 T26N R12W	Gallegos Gallup	10	
Martin Gas Unit #C-1	Pan American Petr.	Sec.11 T27N R10W	Basin wildcat	6	Amoco Core Facility, 2980 Huron Street, Denver, Colorado 80202 Telephone: (303) 830-5020
HOF #1	Louisiana State Univ.	Sec.13 T29N R17W	Hogback Dakota	3	New Mexico Library of Subsurface Data New Mexico Bureau of Mines and Mineral Resources, Socorro, New Mexico 87801 Telephone: (505) 835-5202
HOF #2	Louisiana State Univ.	Sec.19 T29N R16W	Hogback Dakota	9	
HOF #3	Louisiana State Univ.	Sec.19 T29N R16W	Hogback Dakota	8	

Appendix 4. Operation and calibration of the mechanical field permeameter and computer-controlled scanning minipermeameter.

Mechanical Field Permeameter

The flow of gas through the mechanical field permeameter (Fig. 5) and the rock specimen was generated by a compressed nitrogen gas cylinder controlled by a two-stage regulator. The gas flux through the system and the outcrop was measured by three different flow tubes (rotameters), each calibrated by the manufacturer for different rates of gas flow (cc/sec). A pressure gauge downstream of the rotameters monitored the pressure of the flow at the point where the probe tip touched the rock's surface.

The equations required for the conversion from flow-tube graduations to cc/sec of gas flow are provided in the manufacturer's manual (not published). Conversions of cc/sec into millidarcies (md) of permeability are discussed in the "Permeability Calculations" section of this report. The effective range of the mechanical field permeameter is approximately 3.0 md to approximately 5000 md.

Calibration of the mechanical field permeameter

Calibration of the mechanical field permeameter took place at the New Mexico Petroleum Recovery Research Center. Calibration was performed on core plugs provided by Unocal of the Pennsylvanian-Permian Tensleep Sandstone in the South Casper Creek field west of Casper, Wyoming. The permeabilities of the core plugs had been previously measured for Unocal using the Hassler Sleeve method. The permeabilities of the core plugs ranged from 0.01 md to 3551 md.

The gas flux through each end of the 2.5 cm (1 inch) diameter core plugs was measured three times, for a total of six measurements per plug. The measurements were then averaged and converted to determine an average gas flow in cc/sec for each core plug. There were commonly significant variations in the permeability measurements of individual plugs due to clay lenses and cementation within the sandstone samples.

Permeability calculations

The average flow rates were converted into permeabilities (in millidarcies) using:

$$k = q_1 \mu P_1 / aG_0(P_1^2 P_0^2/2) * 1.0X10^{10} \qquad \text{(Goggin et al., 1988b)}$$

where:

q_1 = calibrated rotameter reading at P_1
μ = viscosity of nitrogen = $1.78x10^{-5}$ Pa-s
P_1 = tip-seal injection pressure = 5 psi = 119474 Pa
P_0 = ave. atmospheric pressure in Socorro, NM = 85000 Pa
G_0 = Goggin's geometrical factor, $G_0(b_D, \infty) = 4.45$
where
b_D = dimensionless tip-seal thickness = b/a = 4.04
a = internal radius of tip-seal = 0.1308 cm (0.0515 in)
b = external radius of tip-seal = 0.5283 cm (0.208 in)

This equation eliminates the need for numerous calibrations of different mechanical field permeameters with different probe tips at different injection pressures. Instead, Goggin et al. (1988b) proposed a geometrical factor, G_0, that is a function of tip-seal ratio and the dimensions of the sample measured. If the rock sample is significantly larger than the probe tip-seal size, then a "half-space solution" curve may be utilized (Goggin et al., 1988b). It is from the "half-space solution" curve that the above G_0 was determined for this study.

The resulting product is given in units of μm^2 (Goggin et al., 1988b). To convert to md, the product was multiplied by $1.0x10^{10}$. The tip-seal pressure is simply 5 psi (34474 Pa), plus the average atmospheric pressure in Socorro, NM (85000 Pa). Calibration data is given below.

Permeability results from the mechanical field permeameter were plotted against Unocal's Tensleep core plug permeabilities (Fig. A-1). Correlations are quite good, considering the differences in the techniques employed to measure permeability. The

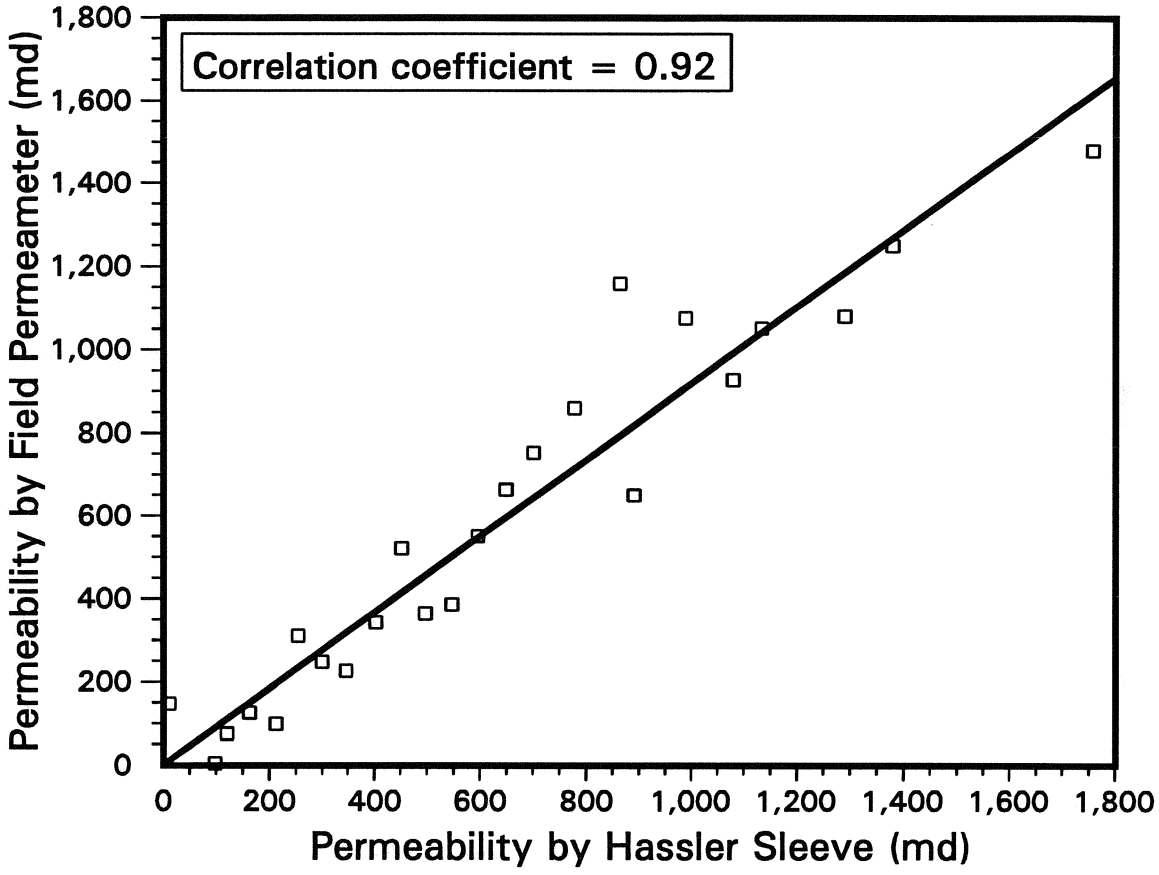

Figure A-1 - Correlation between permeabilities measured on Tensleep Sandstone core plugs by the mechanical field permeameter and the Hassler Sleeve.

Hassler Sleeve method used by Unocal injects gas or fluid through the entire core plug, but prevents the gas or fluid from escaping through the sides of the plug. All heterogeneities within the plug affect the overall permeability measurement, thereby giving an average permeability. The mechanical field permeameter's measurements are much more localized, measuring only a small hemisphere about twice the inside diameter of the probe-tip (sphere of influence is approximately 0.5 cm in diameter). The injected gas is permitted to escape through the rock in all directions.

Tests were performed with various probe tip dimensions at various pressures. The optimum results are with a probe tip inside radius of 0.1308 cm (0.0515 in) at 5 psi. A special polycarbonate plastic sleeve was designed at the New Mexico Petroleum Recovery Research Center to slip around the hand-held probe tip. When in place, it eliminated variations in the sealing pressure in which the silicone foam probe-tip was compressed against the rock sample. These variations in pressure affected gas flow rates. The sleeve also prevented accidental tilting of the probe, thus eliminating the pinching-off or leaking of gas flowing through the probe tip. Although the sleeve proved very useful in measuring smooth-surfaced core plugs and rock slabs, it often prevented the silicone probe tip from achieving a tight seal on the irregular rock surfaces in the outcrop. The sleeve, therefore, was not utilized in the field. Instead, maximum pressure was applied to seal the probe against the outcrop for each permeability measurement. Field data were comparable to core data obtained in the lab because the amount of error produced by minor variations in sealing pressure were small when compared to the high permeabilities of the sandstone.

Muddy or well-cemented lithologies commonly have permeabilities that are too low for the mechanical field permeameter to accurately measure (<5md). To obtain approximate permeability values, a plot of "pressure drop time" (discussed below) versus permeability was developed (Fig. A-2) from low-permeability samples that were

PERM (md)	TIME (min)
0.2	4
0.6	3.35
1.6	3.17
1.7	3.76
1.8	3.25
2.4	2.94
2.7	3.22
4	1.59
4.9	3.08
6.2	0.22
12.3	1.33
21.9	0.13
34.7	0.17
38.4	0.05
38.8	0.08
39.6	1.22
88.1	0.18

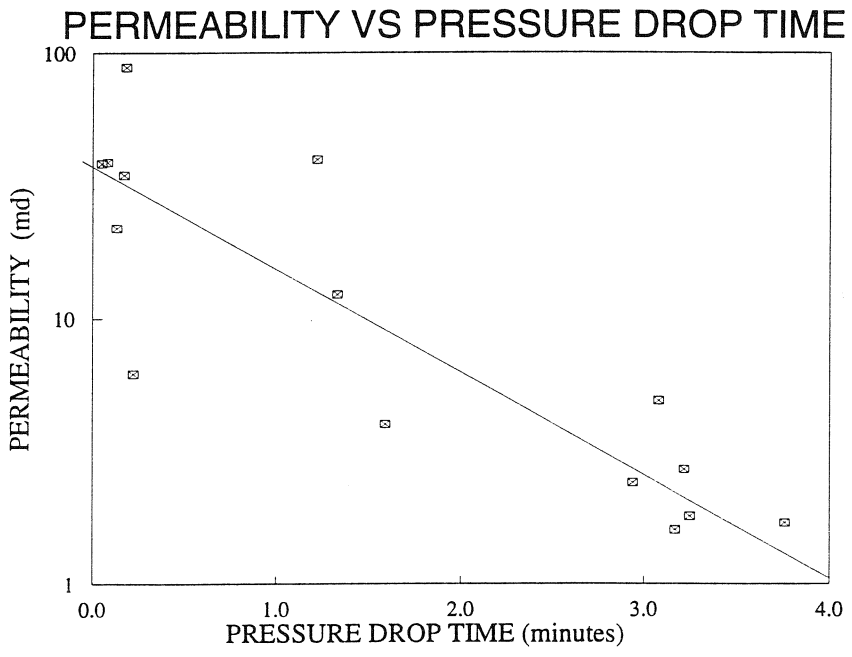

Figure A-2. Plot of permeability vs. pressure drop time for estimating permeability of low-permeability rock, using the mechanical field permeameter.

measured by the computer-controlled scanning minipermeameter. The mechanical field permeameter was first pressurized to 70 psi, the flow of nitrogen was then shut off, and the pressure was permitted to drop. The time that it took the pressure to drop 5 psi was measured with a stop watch. An estimated permeability value was then obtained by plotting the recorded time on a time-permeability curve.

Computer-controlled Scanning Minipermeameter

A computer-controlled scanning minipermeameter (Fig. 7) at the New Mexico Petroleum Recovery Research Center was also used in this study. The minipermeameter consists of a syringe which provides a constant pressure air supply, a network of computer-controlled sensors and actuators to measure air flow, and a silicon rubber probe tip to form a tight seal when pressed against the surface of a specimen (Heller, 1992; Ali, 1993). The probe, syringe and necessary electronics are mounted on a computer-controlled moveable carriage which can scan the length of a core. The table upon which the core rests moves in a direction at right angles to the direction in which the instrument carriage moves, thereby permitting the operator to utilize an x-y grid for permeability studies of the core.

Ali (1993) has run numerous tests on the minipermeameter to test its accuracy and precision. Ali made permeability measurements on core plugs from the Tensleep Sandstone of Wyoming using both Unocal's mechanical fields permeameter and the computer-controlled scanning minipermeameter. Correlation was very good as demonstrated in Fig. A-3 (from Ali, 1993).

The computer-controlled scanning minipermeameter accurately measured permeabilities up to approximately 8.0 darcies, whereas the accuracy of the mechanical field permeameter decreased when sandstone permeabilities exceeded about 4.5 darcies and was incapable of measuring permeabilities over 5.0 darcies.

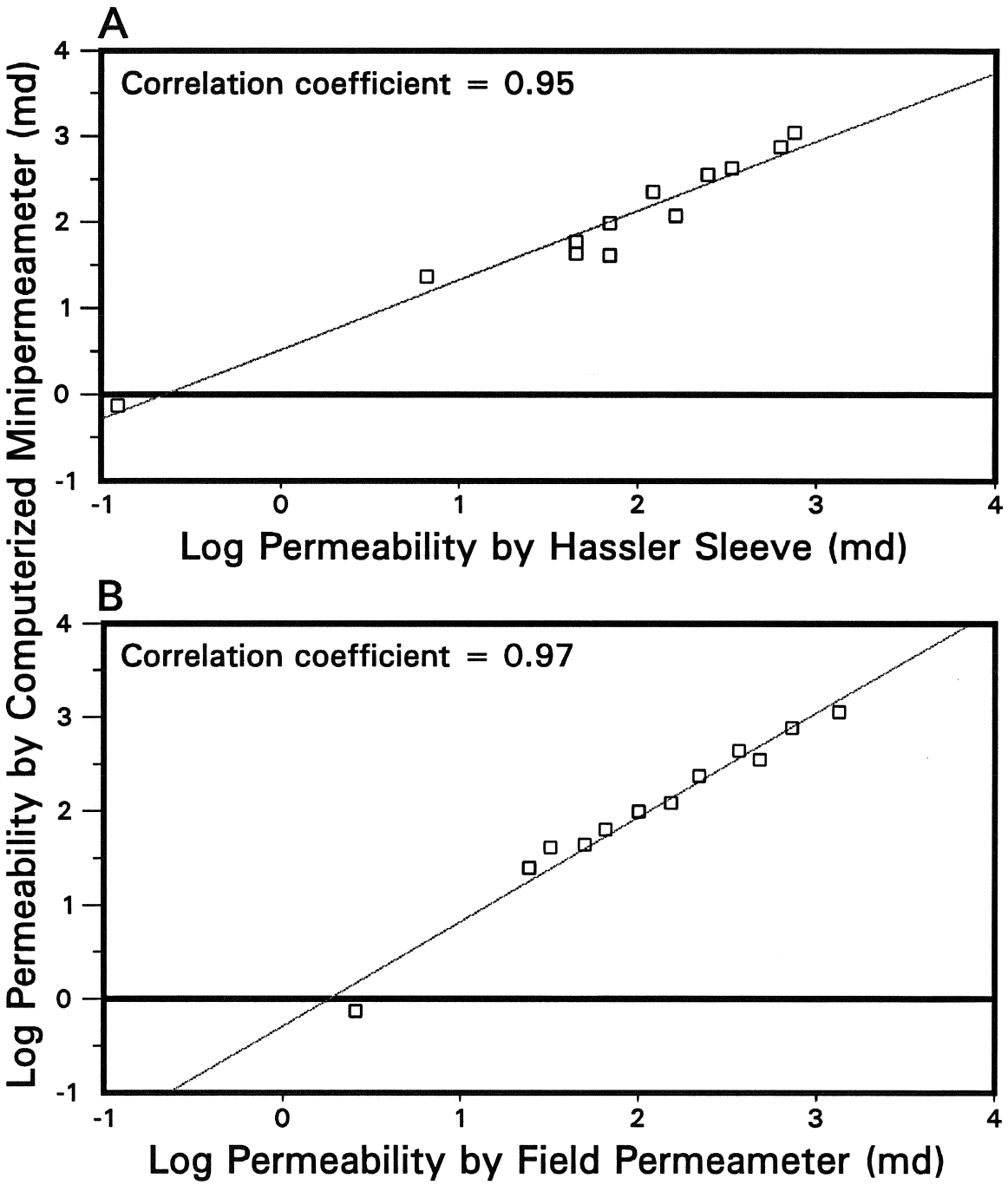

Figure A-3 - Correlation between permeabilities measured on Tensleep Sandstone core plugs by the PRRC minipermeameter and (A) the Hassler Sleeve and (B) the mechanical field permeameter. From Ali (1993).

Appendix 5. Core from Tocito Sandstone oil reservoirs used in permeability studies.

WELL NAME	ORIGINAL OPERATOR	WELL LOCATION	FIELD NAME	THICKNESS OF TOCITO	CURRENT REPOSITORY LOCATION
Navajo Tribal F-151	Solar Petroleum	Sec.10 T31N R17W	Horseshoe Gallup	7.6 m (25 ft)	USGS Core Research Center, Mail Stop 975, Box 25046, Denver Federal Center, Denver, Colorado 80225-0046 Telephone: (303) 236-1930
Martin Gas Unit C-1	Pan American	Sec.11 T27N R10W	Angel's Peak	1.5 m (5 ft)	Amoco Core Facility 2980 Huron Street Denver, Colorado 80202 Telephone: (303) 830-5020
Angel Peak B-37	Union Texas	Sec.24 T28N R11W	Angel's Peak	6.4 m (21 ft)?	
Newsom A-3E (A20)	Union Texas	Sec.4 T26N R8W	Angel's Peak	2.7 m (9 ft)	

Appendix 6. Petrographic data for deep subsurface Tocito Sandstone in four oil fields in the central San Juan Basin.

	CHA CHA GALLUP Pan American Petr. Navajo Tribal E-8				HORSESHOE GALLUP Solar Petroleum Navajo Tribal F-151					TOTAH GALLUP Pan American Petr. Navajo Tribal H-2			
DEPTH (feet)	4837	4838	4844	4847	919.5	924.5	942.5	944.5	944.7	5122	5125	5129	5131
QUARTZ (%)	38.4	61.4	44.8	38.7	23.6	35.5	43.5	54.4	16.5	26.1	60.3		66.9
K-FELDSPAR (%)	1.5	1.8	10.0	12.5	17.5	18.1	13.5	9.0	9.5	17.5	4.0		2.5
PLAGIOCLASE (%)	0.3	0.4	0.8	0.8	0.8	0.8	0.7	0.7	0.5	1.0	0.7		0.5
ROCK FRAGMENTS (%)	5.3	2.2	1.3	1.0	2.2	4.1	3.3	2.7	0.0	4.6	2.6		2.0
DETRITAL CLAY (%)	1.3	1.6	3.0	2.6	34.5	tr	5.9	11.8	19.4	14.3	2.6		1.0
GLAUCONITE (%)	2.0	12.0	7.3	4.3	3.8	9.4	15.1	9.4	0.0	1.6	3.0		3.3
PHOSPHATE (%)	33.3	0.3	0.6	0.3	tr	0.2	tr	1.0	0.0	0.3	1.6		2.0
PYRITE (%)	3.0	1.8	1.3	2.0	6.6	0.7	0.3	1.7	4.0	1.3	1.0		0.3
ORGANICS (%)	0.0	0.7	0.3	1.0	0.4	0.0	0.0	tr	2.0	3.0	0.7		0.0
KAOLINITE (%)	0.0	0.3	0.6	tr	0.7	3.5	0.3	1.4	0.8	tr	tr		0.0
QUARTZ OVERGROWTHS (%)	3.0	3.0	3.0	3.7	tr	3.5	0.7	0.2	0.0	3.3	5.7		7.3
FELDSPAR OVERGROWTHS (%)	0.0	0.0	0.0	0.0	0.0	0.0	0.0	0.0	0.0	0.0	0.4		0.0
CALCITE CEMENT (%)	1.0	0.3	12.0	27.7	0.0	0.7	7.0	0.0	42.5	21.7	1.3		3.0
DOLOMITE (%)	0.3	3.0	2.7	0.0	0.4	4.6	tr	0.0	0.0	0.7	0.3		0.3
GYPSUM (%)	0.0	0.0	0.0	0.0	7.3	0.7	0.0	0.0	0.0	0.0	0.0		0.0
PARTLY DISSOLVED GRAIN (%)	1.3	1.7	2.0	4.7	0.4?	1.4?	1.7?	1.0?	0.0	0.3	3.7		1.3
DISSOLUTION POROSITY (%)	6.7	3.0	5.0	3.0	0.7	16.1	3.3	1.6	0.0	0.2	5.8		1.7
TOTAL POROSITY (%)	9.6	9.3	11.7	4.7	2.3	17.3	9.7	6.6	1.0	0.2	15.0	high	10.6
LAB SERVICES POROSITY (%)	17.0	15.3	16.5	2.5						4.2	6.5	12.6	15.2
LAB SVCS PERMEABILITY (md)	97.0	43.0	35.0	0.03	0.8**	18.5**	80.3**	15.7**	0.8**	0.1	0.1	561	81.0
GRAIN SIZE RANGE (ϕ)					3.0-1.5	4.0-0.5	4.0-0.0	4.0-0.0	<4.0				
GRAIN SIZE AVERAGE (ϕ)					2.5	2.5	2.5	1.75	<4.0				
CALCITE CMT CL*, % BROWN	100	100	100	100	100	100	100	100	100	100	100	100	100
CALCITE CMT CL*, % ORANGE	0.0	0.0	0.0	0.0	0.0	0.0	0.0	0.0	0.0	0.0	0.0	0.0	0.0

* CL = cathodoluminescence ** = Mechanical field permeameter data

Appendix 7. Petrographic data for shallow subsurface cores through the Tocito Sandstone outcrop in the Hogback oil field, San Juan Basin. HOF #2 was spudded in Tocito and HOF #3 was spudded in Upper Mancos Shale. Both core end in the Gallup Sandstone underlying the Tocito.

	HOF #2									HOF #3								
DEPTH (feet)	9.0	17.0	22.0	30.0	36.0	40.0	48.0	50.0	52.0	41.5	44.7	47.6	53.4	59.6	65.5	75.5	75.51	79.5
QUARTZ (%)	38.4	49.3	42.0	42.7	30.1	47.0	49.0	55.2	31.1	12.4	28.9	24.5	27.0	37.9	29.2	28.8	31.8	33.9
K-FELDSPAR (%)	22.5	13.5	23.1	17.5	30.0	7.2	12.5	6.5	18.6	8.4	17.5	16.5	24.0	28.5	18.0	25.0	27.5	26.7
PLAGIOCLASE (%)	1.5	1.0	1.0	0.0	1.5	0.0	1.0	1.0	2.5	2.1	3.5	3.0	1.5	1.5	3.0	1.5	1.5	1.0
ROCK FRAGMENTS (%)	2.1	2.0	1.8	0.8	1.1	0.2	2.0	2.0	2.8	1.4	4.8	3.1	3.1	4.0	1.7	3.7	2.0	2.3
DETRITAL CLAY (%)	1.8	1.7	0.0	10.2	3.4	12.2	4.2	17.4	13.4	52.5	14.0	14.0	13.7	3.1	3.1	2.0	1.4	1.0
GLAUCONITE (%)	0.5	0.8	1.1	0.8	1.7	0.8	1.1	3.1	9.4	0.2	0.2	0.2	1.1	0.2	0.5	0.0	1.1	1.3
PHOSPHATE (%)	0.0	0.0	0.0	0.0	0.3	0.3	0.0	1.1	0.3	2.0	1.1	0.3	0.0	0.3	0.3	4.8	0.0	0.2
PYRITE (%)	1.8	0.8	0.9	0.2	0.2	tr	tr	0.2	0.8	1.7	1.1	4.5	2.0	0.2	0.8	0.5	1.1	1.0
ORGANICS (%)	0.0	0.0	0.0	tr	0.0	tr	tr	tr	tr	tr	tr	tr	tr	0.0	0.0	0.0	0.0	0.0
KAOLINITE (%)	3.7	1.7	2.6	0.1	1.1	1.1	1.7	0.2	0.2	0.2	0.5	2.0	7.1	0.8	0.3	1.7	1.7	3.6
QTZ OVERGROWTHS (%)	2.3	0.6	1.3	0.5	2.2	1.1	0.8	0.8	0.2	0.0	0.0	0.5	2.2	2.8	0.0	2.5	3.4	3.3
FSPAR OVERGROWTH (%)	0.0	0.0	0.0	0.0	0.0	0.0	0.0	0.0	0.0	0.0	0.0	0.0	0.0	0.0	0.0	0.0	0.0	tr
CALCITE CEMENT (%)	0.0	21.8	0.0	21.7	0.2	0.0	3.1	0.6	11.1	11.4	26.0	0.0	2.2	0.2	40.2	17.1	5.7	0.2
DOLOMITE (%)	0.0	0.0	0.0	0.0	0.0	0.2	6.3	0.0	0.0	0.0	0.0	4.0	0.0	0.0	0.0	0.0	0.0	0.0
GYPSUM (%)	0.5	0.3	0.0	0.0	0.0	0.3	0.0	3.9	3.7	0.0	0.0	0.0	0.6	0.5	0.0	0.0	0.0	0.0
REMNANT GRAIN (%)	?	?	?	?	?	?	?	?	?	?	?	?	?	?	?	?	?	?
DISSOLUTION POROSITY	12.2	5.1	2.1	1.2	1.2	?	?	?	?	?	?	?	?	?	?	?	?	?
TOTAL POROSITY (%)	21.1	6.5	26.7	4.2	26.0	28.0	16.2	6.1	5.1	1.1	1.7	6.8	13.4	19.1	0.8	11.1	21.7	24.3
MFP PERMEABILITY (md)	2446	37.6	4433	15.2	5069	1471	200	773	33.2	7.9	3.2	3.3	208	2455	3.2	2076	2076	2641
GRAIN SIZE RANGE (ϕ)	4.-1.0	4.--0.5	4.-1.0	4.-0.5	4.-1.0	4.-1.0	4.-0.5	4.--0.5	4.-0.0	4.-2.5	4.-1.5	4.-2.0	4.-1.0	3.5-0.5	4.-0.0	4.--0.5	4.--0.5	4.-1.5
GRAIN SIZE AVERAGE (ϕ)	2.0	1.8	2.0	1.8	2.0	1.8	2.0	1.8	2.8	3.8	3.3	3.0	2.5	1.8	2.0	1.0	2.0	2.0
CALCITE CL*, % BROWN	50	1	0.0	0.0	100	0.0	40	40	30	50	70	70	1	1				
CALCITE CL, % ORANGE (md)	50	99	0.0	100	0.0	100	60	60	70	50	30	30	99	99				

* = cathodoluminescence

Appendix 8. Cathodoluminescence data for calcite cements in the "upper" Tocito Sandstone cropping out in the Hogback oil field and along the Chaco River.

SAMPLE	CALCITE CEMENT LUMINESCENCE			VISUALLY EST. ABUNDANCE			LITHOFACIES	
	%Brown	%Orange	Relationships or Comments	K-SPAR	PLAG	KAO	DESCRIPTION	THICKNESS
Tocito 1D	0	100					Large cross-bedded ss	140 cm
Tocito 2D	0	100		15-20	1		Interbedded tabular ss & shale	40 cm
Tocito 3D	75	25		20	1-2		Interbedded tabular ss & shale	
Tocito 4D	50	50	Orange fills fracture that cuts brown cement	15-20	1		Interbedded tabular ss & shale	
Tocito #1	0	100	Trace amounts of calcite cement	10	0.3		Large cross-bedded ss (Grid 9, row 1)	137 cm
Tocito #2	0	100	Minor calcite cement, commonly "dirty"	8-10	0.2		Large cross-bedded ss (Grid 9, row 2)	137 cm
Tocito #3	0	0		5	0.2		Large cross-bedded ss (Grid 9, row 2)	137 cm
Tocito #4	50	50		5	0		Lrg x-bd ss (Grid 9 betwn row 2 & 3)	137 cm
Tocito #5	0	0		10	0.3		Large cross-bedded ss (Grid 9, row 3)	137 cm
Tocito #6	0	0		10	0		Large cross-bedded ss (Grid 9, row 5)	137 cm
Tocito #7	0	0		10-15	0.3		Large cross-bedded ss (Grid 9, row 7)	137 cm
Tocito #8	75	25	Local orange cmt, com assoc w/ pores & mud	20	0.3		Phosphatic nodular mudstone (Grid 4)	
Tocito #9	75	25	Kaolinite in pores near brown & orange cmts	15-20	0.5	Abundant	Large cross-bedded ss (Grid 7, row 1)	
Tocito #10	25	75	Orange fills fracture that cuts brown cement	5-8	0		Large cross-bedded ss (Grid 7, row 3)	
Tocito #11	25	75	Orange fills fracture that cuts brown cement	15-20	0.3		Mid of bioturbated ss (intbd w/ shale)	45 cm
Tocito #12	95	5		15-20	0.3		Top of bioturbated ss (intbd w/ shale)	45 cm
Tocito #13	90	10		20-30	1-2		Bioturbated muddy ss & shale	15 cm
Tocito #14	60	40		20-30	1-2	Abundant	Bioturbated muddy ss & shale	15 cm
Tocito #15	75	25	Orange cement filling clusters of pores	10-15	0.5		Bioturbated sandstone (intbd w/ shale)	40 cm
Tocito #16	50	50	Burrows cmtd w/ brn. Orange in porous area	20	0.3		Thin sandstone lens (intbd w/ shale)	5-10 cm

Appendix 8 continued.

SAMPLE	CALCITE CEMENT LUMINESCENCE			VISUALLY EST. ABUNDANCE			LITHOFACIES	
	%Brown	%Orange	Relationships or Comments	K-SPAR	PLAG	KAO	DESCRIPTION	THICKNESS
Tocito #17	15	85	Kao in pores amongst orange & brown cmt	15-20	1	Common	Bioturbated muddy sandstone & shale	26-27 cm
Tocito #18	75	25	Kao in pores amongst orange & brown cmt	15-20	0.3	Abundant	Base of bioturbated ss (intbd w/ shale)	25-27 cm
Tocito #19	20?	80?		15-20	1-2	Common	Bioturbated muddy sandstone & shale	25 cm
Tocito #20	0	100	Minor calcite cement	15-20	0.3		Tabular sandstone (intbd w/ shale)	20+ cm
Tocito #21	40	60		15-20	0.3	V. abundant	Tabular sandstone (intbd w/ shale)	
Tocito #22	0	100		30	1		Medium cross-bedded sandstone	
Tocito #23	0	100	Minor calcite cement	20-15	1-2	Abundant	Tabular sandstone (intbd w/ shale)	8 cm
Tocito #24	0	100	Trace calcite cement	10	0.3		Tabular sandstone (intbd w/ shale)	6 cm
Tocito #25	50	50	Orange cmt appears later than brown cement	15-20	0.3		Tabular sandstone (intbd w/ shale)	6 cm
Tocito #28	5	95					Tabular sandstone (intbd w/ shale)	3 cm
Tocito #30	5	95					Medium cross-bedded sandstone	20+ cm
Tocito #54	25	75					Base of large cross-bedded sandstone	128 cm
Tocito #55	0	100	Minor calcite cement				Top of large cross-bedded sandstone	128 cm
Tocito #56	0	100	Minor calcite cement				Top of medium cross-bedded ss unit	31 cm
Tocito #57	0	100	Minor calcite cement				Base of medium cross-bedded ss unit	19 cm
Tocito #58	0	100	Minor calcite cement				Top of ss w/ reactivation surface	53 cm
Tocito #59	0	100	Abundant calcite cement				Base of ss w/ reactivation surface	53 cm
Tocito #60	0	100	Abundant calcite cement				Base of ss w/ reactivation surface	53 cm
Tocito #61	40	60					Interbedded tabular ss & shale	11 cm
Tocito #62	0	0					Interbedded tabular ss & shale	10 cm
Tocito #63	2	98					Bioturbated planar-bedded ss	14.5 cm

Appendix 9. Isotopic data for calcite cements in the Tocito Sandstone outcrop in the Hogback oil field, San Juan Basin, New Mexico.

SAMPLE NUMBER	BULK ROCK (mg)	CO_2 (μmoles)	$\delta^{13}C‰$ (PDB)	STD. DEV.	FRACTIONATED $\delta^{18}O‰$ (SMOW)	STD. DEV.	CORRECTED $\delta^{18}O‰$ (SMOW)	CORRECTED $\delta^{18}O‰$ (PDB)	LUMINESCENCE % Brown	% Orange
Tocito #3D	32.5	63.5	-3.545	0.049	26.103	0.020	15.497	-14.948	75	25
Tocito #3D	32.5	63.5	-3.535	0.067	26.115	0.048	15.509	-14.936	75	25
Tocito #15	25.2	48.3	-3.824	0.056	25.392	0.054	14.786	-15.637	75	25
Tocito #15	25.2	48.3	-3.852	0.033	25.381	0.086	14.775	-15.648	75	25
Tocito #18	25.1	32.2	-3.666	0.048	25.676	0.033	15.070	-15.362	75	25
Tocito #18	25.1	32.2	-3.681	0.042	25.633	0.035	15.027	-15.404	75	25
Tocito #2D	26.6	82.8	-5.124	0.043	28.618	0.017	18.012	-12.508	0	100
Tocito #2D	26.6	82.8	-5.140	0.045	28.607	0.034	18.001	-12.519	0	100
Tocito #11	100.0	85.5	-4.098	0.049	31.134	0.086	20.528	-10.067	25	75
Tocito #11	100.0	85.5	-4.082	0.023	31.086	0.060	20.480	-10.114	25	75
Tocito #30	25.0	59.6	-4.390	0.044	27.171	0.045	16.565	-13.912	5	95
Tocito #30	25.0	59.6	-4.431	0.029	27.123	0.024	16.517	-13.958	5	95

Appendix 10. Mesoscopic- and macroscopic-scale permeability data for grids along the Tocito Sandstone outcrop in the Hogback oil field and along the Chaco River, San Juan Basin, New Mexico. Grids illustrated in Figures 24-36. Measurements made with a mechanical field permeameter. Geostatistics given in Appendix 11.

GRID 1: Interbedded sandstone and shale lithofacies, "upper" Tocito Sandstone, Hogback oil field. Permeabilities given in darcies.

	Column 1	Column 2	Column 3	Column 4	Column 5
Row 1	0.050	0.028	<0.50	<0.50	<0.50
Row 2	2.640	3.952	2.670	3.674	1.950
Row 3	3.885	2.233	4.929	0.834	4.775
Row 4	>5.15	4.929	4.265	1.749	4.996
Row 5	>5.15	0.720	<0.50	5.140	4.322

GRID 2: Interbedded sandstone and shale lithofacies, "upper" Tocito Sandstone, Hogback oil field. Permeabilities given in darcies.

	Column 1	Column 2	Column 3	Column 4	Column 5
Row 1	3.144	4.476	3.401	4.183	4.327
Row 2	0.659	2.964	2.161	1.126	2.058
Row 3	4.142	4.415	3.967	2.495	4.497

GRID 3: Muddy, bioturbated sandstone lithofacies, "upper" Tocito Sandstone, Hogback oil field. Permeabilities given in darcies.

	Column 1	Column 2	Column 3	Column 4	Column 5
Row 1	3.576	3.365	3.555	2.701	2.995
Row 2	3.190	0.013	0.005	4.374	0.019
Row 3	2.516	0.026	0.798	0.926	2.326
Row 4	0.004	0.020	1.647	3.087	0.055
Row 5	0.540	0.019	0.016	0.004	0.013
Row 6	0.036	0.062	0.069	0.038	0.068

GRID 4: Phosphatic nodular mudstone lithofacies between "upper" and "lower" Tocito Sandstone, Hogback oil field. Permeabilities given in darcies.

	Column 1	Column 2	Column 3	Column 4	Column 5
Row 1	1.235	0.054	0.056	0.076	0.828
Row 2	1.024	2.012	0.100	0.725	0.127
Row 3	0.746	0.140	0.051	0.013	0.016
Row 4	1.158	1.039	0.092	1.055	1.451
Row 5	0.756	0.782	0.049	0.571	0.054

GRID 5: Ripple cross-laminated sandstone lithofacies, "lower" Tocito Sandstone, Hogback oil field. Permeabilities given in darcies.

	Column 1	Column 2	Column 3	Column 4	Column 5	Column 6
Row 1	1.623	0.987	1.143	1.337	1.265	0.038
Row 2	1.684	3.081	2.745	2.232	1.004	2.057
Row 3	4.619	>5.15	>5.15	>5.15	>5.15	>5.15

GRID 6: Ripple cross-laminated sandstone lithofacies, "lower" Tocito Sandstone, Hogback oil field. Permeabilities given in darcies.

Row 1	Row 2
1.158	_
1.039	_
0.011	_
0.695	_
1.075	_
1.075	_
0.021	_
0.022	_
1.024	0.061
0.012	0.689
0.018	1.131

GRID 7: Large-scale cross-bedded sandstone lithofacies, "lower" Tocito Sandstone, Hogback oil field. Permeabilities given in darcies.

	Column 1	Column 2	Column 3	Column 4	Column 5
Row 1	2.665	2.526	1.955	4.363	1.652
Row 2	2.845	3.766	3.982	3.396	4.368
Row 3	3.730	4.029	4.065	4.008	4.430
Row 4	5.145	5.145	5.145	3.782	4.024
Row 5	5.145	5.145	5.145	5.145	5.145
Row 6	5.145	5.145	5.145	3.360	5.145
Row 7	0.664	0.467	0.700	1.019	2.403
Row 8	0.736	1.389	0.022	1.487	1.497
Row 9	1.142	2.007	1.595	0.967	1.446
Row 10	1.698	1.791	0.042	0.931	0.044
Row 11	1.837	-	1.261	-	0.623

	Column 6	Column 7	Column 8	Column 9	Column 10
Row 1	2.717	3.216	4.132	3.967	2.511
Row 2	3.195	2.799	2.820	4.101	3.005
Row 3	2.279	2.748	1.698	3.185	2.598
Row 4	3.885	3.797	4.605	4.224	3.782
Row 5	5.145	5.145	5.145	5.145	5.145
Row 6	5.145	5.145	4.028	5.145	5.145
Row 7	0.952	2.084	0.512	0.967	2.124
Row 8	0.010	0.684	0.782	1.672	1.101
Row 9	1.348	1.749	0.849	0.762	1.379
Row 10	0.705	2.367	0.096	0.083	1.291
Row 11	-	0.149	-	0.772	-

GRID 8: Large-scale cross-bedded sandstone lithofacies, "lower" Tocito Sandstone, Hogback oil field. Permeabilities given in darcies.

	Column 1	Column 2	Column 3	Column 4	Column 5
Row 1	2.670	2.475	2.135	2.413	4.281
Row 2	2.804	2.686	2.645	3.164	4.425
Row 3	3.612	2.341	3.463	3.663	3.128
Row 4	4.111	3.555	3.453	3.046	4.826
Row 5	2.598	2.732	3.396	3.128	3.242
Row 6	3.396	2.459	3.206	3.540	4.291
Row 7	-	3.705	2.449	3.813	3.443
Row 8	2.727	3.473	2.413	3.442	3.607
Row 9	3.406	2.938	2.938	4.106	4.029
Row 10	1.389	2.315	2.881	3.566	4.214
Row 11	1.466	2.583	3.442	2.362	3.746
Row 12	-	3.134	-	2.259	3.504

GRID 9: Large-scale cross-bedded sandstone lithofacies, "lower" Tocito Sandstone, Hogback oil field. Permeabilities given in darcies.

	Column 1	Column 2	Column 3	Column 4	Column 5
Row 1	-	-	-	-	-
Row 2	4.116	4.039	3.000	4.070	4.950
Row 3	5.145	4.893	4.744	5.037	4.060
Row 4	4.641	4.775	4.512	3.591	3.082
Row 5	4.482	3.921	4.173	3.658	3.756
Row 6	4.003	2.840	4.574	3.885	3.566
Row 7	3.468	3.334	3.010	3.478	3.761
Row 8	2.876	1.852	2.279	2.876	3.216

	Column 6	Column 7	Column 8	Column 9	Column 10
Row 1	-	2.176	2.156	1.940	2.748
Row 2	4.512	4.981	3.561	4.734	5.120
Row 3	5.130	4.193	4.070	4.888	4.312
Row 4	3.658	4.132	4.229	3.319	4.338
Row 5	4.173	4.132	4.934	3.643	4.430
Row 6	4.384	4.245	4.482	3.411	2.110
Row 7	2.737	2.964	3.921	3.828	3.180
Row 8	4.024	4.034	3.859	4.948	4.399

	Column 11	Column 12	Column 13	Column 14	Column 15
Row 1	1.142	0.972	-	-	-
Row 2	4.708	3.885	4.667	-	-
Row 3	3.344	4.636	5.145	5.145	5.145
Row 4	4.430	5.145	5.084	4.965	5.145
Row 5	4.934	4.142	4.106	3.535	3.705
Row 6	3.653	5.145	3.766	5.145	4.389
Row 7	3.545	2.887	1.791	3.226	3.931
Row 8	3.874	3.525	4.152	-	-

	Column 16
Row 1	-
Row 2	-
Row 3	5.145
Row 4	5.109
Row 5	2.799
Row 6	3.473
Row 7	1.549
Row 8	-

GRID 10: Large-scale cross-bedded sandstone lithofacies, "upper" Tocito Sandstone, Chaco River near Hogback oil field. Permeabilities given in darcies.

	Column 1	Column 2	Column 3	Column 4	Column 5
Row 1	1.955	4.127	4.363	3.674	4.265
Row 2	3.370	3.622	3.571	2.624	2.495
Row 3	2.722	2.892	2.593	2.058	3.540
Row 4	3.349	3.262	2.511	2.856	2.372
Row 5	3.653	3.247	2.650	3.134	1.935
Row 6	3.844	2.979	2.959	3.216	3.221
Row 7	-	-	2.151	1.389	2.727

GRID 11: Bioturbated tabular sandstone, "upper" Tocito Sandstone, Chaco River near Hogback oil field. Permeabilities given in darcies.

	Column 1	Column 2	Column 3	Column 4	Column 5
Row 1	3.226	2.290	2.691	2.737	2.516
Row 2	2.336	2.465	2.737	2.058	2.562

	Column 6	Column 7	Column 8	Column 9	Column 10
Row 1	2.212	2.393	3.061	2.506	3.267
Row 2	2.588	2.079	2.691	2.511	2.444

GRID 12: Cross-bedded sandstone with reactivation surfaces, "upper" Tocito Sandstone, Chaco River near Hogback oil field. Permeabilities given in darcies.

	Column 1	Column 2	Column 3	Column 4	Column 5
Row 1	2.547	2.881	2.794	2.676	4.394
Row 2	3.149	3.411	4.482	4.291	3.468
Row 3	3.494	3.982	3.473	2.573	4.260
Row 4	4.255	3.998	4.600	4.451	3.895
Row 5	4.291	3.473	4.307	3.458	3.833

	Column 6	Column 7	Column 8	Column 9	Column 10
Row 1	-	-	-	-	-
Row 2	3.442	3.257	4.013	3.483	2.521
Row 3	4.996	5.145	5.145	4.543	5.145
Row 4	4.260	4.451	3.926	-	-
Row 5	3.489	3.406	3.756	-	-

	Column 11	Column 12
Row 1	-	-
Row 2	-	-
Row 3	5.145	5.058
Row 4	-	-
Row 5	-	-

GRID 13: Large-scale cross-bedded sandstone lithofacies, "upper" Tocito Sandstone, Chaco River near Hogback oil field. Permeabilities given in darcies.

	Column 1	Column 2	Column 3	Column 4	Column 5
Row 1	3.730	3.247	3.617	2.995	2.537
Row 2	3.242	3.164	2.521	2.758	3.401
Row 3	2.691	3.741	3.478	3.113	3.231
Row 4	4.368	3.031	2.495	3.442	2.655
Row 5	3.519	2.074	2.758	2.264	2.218
Row 6	2.233	3.154	1.204	-	-

GRID 14: Interbedded sandstone and shale lithofacies, "upper" Tocito Sandstone, Chaco River near Hogback oil field. Permeabilities given in darcies.

	Column 1	Column 2	Column 3	Column 4	Column 5
Row 1	1.909	3.602	2.737	2.485	3.072
Row 2	1.621	0.767	2.207	1.631	1.549
Row 3	1.796	2.048	0.046	0.695	0.033

GRID 15: Contorted medium-scale cross-bedded sandstone lithofacies, "upper" Tocito Sandstone, Chaco River near Hogback oil field. See Figure 33 for sites of stragetically spaced permeability measurements. Permeabilities given in darcies.

3.638	4.229	3.288	4.214
4.121	3.216	4.651	4.662
3.818	4.229	3.916	3.308
3.844	4.322	4.471	4.060
4.101	4.739	4.075	-

GRID 16: Large-scale cross-bedded sandstone lithofacies, "upper" Tocito Sandstone, Chaco River near Hogback oil field. Permeabilities given in darcies.

	Column 1	Column 2	Column 3
Row 1	3.530	3.612	3.139
Row 2	3.025	3.607	3.982
Row 3	3.921	3.303	3.597

GRID 17: Large-scale cross-bedded sandstone lithofacies, "upper" Tocito Sandstone, Chaco River near Hogback oil field. Permeabilities given in darcies.

	Column 1	Column 2	Column 3
Row 1	2.470	2.892	2.115
Row 2	2.923	2.727	2.881
Row 3	2.698	2.737	2.089

GRID 18: Large-scale cross-bedded sandstone lithofacies, "upper" Tocito Sandstone, Chaco River near Hogback oil field. Permeabilities given in darcies.

	Column 1	Column 2	Column 3	Column 4	Column 5
Row 1	1.976	2.506	3.391	2.377	3.607
Row 2	2.531	1.945	2.207	3.252	3.453
Row 3	3.679	3.566	3.324	3.499	3.483
Row 4	3.787	2.933	3.303	3.625	3.175
Row 5	2.002	3.982	4.338	3.607	4.641
Row 6	3.473	4.245	4.368	3.396	3.833
Row 7	4.173	4.163	4.677	3.566	4.245
Row 8	3.648	3.509	3.823	4.235	4.394
Row 9	3.005	2.995	3.483	3.581	4.193
Row 10	2.382	3.535	3.453	4.605	4.116
Row 11	2.506	4.229	4.348	4.621	3.859
Row 12	1.991	3.633	2.634	3.097	3.591
Row 13	3.139	4.291	2.984	3.525	2.876
Row 14	2.938	4.404	3.288	3.031	2.320
Row 15	3.000	3.699	2.583	2.691	2.614
Row 16	2.825	3.499	2.598	-	-

GRID 19: Large-scale cross-bedded sandstone lithofacies, "upper" Tocito Sandstone, Chaco River near Hogback oil field. Permeabilities given in darcies.

	Column 1	Column 2	Column 3	Column 4	Column 5
Row 1	3.442	3.900	1.832	3.082	1.147
Row 2	3.694	3.910	4.106	3.653	2.470
Row 3	2.269	2.099	1.863	2.310	2.331

	Column 6
Row 1	2.676
Row 2	1.348
Row 3	2.598

GRID 20: Contorted large-scale cross-bedded sandstone lithofacies, "upper" Tocito Sandstone, Chaco River near Hogback oil field. Permeabilities given in darcies.

	Column 1	Column 2	Column 3	Column 4
Row 1	3.242	2.315	1.436	3.195
Row 2	2.660	2.326	2.531	1.261
Row 3	4.379	3.190	1.466	2.125
Row 4	2.573	2.480	2.840	2.258

GRID 21: Medium-scale cross-bedded sandstone lithofacies, "upper" Tocito Sandstone, Chaco River near Hogback oil field. Permeabilities given in darcies.

	Column 1	Column 2	Column 3	Column 4
Row 1	2.845	3.061	3.422	3.272
Row 2	3.715	4.286	3.998	3.473
Row 3	3.910	5.145	2.573	3.138
Row 4	4.379	4.389	3.756	3.766
Row 5	4.245	4.347	3.952	4.091
Row 6	2.578	3.663	4.096	4.070
Row 7	4.657	4.024	3.190	1.291

Appendix 11. Geostatistics for outcrop permeability data.

GRID #	LITHOFACIES	# MEASUREMENTS	RANGE (d)	MEAN (d)	STD. DEV.	COEF. OF VARIATION
1	Interbedded ss & sh	25	0.03->5.15	2.76	2.04	0.74
2	Interbedded ss & sh	15	0.66-4.48	3.20	1.30	0.41
3	Muddy bioturbated ss	30	0.00-4.37	1.20	1.50	1.25
4	Phosphatic nodular mdst	25	0.01-2.01	0.57	0.56	0.98
5	Ripple x-laminated ss	18	1.00->5.15	2.85	1.95	0.69
6	Ripple x-laminated ss	14	0.01-1.16	0.57	0.51	0.90
7	Large-scale x-bedded ss	100	0.01->5.15	2.85	1.80	0.63
8	Large-scale x-bedded ss	56	1.39-4.83	3.16	0.71	0.22
9	Large-scale x-bedded ss	113	0.97->5.15	3.92	0.99	0.25
10	Large-scale x-bedded ss	33	1.39-4.36	3.01	0.70	0.23
11	Bioturbated tabular ss	20	2.06-3.26	2.57	0.33	0.13
12	Ss w/ reactivation surface	43	2.55->5.15	3.90	0.75	0.19
13	Large-scale x-bedded ss	28	1.20-4.37	2.96	0.64	0.22
14	Interbedded ss & sh	15	0.00-3.60	1.73	1.04	0.60
15	Ss w/ sediment deformation	20	3.22-4.74	4.04	0.457	0.11
16	Large-scale x-bedded ss	9	3.14-3.98	3.51	0.33	0.09
17	Large-scale x-bedded ss	9	2.09-2.92	2.61	0.31	0.12
18	Large-scale x-bedded ss	79	1.61-4.68	3.41	0.70	0.21
19	Large-scale x-bedded ss	18	1.15-4.11	2.71	0.92	0.34
20	Large-scale x-bedded ss	16	1.26-4.38	2.52	0.78	0.31
21	Medium-scale x-bedded ss	28	2.85-5.15	3.70	0.77	0.21

Appendix 12. Macroscopic-scale permeability data for HOF #2 and HOF #3 core plugs and the vertical outcrop traverse. Measurements made with mechanical field permeameter.

CORE	DEPTH (feet)	PERMEABILITY (md)	PERMEABILITY (d)	POROSITY (%)
HOF-2	7.5	665.2917	0.6653	
HOF-2	8.9	1692.9947	1.6930	
HOF-2	9	1686.6216	1.6866	21.1
HOF-2	11	2728.9264	2.7289	
HOF-2	12	1104.3299	1.1043	
HOF-2	15	2471.1098	2.4711	
HOF-2	17	291.0281	0.2910	6.5
HOF-2	18	1115.7821	1.1158	
HOF-2	19	3069.6099	3.0696	
HOF-2	20	2316.3084	2.3163	
HOF-2	21.5	2398.3542	2.3984	
HOF-2	22	1757.0730	1.7571	26.7
HOF-2	23	35.3314	0.0353	
HOF-2	24	3436.9886	3.4370	
HOF-2	25	3369.3454	3.3693	
HOF-2	27	2397.3484	2.3973	
HOF-2	28	1932.8646	1.9329	
HOF-2	29	3284.3306	3.2843	
HOF-2	30	0.0000	0.0000	4.2
HOF-2	31	2567.1028	2.5671	
HOF-2	32	2171.3978	2.1714	
HOF-2	33	2378.2630	2.3783	
HOF-2	34	2056.1313	2.0561	
HOF-2	35	1922.8628	1.9229	
HOF-2	36	2725.2613	2.7253	26
HOF-2	37	2617.5938	2.6176	
HOF-2	38	3624.2502	3.6243	
HOF-2	39	3156.0081	3.1560	
HOF-2	40	2418.4970	2.4185	28
HOF-2	41	2594.8861	2.5949	
HOF-2	42	1445.6284	1.4456	
HOF-2	43	2121.7741	2.1218	
HOF-2	44	1897.4519	1.8975	
HOF-2	45	177.0296	0.1770	
HOF-2	46	12.6543	0.0127	
HOF-2	47	0.0000	0.0000	
HOF-2	48	569.8303	0.5698	16.2
HOF-2	49	8.1702	0.0082	7.1
HOF-2	51	439.1249	0.4391	
HOF-2	52	3.7603	0.0038	5.1
HOF-2	53	3.4337	0.0034	

Appendix 12 continued.

CORE	DEPTH (feet)	PERMEABILITY (md)	PERMEABILITY (d)	POROSITY (%)
HOF-3	41.5	7.8784	0.0079	1.1
HOF-3	42.5	0.0000	0.0000	
HOF-3	43.5	0.0000	0.0000	
HOF-3	44.7	0.0000	0.0000	1.7
HOF-3	45.4	0.0000	0.0000	
HOF-3	46.5	0.0000	0.0000	
HOF-3	47.6	0.0000	0.0000	6.8
HOF-3	48.5	9.6140	0.0096	
HOF-3	50.7	0.0000	0.0000	
HOF-3	51.4	328.8005	0.3288	
HOF-3	52.4	0.0000	0.0000	
HOF-3	53.4	208.2909	0.2083	13.4
HOF-3	54.5	1646.7072	1.6467	
HOF-3	55.5	2173.3507	2.1734	
HOF-3	56.5	2704.8705	2.7049	
HOF-3	57.5	1090.2663	1.0903	
HOF-3	58.5	1744.2068	1.7442	
HOF-3	59.6	2454.8841	2.4549	19.1
HOF-3	60.5	4356.1555	4.3562	
HOF-3	61.5	3947.2319	3.9472	
HOF-3	64.5	1436.0095	1.4360	
HOF-3	65.5	0.0000	0.0000	0.8
HOF-3	66.5	3060.9056	3.0609	
HOF-3	68.6	352.7889	0.3528	
HOF-3	69.2	3795.0497	3.7950	
HOF-3	70	2398.3542	2.3984	
HOF-3	73.4	2088.3955	2.0884	
HOF-3	74	2580.4682	2.5805	21.7
HOF-3	76.5	2076.3397	2.0763	
HOF-3	77.5	2784.6195	2.7846	
HOF-3	78.5	1730.4496	1.7304	
HOF-3	79.5	2641.4005	2.6414	24.3
HOF-3	80.5	2874.6954	2.8747	
HOF-3	81.5	2061.8993	2.0619	
HOF-3	82.6	11.6356	0.0116	
HOF-3	83.5	240.9009	0.2409	
HOF-3	84.7	800.4609	0.8005	
HOF-3	85.5	1556.9214	1.5569	
HOF-3	86.5	3566.7905	3.5668	
HOF-3	87.5	3731.9830	3.7320	
HOF-3	89.6	221.7871	0.2218	
HOF-3	91.5	355.9387	0.3559	
HOF-3	92.5	0.0000	0.0000	
HOF-3	93.5	4.5292	0.0045	
HOF-3	94.5	0.0000	0.0000	
HOF-3	95.6	0.0000	0.0000	
HOF-3	97.5	7.9495	0.0079	
HOF-3	98.5	0.0000	0.0000	
HOF-3	101	0.0000	0.0000	
HOF-3	104	0.0000	0.0000	
HOF-3	107	0.0000	0.0000	
HOF-3	110	0.0000	0.0000	

Appendix 12 continued.

Vertical traverse of Tocito Sandstone outcrop in Hogback oil field, San Juan Basin, New Mexico. Permeabilities measured with the mechanical field permeameter.

SAMPLE	HEIGHT (ft)	PERMEABILITY (md)	PERMEABILITY (d)	POROSITY (%)
1	17.585	508.5645	0.5086	
2	16.847	49.3010	0.0493	
3	16.109	120.1346	0.1201	
4	15.945	1219.9262	1.2199	
7b	13.976	1516.0532	1.5161	
7a	13.779	3824.9620	3.8250	
9	12.336	884.2953	0.8843	
10	11.516	1939.8556	1.9399	
11	11.155	5248.5907	5.2486	
12	10.499	81.3045	0.0813	
13	9.843	2538.3899	2.5384	
14	9.186	6078.9084	6.0789	
15	8.924	3472.1197	3.4721	
16	8.661	357.2931	0.3573	
17	7.579	6078.9084	6.0789	
18	6.857	628.2800	0.6283	
19	6.234	613.4065	0.6134	
20	4.593	4261.7019	4.2617	
21	1.312	1137.2780	1.1373	
22	0	3053.2961		

Appendix 13. Mesoscopic-scale permeability data for HOF #2 core. Measurements made with computer-controlled scanning minipermeameter.

Depth (ft)	Column 1	Column 2	Column 3	Column 4	Column 5	Column 6	Column 7	Ave. Perm.	Lithofacies
5.00		0.028	0.031	0.038	0.029	0.037		0.0325	ripple x-laminated
5.02		0.023	0.056	0.076	0.047	0.031		0.0466	ripple x-laminated
5.04		0.044	0.064	0.062	0.077	0.033		0.0560	ripple x-laminated
5.06		0.043	0.126	0.278	0.037	0.034		0.1036	ripple x-laminated
5.08		0.044	0.021	0.046	0.008	0.004		0.0248	ripple x-laminated
6.00		0.002	0.002	0.002	0.001	0.002		0.0018	ripple x-laminated
6.02		0.006	0.006	0.004	0.006	0.007		0.0057	ripple x-laminated
6.04		0.019	0.025	0.049	0.022	0.052		0.0333	ripple x-laminated
6.06		0.025	0.020	0.008	0.005	0.005		0.0126	ripple x-laminated
6.08		0.005	0.007	0.005	0.007	0.004		0.0053	ripple x-laminated
6.10		0.007	0.016	0.066	0.097	0.009		0.0389	ripple x-laminated
6.12		0.029	0.055	0.009	0.009	0.018		0.0239	ripple x-laminated
6.15		0.014	0.023	0.018	0.020	0.020		0.0190	ripple x-laminated
6.17		0.009	0.019	0.018	0.016	0.007		0.0138	ripple x-laminated
6.19		0.013	0.012	0.012	0.007	0.004		0.0097	ripple x-laminated
6.21		0.011	0.011	0.006	0.006	0.003		0.0074	ripple x-laminated
6.23		0.006	0.008	0.013	0.013	0.013		0.0106	ripple x-laminated
6.25		0.022	0.012	0.010	0.013	0.008		0.0130	ripple x-laminated
6.27		0.008	0.010	0.021	0.018	0.006		0.0126	ripple x-laminated
6.29		0.015	0.017	0.033	0.013	0.006		0.0166	ripple x-laminated
7.00			7e-04		7e-04		4e-04	0.0006	ripple x-laminated
7.25			0.160		2.335			1.2474	ripple x-laminated
7.50			2.446		1.902			2.1741	ripple x-laminated
8.00			0.032		0.069			0.0503	ripple x-laminated
8.08			0.041		0.031			0.0357	ripple x-laminated
8.50			3e-04		7e-04		4e-04	0.0005	ripple x-laminated
8.86			0.384		0.303			0.3435	ripple x-laminated
8.88			1.604		0.390			0.9971	ripple x-laminated
8.90			1.712		0.765			1.2381	ripple x-laminated
8.98			1.902		1.467			1.6843	ripple x-laminated
9.01			1.446		1.445			1.4457	ripple x-laminated
9.05			0.357		0.984			0.6702	ripple x-laminated
9.09			1.025		0.907			0.9663	ripple x-laminated
9.13			1.374		1.473			1.4233	ripple x-laminated

Appendix 13 continued.

Depth (ft)	Column 1	Column 2	Column 3	Column 4	Column 5	Column 6	Column 7	Ave. Perm.	Lithofacies
9.17			1.510		1.712			1.6107	ripple x-laminated
9.25			1.712		0.665			1.1883	ripple x-laminated
9.33			2.855		0.609			1.7320	ripple x-laminated
9.37			7e-04		5e-04			0.0006	ripple x-laminated
9.42			1.006		1.026			1.0157	ripple x-laminated
9.50			1.426		1.115			1.2705	ripple x-laminated
9.58			3.426		2.446			2.9361	ripple x-laminated
9.62			4e-04		8e-04			0.0006	ripple x-laminated
9.67			1.140		0.582			0.8608	ripple x-laminated
9.75			1.510		1.510			1.5098	ripple x-laminated
9.83			2.855		2.446			2.6504	ripple x-laminated
10.08			1.467		1.712			1.5891	ripple x-laminated
10.17			1.556		1.771			1.6631	ripple x-laminated
10.25			1.556		2.855			2.2051	ripple x-laminated
10.33			3.426		2.335			2.8804	ripple x-laminated
10.42			0.711		0.595			0.6533	interbedded ss & sh
10.50			2.446		2.704			2.5752	interbedded ss & sh
10.58			0.441		0.342			0.3914	interbedded ss & sh
10.67			0.743		0.078			0.4104	interbedded ss & sh
10.75			2.854		2.635			2.7445	interbedded ss & sh
10.83			0.052		0.002			0.0268	interbedded ss & sh
11.04			5e-04		0.003			0.0016	interbedded ss & sh
11.08			0.031		0.107			0.0690	interbedded ss & sh
11.12			4e-04		9e-04			0.0007	interbedded ss & sh
11.17			0.002		0.010			0.0060	interbedded ss & sh
11.21			0.002		5e-04			0.0011	interbedded ss & sh
11.25			4.283		1.656			2.9697	interbedded ss & sh
11.29			5e-04		8e-04			0.0007	interbedded ss & sh
11.33			1.351		1.712			1.5311	interbedded ss & sh
11.37			7e-04		4e-04			0.0006	interbedded ss & sh
11.42			2.855		3.375			3.1148	interbedded ss & sh
11.50			3.212		2.569			2.8902	interbedded ss & sh
11.58			0.465		3.426			1.9453	interbedded ss & sh
11.61			0.002		0.001			0.0017	interbedded ss & sh
11.70			0.026		0.116			0.0712	interbedded ss & sh

Appendix 13 continued.

Depth (ft)	Column 1	Column 2	Column 3	Column 4	Column 5	Column 6	Column 7	Ave. Perm.	Lithofacies
11.78			1.283		1.467			1.3748	interbedded ss & sh
11.95			9e-04		0.001			0.0011	interbedded ss & sh
11.97			1.283		0.899			1.0912	interbedded ss & sh
12.06			1.316		0.496			0.9062	interbedded ss & sh
12.10			5e-04		7e-04			0.0006	interbedded ss & sh
12.15			1.902		2.446			2.1742	interbedded ss & sh
12.19			0.001		0.009			0.0053	interbedded ss & sh
12.22			0.522		1.091			0.8067	interbedded ss & sh
12.30			1.467		2.233			1.8500	interbedded ss & sh
12.39			2.854		1.902			2.3782	interbedded ss & sh
12.43			8e-04		2e-04			0.0005	interbedded ss & sh
12.47			1.556		1.140			1.3479	interbedded ss & sh
12.51			4e-04		6e-04			0.0005	interbedded ss & sh
12.57			3.426		1.069			2.2473	interbedded ss & sh
12.70			5e-04		0.014			0.0071	interbedded ss & sh
12.78			1.347		0.979			1.1625	interbedded ss & sh
12.87			1.633		0.756			1.1944	interbedded ss & sh
13.00			3.807		4.283			4.0449	interbedded ss & sh
13.08			2.140		1.902			2.0211	interbedded ss & sh
13.17			1.140		1.283			1.2115	interbedded ss & sh
13.25			2.233		2.233			2.2333	interbedded ss & sh
13.33			3.426		3.023			3.2242	interbedded ss & sh
13.42			3.426		3.426			3.4259	interbedded ss & sh
13.46			0.002		8e-04			0.0014	interbedded ss & sh
13.50			0.665		0.588			0.6267	interbedded ss & sh
13.58			1.604		1.283			1.4436	interbedded ss & sh
13.66			0.003		0.043			0.0230	interbedded ss & sh
14.47			0.003		9e-04			0.0018	interbedded ss & sh
14.50			1.387		2.140			1.7636	interbedded ss & sh
14.60			1.283		1.712			1.4972	interbedded ss & sh
14.68			2.283		1.656			1.9696	interbedded ss & sh
14.77			2.704		1.115			1.9095	interbedded ss & sh
14.85			2.014		2.704			2.3590	interbedded ss & sh
14.93			3.426		2.704			3.0650	interbedded ss & sh
15.02			2.569		3.023			2.7956	interbedded ss & sh

Appendix 13 continued.

Depth (ft)	Column 1	Column 2	Column 3	Column 4	Column 5	Column 6	Column 7	Ave. Perm.	Lithofacies
15.10			3.807		4.283			4.0450	interbedded ss & sh
15.19			3.426		3.426			3.4257	interbedded ss & sh
15.27			0.002		5e-04			0.0011	interbedded ss & sh
15.35			3.356		3.444			3.4002	interbedded ss & sh
15.43			0.197		0.260			0.2284	interbedded ss & sh
15.52			0.030		0.004			0.0170	interbedded ss & sh
15.68			1.426		2.704			2.0650	interbedded ss & sh
15.77			1.802		3.671			2.7363	interbedded ss & sh
15.82			0.004		0.001			0.0027	interbedded ss & sh
15.85			3.114		4.283			3.6987	interbedded ss & sh
15.93			4.283		3.954			4.1184	interbedded ss & sh
16.02			3.114		3.426			3.2702	interbedded ss & sh
16.10			4.283		3.426			3.8546	interbedded ss & sh
16.15			0.003		0.001			0.0018	interbedded ss & sh
16.17			0.743		0.624			0.6835	interbedded ss & sh
16.25			0.321		0.210			0.2651	interbedded ss & sh
16.48			0.005		0.003			0.0038	interbedded ss & sh
16.50			1.069		1.252			1.1601	interbedded ss & sh
16.67			0.073		0.105			0.0891	interbedded ss & sh
16.75			0.110		0.170			0.1398	interbedded ss & sh
16.92			0.006		0.004			0.0048	interbedded ss & sh
17.00			0.539		0.393			0.4656	interbedded ss & sh
17.08			0.884		0.657			0.7702	interbedded ss & sh
17.17			0.040		0.036			0.0377	interbedded ss & sh
17.25			0.248		0.098			0.1728	interbedded ss & sh
17.33			0.224		0.419			0.3212	interbedded ss & sh
17.50			0.002		0.002			0.0020	interbedded ss & sh
17.58			0.003		0.002			0.0023	interbedded ss & sh
17.62			8e-04		8e-04			0.0008	interbedded ss & sh
17.75			1.510		0.342			0.9261	interbedded ss & sh
17.85			0.002		0.002			0.0018	interbedded ss & sh
17.92			1.426		1.712			1.5687	med-scale x-bedded ss
18.00			4.283		4.283			4.2831	med-scale x-bedded ss
18.08			3.426		2.855			3.1402	med-scale x-bedded ss
18.25			0.127		0.072			0.0994	med-scale x-bedded ss

Appendix 13 continued.

Depth (ft)	Column 1	Column 2	Column 3	Column 4	Column 5	Column 6	Column 7	Ave. Perm.	Lithofacies
18.42			4.283		3.212			3.7474	med-scale x-bedded ss
18.50			2.446		2.446			2.4463	med-scale x-bedded ss
18.58			0.743		0.309			0.5257	med-scale x-bedded ss
18.73			0.012		0.014			0.0128	interbedded ss & sh
18.81			0.002		0.342			0.1722	interbedded ss & sh
18.90			1.510		4.283			2.8965	med-scale x-bedded ss
18.98			3.426		4.283			3.8546	med-scale x-bedded ss
19.06			3.114		4.283			3.6987	med-scale x-bedded ss
19.15			4.283		4.283			4.2832	med-scale x-bedded ss
19.23			4.283		4.283			4.2832	med-scale x-bedded ss
19.31			2.014		1.902			1.9581	med-scale x-bedded ss
19.40			1.902		2.233			2.0677	med-scale x-bedded ss
19.48			2.335		2.233			2.2842	med-scale x-bedded ss
19.56			2.855		2.704			2.7793	med-scale x-bedded ss
19.65			3.807		3.114			3.4606	med-scale x-bedded ss
19.79			6e-04		4e-04			0.0005	med-scale x-bedded ss
19.88			0.006		0.022			0.0138	med-scale x-bedded ss
19.96			0.269		0.556			0.4128	med-scale x-bedded ss
19.98			0.003		8e-04			0.0019	interbedded ss & sh
20.00			1.902		1.902			1.9020	interbedded ss & sh
20.08			2.335		2.446			2.3907	interbedded ss & sh
20.17			2.140		1.656			1.8982	interbedded ss & sh
20.25			0.007		0.010			0.0085	interbedded ss & sh
20.33			0.010		0.022			0.0158	interbedded ss & sh
21.75	2.635	1.556	1.358	1.042	1.426	1.316	1.956	1.3916	interbedded ss & sh
21.79	1.755	1.082	1.358	1.402	1.239	2.253	2.314	1.2984	interbedded ss & sh
21.83	2.314	0.960	1.426	1.755	1.770	2.446	1.975	1.5980	interbedded ss & sh
21.88	2.140	2.054	1.475	1.316	1.770	1.645	1.711	1.6226	interbedded ss & sh
21.92	2.676	1.380	1.426	1.783	1.528	1.155	2.676	1.4766	interbedded ss & sh
21.96	2.362	1.670	1.555	1.902	2.075	2.378	1.902	1.8152	interbedded ss & sh
22.00	2.209	1.475	1.426	1.902	1.614	1.902	1.711	1.5199	interbedded ss & sh
22.04	2.335	1.746	1.902	1.802	1.711	1.902	2.054	1.8066	interbedded ss & sh
22.08	2.054	1.402	2.283	1.770	1.426	1.902	2.740	1.8541	interbedded ss & sh
22.13	1.975	2.195	2.209	2.335	2.209	2.195	3.294	2.2090	interbedded ss & sh
22.17	2.283	3.079	3.031	3.172	2.378	3.283	3.807	2.7044	interbedded ss & sh

Appendix 13 continued.

Depth (ft)	Column 1	Column 2	Column 3	Column 4	Column 5	Column 6	Column 7	Ave. Perm.	Lithofacies
22.20	2.283	1.711	1.755	1.614	1.645	2.140	3.671	1.7004	interbedded ss & sh
22.23	1.902	1.902	1.755	1.556	2.537	3.283	2.740	2.1461	med-scale x-bedded ss
22.25	2.054	1.187	1.975	2.854	3.426	3.283	2.854	2.7004	med-scale x-bedded ss
22.27	1.528	1.316	1.902	1.584	2.762	1.711	3.172	2.3319	med-scale x-bedded ss
23.00	6e-04	0.012	0.003	0.006	0.003	0.008	0.020	0.0034	interbedded ss & sh
23.02	0.118	0.014	0.003	0.002	0.002	0.002	0.073	0.0021	interbedded ss & sh
23.05	8e-04	0.002	1e-04	2e-04	1e-04	0.005	0.013	0.0001	interbedded ss & sh
23.07	0.393	0.539	0.004	0.006	0.170	0.105	0.110	0.0869	interbedded ss & sh
23.09	0.884	0.657	0.548	0.148	0.273	0.096	0.138	0.4105	interbedded ss & sh
23.11	0.004	0.003	0.004	0.004	0.004	8e-04	0.001	0.0040	interbedded ss & sh
23.13	8e-04	0.002	8e-04	4e-04	0.001	0.002	7e-04	0.0010	interbedded ss & sh
23.15	2.789	2.124	4.960	2.860	3.433	2.594	2.824	4.1965	med-scale x-bedded ss
23.17	3.234	5.580	4.058	3.881	5.580	5.580	5.580	4.8191	med-scale x-bedded ss
23.20	5.073	3.938	3.719	4.211	4.376	7.441	7.441	4.0477	med-scale x-bedded ss
23.22	5.315	5.191	5.191	4.376	6.566	4.852	5.191	5.8782	med-scale x-bedded ss
23.24	4.852	4.464	4.650	4.852	4.152	5.953	5.724	4.4010	med-scale x-bedded ss
23.26	5.073	4.555	4.292	4.152	3.658	4.852	4.852	3.9751	med-scale x-bedded ss
23.28	4.960	3.967	5.073	4.852	5.191	4.133	4.211	5.1318	med-scale x-bedded ss
23.30	5.073	7.201	5.874	5.580	4.292	4.749	4.749	5.0831	med-scale x-bedded ss
23.32	4.852	3.643	5.073	5.444	4.464	4.058	3.848	4.7683	med-scale x-bedded ss
23.34	4.749	3.658	4.058	4.464	4.376	3.848	5.315	4.2169	med-scale x-bedded ss
23.36	5.444	4.960	3.719	3.799	3.433	4.749	6.201	3.5762	med-scale x-bedded ss
23.38	5.191	4.852	4.852	3.967	4.650	3.938	4.292	4.7510	med-scale x-bedded ss
23.40	3.719	4.960	4.211	4.650	4.464	3.967	2.656	4.3373	med-scale x-bedded ss
23.42	5.191	3.719	4.464	3.487	4.058	6.378	4.376	4.2607	med-scale x-bedded ss
23.45	5.073	4.152	4.960	4.292	4.211	4.464	2.535	4.5855	med-scale x-bedded ss
23.47	5.073	6.566	4.960	4.650	4.133	4.464	5.874	4.5465	med-scale x-bedded ss
23.49	4.248	5.220	5.075	4.059	5.220	5.075	5.040	5.1471	med-scale x-bedded ss
23.51	5.373	3.971	3.971	5.846	5.220	6.090	5.769	4.5952	med-scale x-bedded ss
23.53	4.567	3.971	4.248	4.455	5.621	5.075	5.075	4.9347	med-scale x-bedded ss
23.55	3.886	3.581	4.455	3.971	4.059	4.567	4.248	4.2573	med-scale x-bedded ss
23.57	5.769	4.059	2.853	3.971	4.567	5.373	4.349	3.7100	med-scale x-bedded ss
23.59	6.090	3.321	0.506	3.728	5.846	6.090	5.709	3.1763	med-scale x-bedded ss
23.61	3.044	2.199	3.321	4.059	7.309	5.846	1.973	5.3146	med-scale x-bedded ss
23.63	4.567	4.684	5.220	4.455	4.059	5.894	6.090	4.6394	med-scale x-bedded ss

Appendix 13 continued.

Depth (ft)	Column 1	Column 2	Column 3	Column 4	Column 5	Column 6	Column 7	Ave. Perm.	Lithofacies
23.65	3.971	2.994	3.581	4.567	4.684	3.512	4.248	4.1326	med-scale x-bedded ss
23.67	5.536	5.536	5.413	4.059	4.248	4.151	4.349	4.8306	med-scale x-bedded ss
23.69	5.075	4.872	3.653	4.248	4.455	4.059	4.937	4.0542	med-scale x-bedded ss
23.72	5.846	3.653	5.075	6.449	4.872	4.937	5.040	4.9731	med-scale x-bedded ss
23.74	4.059	5.040	4.059	3.653	5.220	4.567	3.044	4.6394	med-scale x-bedded ss
23.76	5.373	5.075	6.449	5.769	4.807	4.807	6.090	5.6279	med-scale x-bedded ss
23.78	4.455	3.446	5.220	3.728	3.653	3.971	2.725	4.4363	med-scale x-bedded ss
23.80	3.971	2.572	4.151	5.621	5.846	5.075	2.945	4.9989	med-scale x-bedded ss
23.82	3.095	4.567	6.644	7.309	6.090	5.075	4.937	6.3671	med-scale x-bedded ss
23.84	5.220	4.455	4.349	4.567	4.807	3.446	4.807	4.5783	med-scale x-bedded ss
23.86	6.090	7.309	5.220	6.090	5.709	6.300	3.581	5.4645	med-scale x-bedded ss
23.88	5.075	3.971	5.220	6.644	4.349	2.646	3.044	4.7844	med-scale x-bedded ss
23.90	5.846	8.434	6.852	6.852	6.644	3.581	2.685	6.7479	med-scale x-bedded ss
23.92	4.807	5.709	5.220	6.090	5.220	3.382	3.149	5.2196	med-scale x-bedded ss
23.95	9.137	7.309	5.846	7.309	6.449	2.646	4.349	6.1474	med-scale x-bedded ss
23.97	5.040	6.090	5.075	7.309	6.090	3.321	2.809	5.5824	med-scale x-bedded ss
23.99	5.846	3.446	7.309	9.137	5.769	3.728	2.994	6.5391	med-scale x-bedded ss
24.01	1.755	1.587	2.809	1.587	0.324	0.195	0.110	1.5667	med-scale x-bedded ss
24.03	0.765	3.044	4.807	3.728	3.971	3.247	2.945	4.3891	med-scale x-bedded ss
24.05	3.223	3.971	4.807	3.564	3.971	3.479	3.044	4.3891	med-scale x-bedded ss
24.06	0.001	0.004	9e-04	0.003	7e-04	3e-04	0.003	0.0008	med-scale x-bedded ss
24.07	4.684	3.653	3.044	3.581	3.044	4.248	2.981	3.0436	med-scale x-bedded ss
24.09	3.321	2.809	4.151	2.402	3.108	4.567	2.725	3.6299	med-scale x-bedded ss
24.11	3.321	2.981	1.140	2.282	4.567	4.455	2.226	2.8532	med-scale x-bedded ss
24.13	3.321	1.984	2.006	2.254	1.921	2.123	2.608	1.9635	med-scale x-bedded ss
24.15	5.220	4.455	2.945	2.006	2.646	2.646	2.608	2.7958	med-scale x-bedded ss
24.18	4.059	3.321	2.981	2.467	2.767	3.653	3.653	2.8740	med-scale x-bedded ss
24.20	2.098	2.725	3.653	2.864	4.151	3.512	4.684	3.9022	med-scale x-bedded ss
24.22	3.398	2.467	3.581	3.581	4.349	3.971	4.059	3.9652	med-scale x-bedded ss
24.24	3.261	2.199	3.512	3.971	4.567	2.501	3.971	4.0396	med-scale x-bedded ss
24.26	1.755	2.853	3.261	3.886	3.261	2.501	3.321	3.2612	med-scale x-bedded ss
24.28	2.572	1.587	1.844	2.028	2.123	2.254	3.044	1.9831	med-scale x-bedded ss
24.30	2.341	2.402	2.467	3.095	3.176	2.371	3.108	2.8216	med-scale x-bedded ss
24.32	1.471	1.601	1.722	2.646	2.199	2.341	4.059	1.9605	med-scale x-bedded ss
24.34	2.148	1.520	1.459	2.074	3.131	3.971	3.728	2.2950	med-scale x-bedded ss

Appendix 13 continued.

Depth (ft)	Column 1	Column 2	Column 3	Column 4	Column 5	Column 6	Column 7	Ave. Perm.	Lithofacies
24.36	1.772	1.092	1.176	2.098	2.853	3.653	3.446	2.2986	med-scale x-bedded ss
24.38	1.844	1.520	1.241	3.653	2.467	2.608	3.653	2.4266	med-scale x-bedded ss
24.40	2.123	1.825	2.028	2.853	3.653	4.151	4.684	3.0453	med-scale x-bedded ss
24.42	0.003	0.006	0.004	0.001	8e-04	4e-04	0.003	0.0027	med-scale x-bedded ss
24.43	2.685	2.501	2.173	2.572	3.581	3.886	5.621	3.2886	med-scale x-bedded ss
24.45	3.261	2.572	2.226	2.899	3.971	3.886	4.059	3.2677	med-scale x-bedded ss
24.47	2.899	2.173	2.341	2.254	3.653	4.455	6.090	3.4092	med-scale x-bedded ss
24.49	3.971	3.321	2.945	4.248	5.040	6.090	5.621	4.4622	med-scale x-bedded ss
24.51	5.075	2.725	3.971	3.971	5.040	9.137	6.852	5.2528	med-scale x-bedded ss
24.53	5.075	3.886	3.653	5.769	7.309	7.309	8.434	5.9191	med-scale x-bedded ss
24.55	6.090	3.512	2.899	5.846	6.090	6.852	9.137	5.7751	med-scale x-bedded ss
24.57	3.728	3.095	5.220	4.455	5.040	8.434	6.449	5.2028	med-scale x-bedded ss
24.63	4.151	2.994	3.653	3.044	4.151	7.309	5.894	4.4564	med-scale x-bedded ss
24.65	2.371	4.059	2.402	3.044	3.321	3.581	3.728	3.2150	med-scale x-bedded ss
24.67	3.044	1.942	2.006	2.608	3.728	4.151	4.714	3.1704	med-scale x-bedded ss
24.69	2.981	2.199	2.767	4.684	4.059	4.807	5.075	3.7961	med-scale x-bedded ss
24.71	2.994	3.321	3.446	3.886	3.971	4.349	4.248	3.7449	med-scale x-bedded ss
24.73	2.994	3.321	3.044	3.653	4.151	5.075	5.846	4.0118	med-scale x-bedded ss
24.75	3.321	3.971	3.176	4.684	4.684	5.075	4.248	4.1654	med-scale x-bedded ss
24.78	5.894	4.059	3.581	3.321	3.971	4.349	4.937	4.3017	med-scale x-bedded ss
24.80	4.248	3.223	4.248	3.581	4.807	4.567	4.872	4.2208	med-scale x-bedded ss
24.82	5.220	4.059	3.971	4.059	3.971	4.684	5.536	4.4999	med-scale x-bedded ss
24.84	4.567	5.846	4.428	2.148	3.653	4.684	5.846	4.4532	med-scale x-bedded ss
24.86	3.653	4.349	3.805	3.653	3.971	5.075	6.090	4.3708	med-scale x-bedded ss
24.88	6.090	8.434	7.309	6.090	6.449	6.090	6.852	6.7590	med-scale x-bedded ss
24.90	4.567	4.455	3.581	4.807	3.971	7.309	7.309	5.1427	med-scale x-bedded ss
24.92	5.075	4.349	4.455	5.894	7.309	8.137	6.090	5.9011	med-scale x-bedded ss
24.94	5.220	3.581	3.446	4.151	5.894	4.714	6.090	4.7280	med-scale x-bedded ss
24.96	3.971	5.075	4.455	4.937	5.220	7.309	7.309	5.4679	med-scale x-bedded ss
24.98	4.455	4.684	5.220	6.449	6.090	6.449	5.536	5.5546	med-scale x-bedded ss
25.00	4.455	6.090	1.601	2.341	2.123	4.567	0.889	3.1521	med-scale x-bedded ss
25.02	8.656	8.442	4.937	3.176	4.937	4.151	7.309	5.9441	med-scale x-bedded ss
25.04	4.455	3.176	4.807	5.846	4.151	4.349	7.309	4.8706	med-scale x-bedded ss
25.06	4.567	5.846	4.455	6.090	6.090	8.616	6.852	6.0738	med-scale x-bedded ss
25.08	8.434	6.449	7.831	6.090	7.309	8.967	3.971	7.0071	med-scale x-bedded ss

Appendix 13 continued.

Depth (ft)	Column 1	Column 2	Column 3	Column 4	Column 5	Column 6	Column 7	Ave. Perm.	Lithofacies
25.10	5.075	3.512	5.220	3.728	3.261	2.467	2.767	3.7184	med-scale x-bedded ss
25.12	4.567	2.725	2.922	4.151	4.349	3.728	4.684	3.8751	med-scale x-bedded ss
25.15	3.728	3.131	2.994	4.567	3.581	3.886	4.567	3.7790	med-scale x-bedded ss
25.17	5.846	4.151	2.994	3.512	2.809	3.886	3.971	3.8814	med-scale x-bedded ss
25.19	4.937	4.248	3.512	3.044	2.994	2.981	2.767	3.4975	med-scale x-bedded ss
25.21	2.646	2.608	2.371	2.434	2.173	2.646	2.467	2.4781	med-scale x-bedded ss
25.23	2.767	2.402	2.608	2.572	3.971	3.044	2.536	2.8427	med-scale x-bedded ss
25.25	2.725	2.311	2.051	1.738	0.930	1.984	1.659	1.9139	med-scale x-bedded ss
25.27	2.501	2.123	1.738	0.740	1.208	1.303	1.705	1.6168	med-scale x-bedded ss
25.29	2.123	3.131	1.722	2.199	1.587	2.199	2.501	2.2087	med-scale x-bedded ss
25.31	3.971	2.994	3.728	2.341	1.882	1.425	1.844	2.5975	med-scale x-bedded ss
25.33	2.685	2.028	1.844	2.282	2.226	3.247	2.809	2.4458	med-scale x-bedded ss
25.35	2.646	2.536	2.646	3.044	2.864	1.772	2.725	2.6048	med-scale x-bedded ss
25.37	2.123	2.501	1.921	2.148	1.382	1.722	1.249	1.8636	med-scale x-bedded ss
25.39	1.294	1.659	2.371	1.331	2.646	2.311	2.739	2.0501	med-scale x-bedded ss
25.45	0.127	0.206	0.048	0.037	0.031	0.066	0.048	0.0803	med-scale x-bedded ss
25.47	0.085	0.110	0.060	0.048	0.102	0.776	0.439	0.2314	med-scale x-bedded ss
25.49	2.112	2.014	2.209	1.336	1.501	1.902	1.701	1.8250	med-scale x-bedded ss
25.51	1.988	2.362	1.614	1.630	1.450	2.314	1.882	1.8913	med-scale x-bedded ss
25.53	2.636	2.362	2.953	2.595	4.350	2.446	2.520	2.8374	med-scale x-bedded ss
25.55	2.258	2.283	2.233	2.595	2.253	1.902	2.077	2.2286	med-scale x-bedded ss
25.58	1.105	1.005	1.204	1.426	2.740	1.426	2.078	1.5691	med-scale x-bedded ss
25.60	1.752	1.902	1.380	1.975	2.054	2.075	2.065	1.8860	med-scale x-bedded ss
25.62	2.059	2.446	1.592	2.140	2.854	4.283	3.569	2.7061	med-scale x-bedded ss
25.70	0.057	0.059	0.057	0.031	0.017	0.016	0.032	0.0384	med-scale x-bedded ss
25.72	0.172	0.268	0.394	0.394	0.460	0.632	1.450	0.5385	med-scale x-bedded ss
25.74	1.239	0.755	0.637	1.155	1.450	1.017	2.594	1.2640	med-scale x-bedded ss
25.77	0.939	0.513	0.498	0.609	0.550	1.155	0.949	0.7449	med-scale x-bedded ss
25.79	0.378	0.450	0.196	0.115	0.181	0.390	0.387	0.2995	med-scale x-bedded ss
26.18	5e-04	5e-04	8e-04	6e-04	3e-04	4e-04	5e-04	0.0005	med-scale x-bedded ss
26.20	0.039	0.056	0.149	0.006	2.399	2.506	1.198	0.9075	med-scale x-bedded ss
26.22	1.664	0.697	2.124	3.138	4.152	3.717	3.281	2.6819	med-scale x-bedded ss
26.24	1.273	1.288	1.311	4.749	4.376	2.936	3.658	2.7987	med-scale x-bedded ss
26.26	2.754	2.373	2.688	3.770	4.852	3.039	3.251	3.2468	med-scale x-bedded ss
26.28	3.281	0.870	4.211	4.960	3.848	3.143	3.056	3.3383	med-scale x-bedded ss

Appendix 13 continued.

Depth (ft)	Column 1	Column 2	Column 3	Column 4	Column 5	Column 6	Column 7	Ave. Perm.	Lithofacies
26.30	3.542	3.056	2.656	2.373	3.626	3.433	3.599	3.1837	med-scale x-bedded ss
26.32	2.535	2.789	1.651	1.991	3.476	3.253	2.721	2.6307	med-scale x-bedded ss
26.35	2.399	1.874	2.721	3.143	4.852	3.634	3.056	3.0969	med-scale x-bedded ss
26.37	2.399	2.399	3.643	3.719	3.330	3.381	3.658	3.2185	med-scale x-bedded ss
26.39	3.626	4.852	4.650	3.643	3.015	3.433	3.330	3.7927	med-scale x-bedded ss
26.41	3.926	4.259	3.938	2.936	3.330	3.719	3.291	3.6284	med-scale x-bedded ss
26.43	3.893	3.985	4.650	2.373	3.234	1.784	2.824	3.2489	med-scale x-bedded ss
26.45	3.800	4.058	2.754	2.860	3.719	2.721	2.124	3.1480	med-scale x-bedded ss
26.47	3.542	3.234	3.188	2.104	2.253	1.974	1.548	2.5488	med-scale x-bedded ss
26.49	3.719	2.860	1.956	2.564	1.570	1.616	1.651	2.2767	med-scale x-bedded ss
26.51	4.058	2.065	2.594	2.936	2.373	2.399	2.399	2.6889	med-scale x-bedded ss
26.53	3.599	4.555	2.936	3.330	2.721	3.967	3.433	3.5059	med-scale x-bedded ss
26.55	4.292	2.721	3.015	3.967	3.658	2.975	3.281	3.4157	med-scale x-bedded ss
26.57	3.506	2.721	3.188	3.658	4.292	3.143	3.143	3.3786	med-scale x-bedded ss
26.60	3.711	3.915	4.749	4.960	3.143	3.613	3.492	3.9404	med-scale x-bedded ss
26.62	3.521	3.330	4.852	3.234	3.967	4.555	3.719	3.8826	med-scale x-bedded ss
26.64	4.186	4.852	3.433	3.381	3.487	4.650	4.248	4.0339	med-scale x-bedded ss
26.66	3.300	3.610	3.967	4.251	2.928	2.625	4.376	3.5795	med-scale x-bedded ss
26.68	2.104	2.009	1.376	3.281	1.351	2.165	1.592	1.9826	med-scale x-bedded ss
26.70	1.858	1.939	2.124	3.143	4.292	1.559	3.719	2.6620	med-scale x-bedded ss
26.72	7e-04	8e-04	8e-04	5e-04	8e-04	6e-04	5e-04	0.0007	med-scale x-bedded ss
26.74	4.376	3.719	4.852	3.281	4.852	5.580	3.099	4.2515	med-scale x-bedded ss
26.76	6.033	5.073	3.433	3.281	5.724	3.658	5.073	4.6107	med-scale x-bedded ss
26.78	3.967	2.860	3.330	5.444	4.852	5.073	3.433	4.1372	med-scale x-bedded ss
26.80	4.555	5.073	3.967	5.191	3.599	4.376	4.749	4.5014	med-scale x-bedded ss
26.82	4.292	4.133	6.201	5.191	4.650	3.719	4.960	4.7351	med-scale x-bedded ss
26.84	3.782	3.487	2.479	4.292	4.211	2.789	3.234	3.4676	med-scale x-bedded ss
26.86	2.425	3.658	4.749	4.376	3.792	3.648	4.292	3.8485	med-scale x-bedded ss
26.88	3.719	3.599	4.058	2.975	2.789	3.719	4.555	3.6306	med-scale x-bedded ss
26.91	3.381	3.799	2.564	3.570	4.133	3.542	3.719	3.5297	med-scale x-bedded ss
26.93	3.599	4.152	3.782	3.234	3.234	4.251	3.433	3.6693	med-scale x-bedded ss
26.95	2.898	2.789	3.381	3.143	2.564	3.487	4.058	3.1883	med-scale x-bedded ss
26.97	3.487	4.555	5.444	4.058	3.719	3.826	3.381	4.0670	med-scale x-bedded ss
26.99	4.058	3.281	3.719	4.852	3.799	4.464	4.749	4.1316	med-scale x-bedded ss
27.01	4.292	4.464	7.441	5.580	3.719	3.719	4.292	4.7868	med-scale x-bedded ss

Appendix 13 continued.

Depth (ft)	Column 1	Column 2	Column 3	Column 4	Column 5	Column 6	Column 7	Ave. Perm.	Lithofacies
27.03	2.425	3.234	5.580	4.292	3.234	2.348	2.860	3.4247	med-scale x-bedded ss
27.05	7e-04	5e-04	7e-04	4e-04	9e-04	6e-04	5e-04	0.0006	med-scale x-bedded ss
27.07	4.211	2.594	4.292	3.599	2.656	2.688	2.824	3.2662	med-scale x-bedded ss
27.10	5.043	5.874	3.719	3.330	3.719	4.211	2.594	4.0701	med-scale x-bedded ss
27.12	4.830	5.874	4.852	2.451	1.991	1.061	2.160	3.3170	med-scale x-bedded ss
27.14	2.373	1.429	1.728	1.818	1.218	1.999	2.824	1.9126	med-scale x-bedded ss
27.16	2.479	3.188	2.386	1.874	1.843	2.898	3.188	2.5506	med-scale x-bedded ss
27.18	3.719	3.487	2.754	2.594	2.208	1.991	3.381	2.8763	med-scale x-bedded ss
27.20	3.550	3.381	3.719	2.324	1.798	3.099	4.058	3.1326	med-scale x-bedded ss
27.22	3.249	2.479	1.922	1.137	1.627	2.824	2.594	2.2617	med-scale x-bedded ss
27.25	3.719	2.441	1.288	1.303	1.548	2.824	3.719	2.4061	med-scale x-bedded ss
27.27	3.658	2.276	1.991	1.438	2.104	2.860	2.789	2.4452	med-scale x-bedded ss
27.29	3.188	2.936	2.625	2.208	1.537	1.939	3.381	2.5448	med-scale x-bedded ss
27.31	2.065	2.027	1.874	1.527	1.991	2.009	3.099	2.0846	med-scale x-bedded ss
27.33	2.348	1.506	1.843	1.968	1.863	1.651	1.516	1.8138	med-scale x-bedded ss
27.35	2.230	1.784	1.359	2.535	1.843	1.438	1.974	1.8803	med-scale x-bedded ss
27.37	2.324	1.689	1.991	1.581	1.974	1.402	1.798	1.8226	med-scale x-bedded ss
27.39	1.874	1.843	1.702	2.789	2.506	3.188	1.858	2.2513	med-scale x-bedded ss
27.41	1.702	2.230	2.104	3.143	3.643	2.975	3.143	2.7057	med-scale x-bedded ss
27.43	3.799	2.824	2.936	3.915	2.721	2.046	3.719	3.1371	med-scale x-bedded ss
27.46	2.860	2.975	4.058	4.749	4.555	5.073	4.464	4.1047	med-scale x-bedded ss
27.48	3.487	2.451	5.580	5.444	4.292	4.292	3.658	4.1721	med-scale x-bedded ss
27.50	2.975	3.719	3.938	3.188	3.188	5.191	3.542	3.6772	med-scale x-bedded ss
27.52	2.898	3.381	3.658	2.688	3.487	4.211	3.381	3.3861	med-scale x-bedded ss
27.54	3.487	5.073	4.464	4.058	4.292	4.292	5.191	4.4079	med-scale x-bedded ss
27.56	2.479	1.858	3.056	4.058	4.058	3.330	6.378	3.6024	med-scale x-bedded ss
27.58	4.650	3.433	2.276	2.754	3.015	4.464	6.033	3.8036	med-scale x-bedded ss
27.60	5.874	5.073	4.211	3.542	5.444	6.201	4.211	4.9365	med-scale x-bedded ss
27.62	2.688	1.784	2.230	2.625	5.580	3.643	3.927	3.2110	med-scale x-bedded ss
27.64	2.564	2.253	1.548	2.564	5.724	4.058	3.992	3.2433	med-scale x-bedded ss
27.66	4e-04	6e-04	5e-04	4e-04	5e-04	4e-04	4e-04	0.0005	med-scale x-bedded ss
27.68	4.852	3.938	5.580	6.378	4.292	7.441	6.765	5.6067	med-scale x-bedded ss
27.70	7.879	7.441	4.650	5.724	6.201	5.444	4.464	5.9718	med-scale x-bedded ss
27.72	4.749	6.033	5.073	5.315	5.953	5.315	3.056	5.0704	med-scale x-bedded ss
27.74	4.133	4.376	4.376	4.960	5.191	2.625	3.848	4.2154	med-scale x-bedded ss

Appendix 13 continued.

Depth (ft)	Column 1	Column 2	Column 3	Column 4	Column 5	Column 6	Column 7	Ave. Perm.	Lithofacies
27.76	3.953	3.807	3.426	3.426	4.283	3.807	3.658	3.7656	med-scale x-bedded ss
27.78	3.172	4.283	4.031	3.294	3.807	1.850	2.283	3.2456	med-scale x-bedded ss
27.81	2.283	1.678	2.054	1.902	2.854	2.140	1.711	2.0888	med-scale x-bedded ss
27.83	2.762	1.711	1.678	1.555	1.068	1.316	0.798	1.5555	med-scale x-bedded ss
27.85	1.956	2.054	2.762	1.850	1.380	2.335	1.902	2.0341	med-scale x-bedded ss
27.87	2.953	1.645	1.121	1.155	1.475	0.899	3.426	1.8106	med-scale x-bedded ss
27.89	2.446	2.195	1.711	1.450	1.055	1.711	2.253	1.8316	med-scale x-bedded ss
27.91	2.854	1.426	1.380	1.755	1.850	2.209	2.446	1.9886	med-scale x-bedded ss
27.93	2.676	1.188	1.171	1.475	1.121	0.769	2.446	1.5494	med-scale x-bedded ss
27.95	2.140	1.678	1.902	0.881	1.426	0.909	1.380	1.4734	med-scale x-bedded ss
27.97	0.656	0.641	0.899	0.939	1.030	0.798	1.711	0.9535	med-scale x-bedded ss
27.99	5e-04	9e-04	4e-04	5e-04	9e-04	5e-04	3e-04	0.0006	med-scale x-bedded ss
28.02	1.555	1.402	0.484	1.678	2.233	2.595	3.274	1.8887	med-scale x-bedded ss
28.04	3.294	3.058	2.335	2.446	3.262	3.953	3.608	3.1366	med-scale x-bedded ss
28.06	3.058	1.426	1.902	2.283	3.058	3.262	3.217	2.6009	med-scale x-bedded ss
28.08	3.724	2.953	2.054	4.542	4.647	3.172	1.903	3.2848	med-scale x-bedded ss
28.10	2.314	2.446	1.052	2.378	2.595	3.114	3.294	2.4560	med-scale x-bedded ss
28.12	0.113	0.093	0.114	0.054	0.034	0.060	0.045	0.0731	med-scale x-bedded ss
28.14	3.426	2.854	3.606	3.807	4.079	3.606	2.740	3.4454	med-scale x-bedded ss
28.16	2.762	2.446	4.283	4.283	4.157	4.031	3.426	3.6267	med-scale x-bedded ss
28.18	2.646	2.608	2.371	2.434	2.173	2.646	2.467	2.4781	med-scale x-bedded ss
28.20	0.003	0.003	0.003	9e-04	5e-04	0.002	7e-04	0.0020	med-scale x-bedded ss
28.22	2.725	2.311	2.051	1.738	0.930	1.984	1.659	1.9139	med-scale x-bedded ss
28.24	2.501	2.123	1.738	0.740	1.208	1.303	1.705	1.6168	med-scale x-bedded ss
28.26	2.123	3.131	1.722	2.199	1.587	2.199	2.501	2.2087	med-scale x-bedded ss
28.28	3.971	2.994	3.728	2.341	1.882	1.425	1.844	2.5975	med-scale x-bedded ss
28.30	2.685	2.028	1.844	2.282	2.226	3.247	2.809	2.4458	med-scale x-bedded ss
28.32	2.646	2.536	2.646	3.044	2.864	1.772	2.725	2.6048	med-scale x-bedded ss
28.34	2.123	2.501	1.921	2.148	1.382	1.722	1.249	1.8636	med-scale x-bedded ss
28.36	1.294	1.659	2.371	1.331	2.646	2.311	2.739	2.0501	med-scale x-bedded ss
28.38	2.187	2.451	2.656	4.251	6.378	3.381	3.719	3.5747	med-scale x-bedded ss
28.40	1.691	2.253	0.846	1.974	2.065	1.108	1.716	1.6646	med-scale x-bedded ss
28.44	1e-04	7e-04	8e-04	6e-04	3e-04	3e-04	6e-04	0.0005	ripple x-laminated ss
28.46	0.837	0.570	1.166	0.207	0.454	0.376	0.469	0.5827	ripple x-laminated ss
28.48	0.421	0.725	0.551	0.193	0.114	0.070	0.664	0.3910	ripple x-laminated ss

Appendix 13 continued.

Depth (ft)	Column 1	Column 2	Column 3	Column 4	Column 5	Column 6	Column 7	Ave. Perm.	Lithofacies
28.50	0.412	0.167	0.228	0.166	0.273	0.123	0.230	0.2282	ripple x-laminated ss
28.52	3.433	1.858	2.373	2.300	1.051	0.415	1.906	1.9051	med-scale x-bedded ss
28.54	5.874	4.133	5.073	3.330	3.056	3.281	4.152	4.1286	med-scale x-bedded ss
28.56	4.376	7.144	3.368	5.724	4.464	5.874	7.441	5.4844	med-scale x-bedded ss
28.58	7e-04	3e-04	6e-04	9e-04	5e-04	3e-04	8e-04	0.0006	med-scale x-bedded ss
28.60	8.930	5.580	7.698	3.599	3.848	1.828	5.073	5.2223	med-scale x-bedded ss
28.62	8.924	8.977	8.930	7.144	6.869	7.441	5.874	7.7370	med-scale x-bedded ss
28.64	8.930	7.879	8.999	8.505	12.18	8.372	8.930	9.1135	med-scale x-bedded ss
28.66	8.930	7.144	7.144	8.956	8.930	8.505	8.899	8.3583	med-scale x-bedded ss
28.68	8.930	7.441	8.930	8.505	7.144	7.441	6.378	7.8243	med-scale x-bedded ss
28.70	5.724	6.158	7.765	6.201	7.441	8.930	8.943	7.3089	med-scale x-bedded ss
28.72	8.930	6.378	8.930	7.879	7.765	5.580	8.118	7.6545	med-scale x-bedded ss
28.74	7.441	7.144	8.937	5.724	8.985	5.580	4.852	6.9518	med-scale x-bedded ss
28.76	8.372	8.372	8.372	7.441	6.378	7.201	6.378	7.5021	med-scale x-bedded ss
28.78	6.378	7.698	7.441	7.879	7.201	4.852	7.144	6.9420	med-scale x-bedded ss
28.81	6.566	8.976	8.930	7.441	8.930	7.144	7.441	7.9184	med-scale x-bedded ss
28.83	7.441	7.879	8.505	8.372	8.930	7.441	6.378	7.8496	med-scale x-bedded ss
28.85	3.381	3.599	4.464	4.749	4.852	6.378	7.144	4.9381	med-scale x-bedded ss
28.87	5.444	7.201	4.852	3.099	2.145	4.960	5.073	4.6820	med-scale x-bedded ss
28.89	5.724	5.073	4.376	6.158	4.960	5.315	4.852	5.2081	med-scale x-bedded ss
28.91	4e-04	8e-04	6e-04	9e-04	6e-04	3e-04	5e-04	0.0006	med-scale x-bedded ss
28.93	8.372	8.118	7.144	5.315	5.724	6.765	6.765	6.8859	med-scale x-bedded ss
28.95	5.444	5.724	7.144	8.940	8.930	5.073	7.201	6.9222	med-scale x-bedded ss
28.97	4.852	4.292	3.658	4.852	6.378	7.441	6.201	5.3821	med-scale x-bedded ss
28.99	8.505	7.879	5.580	3.056	4.376	4.464	4.960	5.5458	med-scale x-bedded ss
29.01	6.158	5.724	7.144	7.441	7.441	6.033	7.441	6.7689	med-scale x-bedded ss
29.03	7.201	7.441	6.033	5.953	7.441	6.201	7.201	6.7817	med-scale x-bedded ss
29.06	8.949	8.951	8.953	7.144	6.033	4.960	5.724	7.2447	med-scale x-bedded ss
29.08	8.372	7.441	7.201	8.505	7.201	6.033	6.614	7.3383	med-scale x-bedded ss
29.10	5.874	5.580	8.505	7.201	8.372	8.505	8.930	7.5669	med-scale x-bedded ss
29.12	3.433	4.852	5.073	6.378	6.378	8.956	8.957	6.2896	med-scale x-bedded ss
29.14	4.749	4.464	4.650	3.658	3.433	4.133	7.441	4.6468	med-scale x-bedded ss
29.16	6.614	5.073	5.191	4.292	4.376	4.960	5.073	5.0827	med-scale x-bedded ss
29.18	7.441	7.144	6.201	5.580	5.874	5.724	6.158	6.3031	med-scale x-bedded ss
29.20	8.930	6.566	6.378	6.378	6.378	7.144	5.953	6.8180	med-scale x-bedded ss

Appendix 13 continued.

Depth (ft)	Column 1	Column 2	Column 3	Column 4	Column 5	Column 6	Column 7	Ave. Perm.	Lithofacies
29.22	7.765	7.441	6.378	5.724	5.580	8.372	8.930	7.1701	med-scale x-bedded ss
29.24	0.702	1.273	0.952	4.292	3.719	5.580	6.378	3.2710	med-scale x-bedded ss
29.30	4e-04	4e-04	9e-04	6e-04	5e-04	6e-04	3e-04	0.0005	med-scale x-bedded ss
29.32	3.188	4.852	4.292	4.292	4.058	4.852	5.580	4.4448	med-scale x-bedded ss
29.34	9e-04	9e-04	9e-04	6e-04	5.580	4.960	5.191	2.2478	med-scale x-bedded ss
29.36	5.191	4.960	3.143	3.188	6e-04	5.191	7.201	4.1248	med-scale x-bedded ss
29.38	6e-04	9e-04	6.378	4.152	2.187	4e-04	4.650	2.4812	med-scale x-bedded ss
29.40	3.938	4.133	4e-04	4e-04	2e-04	4e-04	4e-04	1.1533	med-scale x-bedded ss
29.42	5.444	4.292	3.799	5.191	3.848	6.033	5.953	4.9370	med-scale x-bedded ss
29.44	4.749	4.650	4.960	4.152	4.464	5.444	4.960	4.7684	med-scale x-bedded ss
29.47	6.201	4.376	6.033	4.749	5.444	4.464	5.315	5.2259	med-scale x-bedded ss
29.49	3.881	4.960	4.960	5.191	6.614	6.158	5.724	5.3554	med-scale x-bedded ss
29.51	4.749	5.724	5.073	4.555	5.191	6.378	7.441	5.5872	med-scale x-bedded ss
29.53	4.133	3.643	4.464	4.292	6.201	5.724	5.444	4.8429	med-scale x-bedded ss
29.55	2.824	4.555	4.376	3.234	3.433	6.378	5.874	4.3820	med-scale x-bedded ss
29.57	7.441	4.376	3.719	4.749	4.555	3.487	4.464	4.6844	med-scale x-bedded ss
29.59	7.441	8.372	5.580	3.719	2.721	5.073	4.464	5.3386	med-scale x-bedded ss
29.61	5.191	5.444	6.158	5.580	6.614	5.315	3.381	5.3833	med-scale x-bedded ss
29.63	5.073	4.464	5.444	5.444	4.960	5.724	4.852	5.1372	med-scale x-bedded ss
29.65	5.580	4.852	5.580	4.960	5.874	6.378	5.874	5.5856	med-scale x-bedded ss
29.67	4.743	4.649	4.387	5.444	5.346	5.347	4.625	4.9346	med-scale x-bedded ss
29.69	3.673	3.860	3.762	4.864	4.753	4.876	2.953	4.1060	med-scale x-bedded ss
29.71	2.535	3.381	2.594	3.622	3.575	3.436	1.273	2.9167	med-scale x-bedded ss
29.73	3e-04	1.142	1.956	2.656	2.898	2.104	1.581	1.7625	med-scale x-bedded ss
29.75	2.399	6e-04	2e-04	4e-04	3e-04	3e-04	4e-04	0.3430	med-scale x-bedded ss
29.77	2.936	5.580	4.960	4.555	5.953	5.073	3.381	4.6339	med-scale x-bedded ss
29.79	3.881	4.960	5.191	4.058	4.555	4.152	4.852	4.5212	med-scale x-bedded ss
29.81	4.749	5.724	5.073	6.201	7.441	5.315	5.191	5.6704	med-scale x-bedded ss
29.83	4.133	3.643	5.191	6.201	6.201	5.444	5.315	5.1610	med-scale x-bedded ss
29.87	0.543	0.656	0.683	0.029	0.027	0.023	0.026	0.2838	muddy bioturbated ss
29.89	0.004	0.005	0.004	0.009	0.016	1.296	0.368	0.2429	muddy bioturbated ss
29.91	5e-04	5e-04	5e-04	7e-04	5e-04	0.001	0.001	0.0007	muddy bioturbated ss
29.93	6e-04	3e-04	3e-04	5e-04	8e-04	6e-04	4e-04	0.0005	muddy bioturbated ss
29.95	4e-04	5e-04	4e-04	0.002	0.001	6e-04	6e-04	0.0008	muddy bioturbated ss
29.97	7e-04	5e-04	3e-04	5e-04	2e-04	4e-04	3e-04	0.0004	muddy bioturbated ss

Appendix 13 continued.

Depth (ft)	Column 1	Column 2	Column 3	Column 4	Column 5	Column 6	Column 7	Ave. Perm.	Lithofacies
29.99	0.003	0.008	8e-04	3e-04	3e-04	3e-04	5e-04	0.0018	muddy bioturbated ss
30.01	0.008	0.014	0.019	0.019	0.010	0.007	0.030	0.0152	muddy bioturbated ss
30.03	5.315	1.742	1.559	3.143	3.985	5.724	2.348	3.4021	med-scale x-bedded ss
30.05	9e-04	9e-04	6e-04	2e-04	9e-04	7e-04	2e-04	0.0006	med-scale x-bedded ss
30.07	7.879	8.372	4.211	7.441	7.201	5.761	3.719	6.3692	med-scale x-bedded ss
30.09	6.765	7.879	2.754	7.050	5.580	7.441	7.144	6.3733	med-scale x-bedded ss
30.11	2.399	4.650	4.650	5.444	4.749	6.201	4.152	4.6063	med-scale x-bedded ss
30.13	7.441	5.580	4.852	5.724	2.754	2.594	2.754	4.5286	med-scale x-bedded ss
30.15	2.027	2.936	1.191	1.393	1.874	2.253	2.276	1.9929	med-scale x-bedded ss
30.17	0.009	0.003	0.004	0.002	0.007	0.003	0.006	0.0048	med-scale x-bedded ss
30.19	1.516	1.616	0.977	1.114	0.582	0.538	0.340	0.9546	med-scale x-bedded ss
30.21	2.399	2.955	2.623	2.020	1.165	1.475	1.512	2.0213	med-scale x-bedded ss
30.23	3.719	4.852	3.938	2.324	0.894	2.721	2.870	3.0453	med-scale x-bedded ss
30.25	7.441	5.073	1.874	1.874	2.721	3.799	4.376	3.8796	med-scale x-bedded ss
30.27	4.555	1.131	1.311	0.968	1.813	1.890	2.975	2.0917	med-scale x-bedded ss
30.29	2.300	1.702	2.065	1.384	2.425	2.594	3.099	2.2240	med-scale x-bedded ss
30.31	4.555	2.721	2.027	1.676	1.486	1.858	1.874	2.3139	med-scale x-bedded ss
30.33	4.464	2.824	2.230	1.858	2.124	2.898	2.898	2.7565	med-scale x-bedded ss
30.35	2.479	2.451	1.537	2.688	2.754	2.208	1.438	2.2222	med-scale x-bedded ss
30.37	2.789	2.399	1.702	1.939	2.253	2.208	2.208	2.2140	med-scale x-bedded ss
30.4	4.251	3.188	1.676	2.187	1.956	2.348	2.789	2.6278	med-scale x-bedded ss
30.42	2.348	2.451	3.433	3.487	3.234	2.479	2.975	2.9152	med-scale x-bedded ss
30.44	2.084	2.046	1.742	1.770	2.124	2.656	2.564	2.1408	med-scale x-bedded ss
30.46	2.789	1.922	1.715	1.334	1.828	2.230	2.754	2.0818	med-scale x-bedded ss
30.48	2.373	3.143	2.348	4.211	3.719	4.555	5.191	3.6485	med-scale x-bedded ss
30.50	4.355	4.152	4.852	4.960	3.658	5.724	4.797	4.6426	med-scale x-bedded ss
30.52	2.721	3.719	1.784	2.065	2.348	3.719	4.550	2.9866	med-scale x-bedded ss
30.54	2.721	2.208	2.754	2.860	3.529	4.231	5.133	3.3481	med-scale x-bedded ss
30.56	3.051	3.247	3.618	3.974	5.379	5.444	5.724	4.3482	med-scale x-bedded ss
30.58	3.381	4.464	4.852	5.444	5.315	5.580	5.315	4.9072	med-scale x-bedded ss
30.60	4.376	2.656	3.599	4.152	5.580	6.697	7.441	4.9289	med-scale x-bedded ss
30.62	3.938	4.376	6.201	5.724	6.378	6.158	6.033	5.5439	med-scale x-bedded ss
30.64	5.315	5.724	3.881	4.555	6.976	5.874	6.765	5.5842	med-scale x-bedded ss
30.66	9e-04	6e-04	2e-04	3e-04	2e-04	5e-04	8e-04	0.0005	med-scale x-bedded ss
30.68	6.614	6.378	5.580	4.852	6.614	5.073	3.719	5.5473	med-scale x-bedded ss

Appendix 13 continued.

Depth (ft)	Column 1	Column 2	Column 3	Column 4	Column 5	Column 6	Column 7	Ave. Perm.	Lithofacies
30.70	7.201	6.566	6.566	8.372	7.441	6.201	7.441	7.1126	med-scale x-bedded ss
30.72	5e-04	8e-04	9e-04	7e-04	8e-04	2e-04	2e-04	0.0006	med-scale x-bedded ss
30.74	5.580	4.960	5.724	0.005	7.879	8.372	6.566	5.5837	med-scale x-bedded ss
30.76	6.033	6.566	6.378	6.976	8.930	7.765	7.201	7.1214	med-scale x-bedded ss
30.78	7.441	6.614	6.378	5.580	7.441	6.033	7.441	6.7043	med-scale x-bedded ss
30.80	5.874	6.033	6.614	7.441	7.441	7.201	7.765	6.9101	med-scale x-bedded ss
30.82	6.976	8.930	6.614	6.378	8.372	9.707	7.441	7.7742	med-scale x-bedded ss
30.84	8.372	6.378	5.724	6.158	7.765	7.050	5.724	6.7385	med-scale x-bedded ss
30.87	5.580	5.724	5.444	6.378	6.614	7.201	7.441	6.3404	med-scale x-bedded ss
30.89	5.580	6.378	6.378	7.201	6.378	4.960	5.874	6.1071	med-scale x-bedded ss
30.91	4.960	6.614	6.378	4.749	4.464	6.378	6.378	5.7030	med-scale x-bedded ss
30.93	5.444	4.852	4.960	6.378	6.378	6.158	5.580	5.6787	med-scale x-bedded ss
30.95	5.444	7.441	6.201	6.614	5.724	6.158	4.960	6.0774	med-scale x-bedded ss
30.97	7.201	5.444	6.765	5.444	6.158	6.201	6.033	6.1780	med-scale x-bedded ss
30.99	7.144	6.976	7.144	5.580	5.580	5.444	6.158	6.2895	med-scale x-bedded ss
31.01	5e-04	6e-04	3e-04	2e-04	2e-04	6e-04	2e-04	0.0004	med-scale x-bedded ss
31.03	1.296	0.670	0.561	0.611	0.737	0.279	0.095	0.6068	med-scale x-bedded ss
31.05	1.486	0.451	0.729	1.008	0.870	1.828	1.828	1.1713	med-scale x-bedded ss
31.07	2.247	1.379	1.457	2.457	1.957	2.367	2.943	2.1150	med-scale x-bedded ss
31.09	3.124	3.166	2.625	2.456	3.622	3.144	4.058	3.1704	med-scale x-bedded ss
31.11	4.852	4.133	2.975	2.688	5.073	3.599	4.058	3.9111	med-scale x-bedded ss
31.13	4.376	3.967	5.580	3.099	5.191	4.464	2.253	4.1329	med-scale x-bedded ss
31.15	2.065	2.208	1.204	3.915	6.201	5.315	4.852	3.6800	med-scale x-bedded ss
31.17	3.330	3.542	4.464	5.580	3.188	2.860	2.975	3.7056	med-scale x-bedded ss
31.19	5e-04	3e-04	6e-04	6e-04	3e-04	3e-04	2e-04	0.0004	med-scale x-bedded ss
31.21	5.191	6.201	6.033	5.073	5.580	4.852	5.315	5.4635	med-scale x-bedded ss
31.23	5.444	5.444	4.852	3.799	3.658	4.555	4.464	4.6023	med-scale x-bedded ss
31.25	3.719	3.848	3.799	4.555	5.073	5.191	4.960	4.4491	med-scale x-bedded ss
31.28	4.555	3.967	4.960	3.487	3.143	4.555	4.852	4.2169	med-scale x-bedded ss
31.30	4.152	5.580	4.749	2.348	3.188	4.376	4.464	4.1224	med-scale x-bedded ss
31.32	6.201	6.158	4.852	3.381	5.444	4.058	5.724	5.1167	med-scale x-bedded ss
31.34	6.201	6.976	3.570	5.580	5.580	4.960	5.953	5.5458	med-scale x-bedded ss
31.36	6.201	3.433	6.158	6.033	6.158	6.765	7.144	5.9844	med-scale x-bedded ss
31.38	6.033	7.201	7.144	5.953	6.378	6.614	6.879	6.6003	med-scale x-bedded ss
31.40	4.852	6.566	5.444	7.441	8e-04	9e-04	8e-04	3.4723	med-scale x-bedded ss

Appendix 13 continued.

Depth (ft)	Column 1	Column 2	Column 3	Column 4	Column 5	Column 6	Column 7	Ave. Perm.	Lithofacies
31.42	5.315	6.158	5.761	7.441	5.073	4.376	5.687	5.6872	med-scale x-bedded ss
31.44	2.230	3.188	0.473	2.535	6.033	6.201	9.923	4.3690	med-scale x-bedded ss
31.46	0.115	0.096	2.506	0.846	6e-04	5e-04	0.505	0.5814	med-scale x-bedded ss
31.48	2.124	2.276	1.137	1.303	3.967	5.444	4.650	2.9859	med-scale x-bedded ss
31.50	4.058	4.058	4.464	3.881	6.976	5.724	6.697	5.1224	med-scale x-bedded ss
31.52	5.444	4.133	5.315	5.444	6.378	5.580	5.580	5.4107	med-scale x-bedded ss
31.54	5.444	5.444	4.960	4.133	6.033	6.158	4.960	5.3046	med-scale x-bedded ss
31.56	5.444	3.719	3.782	4.749	5.444	6.378	5.724	5.0343	med-scale x-bedded ss
31.58	4.852	2.789	2.594	3.967	5.580	4.852	6.378	4.4304	med-scale x-bedded ss
31.60	3.599	2.898	2.506	3.719	3.143	5.191	5.191	3.7495	med-scale x-bedded ss
31.62	2.688	3.433	3.487	4.376	2.789	2.506	2.594	3.1247	med-scale x-bedded ss
31.64	1.715	3.985	1.012	1.715	1.036	2.046	2.656	2.0236	med-scale x-bedded ss
31.66	2.084	2.594	3.658	3.234	1.137	1.198	1.527	2.2045	med-scale x-bedded ss
31.68	4.464	2.936	2.230	1.828	2.084	1.728	1.715	2.4265	med-scale x-bedded ss
31.70	4.376	4.852	3.938	2.975	2.789	2.479	3.330	3.5341	med-scale x-bedded ss
31.72	4.960	4.555	3.938	3.719	3.015	2.754	2.789	3.6758	med-scale x-bedded ss
31.74	6.201	5.444	4.555	2.824	3.099	4.292	4.133	4.3639	med-scale x-bedded ss
31.76	4.852	4.749	4.058	3.719	4.464	3.433	4.133	4.2011	med-scale x-bedded ss
31.78	5.444	3.658	2.479	1.956	3.826	4.211	4.292	3.6951	med-scale x-bedded ss
31.80	4.852	4.852	3.719	4.058	2.936	2.564	2.936	3.7024	med-scale x-bedded ss
31.82	5.724	3.967	3.056	2.975	2.898	3.234	3.188	3.5773	med-scale x-bedded ss
31.84	4.852	3.799	3.487	3.234	4.058	4.650	4.292	4.0529	med-scale x-bedded ss
31.86	4.650	3.643	3.719	4.464	4.133	4.555	4.555	4.2455	med-scale x-bedded ss
31.88	4.251	3.848	4.058	3.915	3.719	4.960	3.619	4.0528	med-scale x-bedded ss
31.91	7.201	6.201	3.719	2.721	4.749	2.754	2.373	4.2454	med-scale x-bedded ss
31.93	5.874	6.158	3.487	3.719	3.381	4.464	3.056	4.3056	med-scale x-bedded ss
31.95	1.715	2.065	1.922	1.537	1.185	1.114	0.909	1.4925	med-scale x-bedded ss
31.97	1.252	0.729	0.693	0.497	0.537	0.447	0.668	0.6889	med-scale x-bedded ss
31.99	2e-04	7e-04	2e-04	8e-04	2e-04	3e-04	2e-04	0.0004	med-scale x-bedded ss
32.01	3.719	4.133	3.967	3.33	2.348	2.027	1.756	3.0401	med-scale x-bedded ss
32.03	4.852	3.234	3.658	3.719	2.564	2.451	2.165	3.2349	med-scale x-bedded ss
32.05	4.375	4.555	4.251	2.187	2.721	2.399	3.099	3.3694	med-scale x-bedded ss
32.07	3.719	3.188	2.789	2.084	1.906	2.824	2.975	2.7835	med-scale x-bedded ss
32.09	3.143	2.824	2.936	2.789	3.433	2.625	2.479	2.8896	med-scale x-bedded ss
32.11	2.936	2.535	1.922	3.143	3.330	3.381	2.276	2.7890	med-scale x-bedded ss

Appendix 13 continued.

Depth (ft)	Column 1	Column 2	Column 3	Column 4	Column 5	Column 6	Column 7	Ave. Perm.	Lithofacies
32.13	2.065	2.324	2.324	3.281	2.451	2.373	2.754	2.5103	med-scale x-bedded ss
32.16	2.124	2.479	3.099	2.754	2.348	1.858	2.208	2.4101	med-scale x-bedded ss
32.18	3.719	2.564	2.594	2.324	1.756	2.564	2.479	2.5713	med-scale x-bedded ss
32.20	4.555	4.133	2.754	2.187	2.625	2.165	1.476	2.8421	med-scale x-bedded ss
32.22	3.281	2.479	4.555	3.658	4.058	3.015	2.046	3.2989	med-scale x-bedded ss
32.24	2.898	3.643	3.915	3.143	3.719	6.033	4.376	3.9610	med-scale x-bedded ss
32.26	1.548	1.784	2.124	4.464	4.555	2.564	2.065	2.7291	med-scale x-bedded ss
32.28	2.479	0.859	1.604	2.046	0.124	0.122	1.438	1.2389	med-scale x-bedded ss
32.30	7e-04	5e-04	5e-04	8e-04	1.447	2.208	1.276	0.7048	interbedded ss & sh
32.32	0.784	1.393	1.359	1.012	3e-04	3e-04	1.114	0.8089	interbedded ss & sh
32.34	1.939	1.939	2.373	1.527	0.781	0.943	8e-04	1.3576	interbedded ss & sh
32.36	1.770	1.974	2.084	2.506	1.843	1.393	0.837	1.7723	interbedded ss & sh
32.38	1.813	2.535	2.027	2.300	1.506	0.749	0.809	1.6770	interbedded ss & sh
32.42	3e-04	3e-04	2e-04	3e-04	3e-04	4e-04	2e-04	0.0003	interbedded ss & sh
32.44	0.122	0.060	0.013	0.018	0.018	0.100	0.025	0.0509	interbedded ss & sh
32.47	0.341	0.199	0.863	0.706	2.276	1.327	2.425	1.1622	interbedded ss & sh
32.49	4.464	3.967	4.852	4.464	2.824	2.789	4.464	3.9748	interbedded ss & sh
32.51	3.234	2.451	0.660	2.535	2.688	4.152	2.860	2.6543	interbedded ss & sh
32.53	4.058	5.724	3.330	3.719	5.073	5.953	6.378	4.8906	interbedded ss & sh
32.55	5.846	3.967	3.487	4.133	3.967	3.719	3.967	4.1552	interbedded ss & sh
32.57	4.555	2.754	3.658	3.658	4.133	2.027	2.425	3.3158	interbedded ss & sh
32.60	3.143	2.104	1.939	1.604	1.742	1.581	2.451	2.0805	interbedded ss & sh
32.62	4.211	4.133	3.719	4.376	3.719	3.281	3.719	3.8799	interbedded ss & sh
32.64	2.754	2.898	3.487	4.852	4.211	2.789	7.144	4.0191	interbedded ss & sh
32.66	3.848	4.555	4.376	6.378	6.614	7.441	8.930	6.0204	interbedded ss & sh
32.68	3.099	2.594	2.975	1.956	2.084	2.721	2.124	2.5076	interbedded ss & sh
32.70	2.721	2.124	2.399	2.479	2.208	2.104	2.594	2.3755	interbedded ss & sh
32.72	2.009	1.559	2.625	1.447	2.165	2.165	1.813	1.9691	interbedded ss & sh
32.74	2.124	2.373	2.027	1.148	0.757	0.827	0.789	1.4352	interbedded ss & sh
32.76	2e-04	4e-04	4e-04	3e-04	9e-04	2e-04	2e-04	0.0004	interbedded ss & sh
32.78	2.824	1.581	2.027	1.438	2.936	4.852	4.852	2.9301	interbedded ss & sh
32.80	2.898	3.381	2.348	1.570	1.142	2.373	1.828	2.2199	interbedded ss & sh
32.82	2.425	3.143	3.433	2.898	3.967	3.799	2.027	3.0987	interbedded ss & sh
32.84	2.789	2.564	3.433	3.015	4.058	4.292	4.464	3.5163	interbedded ss & sh
32.86	3.143	2.208	2.625	2.789	4.292	3.188	2.594	2.9768	interbedded ss & sh

Appendix 13 continued.

Depth (ft)	Column 1	Column 2	Column 3	Column 4	Column 5	Column 6	Column 7	Ave. Perm.	Lithofacies
32.88	2.451	2.824	1.770	2.009	2.373	3.433	2.564	2.4892	interbedded ss & sh
32.90	3.381	2.625	2.165	2.124	3.643	4.152	3.281	3.0531	interbedded ss & sh
32.92	3.381	2.506	3.330	3.658	3.881	4.650	5.444	3.8359	interbedded ss & sh
32.95	2.373	2.564	3.056	4.058	5.073	5.444	2.721	3.6127	interbedded ss & sh
32.97	1.108	2.027	1.218	1.012	1.728	0.759	0.924	1.2538	interbedded ss & sh
32.99	3.381	3.719	4.555	5.580	3.281	2.824	4.960	4.0430	interbedded ss & sh
33.01	3.881	1.343	2.300	2.975	2.975	4.960	4.376	3.2584	interbedded ss & sh
33.03	1.457	2.975	3.938	0.960	1.843	2.898	4.211	2.6116	interbedded ss & sh
33.05	2.656	1.288	2.721	2.824	3.015	4.852	5.580	3.2766	interbedded ss & sh
33.07	3.542	3.619	3.985	3.381	3.281	5.874	6.765	4.3496	interbedded ss & sh
33.09	4.650	5.444	3.368	4.464	4.749	3.643	4.058	4.3394	interbedded ss & sh
33.11	6e-04	5e-04	3e-04	6e-04	2e-04	1e-04	2e-04	0.0004	interbedded ss & sh
33.14	1.218	0.806	1.056	0.981	1.476	1.266	1.191	1.1420	interbedded ss & sh
33.16	1.204	0.515	0.351	0.397	0.419	0.215	0.378	0.4970	interbedded ss & sh
33.18	0.674	0.713	0.507	0.483	0.302	0.460	0.167	0.4721	interbedded ss & sh
33.20	0.175	0.449	0.853	0.856	0.952	0.521	0.781	0.6552	interbedded ss & sh
33.22	0.686	1.173	0.952	0.824	0.952	1.327	1.327	1.0342	interbedded ss & sh
33.24	0.981	0.887	0.648	0.432	1.784	2.145	1.770	1.2351	interbedded ss & sh
33.26	1.581	0.939	1.664	1.890	1.728	2.084	1.616	1.6432	interbedded ss & sh
33.29	1.676	1.581	1.319	2.324	2.754	2.721	1.728	2.0147	interbedded ss & sh
33.31	2.754	2.348	2.324	2.721	2.564	1.476	1.770	2.2795	interbedded ss & sh
33.33	2.230	2.208	2.065	1.939	1.204	2.348	3.381	2.1966	interbedded ss & sh
33.35	1.173	1.097	1.701	2e-04	6e-04	5e-04	4e-04	0.5674	interbedded ss & sh
33.37	4e-04	2e-04	3e-04	1.405	1.166	1.438	1.142	0.7361	interbedded ss & sh
33.39	0.693	1.548	1.384	1.664	1.742	0.994	0.237	1.1802	interbedded ss & sh
33.41	1.022	0.270	0.382	0.260	0.187	0.057	0.070	0.3210	interbedded ss & sh
33.43	0.131	0.119	0.249	0.179	0.151	0.187	0.291	0.1868	interbedded ss & sh
33.45	0.229	0.291	0.345	2.324	2.046	0.257	1.211	0.9574	interbedded ss & sh
33.47	1.728	2.594	3.881	3.487	3.658	3.234	2.824	3.0581	interbedded ss & sh
33.49	2.451	3.381	1.858	3.143	3.056	2.936	3.967	2.9704	interbedded ss & sh
33.51	3.381	3.330	2.975	3.381	3.099	2.276	1.922	2.9092	interbedded ss & sh
33.54	2.564	2.373	1.939	2.253	2.324	1.770	1.570	2.1132	interbedded ss & sh
33.56	2.446	2.140	1.755	1.902	1.475	1.528	1.171	1.7737	interbedded ss & sh
33.58	1.528	1.834	1.902	2.335	1.746	1.711	1.042	1.7282	interbedded ss & sh
33.60	2.314	1.711	2.054	1.755	2.446	1.669	1.902	1.9787	interbedded ss & sh

Appendix 13 continued.

Depth (ft)	Column 1	Column 2	Column 3	Column 4	Column 5	Column 6	Column 7	Ave. Perm.	Lithofacies
33.62	1.975	1.711	2.014	1.669	1.755	1.276	1.501	1.7002	interbedded ss & sh
33.71	4.852	3.143	3.719	2.789	2.594	2.208	3.143	3.2068	lrg-scale x-bedded ss
33.73	4.376	4.376	2.084	2.824	3.719	5.315	4.464	3.8797	lrg-scale x-bedded ss
33.75	3.433	3.433	2.898	4.211	4.960	3.881	3.143	3.7083	lrg-scale x-bedded ss
33.77	5.444	3.234	3.281	3.330	3.826	4.058	4.152	3.9036	lrg-scale x-bedded ss
33.79	3.099	2.145	2.975	3.826	3.433	3.056	4.464	3.2853	lrg-scale x-bedded ss
33.81	2.789	2.009	4.464	5.874	4.650	4.960	2.789	3.9335	lrg-scale x-bedded ss
33.83	4.960	4.058	1.066	2.451	3.143	3.015	3.234	3.1323	lrg-scale x-bedded ss
33.86	3.848	2.688	3.487	4.133	3.487	3.719	3.500	3.5516	lrg-scale x-bedded ss
33.88	4.960	4.464	6.201	5.315	5.724	6.158	7.441	5.7517	lrg-scale x-bedded ss
33.90	5.444	6.378	6.158	4.960	3.330	4.960	4.555	5.1122	lrg-scale x-bedded ss
33.92	6.378	5.073	4.852	4.464	3.188	2.936	4.133	4.4318	lrg-scale x-bedded ss
33.94	4.583	3.481	3.195	3.644	2.589	2.694	3.216	3.3432	lrg-scale x-bedded ss
33.96	2.789	1.890	1.537	2.824	1.991	2.451	2.300	2.2545	lrg-scale x-bedded ss
33.98	2.824	2.425	2.373	2.975	2.656	2.027	2.506	2.5409	lrg-scale x-bedded ss
34.00	2.688	2.104	1.185	1.438	2.594	3.487	3.826	2.4745	lrg-scale x-bedded ss
34.02	1.218	1.874	3.381	4.464	3.015	4.960	4.376	3.3267	lrg-scale x-bedded ss
34.04	1.639	1.702	1.616	1.991	2.754	2.535	5.444	2.5259	lrg-scale x-bedded ss
34.06	1.359	1.457	2.009	3.487	6.976	5.953	5.580	3.8315	lrg-scale x-bedded ss
34.08	1.548	1.991	4.852	4.852	5.444	5.073	5.724	4.2120	lrg-scale x-bedded ss
34.11	1.664	3.330	2.253	3.368	5.444	2.789	1.676	2.9321	lrg-scale x-bedded ss
34.13	1.548	1.527	0.977	1.343	1.457	1.281	1.114	1.3207	lrg-scale x-bedded ss
34.15	0.537	0.452	0.654	1.173	0.876	1.281	1.224	0.8852	lrg-scale x-bedded ss
34.17	0.901	0.778	0.767	0.784	1.516	1.457	1.922	1.1608	lrg-scale x-bedded ss
34.19	0.968	0.943	0.876	1.457	2.065	2.009	1.813	1.4474	lrg-scale x-bedded ss
34.21	1.303	1.081	1.296	1.486	1.359	1.211	1.592	1.3326	lrg-scale x-bedded ss
34.23	2.009	1.639	1.252	0.952	1.293	1.633	1.693	1.4958	lrg-scale x-bedded ss
34.25	3.193	3.194	2.731	3.133	3.072	3.353	3.824	3.2144	lrg-scale x-bedded ss
34.27	4.376	4.749	4.211	5.315	4.852	5.073	5.724	4.8998	lrg-scale x-bedded ss
34.29	5.724	4.852	5.724	5.191	4.211	6.378	7.144	5.6032	lrg-scale x-bedded ss
34.31	5.444	5.724	5.724	7.201	6.614	7.201	6.201	6.3013	lrg-scale x-bedded ss
34.33	5.315	5.874	4.376	5.073	5.580	6.201	5.315	5.3905	lrg-scale x-bedded ss
34.35	5.580	4.852	3.433	2.324	4.133	5.580	6.869	4.6816	lrg-scale x-bedded ss
34.37	4.960	5.073	6.869	6.201	3.967	4.292	4.464	5.1179	lrg-scale x-bedded ss
34.39	8.930	5.191	5.315	4.376	3.542	4.650	3.099	5.0146	lrg-scale x-bedded ss

Appendix 13 continued.

Depth (ft)	Column 1	Column 2	Column 3	Column 4	Column 5	Column 6	Column 7	Ave. Perm.	Lithofacies
34.41	4.749	4.464	2.936	2.898	3.967	4.211	5.580	4.1149	lrg-scale x-bedded ss
34.43	4.852	5.444	7.441	6.378	7.879	6.378	3.599	5.9960	lrg-scale x-bedded ss
34.45	7.201	7.144	8.505	5.724	5.073	5.315	4.133	6.1562	lrg-scale x-bedded ss
34.47	6.201	4.650	5.444	4.852	5.444	5.315	7.441	5.6210	lrg-scale x-bedded ss
34.49	5.315	6.201	5.724	5.444	6.158	3.433	5.874	5.4497	lrg-scale x-bedded ss
34.51	5.724	6.201	5.444	5.444	5.315	6.566	3.938	5.5187	lrg-scale x-bedded ss
34.53	4.749	4.960	7.144	6.201	6.697	4.960	6.378	5.8697	lrg-scale x-bedded ss
34.55	4.251	7.201	5.580	7.441	8.372	7.441	6.158	6.6351	lrg-scale x-bedded ss
34.57	5.444	5.953	8.372	6.201	4.555	5.444	2.535	5.5005	lrg-scale x-bedded ss
34.59	7.201	7.144	6.378	5.874	5.580	5.874	4.960	6.1445	lrg-scale x-bedded ss
34.61	7.441	7.441	5.580	5.315	5.953	4.852	3.381	5.7090	lrg-scale x-bedded ss
34.64	4.852	5.874	4.960	3.570	3.381	4.251	2.721	4.2299	lrg-scale x-bedded ss
34.66	3.719	2.425	3.433	2.688	1.676	2.898	3.330	2.8813	lrg-scale x-bedded ss
34.68	2.594	3.719	2.936	3.143	3.782	5.874	6.378	4.0609	lrg-scale x-bedded ss
34.70	7.201	6.201	4.852	5.073	7.201	7.144	6.201	6.2675	lrg-scale x-bedded ss
34.72	5.580	4.376	3.719	4.058	3.967	2.373	1.922	3.7138	lrg-scale x-bedded ss
34.74	3.056	2.124	3.143	3.099	3.056	4.251	6.614	3.6205	lrg-scale x-bedded ss
34.76	3.915	2.754	4.960	4.152	6.765	5.724	5.823	4.8704	lrg-scale x-bedded ss
34.78	6.378	5.724	5.953	5.580	5.191	5.315	4.650	5.5414	lrg-scale x-bedded ss
34.80	5.580	3.938	3.643	2.789	2.656	4.555	3.368	3.7899	lrg-scale x-bedded ss
34.82	3.381	3.281	3.719	2.824	3.143	3.281	3.848	3.3539	lrg-scale x-bedded ss
34.84	2.594	2.165	2.688	2.564	3.433	4.355	3.658	3.0653	lrg-scale x-bedded ss
34.86	3.015	1.939	3.234	3.099	4.058	2.253	2.373	2.8529	lrg-scale x-bedded ss
34.89	2.824	2.754	2.451	1.956	3.658	4.650	3.938	3.1760	lrg-scale x-bedded ss
34.91	3.234	3.487	3.915	4.292	4.376	4.555	3.281	3.8771	lrg-scale x-bedded ss
34.93	7.201	3.782	3.188	3.143	4.650	5.580	3.381	4.4179	lrg-scale x-bedded ss
34.95	3.281	3.881	3.719	2.789	3.381	2.721	2.046	3.1169	lrg-scale x-bedded ss
34.97	2.348	2.594	1.702	2.506	3.542	2.898	3.782	2.7675	lrg-scale x-bedded ss
34.99	3.500	2.975	1.438	2.754	5.191	4.852	5.444	3.7364	lrg-scale x-bedded ss
35.01	3.143	3.542	4.058	3.330	3.487	2.253	4.058	3.4100	lrg-scale x-bedded ss
35.03	6.033	3.967	1.728	1.402	3.719	3.643	3.938	3.4902	lrg-scale x-bedded ss
35.05	3.381	3.433	3.967	2.936	4.058	4.464	3.826	3.7234	lrg-scale x-bedded ss
35.07	5.191	4.749	3.381	3.967	3.433	4.960	3.433	4.1591	lrg-scale x-bedded ss
35.09	4.058	4.464	2.936	3.433	3.281	3.234	4.852	3.7511	lrg-scale x-bedded ss
35.11	2.187	2.789	5.444	3.915	4.852	5.580	4.555	4.1889	lrg-scale x-bedded ss

Appendix 13 continued.

Depth (ft)	Column 1	Column 2	Column 3	Column 4	Column 5	Column 6	Column 7	Ave. Perm.	Lithofacies
35.14	6.765	7.144	6.378	6.378	5.191	4.852	6.201	6.1297	lrg-scale x-bedded ss
35.16	6.033	4.292	4.464	6.765	6.378	4.292	5.371	5.3706	lrg-scale x-bedded ss
35.18	5.580	6.378	5.580	6.033	4.464	5.444	5.444	5.5606	lrg-scale x-bedded ss
35.20	5.444	6.033	4.650	6.566	4.355	5.444	4.133	5.2321	lrg-scale x-bedded ss
35.22	5.580	4.749	4.852	5.724	5.953	5.874	5.580	5.4731	lrg-scale x-bedded ss
35.24	4.251	3.143	5.315	5.580	6.201	6.378	5.874	5.2488	lrg-scale x-bedded ss
35.27	6.201	5.580	5.073	6.088	4.376	4.749	5.444	5.3587	lrg-scale x-bedded ss
35.29	3.487	4.555	4.133	5.315	4.852	4.211	4.852	4.4863	lrg-scale x-bedded ss
35.31	5.444	4.555	5.073	4.058	4.960	4.960	4.960	4.8585	lrg-scale x-bedded ss
35.33	4.650	4.749	5.444	6.201	4.960	3.881	2.564	4.6355	lrg-scale x-bedded ss
35.35	4.852	4.852	4.464	3.643	2.975	4.852	5.191	4.4041	lrg-scale x-bedded ss
35.37	3.433	5.874	6.378	4.133	3.433	3.799	4.058	4.4439	lrg-scale x-bedded ss
35.39	7.441	5.444	5.191	3.487	3.719	4.749	4.555	4.9409	lrg-scale x-bedded ss
35.41	2.936	2.656	3.938	5.724	5.073	5.580	4.292	4.3140	lrg-scale x-bedded ss
35.43	5.580	4.749	4.852	5.724	5.953	5.874	5.580	5.4731	lrg-scale x-bedded ss
35.45	5.580	6.378	5.580	6.033	4.464	5.444	5.444	5.5606	lrg-scale x-bedded ss
35.47	5.444	6.033	4.650	6.566	4.355	5.444	4.133	5.2321	lrg-scale x-bedded ss
35.49	5.761	5.724	4.852	4.292	3.967	6.566	7.441	5.5146	lrg-scale x-bedded ss
35.52	4.211	5.444	5.191	5.580	5.315	8.118	7.780	5.9484	lrg-scale x-bedded ss
35.54	6.378	6.088	6.976	6.278	4.052	5.186	5.377	5.7621	lrg-scale x-bedded ss
35.56	7.441	6.158	5.761	4.650	2.789	2.253	2.975	4.5752	lrg-scale x-bedded ss
35.58	4.152	2.564	1.715	3.487	4.211	4.058	4.058	3.4635	lrg-scale x-bedded ss
35.60	3.188	3.433	3.281	3.719	4.749	4.852	3.782	3.8578	lrg-scale x-bedded ss
35.62	3.719	5.191	5.444	5.315	4.852	5.073	4.058	4.8073	lrg-scale x-bedded ss
35.64	6.614	5.191	4.960	5.444	4.555	2.936	5.191	4.9844	lrg-scale x-bedded ss
35.66	6.378	5.315	5.073	3.782	5.315	3.643	6.201	5.1009	lrg-scale x-bedded ss
35.68	3.967	4.464	4.376	5.444	5.580	4.376	3.500	4.5297	lrg-scale x-bedded ss
35.70	7.201	5.953	6.614	5.444	4.464	4.133	2.373	5.1689	lrg-scale x-bedded ss
35.72	6.158	6.378	4.292	3.381	2.789	2.975	2.479	4.0644	lrg-scale x-bedded ss
35.74	3.658	3.719	4.058	4.464	3.967	2.625	2.165	3.5223	lrg-scale x-bedded ss
35.76	3.719	1.351	2.789	2.479	1.676	1.715	5.724	2.7789	lrg-scale x-bedded ss
35.79	1.592	1.359	2.479	5.315	6.158	5.724	5.444	4.0100	lrg-scale x-bedded ss
35.81	3.985	5.724	5.315	5.580	3.487	4.555	4.555	4.7429	lrg-scale x-bedded ss
35.83	6.378	4.960	7.050	5.191	5.444	5.580	4.852	5.6364	lrg-scale x-bedded ss
35.85	4.464	5.444	4.555	3.487	2.451	4.058	5.580	4.2913	lrg-scale x-bedded ss

Appendix 13 continued.

Depth (ft)	Column 1	Column 2	Column 3	Column 4	Column 5	Column 6	Column 7	Ave. Perm.	Lithofacies
35.87	2.860	3.487	4.292	4.960	5.761	5.580	4.650	4.5128	lrg-scale x-bedded ss
35.89	5.444	5.191	5.444	4.749	4.852	3.848	5.315	4.9775	lrg-scale x-bedded ss
35.91	4.292	3.281	4.292	4.960	5.191	6.201	5.580	4.8282	lrg-scale x-bedded ss
35.93	6.378	6.378	5.580	4.749	3.826	4.555	4.376	5.1203	lrg-scale x-bedded ss
35.95	6.033	4.292	3.719	4.464	3.719	4.852	5.953	4.7189	lrg-scale x-bedded ss
35.97	2.975	4.133	3.967	4.749	4.555	6.378	3.915	4.3817	lrg-scale x-bedded ss
35.99	2.860	5.580	5.823	5.724	5.073	6.201	6.378	5.3770	lrg-scale x-bedded ss
36.01	2.104	6.614	3.719	3.381	4.277	6.289	6.496	4.6972	lrg-scale x-bedded ss
36.04	3.719	4.292	4.152	5.953	4.376	6.378	6.614	5.0692	lrg-scale x-bedded ss
36.06	4.852	5.874	5.724	3.985	5.073	3.056	2.506	4.4387	lrg-scale x-bedded ss
36.08	5.315	4.852	3.381	3.188	4.852	4.852	4.852	4.4702	lrg-scale x-bedded ss
36.10	6.378	6.378	5.874	6.088	5.580	5.191	4.650	5.7342	lrg-scale x-bedded ss
36.12	4.852	4.464	4.650	4.464	4.555	4.058	3.599	4.3773	lrg-scale x-bedded ss
36.14	5.073	4.852	4.464	3.658	5.444	6.201	7.144	5.2622	lrg-scale x-bedded ss
36.16	4.555	5.724	6.378	6.201	6.566	6.158	4.749	5.7613	lrg-scale x-bedded ss
36.18	7.050	6.976	5.191	4.133	5.823	6.378	6.378	5.9898	lrg-scale x-bedded ss
36.20	5.724	7.441	4.960	7.201	8.930	8.372	7.441	7.1528	lrg-scale x-bedded ss
36.22	4.960	6.201	7.201	6.869	7.441	7.441	6.201	6.6163	lrg-scale x-bedded ss
36.24	7.144	7.441	6.378	5.444	6.614	6.614	5.724	6.4799	lrg-scale x-bedded ss
36.26	5.580	5.315	6.378	3.967	4.464	5.724	6.378	5.4008	lrg-scale x-bedded ss
36.28	4.376	4.464	7.201	7.441	7.765	8.118	6.614	6.5686	lrg-scale x-bedded ss
36.31	7.441	6.378	6.201	5.724	5.444	3.881	6.158	5.8895	lrg-scale x-bedded ss
36.33	4.464	4.152	5.580	6.158	6.378	6.033	7.050	5.6878	lrg-scale x-bedded ss
36.35	7.441	6.201	7.441	7.050	7.441	6.614	5.073	6.7517	lrg-scale x-bedded ss
36.37	7.441	5.724	5.315	5.580	7.441	8.118	7.441	6.7230	lrg-scale x-bedded ss
36.43	5.580	6.378	5.953	4.852	4.133	6.201	6.378	5.6392	lrg-scale x-bedded ss
36.45	5.724	4.058	4.852	7.441	8.930	7.201	6.033	6.3199	lrg-scale x-bedded ss
36.47	5.444	6.378	5.724	3.719	3.719	5.580	4.650	5.0306	lrg-scale x-bedded ss
36.49	4.960	4.960	4.376	6.765	6.869	7.144	6.378	5.9216	lrg-scale x-bedded ss
36.51	5.953	6.378	6.378	5.191	6.201	5.724	5.724	5.9353	lrg-scale x-bedded ss
36.53	5.444	5.580	7.698	7.879	7.441	5.724	6.088	6.5507	lrg-scale x-bedded ss
36.55	6.201	5.953	5.724	5.444	4.852	4.852	4.251	5.3252	lrg-scale x-bedded ss
36.57	7.144	5.315	5.315	6.378	7.441	6.378	6.614	6.3692	lrg-scale x-bedded ss
36.60	8.372	8.926	8.953	8.930	8.930	8.930	6.378	8.4886	lrg-scale x-bedded ss
36.62	8.967	7.201	8.372	7.441	4.133	3.143	2.625	5.9831	lrg-scale x-bedded ss

Appendix 13 continued.

Depth (ft)	Column 1	Column 2	Column 3	Column 4	Column 5	Column 6	Column 7	Ave. Perm.	Lithofacies
36.64	4.292	3.433	3.599	4.555	2.506	2.451	1.728	3.2236	lrg-scale x-bedded ss
36.66	3.487	2.165	2.754	3.487	2.208	1.784	2.187	2.5817	lrg-scale x-bedded ss
36.68	5.073	3.500	1.843	3.658	3.719	6.378	2.824	3.8565	lrg-scale x-bedded ss
36.70	4.227	3.896	3.348	3.798	4.286	5.049	4.587	4.1700	lrg-scale x-bedded ss
36.72	3.381	4.292	4.852	3.938	4.852	3.719	6.378	4.4875	lrg-scale x-bedded ss
36.74	5.191	5.444	6.201	4.464	4.251	3.542	3.658	4.6787	lrg-scale x-bedded ss
36.76	3.330	5.073	4.211	4.960	3.719	4.960	6.201	4.6363	lrg-scale x-bedded ss
36.78	6.378	5.444	4.376	3.967	4.376	3.381	3.433	4.4794	lrg-scale x-bedded ss
36.81	3.782	4.058	3.234	3.719	4.376	4.650	6.158	4.2824	lrg-scale x-bedded ss
36.83	4.376	4.292	4.152	3.015	2.373	3.281	2.253	3.3918	lrg-scale x-bedded ss
36.85	3.234	4.376	4.211	2.975	2.208	2.860	2.399	3.1804	lrg-scale x-bedded ss
36.87	3.330	2.754	4.852	4.376	4.852	4.960	5.315	4.3485	lrg-scale x-bedded ss
36.89	3.848	4.852	5.315	6.765	8.949	8.972	9.303	6.8575	lrg-scale x-bedded ss
36.91	8.930	8.930	8.930	8.955	8.967	7.144	6.158	8.2878	lrg-scale x-bedded ss
36.93	7.144	7.201	4.211	3.542	2.789	3.433	2.656	4.4251	lrg-scale x-bedded ss
36.95	1.939	3.143	3.719	3.799	5.580	4.852	4.852	3.9834	lrg-scale x-bedded ss
36.97	8.930	7.765	5.953	4.960	3.487	3.719	3.234	5.4354	lrg-scale x-bedded ss
37.00	4.058	3.719	4.292	4.133	5.191	4.852	4.376	4.3744	lrg-scale x-bedded ss
37.02	4.376	4.650	7.144	9.568	8.930	7.201	7.441	7.0444	lrg-scale x-bedded ss
37.04	8.933	9.568	7.879	8.935	5.724	6.201	6.378	7.6596	lrg-scale x-bedded ss
37.06	7.879	8.930	7.441	7.050	7.441	8.372	8.930	8.0063	lrg-scale x-bedded ss
37.08	7.441	8.930	8.925	9.401	8.930	6.378	7.441	8.2066	lrg-scale x-bedded ss
37.10	7.441	8.930	7.441	9.568	8.930	8.973	6.378	8.2376	lrg-scale x-bedded ss
37.12	8.118	6.566	6.765	7.441	7.201	6.765	6.378	7.0334	lrg-scale x-bedded ss
37.14	7.144	6.869	5.874	5.874	5.073	3.188	2.046	5.1525	lrg-scale x-bedded ss
37.16	8.372	7.441	6.201	2.253	0.754	0.920	2.348	4.0413	lrg-scale x-bedded ss
37.18	2.009	2.300	1.813	1.756	3.381	3.056	4.960	2.7535	lrg-scale x-bedded ss
37.20	5.580	5.580	5.315	7.441	6.201	7.441	7.441	6.4286	lrg-scale x-bedded ss
37.22	8.915	4.133	8.964	8.978	8.526	8.127	7.974	7.9451	lrg-scale x-bedded ss
37.24	5.938	3.045	2.860	2.656	2.348	2.425	3.658	3.2756	lrg-scale x-bedded ss
37.26	2.975	1.956	1.527	2.754	4.058	2.594	4.058	2.8459	lrg-scale x-bedded ss
37.28	4.292	2.506	5.315	5.444	3.799	1.351	0.573	3.3255	lrg-scale x-bedded ss
37.30	1.142	0.890	1.393	1.828	1.858	4.376	2.898	2.0550	lrg-scale x-bedded ss
37.32	1.858	2.975	5.073	4.650	6.378	5.724	4.852	4.5013	lrg-scale x-bedded ss
37.35	3.599	3.643	2.451	3.487	3.658	3.056	1.858	3.1076	lrg-scale x-bedded ss

Appendix 13 continued.

Depth (ft)	Column 1	Column 2	Column 3	Column 4	Column 5	Column 6	Column 7	Ave. Perm.	Lithofacies
37.37	1.939	2.276	1.081	1.581	2.253	1.311	1.858	1.7571	lrg-scale x-bedded ss
37.39	3.143	3.433	2.824	2.564	1.939	1.252	1.066	2.3172	lrg-scale x-bedded ss
37.41	0.648	1.137	0.495	1.191	0.972	1.828	2.594	1.2664	lrg-scale x-bedded ss
37.43	2.084	2.276	2.276	4.464	5.444	3.915	3.433	3.4132	lrg-scale x-bedded ss
37.45	3.056	1.956	2.187	3.643	4.852	6.158	4.852	3.8149	lrg-scale x-bedded ss
37.47	5.724	6.378	6.378	11.16	10.300	6.566	3.826	7.1913	lrg-scale x-bedded ss
37.49	7.201	3.985	4.376	6.378	5.444	7.201	7.144	5.9614	lrg-scale x-bedded ss
37.51	4.960	4.058	4.960	6.378	7.441	5.724	4.058	5.3683	lrg-scale x-bedded ss
37.53	3.782	4.292	3.015	1.974	1.991	2.789	2.253	2.8708	lrg-scale x-bedded ss
37.55	2.656	2.276	4.376	4.133	3.719	3.099	2.479	3.2482	lrg-scale x-bedded ss
37.57	2.898	3.500	2.506	4.133	4.555	3.487	3.487	3.5093	lrg-scale x-bedded ss
37.59	2.824	2.027	4.058	6.566	7.441	3.330	4.376	4.3747	lrg-scale x-bedded ss
37.62	3.143	4.058	4.211	2.860	3.234	4.555	4.251	3.7587	lrg-scale x-bedded ss
37.64	7.441	7.879	7.441	8.930	3.643	3.487	3.143	5.9950	lrg-scale x-bedded ss
37.66	4.852	7.144	2.975	2.625	3.330	4.650	3.826	4.2001	lrg-scale x-bedded ss
37.68	3.967	5.874	3.570	3.433	5.724	7.201	8.930	5.5286	lrg-scale x-bedded ss
37.70	3.719	5.315	6.869	7.879	9.707	5.953	7.050	6.6416	lrg-scale x-bedded ss
37.72	8.930	8.372	7.144	7.144	7.441	5.444	2.656	6.7330	lrg-scale x-bedded ss
37.74	7.144	6.158	2.975	3.848	6.378	3.433	1.296	4.4615	lrg-scale x-bedded ss
37.76	4.852	2.936	5.073	4.555	3.719	4.376	4.852	4.3376	lrg-scale x-bedded ss
37.78	0.863	3.719	4.650	6.378	5.874	5.073	4.058	4.3735	lrg-scale x-bedded ss
37.80	3.487	4.852	5.444	5.315	4.555	5.073	4.749	4.7820	lrg-scale x-bedded ss
37.82	4.376	7.144	7.441	7.144	6.378	6.378	7.441	6.6146	lrg-scale x-bedded ss
37.84	7.144	8.930	7.201	5.073	7.441	5.191	5.315	6.6135	lrg-scale x-bedded ss
37.87	5.724	4.376	5.580	5.580	4.292	1.359	2.721	4.2331	lrg-scale x-bedded ss
37.89	4.555	4.960	3.719	5.191	4.152	3.188	3.719	4.2120	lrg-scale x-bedded ss
37.91	4.555	4.376	4.960	4.852	5.580	5.444	8.118	5.4123	lrg-scale x-bedded ss
37.93	8.372	6.614	4.211	5.580	4.464	2.789	4.152	5.1689	lrg-scale x-bedded ss
37.95	7.765	7.879	4.464	3.330	3.658	4.211	3.433	4.9630	lrg-scale x-bedded ss
38.01	6.033	3.143	3.330	3.433	2.898	1.676	2.535	3.2926	lrg-scale x-bedded ss
38.03	1.496	1.756	0.789	2.451	3.487	6.378	7.441	3.3997	lrg-scale x-bedded ss
38.05	2.975	2.324	4.852	2.754	5.191	4.152	4.852	3.8714	lrg-scale x-bedded ss
38.07	3.381	2.860	3.143	3.433	1.843	3.281	1.858	2.8285	lrg-scale x-bedded ss
38.09	4.058	3.658	4.058	3.658	5.874	7.441	7.441	5.1699	lrg-scale x-bedded ss
38.11	5.874	7.441	11.160	4.852	6.378	5.191	2.253	6.1647	lrg-scale x-bedded ss

Appendix 13 continued.

Depth (ft)	Column 1	Column 2	Column 3	Column 4	Column 5	Column 6	Column 7	Ave. Perm.	Lithofacies
38.14	3.658	3.719	1.702	1.238	0.729	1.429	1.166	1.9488	lrg-scale x-bedded ss
38.16	1.537	1.527	2.104	1.890	1.676	1.081	1.770	1.6550	lrg-scale x-bedded ss
38.18	0.990	2.399	1.281	1.343	1.592	1.639	1.702	1.5635	lrg-scale x-bedded ss
38.20	2.975	3.281	2.975	2.975	3e-04	3e-04	2e-04	1.7438	lrg-scale x-bedded ss
38.22	3e-04	2e-04	2e-04	2e-04	2.479	2.348	4.133	1.2801	lrg-scale x-bedded ss
38.24	3.643	3.099	3.487	3.985	2.479	4.292	3.330	3.4736	lrg-scale x-bedded ss
38.26	4.749	4.960	5.761	5.315	4.852	5.724	6.378	5.3911	lrg-scale x-bedded ss
38.28	3.658	6.201	5.580	5.191	4.852	6.378	4.650	5.2157	lrg-scale x-bedded ss
38.30	5.444	4.960	4.555	4.852	4.749	5.315	6.378	5.1789	lrg-scale x-bedded ss
38.32	4.464	5.724	4.960	7.144	4.960	6.033	6.201	5.6407	lrg-scale x-bedded ss
38.34	8.372	6.201	6.378	8.118	7.201	7.879	7.441	7.3701	lrg-scale x-bedded ss
38.36	5.073	7.050	5.580	7.201	4.152	4.211	5.761	5.5754	lrg-scale x-bedded ss
38.39	3.433	5.315	3.381	5.874	4.960	3.915	2.936	4.2591	lrg-scale x-bedded ss
38.41	5.073	5.724	4.852	7.441	4.960	5.444	3.967	5.3516	lrg-scale x-bedded ss
38.43	6.201	7.698	5.874	7.441	5.580	7.441	7.698	6.8478	lrg-scale x-bedded ss
38.45	7.441	8.372	6.378	5.444	1.384	4.464	6.378	5.6945	lrg-scale x-bedded ss
38.47	4.555	3.433	4.749	5.874	4.960	4.555	6.378	4.9291	lrg-scale x-bedded ss
38.49	3.487	6.378	6.378	6.765	4.852	5.191	6.201	5.6073	lrg-scale x-bedded ss
38.51	6.033	4.650	7.144	4.749	4.133	3.938	3.381	4.8611	lrg-scale x-bedded ss
38.53	7.441	6.765	3.099	4.292	3.570	3.433	5.315	4.8450	lrg-scale x-bedded ss
38.55	4.555	4.292	6.765	8.930	8.930	6.378	5.846	6.5281	lrg-scale x-bedded ss
38.57	8.269	7.050	4.292	8.953	8.953	8.953	5.580	7.4356	lrg-scale x-bedded ss
38.59	8.372	8.462	5.335	7.967	7.424	6.614	5.315	7.0697	lrg-scale x-bedded ss
38.61	6.374	7.973	6.378	7.441	6.378	7.201	7.441	7.0266	lrg-scale x-bedded ss
38.63	6.201	7.266	8.930	8.505	7.441	6.378	4.852	7.0819	lrg-scale x-bedded ss
38.66	6.378	6.614	4.749	4.376	3.015	3.719	4.058	4.7013	lrg-scale x-bedded ss
38.68	2.754	2.564	3.643	5.580	5.444	3.381	3.719	3.8695	lrg-scale x-bedded ss
38.70	3.099	3.599	3.330	4.749	5.724	5.724	7.050	4.7534	lrg-scale x-bedded ss
38.72	5.315	6.566	7.441	7.698	6.201	3.188	4.464	5.8388	lrg-scale x-bedded ss
38.74	7.441	4.555	4.251	3.967	4.852	5.724	6.378	5.3098	lrg-scale x-bedded ss
38.76	5.444	5.580	4.464	5.580	5.444	4.852	6.378	5.3919	lrg-scale x-bedded ss
38.78	5.724	7.144	6.158	6.614	7.441	8.930	8.953	7.2805	lrg-scale x-bedded ss
38.80	8.955	8.372	8.926	8.952	7.201	8.951	8.930	8.6125	lrg-scale x-bedded ss
38.82	8.930	8.372	7.879	8.372	5.444	6.378	5.580	7.2795	lrg-scale x-bedded ss
38.84	6.378	6.201	6.614	4.960	4.852	7.441	5.073	5.9313	lrg-scale x-bedded ss

Appendix 13 continued.

Depth (ft)	Column 1	Column 2	Column 3	Column 4	Column 5	Column 6	Column 7	Ave. Perm.	Lithofacies
38.86	5.444	4.960	4.749	4.960	7.201	8.372	8.372	6.2940	lrg-scale x-bedded ss
38.88	7.441	8.953	5.444	7.144	5.315	3.719	3.643	5.9513	lrg-scale x-bedded ss
38.91	6.765	4.133	3.658	2.975	3.188	5.580	7.201	4.7857	lrg-scale x-bedded ss
38.93	4.376	4.650	7.441	6.033	7.201	5.874	8.372	6.2783	lrg-scale x-bedded ss
38.95	8.118	8.118	7.441	6.976	8.956	8.953	8.930	8.2132	lrg-scale x-bedded ss
38.97	8.930	7.050	8.372	8.930	8.372	6.566	4.058	7.4682	lrg-scale x-bedded ss
38.99	8.930	8.930	7.144	2.824	2.975	3.433	3.487	5.3890	lrg-scale x-bedded ss
39.01	2.754	3.381	4.251	5.580	5.315	5.580	5.761	4.6603	lrg-scale x-bedded ss
39.03	5.724	5.724	4.852	4.749	5.724	4.555	5.191	5.2167	lrg-scale x-bedded ss
39.05	5.444	5.580	4.464	2.975	1.012	1.702	3.381	3.5083	lrg-scale x-bedded ss
39.07	2.754	1.939	2.230	2.860	4.852	3.938	5.073	3.3782	lrg-scale x-bedded ss
39.09	3.381	4.749	4.555	4.464	4.211	3.881	6.378	4.5169	lrg-scale x-bedded ss
39.11	5.874	8.372	5.580	6.378	4.960	6.158	8.118	6.4915	lrg-scale x-bedded ss
39.13	6.614	7.201	5.580	6.201	4.960	5.444	6.033	6.0049	lrg-scale x-bedded ss
39.15	3.487	4.464	5.444	6.201	6.765	5.191	5.580	5.3045	lrg-scale x-bedded ss
39.18	8.930	7.144	6.869	6.378	6.378	8.951	7.765	7.4879	lrg-scale x-bedded ss
39.20	4.376	7.050	7.441	7.441	6.201	8.953	8.930	7.1989	lrg-scale x-bedded ss
39.22	2.656	4.376	8.930	8.372	8.958	8.953	8.930	7.3107	lrg-scale x-bedded ss
39.24	6.201	5.580	8.738	7.765	8.953	8.930	6.378	7.5064	lrg-scale x-bedded ss
39.26	5.411	8.930	5.580	8.984	8.976	8.952	7.144	7.7111	lrg-scale x-bedded ss
39.28	8.953	6.201	8.930	8.372	7.698	6.378	4.555	7.2982	lrg-scale x-bedded ss
39.30	7.441	8.930	5.444	5.315	6.378	6.869	5.580	6.5654	lrg-scale x-bedded ss
39.32	7.050	5.724	5.874	8.930	8.736	7.441	2.936	6.6701	lrg-scale x-bedded ss
39.34	6.378	8.963	8.954	8.424	8.628	8.372	8.118	8.2624	lrg-scale x-bedded ss
39.36	8.930	8.856	8.958	8.753	8.953	8.963	3.967	8.1971	lrg-scale x-bedded ss
39.38	8.930	8.957	7.441	8.963	8.930	8.973	5.191	8.1978	lrg-scale x-bedded ss
39.40	8.957	7.441	4.852	6.088	4.292	7.973	7.050	6.6648	lrg-scale x-bedded ss
39.42	5.444	7.144	8.118	7.144	8.372	8.372	8.984	7.6540	lrg-scale x-bedded ss
39.45	8.505	8.118	8.965	8.973	8.372	5.953	8.505	8.1987	lrg-scale x-bedded ss
39.47	6.378	8.930	7.144	7.441	7.144	8.957	8.951	7.8493	lrg-scale x-bedded ss
39.49	8.963	8.974	7.879	7.973	8.372	7.144	8.930	8.3193	lrg-scale x-bedded ss
39.53	6.201	2.789	5.315	8.372	7.441	3.433	3.487	5.2910	lrg-scale x-bedded ss
39.55	5.580	5.580	4.852	5.724	6.378	3.487	4.555	5.1651	lrg-scale x-bedded ss
39.57	5.580	3.719	5.580	4.464	3.433	3.188	3.056	4.1458	lrg-scale x-bedded ss
39.59	3.967	3.056	3.330	3.658	4.960	1.548	1.742	3.1803	lrg-scale x-bedded ss

Appendix 13 continued.

Depth (ft)	Column 1	Column 2	Column 3	Column 4	Column 5	Column 6	Column 7	Ave. Perm.	Lithofacies
39.61	3.381	1.974	1.715	4.376	6.566	2.975	1.639	3.2322	lrg-scale x-bedded ss
39.63	2.009	1.715	3.015	2.625	6.201	5.073	3.719	3.4795	lrg-scale x-bedded ss
39.65	2.975	1.402	1.476	1.351	4.211	8.953	8.372	4.1057	lrg-scale x-bedded ss
39.67	4.464	2.824	3.719	3.967	1.008	7.144	7.050	4.3108	lrg-scale x-bedded ss
39.70	7.144	2.860	3.330	3.015	4.058	6.869	8.930	5.1723	lrg-scale x-bedded ss
39.72	3.188	1.890	1.922	2.124	4.960	4.960	6.201	3.6064	lrg-scale x-bedded ss
39.74	7.441	6.566	6.378	7.144	8.957	8.930	5.724	7.3056	lrg-scale x-bedded ss
39.76	6.033	2.208	1.858	0.531	1.224	6.378	7.441	3.6678	lrg-scale x-bedded ss
39.78	8.954	7.144	2.936	7.144	8.372	7.144	2.564	6.3224	lrg-scale x-bedded ss
39.80	7.441	8.953	8.956	8.951	8.372	7.441	8.953	8.4383	lrg-scale x-bedded ss
39.82	8.118	8.930	8.930	8.953	8.953	6.158	7.441	8.2121	lrg-scale x-bedded ss
39.84	8.930	8.953	7.879	8.954	5.874	4.960	2.721	6.8960	lrg-scale x-bedded ss
39.86	1.376	3.881	6.614	8.505	0.024	2.656	6.201	4.1795	lrg-scale x-bedded ss
39.88	7.441	7.879	6.378	5.315	4.960	7.144	5.444	6.3659	lrg-scale x-bedded ss
39.90	5.724	7.765	7.441	6.765	6.765	5.874	3.542	6.2679	lrg-scale x-bedded ss
39.92	3.881	6.201	7.441	6.976	6.033	5.761	3.433	5.6751	lrg-scale x-bedded ss
39.94	4.960	4.650	5.874	5.724	5.823	4.960	4.464	5.2078	lrg-scale x-bedded ss
39.97	8.930	6.976	6.033	5.953	3.967	2.009	1.131	4.9999	lrg-scale x-bedded ss
39.99	2.324	2.208	1.974	1.252	1.026	0.853	4.555	2.0273	lrg-scale x-bedded ss
40.01	1.008	1.559	0.853	1.651	5.751	5.823	5.444	3.1555	lrg-scale x-bedded ss
40.03	4.965	5.874	4.649	5.724	5.366	5.783	5.761	5.4460	lrg-scale x-bedded ss
40.05	4.666	5.728	6.378	8.930	5.073	6.723	6.728	6.3179	lrg-scale x-bedded ss
40.07	4.852	5.724	5.724	2.506	3.143	7.698	7.784	5.3471	lrg-scale x-bedded ss
40.09	4.058	1.148	3.188	7.441	8.957	7.441	8.930	5.8806	lrg-scale x-bedded ss
40.11	4.960	8.953	8.930	5.874	7.201	6.378	4.650	6.7066	lrg-scale x-bedded ss
40.13	5.669	8.196	6.891	6.244	5.460	7.072	6.800	6.6189	lrg-scale x-bedded ss
40.15	6.378	7.441	4.852	6.614	3.719	7.765	8.118	6.4126	lrg-scale x-bedded ss
40.17	1.581	1.108	0.567	0.968	3.281	6.378	6.201	2.8692	lrg-scale x-bedded ss
40.19	1.676	1.922	1.160	1.858	4.464	4.852	8.930	3.5519	lrg-scale x-bedded ss
40.21	2.975	2.425	2.399	1.715	2.754	4.152	8.505	3.5606	lrg-scale x-bedded ss
40.24	3.188	3.143	3.281	1.384	5.724	8.930	6.614	4.6091	lrg-scale x-bedded ss
40.26	1.843	1.211	0.565	0.630	3.234	5.874	4.852	2.6013	interbedded ss & sh
40.28	0.291	0.699	0.856	1.031	1.581	2.399	3.381	1.4626	interbedded ss & sh
40.30	0.563	0.948	1.343	1.486	1.756	3.381	3.658	1.8762	interbedded ss & sh
40.32	0.840	1.036	1.639	1.784	1.843	3.643	3.719	2.0720	interbedded ss & sh

Appendix 13 continued.

Depth (ft)	Column 1	Column 2	Column 3	Column 4	Column 5	Column 6	Column 7	Ave. Perm.	Lithofacies
40.34	0.722	1.211	0.846	1.017	1.974	3.143	3.143	1.7221	interbedded ss & sh
40.36	0.635	1.036	1.081	1.359	1.874	2.936	2.084	1.5722	interbedded ss & sh
40.38	1.041	1.224	1.334	1.476	2.324	2.688	2.688	1.8249	interbedded ss & sh
40.40	1.676	1.476	1.081	1.384	2.535	2.594	2.564	1.9016	interbedded ss & sh
40.42	2.208	1.702	1.922	2.373	2.506	4.852	4.852	2.9166	interbedded ss & sh
40.44	1.114	1.022	1.604	1.939	2.535	3.056	4.058	2.1896	interbedded ss & sh
40.46	0.928	1.466	1.092	1.890	2.300	2.898	3.599	2.0246	interbedded ss & sh
40.49	1.097	1.166	1.592	2.898	3.281	3.433	3.433	2.4144	interbedded ss & sh
40.51	2.065	1.798	2.027	2.594	0.524	2.824	4.960	2.3989	interbedded ss & sh
40.53	2.688	2.253	2.656	3.719	5.444	3.015	3.643	3.3455	interbedded ss & sh
40.55	4.211	1.906	3.143	2.936	3.234	3.719	5.724	3.5531	interbedded ss & sh
40.57	3.099	2.656	2.789	4.749	4.852	4.852	3.848	3.8349	interbedded ss & sh
40.59	3.881	2.253	2.936	2.936	3.487	2.373	3.015	2.9829	interbedded ss & sh
40.61	2.594	1.939	1.238	1.245	1.476	2.065	1.890	1.7781	interbedded ss & sh
40.63	2.009	2.027	1.639	1.627	0.999	0.994	1.537	1.5476	interbedded ss & sh
40.65	2.479	1.974	1.496	1.496	1.506	1.906	1.922	1.8255	interbedded ss & sh
40.67	2.208	1.639	1.828	1.592	1.076	1.627	2.009	1.7114	interbedded ss & sh
40.69	2.399	2.046	1.843	1.537	1.238	1.784	2.046	1.8417	interbedded ss & sh
40.71	3.433	2.625	1.476	0.786	1.198	1.581	2.009	1.8725	interbedded ss & sh
40.73	4.376	2.975	2.104	1.114	1.154	1.273	1.798	2.1135	interbedded ss & sh
40.76	3.330	2.425	1.376	2.084	1.715	2.594	3.433	2.4224	interbedded ss & sh
40.78	0.999	1.131	0.870	0.968	0.630	2.027	2.348	1.2817	interbedded ss & sh
40.82	5.580	7.050	7.144	3.799	3.433	4.058	3.234	4.8995	interbedded ss & sh
40.83	4.650	4.185	4.292	6.158	4.464	3.281	2.754	4.2548	interbedded ss & sh
40.85	4.292	3.938	3.433	7.201	4.464	2.564	3.542	4.2049	interbedded ss & sh
40.88	4.058	5.315	4.650	4.464	3.234	3.433	3.599	4.1074	interbedded ss & sh
40.90	4.058	4.852	4.292	3.143	3.433	4.852	3.719	4.0498	interbedded ss & sh
40.92	3.938	5.580	5.823	4.185	3.330	4.133	4.464	4.4933	interbedded ss & sh
40.94	3.119	5.191	5.724	4.251	2.824	4.376	5.073	4.3653	interbedded ss & sh
40.96	2.300	4.376	2.789	2.324	4.555	3.433	3.143	3.2740	interbedded ss & sh
40.98	4.960	4.292	3.143	3.719	4.292	3.938	2.721	3.8664	interbedded ss & sh
41.01	3.487	4.292	2.789	3.719	3.188	2.824	2.975	3.3247	interbedded ss & sh
41.03	3.570	4.152	3.015	2.625	2.324	2.898	2.535	3.0169	interbedded ss & sh
41.05	2.898	2.824	2.656	2.656	2.084	1.537	2.230	2.4122	interbedded ss & sh
41.07	1.770	1.592	1.828	2.399	1.843	1.604	1.548	1.7975	interbedded ss & sh

Appendix 13 continued.

Depth (ft)	Column 1	Column 2	Column 3	Column 4	Column 5	Column 6	Column 7	Ave. Perm.	Lithofacies
41.09	0.268	0.394	0.194	0.477	0.500	0.639	3.099	0.7958	interbedded ss & sh
41.11	6e-04	5e-04	2e-04	3e-04	2e-04	2e-04	3e-04	0.0003	interbedded ss & sh
41.13	0.024	0.018	0.104	0.021	0.018	0.013	0.185	0.0547	interbedded ss & sh
41.15	0.041	0.396	1.108	1.185	1.076	0.676	1.664	0.8780	interbedded ss & sh
41.17	2.084	1.858	1.639	2.324	1.770	1.858	2.009	1.9346	interbedded ss & sh
41.19	2.594	2.373	2.253	2.399	1.784	2.936	2.124	2.3517	interbedded ss & sh
41.21	3.368	2.230	3.143	2.479	2.027	2.187	1.516	2.4214	interbedded ss & sh
41.23	1.017	2.688	3.826	2.104	0.514	0.405	0.351	1.5578	interbedded ss & sh
41.26	0.674	1.252	0.708	2e-04	3e-04	0.247	5e-04	0.4117	interbedded ss & sh
41.28	2e-04	0.156	0.262	0.286	0.543	0.280	0.208	0.2480	interbedded ss & sh
41.30	0.155	5e-04	0.151	2e-04	3e-04	0.238	0.311	0.1221	interbedded ss & sh
41.32	0.180	0.314	3e-04	0.191	0.307	4e-04	3e-04	0.1418	interbedded ss & sh
41.34	0.469	0.380	0.725	0.964	1.351	1.537	0.939	0.9092	interbedded ss & sh
41.36	1.570	2.594	1.770	1.486	2.451	2.230	2.373	2.0677	interbedded ss & sh
41.38	3.330	2.754	2.230	1.858	2.124	2.451	2.975	2.5319	interbedded ss & sh
41.40	2.479	3.719	3.234	3.099	2.594	2.506	2.535	2.8809	interbedded ss & sh
41.42	2.898	2.721	3.967	2.824	3.015	2.451	2.688	2.9377	interbedded ss & sh
41.44	2.975	2.253	2.373	3.330	2.656	2.230	2.425	2.6060	interbedded ss & sh
41.46	2.124	1.939	2.594	2.754	2.451	3.015	2.425	2.4718	interbedded ss & sh
41.48	1.742	1.651	0.635	1.420	1.689	2.721	2.451	1.7584	interbedded ss & sh
41.50	1.627	1.651	2.104	1.592	2.625	2.564	2.104	2.0382	interbedded ss & sh
41.53	0.633	0.088	0.264	3.433	1.537	0.034	0.645	0.9477	interbedded ss & sh
41.55	0.073	0.087	0.786	2.124	0.920	0.005	1.359	0.7649	interbedded ss & sh
41.57	0.002	0.014	0.036	0.029	0.084	0.003	0.003	0.0244	muddy bioturbated ss
41.59	0.001	0.002	0.034	0.021	0.099	0.004	0.004	0.0236	muddy bioturbated ss
41.61	0.003	0.003	0.078	0.020	0.015	0.017	0.018	0.0219	muddy bioturbated ss
41.63	0.002	0.010	0.054	0.226	0.049	0.028	0.010	0.0542	muddy bioturbated ss
41.65	0.019	0.020	0.045	0.223	0.063	0.009	0.009	0.0554	muddy bioturbated ss
41.67	0.017	0.009	0.027	0.099	0.109	0.036	0.128	0.0608	muddy bioturbated ss
41.69	0.068	0.021	0.008	0.028	0.003	0.005	0.002	0.0193	muddy bioturbated ss
41.71	0.184	0.078	0.061	0.014	0.012	0.140	0.090	0.0825	muddy bioturbated ss
41.73	0.014	0.008	0.011	0.017	0.048	0.041	0.035	0.0248	muddy bioturbated ss
41.75	0.016	0.029	0.005	0.004	0.004	0.004	0.002	0.0091	muddy bioturbated ss
41.78	0.059	0.027	0.009	0.010	0.014	0.006	0.003	0.0182	muddy bioturbated ss
41.80	0.012	0.034	0.074	0.048	0.026	0.010	0.024	0.0326	muddy bioturbated ss

Appendix 13 continued.

Depth (ft)	Column 1	Column 2	Column 3	Column 4	Column 5	Column 6	Column 7	Ave. Perm.	Lithofacies
41.82	0.023	0.009	0.129	0.032	0.011	0.028	0.046	0.0397	muddy bioturbated ss
41.84	0.015	0.010	0.024	0.053	0.037	0.011	0.049	0.0286	muddy bioturbated ss
41.86	0.027	0.039	0.043	0.225	0.028	0.104	0.042	0.0726	muddy bioturbated ss
41.88	0.381	0.447	0.491	0.815	0.043	0.098	0.140	0.3452	muddy bioturbated ss
41.90	1.097	1.142	0.704	0.806	0.574	0.812	0.742	0.8397	muddy bioturbated ss
41.92	1.166	1.218	1.119	1.066	1.252	0.928	0.339	1.0124	med-scale x-bedded ss
41.94	1.420	1.061	1.051	1.137	2.373	1.466	1.166	1.3819	med-scale x-bedded ss
41.96	1.411	1.486	1.319	1.296	1.319	1.906	1.991	1.5323	med-scale x-bedded ss
41.98	1.702	1.238	1.376	1.756	2.230	2.208	2.208	1.8169	med-scale x-bedded ss
42.00	1.506	1.813	2.230	2.451	1.664	2.898	2.046	2.0868	med-scale x-bedded ss
42.02	1.922	1.125	1.639	1.974	1.742	1.906	1.429	1.6767	med-scale x-bedded ss
42.05	1.296	1.426	1.276	2.451	1.664	2.208	1.756	1.7252	med-scale x-bedded ss
42.07	1.336	1.276	1.645	1.711	2.283	2.378	1.711	1.7631	med-scale x-bedded ss
42.09	1.555	1.711	1.902	1.755	1.902	1.585	1.358	1.6811	med-scale x-bedded ss
42.11	1.770	1.711	1.902	1.85	1.555	2.362	2.233	1.9119	med-scale x-bedded ss
42.13	1.902	1.402	1.584	1.902	1.155	1.276	1.188	1.4870	med-scale x-bedded ss
42.15	1.746	1.426	1.222	1.055	1.380	1.614	1.110	1.3647	med-scale x-bedded ss
42.17	1.296	1.450	1.450	1.802	1.475	1.770	1.850	1.5846	med-scale x-bedded ss
42.19	2.314	3.114	2.140	1.902	2.674	3.426	1.556	2.4463	med-scale x-bedded ss
42.21	2.283	1.528	2.378	2.676	2.446	2.676	1.902	2.2697	med-scale x-bedded ss
42.23	1.501	2.518	2.762	1.902	2.676	2.676	3.426	2.4943	med-scale x-bedded ss
42.25	2.854	2.378	2.362	2.518	1.975	2.595	3.172	2.5504	med-scale x-bedded ss
42.27	2.676	2.854	3.114	1.902	1.755	2.014	1.711	2.2895	med-scale x-bedded ss
42.30	2.518	2.209	2.446	1.902	2.253	2.054	1.783	2.1664	med-scale x-bedded ss
42.32	1.711	2.446	2.595	1.711	2.378	2.518	2.854	2.3162	med-scale x-bedded ss
42.34	2.362	2.446	2.446	2.595	2.195	2.854	2.283	2.4543	med-scale x-bedded ss
42.36	1.850	2.140	1.902	3.172	2.854	2.740	2.314	2.4245	med-scale x-bedded ss
42.38	2.362	1.902	3.294	2.209	2.233	1.670	1.614	2.1833	med-scale x-bedded ss
42.42	1.188	1.017	1.296	1.556	1.296	1.426	1.426	1.3147	med-scale x-bedded ss
42.44	0.909	1.380	1.584	1.678	1.902	1.171	1.316	1.4198	med-scale x-bedded ss
42.46	1.902	1.276	1.711	1.204	1.140	1.555	0.949	1.3912	med-scale x-bedded ss
42.48	1.670	1.746	1.450	1.475	1.096	1.296	1.528	1.4657	med-scale x-bedded ss
42.50	1.902	1.755	1.005	1.222	1.614	1.239	1.501	1.4626	med-scale x-bedded ss
42.52	1.746	1.670	1.555	2.595	1.402	1.670	1.276	1.7019	med-scale x-bedded ss
42.54	1.902	2.446	4.283	3.262	2.140	1.296	1.159	2.3554	med-scale x-bedded ss

Appendix 13 continued.

Depth (ft)	Column 1	Column 2	Column 3	Column 4	Column 5	Column 6	Column 7	Ave. Perm.	Lithofacies
42.56	2.253	2.209	2.953	2.209	1.528	0.971	0.543	1.8093	med-scale x-bedded ss
42.59	3.114	2.518	3.807	2.253	1.975	1.584	0.421	2.2389	med-scale x-bedded ss
42.61	1.902	1.501	1.239	0.919	1.475	0.700	0.368	1.1575	med-scale x-bedded ss
42.63	3e-04	0.236	0.234	3.807	3.058	0.178	0.106	1.0886	med-scale x-bedded ss
42.65	4e-04	3e-04	5e-04	8e-04	4e-04	2e-04	9e-04	0.0005	muddy bioturbated ss
42.67	0.351	0.145	0.195	0.035	0.196	0.098	0.208	0.1754	muddy bioturbated ss
42.69	6e-04	7e-04	3e-04	2e-04	5e-04	8e-04	4e-04	0.0005	muddy bioturbated ss
42.71	0.303	0.167	0.058	0.160	0.205	0.646	1.755	0.4707	muddy bioturbated ss
42.73	0.899	1.171	1.140	0.580	1.802	1.711	2.209	1.3589	muddy bioturbated ss
42.75	0.813	1.316	1.670	1.556	1.755	1.556	1.556	1.4600	muddy bioturbated ss
42.77	1.171	1.475	1.316	1.556	1.711	1.276	1.755	1.4657	muddy bioturbated ss
42.79	0.783	0.769	0.776	0.711	0.846	0.846	0.450	0.7402	muddy bioturbated ss
42.81	0.806	0.565	1.030	0.929	0.971	0.919	0.513	0.8188	muddy bioturbated ss
42.83	0.730	0.791	0.479	0.949	1.030	1.402	0.899	0.8970	muddy bioturbated ss
42.86	0.421	0.463	0.314	0.688	1.125	1.296	0.332	0.6627	muddy bioturbated ss
42.88	7e-04	3e-04	2e-04	3e-04	2e-04	1e-04	5e-04	0.0003	muddy bioturbated ss
42.90	0.643	0.581	1.184	1.024	0.708	0.058	0.036	0.6050	muddy bioturbated ss
42.92	0.473	0.672	1.258	1.154	1.587	0.687	0.840	0.9528	muddy bioturbated ss
42.94	0.159	0.417	0.272	0.436	1.312	0.514	0.303	0.4875	muddy bioturbated ss
42.96	0.806	1.169	1.483	0.847	0.954	0.312	0.728	0.8999	muddy bioturbated ss
42.98	1.224	1.382	1.789	1.436	2.282	2.371	1.414	1.6998	med-scale x-bedded ss
43.00	1.807	1.471	1.232	1.169	1.036	1.403	2.074	1.4560	med-scale x-bedded ss
43.02	1.659	1.351	1.533	1.471	1.921	1.161	2.006	1.5861	med-scale x-bedded ss
43.04	1.901	1.508	1.615	0.679	1.060	2.098	1.393	1.4648	med-scale x-bedded ss
43.06	3.321	2.148	2.311	2.434	2.994	1.674	2.809	2.5272	med-scale x-bedded ss
43.08	2.608	1.901	1.844	1.705	1.901	2.098	2.123	2.0258	med-scale x-bedded ss
43.11	2.254	2.282	1.105	1.147	1.674	2.311	2.123	1.8421	med-scale x-bedded ss
43.13	2.767	2.006	1.807	0.954	1.267	1.825	2.767	1.9131	med-scale x-bedded ss
43.15	2.685	2.006	1.436	1.072	2.006	3.581	2.809	2.2280	med-scale x-bedded ss
43.17	2.945	1.573	2.006	2.199	1.674	2.402	3.728	2.3610	med-scale x-bedded ss
43.19	4.059	2.402	2.254	2.899	2.572	2.945	2.572	2.8146	med-scale x-bedded ss
43.21	4.567	2.572	2.767	3.971	2.767	3.728	4.714	3.5834	med-scale x-bedded ss
43.23	2.767	3.044	2.282	2.282	4.684	3.321	3.044	3.0603	med-scale x-bedded ss
43.25	1.559	0.985	1.508	1.825	2.098	4.151	2.981	2.1583	med-scale x-bedded ss
43.27	1.520	1.644	1.216	1.644	1.520	2.006	2.767	1.7595	med-scale x-bedded ss

Appendix 13 continued.

Depth (ft)	Column 1	Column 2	Column 3	Column 4	Column 5	Column 6	Column 7	Ave. Perm.	Lithofacies
43.29	1.844	1.705	2.006	1.258	3.247	3.223	3.728	2.4299	med-scale x-bedded ss
43.31	1.520	3.512	2.608	3.223	3.247	3.971	4.248	3.1899	med-scale x-bedded ss
43.33	3.131	2.809	3.204	2.434	4.059	3.581	4.059	3.3253	med-scale x-bedded ss
43.35	3.247	2.074	2.767	1.807	2.994	4.349	4.059	3.0423	med-scale x-bedded ss
43.38	3.044	3.321	2.006	2.994	2.572	4.455	5.769	3.4514	med-scale x-bedded ss
43.40	3.581	2.646	4.455	3.044	4.349	4.807	4.872	3.9649	med-scale x-bedded ss
43.42	4.455	3.653	3.247	1.882	2.767	2.434	2.341	2.9683	med-scale x-bedded ss
43.44	2.402	1.921	1.393	1.882	1.414	2.994	3.971	2.2823	med-scale x-bedded ss
43.46	2.051	1.241	2.282	2.341	2.572	3.321	3.653	2.4942	med-scale x-bedded ss
43.48	1.963	2.402	2.945	2.646	3.044	4.937	4.059	3.1423	med-scale x-bedded ss
43.50	2.402	2.608	2.981	3.581	2.899	3.971	3.382	3.1178	med-scale x-bedded ss
43.52	3.653	2.371	3.581	2.646	3.728	1.448	3.044	2.9243	med-scale x-bedded ss
43.54	3.149	3.095	3.398	2.536	2.434	2.467	3.479	2.9368	med-scale x-bedded ss
43.56	3.261	2.467	3.398	2.767	3.446	2.767	3.728	3.1190	med-scale x-bedded ss
43.58	2.608	2.199	2.994	2.994	2.608	2.809	3.728	2.8486	med-scale x-bedded ss
43.60	2.028	2.282	2.756	2.434	3.108	3.512	3.728	2.8355	med-scale x-bedded ss
43.62	2.371	1.921	1.942	2.028	1.921	2.899	4.684	2.5380	med-scale x-bedded ss
43.65	1.459	2.402	1.844	2.173	3.653	3.728	3.886	2.7350	med-scale x-bedded ss
43.67	2.074	1.331	2.028	3.564	3.321	4.059	4.684	3.0087	med-scale x-bedded ss
43.69	1.674	0.985	2.148	2.402	3.971	3.581	3.728	2.6412	med-scale x-bedded ss
43.71	0.652	1.601	1.495	2.074	2.809	3.382	3.512	2.2180	med-scale x-bedded ss
43.73	0.740	1.414	3.176	2.899	5.220	3.971	4.872	3.1844	med-scale x-bedded ss
43.75	1.901	1.644	2.006	3.653	4.455	5.220	5.220	3.4426	med-scale x-bedded ss
43.77	3.321	3.044	2.254	3.044	3.149	4.807	3.581	3.3141	med-scale x-bedded ss
43.79	2.756	2.572	3e-04	5e-04	3e-04	2e-04	6e-04	0.7614	med-scale x-bedded ss
43.81	2e-04	7e-04	2.434	2.467	2.557	2.646	2.572	1.8110	med-scale x-bedded ss
43.83	2.555	2.608	2.572	3.581	2.608	2.809	2.725	2.7798	med-scale x-bedded ss
43.85	2.501	1.459	1.644	2.254	2.173	1.789	3.044	2.1235	med-scale x-bedded ss
43.87	1.772	1.882	2.809	2.994	1.942	2.994	2.501	2.4132	med-scale x-bedded ss
43.90	1.902	1.336	1.902	1.783	2.335	2.123	0.902	1.7546	med-scale x-bedded ss
43.92	1.316	1.821	2.676	3.058	2.537	2.762	0.960	2.1614	med-scale x-bedded ss
43.94	2.446	2.854	1.783	2.209	1.956	1.975	2.595	2.2597	med-scale x-bedded ss
43.96	3e-04	4e-04	3e-04	3e-04	6e-04	4e-04	2e-04	0.0004	med-scale x-bedded ss
43.98	2.226	1.882	1.508	1.644	3.653	2.725	2.467	2.3007	med-scale x-bedded ss
44.00	1.258	2.311	1.722	2.767	2.434	2.311	3.886	2.3840	med-scale x-bedded ss

Appendix 13 continued.

Depth (ft)	Column 1	Column 2	Column 3	Column 4	Column 5	Column 6	Column 7	Ave. Perm.	Lithofacies
44.02	2.311	1.825	2.685	2.199	2.809	1.659	2.809	2.3282	med-scale x-bedded ss
44.04	2.123	1.984	2.536	2.646	2.434	2.402	2.646	2.3959	med-scale x-bedded ss
44.06	2.341	2.809	2.536	3.176	2.994	3.805	2.809	2.9242	med-scale x-bedded ss
44.08	3.653	2.994	2.981	3.886	3.261	3.044	3.044	3.2661	med-scale x-bedded ss
44.10	2.282	3.321	3.653	3.653	3.564	3.223	3.247	3.2774	med-scale x-bedded ss
44.12	2.608	3.653	4.248	3.728	3.321	3.653	3.321	3.5044	med-scale x-bedded ss
44.14	2.854	3.671	3.606	3.807	2.676	3.426	2.953	3.2845	med-scale x-bedded ss
44.17	3.833	2.446	3.807	3.172	2.676	4.283	3.807	3.4318	med-scale x-bedded ss
44.19	2.446	2.378	2.762	3.058	1.755	2.740	2.362	2.5002	med-scale x-bedded ss
44.21	0.299	0.463	0.144	0.044	0.168	1.082	0.188	0.3411	muddy bioturbated ss
44.23	0.011	0.003	0.027	0.011	0.091	0.043	0.013	0.0283	muddy bioturbated ss
44.25	0.005	0.014	0.033	0.028	0.040	0.063	0.019	0.0289	muddy bioturbated ss
44.27	0.056	0.013	0.014	0.012	0.025	0.001	0.001	0.0173	muddy bioturbated ss
44.29	0.082	0.013	0.012	0.045	0.060	0.002	6e-04	0.0306	muddy bioturbated ss
44.31	0.007	0.007	0.005	0.043	0.045	0.142	0.235	0.0692	muddy bioturbated ss
44.33	0.010	0.010	0.005	0.031	0.048	0.065	0.002	0.0242	muddy bioturbated ss
44.35	0.035	0.022	0.049	0.022	0.006	0.138	0.009	0.0399	muddy bioturbated ss
44.37	0.051	0.062	0.052	0.014	0.035	0.111	0.006	0.0470	muddy bioturbated ss
44.39	0.008	0.011	0.009	0.003	0.031	0.045	0.042	0.0212	muddy bioturbated ss
44.42	0.012	0.002	0.004	0.004	0.008	0.001	9e-04	0.0044	muddy bioturbated ss
44.44	0.022	0.004	5e-04	4e-04	0.021	0.022	0.039	0.0155	muddy bioturbated ss
44.46	0.015	0.004	0.008	0.014	0.020	0.002	5e-04	0.0089	muddy bioturbated ss
44.48	0.031	0.002	0.002	0.003	0.000	0.000	0.298	0.0479	muddy bioturbated ss
44.50	0.003	0.003	0.009	0.007	0.002	0.002	0.160	0.0265	muddy bioturbated ss
44.52	0.037	0.017	0.060	0.028	0.009	0.007	0.002	0.0229	muddy bioturbated ss
44.54	0.076	0.034	0.029	0.001	0.003	0.008	0.002	0.0219	muddy bioturbated ss
44.56	0.099	0.006	0.005	0.007	0.009	0.007	0.010	0.0203	muddy bioturbated ss
44.58	0.008	0.006	0.006	0.007	0.005	0.006	0.011	0.0070	muddy bioturbated ss
44.60	0.004	0.017	0.012	0.015	0.009	0.002	0.003	0.0089	muddy bioturbated ss
44.62	0.047	0.050	0.131	0.205	0.017	0.005	0.002	0.0652	muddy bioturbated ss
44.64	0.007	0.008	0.197	0.030	0.012	0.003	0.001	0.0367	muddy bioturbated ss
44.66	0.007	0.005	0.028	0.033	0.013	0.010	7e-04	0.0137	muddy bioturbated ss
44.69	0.002	6e-04	0.002	0.002	0.002	0.001	7e-04	0.0013	muddy bioturbated ss
44.71	0.002	7e-04	0.001	0.002	0.002	0.001	0.001	0.0013	muddy bioturbated ss
44.73	0.002	5e-04	8e-04	9e-04	0.001	9e-04	7e-04	0.0009	muddy bioturbated ss

Appendix 13 continued.

Depth (ft)	Column 1	Column 2	Column 3	Column 4	Column 5	Column 6	Column 7	Ave. Perm.	Lithofacies
44.81	0.300	0.163	0.159	0.167	0.180	0.097	0.334	0.2000	med-scale x-bedded ss
44.83	0.487	0.198	0.254	0.471	0.320	0.080	0.018	0.2610	med-scale x-bedded ss
44.85	0.309	0.277	0.490	0.370	0.258	0.178	0.047	0.2754	med-scale x-bedded ss
44.87	0.153	0.155	0.165	0.134	0.194	0.113	0.050	0.1376	med-scale x-bedded ss
44.89	0.142	0.405	0.143	0.141	0.166	0.104	0.118	0.1741	med-scale x-bedded ss
44.91	0.198	0.192	0.218	0.287	0.479	0.292	0.421	0.2979	med-scale x-bedded ss
44.94	0.441	0.415	0.495	0.421	0.368	0.308	0.546	0.4278	med-scale x-bedded ss
44.96	0.683	0.266	0.609	0.297	0.723	0.490	0.688	0.5364	med-scale x-bedded ss
44.98	0.378	0.458	0.481	0.618	0.756	0.705	0.317	0.5304	med-scale x-bedded ss
45.00	0.550	0.487	0.536	0.854	0.929	0.982	0.762	0.7285	med-scale x-bedded ss
45.02	0.446	0.526	0.736	0.829	0.813	0.688	0.776	0.6878	med-scale x-bedded ss
45.04	9e-04	9e-04	2e-04	9e-04	8e-04	3e-04	8e-04	0.0007	med-scale x-bedded ss
45.06	0.134	0.453	0.821	0.504	0.366	0.565	0.451	0.4705	med-scale x-bedded ss
45.08	0.316	1.055	1.239	1.556	1.276	1.258	1.336	1.1479	med-scale x-bedded ss
45.10	0.656	0.884	0.112	1.202	1.528	1.239	1.204	0.9750	med-scale x-bedded ss
45.12	0.949	1.711	1.199	1.614	1.592	1.902	1.528	1.4993	med-scale x-bedded ss
45.14	1.239	1.121	1.358	1.450	1.296	1.121	0.776	1.1944	med-scale x-bedded ss
45.16	0.948	1.239	0.889	1.422	1.472	1.421	1.169	1.2229	med-scale x-bedded ss
45.31	1.770	0.458	0.403	0.270	0.199	0.110	0.093	0.4719	med-scale x-bedded ss
45.33	0.694	0.490	0.783	0.026	0.126	0.203	0.510	0.4045	med-scale x-bedded ss
45.35	0.929	0.430	0.407	0.016	0.109	0.031	0.029	0.2785	med-scale x-bedded ss
45.37	2.362	0.576	0.520	1.614	0.016	1.614	3.426	1.4468	med-scale x-bedded ss
45.39	0.252	0.156	1.258	0.243	0.460	1.171	0.769	0.6156	med-scale x-bedded ss
45.41	0.711	0.667	0.618	0.929	0.919	0.829	1.125	0.8282	med-scale x-bedded ss
45.43	0.769	0.529	0.982	0.994	0.939	1.222	1.426	0.9801	med-scale x-bedded ss
45.45	0.783	0.881	1.222	1.030	0.919	1.017	2.233	1.1549	med-scale x-bedded ss
45.48	1.005	0.899	1.276	1.380	1.426	1.316	0.971	1.1818	med-scale x-bedded ss
45.50	0.899	1.030	1.239	1.402	1.125	1.426	1.450	1.2244	med-scale x-bedded ss
45.52	1.222	1.475	1.121	1.258	1.475	1.614	1.501	1.3807	med-scale x-bedded ss
45.54	1.614	1.276	1.042	1.140	1.222	1.171	1.336	1.2574	med-scale x-bedded ss
45.56	1.358	1.222	1.204	1.188	1.380	1.501	1.380	1.3187	med-scale x-bedded ss
45.58	1.358	1.475	1.645	1.276	1.188	1.171	1.258	1.3386	med-scale x-bedded ss
45.60	1.614	1.239	1.678	1.902	1.592	1.380	1.188	1.5131	med-scale x-bedded ss
45.62	0.890	1.645	1.975	1.711	2.014	1.975	1.450	1.6658	med-scale x-bedded ss
45.64	1.121	1.085	0.899	0.798	1.556	1.358	1.258	1.1535	med-scale x-bedded ss

Appendix 13 continued.

Depth (ft)	Column 1	Column 2	Column 3	Column 4	Column 5	Column 6	Column 7	Ave. Perm.	Lithofacies
45.66	2.140	1.140	1.380	1.276	1.110	0.821	1.042	1.2727	med-scale x-bedded ss
45.68	2.252	2.364	2.209	2.518	1.770	0.919	0.749	1.8258	med-scale x-bedded ss
45.73	1.584	0.881	1.556	3.426	3.426	4.031	3.172	2.5820	med-scale x-bedded ss
45.75	1.276	1.711	2.446	2.762	2.518	3.172	2.518	2.3434	med-scale x-bedded ss
45.77	1.614	1.426	1.239	2.518	2.854	2.762	3.426	2.2627	med-scale x-bedded ss
45.79	3.172	3.606	2.446	3.953	3.426	3.426	2.335	3.1948	med-scale x-bedded ss
45.81	1.902	2.762	3.426	2.953	3.262	3.807	3.426	3.0767	med-scale x-bedded ss
45.83	3.114	1.426	0.307	1.140	2.762	0.846	2.854	1.7784	med-scale x-bedded ss
45.85	1.916	1.276	2.676	1.902	1.316	2.446	1.336	1.8382	med-scale x-bedded ss
45.87	1.358	2.854	2.446	2.378	2.071	1.956	2.378	2.2057	med-scale x-bedded ss
45.89	2.446	1.380	0.736	0.656	2.518	0.929	3.426	1.7271	med-scale x-bedded ss
45.91	1.670	1.528	1.239	0.982	1.755	1.902	1.711	1.5410	med-scale x-bedded ss
46.00	0.588	1.179	1.103	2.283	1.902	1.902	2.283	1.6057	med-scale x-bedded ss
46.02	0.053	0.053	0.051	0.049	0.123	0.087	0.104	0.0743	phosphatic nodular mdst
46.04	0.012	0.017	0.073	0.078	0.187	0.171	0.080	0.0881	phosphatic nodular mdst
46.06	0.020	0.006	0.018	0.044	0.034	0.061	0.034	0.0308	phosphatic nodular mdst
46.08	0.030	0.009	0.016	0.027	0.041	0.095	0.041	0.0369	phosphatic nodular mdst
46.10	0.019	0.027	0.037	0.027	0.025	0.046	0.027	0.0296	phosphatic nodular mdst
46.12	0.046	0.030	0.033	0.015	0.012	0.020	0.011	0.0238	phosphatic nodular mdst
46.14	0.033	0.037	0.027	0.031	0.017	0.021	0.021	0.0266	phosphatic nodular mdst
46.16	0.081	0.068	0.061	0.050	0.028	0.014	0.022	0.0463	phosphatic nodular mdst
46.18	0.095	0.103	0.113	0.067	0.055	0.020	0.033	0.0694	phosphatic nodular mdst
46.20	0.068	0.059	0.064	0.083	0.070	0.048	0.028	0.0598	phosphatic nodular mdst
46.22	0.042	0.054	0.086	0.044	0.051	0.035	0.043	0.0507	phosphatic nodular mdst
46.25	0.037	0.029	0.071	0.069	0.031	0.045	0.039	0.0459	phosphatic nodular mdst
46.27	0.032	0.033	0.059	0.027	0.017	0.021	0.028	0.0310	phosphatic nodular mdst
46.29	0.065	0.034	0.021	0.036	0.029	0.039	0.062	0.0407	phosphatic nodular mdst
46.31	0.104	0.041	0.031	0.031	0.057	0.074	0.090	0.0611	phosphatic nodular mdst
46.33	0.020	0.015	0.061	0.100	0.096	0.064	0.057	0.0588	phosphatic nodular mdst
46.35	0.048	0.036	0.065	0.157	0.168	0.107	0.093	0.0962	phosphatic nodular mdst
46.37	0.048	0.073	0.067	0.094	0.133	0.091	0.080	0.0836	phosphatic nodular mdst
46.39	0.130	0.055	0.101	0.113	0.069	0.050	0.088	0.0866	phosphatic nodular mdst
46.41	0.448	0.267	0.599	0.124	0.068	0.100	0.083	0.2414	phosphatic nodular mdst
46.47	0.036	0.045	0.136	0.153	0.103	0.113	0.164	0.1071	phosphatic nodular mdst
46.49	2e-04	3e-04	0.014	0.093	0.176	0.215	0.052	0.0786	phosphatic nodular mdst

Appendix 13 continued.

Depth (ft)	Column 1	Column 2	Column 3	Column 4	Column 5	Column 6	Column 7	Ave. Perm.	Lithofacies
46.52	2e-04	0.000	1e-04	0.006	0.008	4e-04	2e-04	0.0021	phosphatic nodular mdst
46.54	1e-04	0.000	1e-04	0.000	0.000	6e-04	1e-04	0.0001	phosphatic nodular mdst
46.56	1e-04	1e-04	0.000	0.000	1e-04	1e-04	0.000	6e-05	phosphatic nodular mdst
46.58	0.015	3e-04	0.000	0.000	1e-04	1e-04	4e-04	0.0022	phosphatic nodular mdst
46.60	0.202	0.038	0.019	7e-04	2e-04	3e-04	0.001	0.0373	phosphatic nodular mdst
46.62	0.004	0.092	0.019	0.007	0.019	0.024	0.030	0.0279	phosphatic nodular mdst
46.64	0.006	0.015	0.016	0.009	0.017	0.018	0.011	0.0130	phosphatic nodular mdst
46.66	0.006	0.005	0.005	0.009	0.014	0.028	0.027	0.0133	phosphatic nodular mdst
46.68	0.003	0.003	0.004	0.014	0.008	0.018	0.032	0.0117	phosphatic nodular mdst
46.70	0.003	0.004	0.005	0.032	0.061	0.028	0.011	0.0206	phosphatic nodular mdst
46.72	0.005	0.004	0.007	0.051	0.053	0.050	0.022	0.0273	phosphatic nodular mdst
46.74	0.003	0.025	0.004	0.048	0.010	0.047	0.023	0.0228	phosphatic nodular mdst
46.77	0.020	0.034	0.026	0.017	0.019	0.034	0.003	0.0219	phosphatic nodular mdst
46.79	0.003	0.003	0.027	0.019	0.024	0.013	0.017	0.0150	phosphatic nodular mdst
46.81	0.032	0.006	0.008	0.010	0.014	0.009	0.009	0.0125	phosphatic nodular mdst
46.87	0.008	0.007	0.029	0.021	0.022	0.014	0.005	0.0151	phosphatic nodular mdst
46.89	0.007	0.007	0.011	0.013	0.025	0.011	0.011	0.0121	phosphatic nodular mdst
46.91	0.010	0.028	0.015	0.006	0.011	0.010	0.021	0.0142	phosphatic nodular mdst
46.93	0.040	0.011	0.003	0.002	0.010	0.009	0.004	0.0114	phosphatic nodular mdst
46.95	0.003	0.006	0.017	0.008	0.002	0.004	0.006	0.0065	phosphatic nodular mdst
46.97	0.005	0.004	0.007	0.024	0.004	0.003	0.010	0.0080	phosphatic nodular mdst
46.99	0.004	0.005	0.010	0.026	0.016	0.004	0.003	0.0098	phosphatic nodular mdst
47.01	0.002	0.004	0.014	0.010	0.010	0.003	0.003	0.0065	phosphatic nodular mdst
47.04	0.006	0.008	0.006	0.010	0.004	0.007	0.008	0.0069	phosphatic nodular mdst
47.06	0.253	0.031	0.002	0.003	0.004	0.002	0.003	0.0425	phosphatic nodular mdst
47.08	0.001	0.002	0.001	0.001	0.013	0.038	0.004	0.0088	phosphatic nodular mdst
47.10	9e-04	0.001	0.001	0.001	0.002	0.001	0.004	0.0016	phosphatic nodular mdst
47.12	7e-04	8e-04	0.001	9e-04	8e-04	0.004	0.002	0.0015	phosphatic nodular mdst
47.14	6e-04	8e-04	0.001	0.001	7e-04	0.003	0.003	0.0014	phosphatic nodular mdst
47.16	5e-04	8e-04	6e-04	6e-04	4e-04	7e-04	0.005	0.0012	phosphatic nodular mdst
47.18	7e-04	6e-04	5e-04	5e-04	9e-04	0.001	4e-04	0.0007	phosphatic nodular mdst
47.20	4e-04	5e-04	5e-04	9e-04	0.004	0.003	7e-04	0.0014	phosphatic nodular mdst
47.22	4e-04	9e-04	4e-04	0.002	0.003	0.003	0.002	0.0015	phosphatic nodular mdst
47.24	2e-04	2e-04	3e-04	0.001	0.005	6e-04	5e-04	0.0011	phosphatic nodular mdst
47.26	2e-04	2e-04	2e-04	4e-04	4e-04	7e-04	6e-04	0.0004	phosphatic nodular mdst

Appendix 13 continued.

Depth (ft)	Column 1	Column 2	Column 3	Column 4	Column 5	Column 6	Column 7	Ave. Perm.	Lithofacies
47.29	2e-04	3e-04	5e-04	4e-04	4e-04	4e-04	5e-04	0.0004	phosphatic nodular mdst
47.31	3e-04	3e-04	0.001	5e-04	3e-04	3e-04	6e-04	0.0005	phosphatic nodular mdst
47.33	3e-04	3e-04	8e-04	4e-04	3e-04	5e-04	5e-04	0.0004	phosphatic nodular mdst
47.35	4e-04	3e-04	3e-04	5e-04	3e-04	5e-04	4e-04	0.0004	phosphatic nodular mdst
47.37	0.025	6e-04	3e-04	3e-04	5e-04	3e-04	4e-04	0.0040	phosphatic nodular mdst
47.39	0.533	0.062	0.001	2e-04	2e-04	6e-04	0.032	0.0899	phosphatic nodular mdst
47.41	0.381	0.160	0.001	9e-04	6e-04	0.002	0.016	0.0801	phosphatic nodular mdst
47.43	0.460	0.219	0.200	0.175	0.002	0.002	2e-04	0.1511	phosphatic nodular mdst
47.45	0.300	0.136	0.111	0.021	0.010	0.003	1e-04	0.0829	phosphatic nodular mdst
47.47	0.283	0.259	1.026	0.196	0.018	0.014	0.004	0.2572	phosphatic nodular mdst
47.49	0.511	1.166	0.198	0.186	0.054	0.011	0.032	0.3083	phosphatic nodular mdst
47.51	0.617	3.426	0.575	0.702	0.399	0.030	0.107	0.8364	phosphatic nodular mdst
47.53	0.827	2.854	0.732	1.350	0.721	0.199	0.932	1.0878	phosphatic nodular mdst
47.56	1.068	1.711	0.967	1.387	1.166	0.788	1.068	1.1652	phosphatic nodular mdst
47.58	0.460	1.466	0.967	1.510	1.222	0.776	0.517	0.9883	phosphatic nodular mdst
47.60	0.045	0.061	0.019	0.015	0.042	0.238	0.093	0.0732	phosphatic nodular mdst
47.62	0.058	0.048	0.015	0.188	0.043	0.010	0.015	0.0538	phosphatic nodular mdst
47.64	0.069	0.114	0.046	0.042	0.048	0.142	0.120	0.0829	phosphatic nodular mdst
47.66	7e-04	2e-04	0.072	0.027	0.003	0.003	0.034	0.0200	phosphatic nodular mdst
47.68	7e-04	4e-04	0.043	0.016	0.002	0.053	0.429	0.0778	phosphatic nodular mdst
47.70	0.083	0.241	0.370	0.126	0.402	0.408	1.026	0.3792	phosphatic nodular mdst
47.72	0.674	0.648	0.119	7e-04	0.280	0.298	0.533	0.3645	phosphatic nodular mdst
47.74	0.327	0.765	0.568	0.801	0.538	0.061	0.340	0.4855	phosphatic nodular mdst
47.89	0.088	0.057	0.142	0.409	0.334	0.453	0.388	0.2674	med-scale x-bedded ss
47.91	0.529	0.399	0.609	0.526	0.439	0.557	0.568	0.5183	med-scale x-bedded ss
47.93	0.605	0.632	0.392	0.257	0.371	0.091	0.205	0.3648	med-scale x-bedded ss
47.95	0.478	0.311	0.354	0.375	0.383	0.343	0.688	0.4188	med-scale x-bedded ss
47.97	1.017	0.463	0.837	0.700	0.434	0.308	0.407	0.5951	med-scale x-bedded ss
47.99	1.222	0.829	0.070	0.333	0.269	1.501	2.740	0.9948	med-scale x-bedded ss
48.01	0.501	0.683	0.122	0.392	0.191	0.949	0.350	0.4555	med-scale x-bedded ss
48.03	1.614	0.776	0.798	0.637	0.492	0.846	0.627	0.8272	med-scale x-bedded ss
48.05	1.380	1.711	1.850	1.017	1.042	0.550	0.526	1.1538	med-scale x-bedded ss
48.08	0.520	1.426	1.068	1.678	0.443	1.171	1.017	1.0461	med-scale x-bedded ss
48.10	1.834	1.755	1.860	1.614	1.711	0.994	1.475	1.6061	med-scale x-bedded ss
48.12	1.645	2.314	2.054	1.501	1.975	1.140	1.501	1.7327	med-scale x-bedded ss

Appendix 13 continued.

Depth (ft)	Column 1	Column 2	Column 3	Column 4	Column 5	Column 6	Column 7	Ave. Perm.	Lithofacies
48.14	3.172	2.634	1.584	1.528	1.614	1.555	1.669	1.9652	med-scale x-bedded ss
48.16	3.671	2.446	1.555	1.711	1.555	1.336	1.783	2.0082	med-scale x-bedded ss
48.18	1.556	1.068	0.776	0.539	0.949	1.096	0.821	0.9723	med-scale x-bedded ss
48.20	2.446	0.756	0.601	0.605	0.730	1.121	0.661	0.9885	med-scale x-bedded ss
48.22	0.417	0.568	0.742	0.667	0.484	0.762	1.030	0.6672	med-scale x-bedded ss
48.24	0.043	0.529	0.565	0.267	1.204	0.949	1.042	0.6571	med-scale x-bedded ss
48.70	0.338	0.422	0.318	0.072	0.067	0.086	0.085	0.1981	glauconitic ss
48.72	0.068	0.030	0.204	0.170	0.147	0.121	0.122	0.1232	glauconitic ss
48.74	0.045	0.026	0.031	0.034	0.026	0.070	0.335	0.0811	glauconitic ss
48.76	0.021	0.033	0.033	0.047	0.108	0.298	0.036	0.0823	glauconitic ss
48.78	0.015	0.016	0.029	0.011	0.061	0.219	0.071	0.0603	glauconitic ss
48.80	0.013	0.006	0.053	0.066	0.016	0.029	0.030	0.0304	glauconitic ss
48.82	0.024	0.013	0.014	0.013	0.037	0.015	0.017	0.0190	glauconitic ss
48.84	0.009	0.019	0.067	0.040	0.122	0.117	0.048	0.0602	glauconitic ss
48.87	0.013	0.005	0.017	0.013	0.082	0.219	0.134	0.0689	glauconitic ss
48.89	0.033	0.062	0.030	0.017	0.046	0.035	0.051	0.0391	glauconitic ss
48.91	0.041	0.036	0.030	0.032	0.037	0.037	0.067	0.0399	glauconitic ss
48.93	0.025	0.017	0.039	0.093	0.093	0.049	0.062	0.0539	glauconitic ss
48.95	0.026	0.038	0.048	0.084	0.062	0.117	0.045	0.0599	glauconitic ss
48.97	0.047	0.015	0.033	0.052	0.103	0.072	0.044	0.0522	glauconitic ss
48.99	0.068	0.045	0.040	0.047	0.021	0.032	0.028	0.0399	glauconitic ss
49.01	0.183	0.069	0.057	0.054	0.048	0.048	0.024	0.0688	glauconitic ss
49.03	0.047	0.049	0.072	0.071	0.147	0.075	0.043	0.0722	glauconitic ss
49.05	0.086	0.122	0.076	0.056	0.096	0.085	0.036	0.0794	glauconitic ss
49.07	0.090	0.070	0.142	0.090	0.074	0.155	0.084	0.1007	glauconitic ss
49.09	0.087	0.121	0.180	0.078	0.063	0.032	0.056	0.0882	glauconitic ss
49.12	0.440	0.115	0.331	0.166	0.102	0.076	0.049	0.1827	glauconitic ss
49.14	0.196	0.289	0.344	0.109	0.137	0.039	0.052	0.1666	glauconitic ss
49.16	0.381	0.101	0.127	0.068	0.050	0.050	0.030	0.1152	glauconitic ss
49.18	0.301	0.258	0.204	0.211	0.166	0.119	0.257	0.2165	glauconitic ss
49.20	0.123	0.115	0.252	0.482	0.158	0.478	0.163	0.2531	glauconitic ss
49.22	0.487	0.252	0.202	0.342	0.492	0.632	0.399	0.4006	glauconitic ss
49.24	0.113	0.320	0.210	0.364	0.473	0.034	0.487	0.2859	glauconitic ss
49.26	0.166	0.093	0.142	0.177	0.101	0.185	0.568	0.2045	glauconitic ss
49.28	0.440	0.276	0.202	0.170	0.550	0.325	0.294	0.3224	glauconitic ss

Appendix 13 continued.

Depth (ft)	Column 1	Column 2	Column 3	Column 4	Column 5	Column 6	Column 7	Ave. Perm.	Lithofacies
49.34	0.721	0.624	0.617	0.408	0.088	0.765	0.743	0.5665	glauconitic ss
49.37	0.009	0.003	0.171	0.006	0.001	0.320	0.004	0.0736	glauconitic ss
49.39	0.189	0.437	0.099	7e-04	0.004	0.168	0.004	0.1287	glauconitic ss
49.41	0.028	0.041	0.004	0.009	0.022	0.412	0.058	0.0821	glauconitic ss
49.43	0.099	0.002	0.002	0.031	0.002	0.005	0.071	0.0303	glauconitic ss
49.45	0.102	0.148	0.056	0.007	0.017	0.027	0.027	0.0547	glauconitic ss
49.47	0.027	0.040	0.069	0.051	0.013	0.006	0.006	0.0302	glauconitic ss
49.49	0.038	0.039	0.056	0.023	0.011	0.008	0.008	0.0261	glauconitic ss
49.51	0.141	0.034	0.053	0.013	0.014	0.022	0.019	0.0423	glauconitic ss
49.53	0.156	0.110	0.194	0.099	0.142	0.015	0.003	0.1027	glauconitic ss
49.78	0.442	0.100	0.711	0.541	0.138	0.133	0.002	0.2953	glauconitic ss
49.80	0.166	0.669	0.161	0.216	0.304	0.457	0.063	0.2909	glauconitic ss
49.82	0.020	0.028	0.057	0.037	0.012	0.013	0.040	0.0297	glauconitic ss
49.84	0.057	0.031	0.013	0.027	0.031	0.025	0.025	0.0298	glauconitic ss
49.86	0.039	0.083	0.064	0.063	0.056	0.032	0.015	0.0504	glauconitic ss
49.89	0.093	0.103	0.119	0.109	0.021	0.037	0.058	0.0771	glauconitic ss
49.91	0.041	0.020	0.029	0.063	0.003	0.014	0.013	0.0260	glauconitic ss
49.93	0.035	0.051	0.027	0.056	0.027	0.037	0.012	0.0349	glauconitic ss
49.95	0.029	0.042	0.029	0.033	0.026	0.200	0.719	0.1540	glauconitic ss
49.97	0.209	0.275	0.101	0.533	1.316	0.537	0.420	0.4842	glauconitic ss
49.99	0.813	1.159	0.439	0.742	0.288	0.168	0.340	0.5641	glauconitic ss
50.01	2.362	0.632	1.068	0.813	1.052	1.368	0.888	1.1690	glauconitic ss
50.03	0.034	0.529	0.911	0.092	0.199	0.854	0.632	0.4643	glauconitic ss
50.05	0.014	0.027	0.033	0.122	0.126	0.319	0.372	0.1447	glauconitic ss
50.07	0.190	0.169	0.110	0.312	0.071	0.062	0.126	0.1484	glauconitic ss
50.09	0.238	0.298	0.178	0.268	0.374	0.362	0.376	0.2989	glauconitic ss
50.11	0.149	0.097	0.035	0.102	0.175	0.347	0.380	0.1835	glauconitic ss
50.13	0.347	0.199	0.494	0.490	0.134	0.104	0.050	0.2598	glauconitic ss
50.16	0.051	0.076	0.405	0.366	0.167	0.408	0.146	0.2312	glauconitic ss
50.18	0.272	0.027	0.108	0.048	0.133	0.509	0.265	0.1944	glauconitic ss
50.20	1.592	0.876	0.086	0.442	0.865	1.068	1.316	0.8921	glauconitic ss
50.22	1.850	1.902	0.644	0.408	1.342	1.140	0.794	1.1542	glauconitic ss
50.24	0.358	0.768	0.454	0.439	0.140	0.632	0.949	0.5343	glauconitic ss
50.26	0.022	0.100	0.003	0.003	0.776	0.949	1.103	0.4224	glauconitic ss
50.28	0.794	1.267	1.036	0.347	1.159	2.140	0.936	1.0971	glauconitic ss

Appendix 13 continued.

Depth (ft)	Column 1	Column 2	Column 3	Column 4	Column 5	Column 6	Column 7	Ave. Perm.	Lithofacies
50.30	1.291	0.190	0.067	0.564	1.222	1.267	0.656	0.7508	glauconitic ss
50.32	0.011	0.022	0.012	0.010	0.053	0.155	0.727	0.1411	glauconitic ss
50.34	0.165	0.039	0.030	0.053	0.053	0.244	0.963	0.2208	glauconitic ss
50.36	0.751	0.245	0.191	0.330	0.564	0.192	0.058	0.3329	glauconitic ss
50.38	1.342	0.899	1.068	0.663	0.865	0.823	0.280	0.8486	glauconitic ss
50.41	0.823	0.977	0.936	0.352	0.208	0.109	0.541	0.5638	glauconitic ss
50.43	0.609	0.256	0.191	0.257	0.583	0.865	0.448	0.4583	glauconitic ss
50.45	0.175	0.320	0.340	1.291	1.342	0.437	0.089	0.5704	glauconitic ss
50.47	0.378	0.537	0.578	0.963	0.555	0.356	0.258	0.5177	glauconitic ss
50.49	0.876	1.244	0.437	0.759	0.711	0.683	0.463	0.7390	glauconitic ss
50.51	1.036	1.068	0.727	0.055	1.222	1.556	1.244	0.9867	glauconitic ss
50.53	1.244	0.977	1.121	1.397	1.426	1.103	0.899	1.1666	glauconitic ss
50.55	0.396	0.609	1.426	1.592	1.397	1.159	0.302	0.9828	glauconitic ss
50.57	1.397	1.902	2.283	1.592	1.159	1.711	1.103	1.5923	glauconitic ss
50.59	1.630	1.834	2.140	1.630	1.711	1.771	1.902	1.8024	glauconitic ss
50.61	1.488	1.630	1.267	1.179	1.426	1.902	1.711	1.5146	glauconitic ss
50.63	2.362	1.426	1.369	1.902	1.711	2.054	0.501	1.6177	glauconitic ss
50.65	2.335	0.977	1.556	1.342	1.488	0.924	0.767	1.3410	glauconitic ss
50.68	1.091	1.179	0.911	1.316	0.844	0.813	0.963	1.0167	glauconitic ss
50.70	0.032	0.016	0.311	0.561	0.596	1.068	0.971	0.5080	glauconitic ss
50.72	0.201	0.539	0.030	0.550	0.516	0.492	0.971	0.4715	glauconitic ss
50.74	0.490	0.166	0.439	0.441	0.546	0.179	0.672	0.4189	glauconitic ss
50.76	0.168	0.899	1.055	1.222	0.909	1.096	1.426	0.9677	glauconitic ss
50.78	0.641	0.982	1.258	1.336	1.528	1.402	1.276	1.2034	glauconitic ss
50.80	1.501	1.296	1.005	1.528	0.783	0.204	0.837	1.0219	glauconitic ss
50.82	1.501	1.296	1.902	1.358	1.358	2.378	2.854	1.8065	glauconitic ss
50.93	2.635	2.209	1.244	2.335	1.068	1.902	2.979	2.0529	glauconitic ss
50.95	0.554	1.005	1.555	2.446	0.473	2.740	2.537	1.6159	glauconitic ss
50.97	0.212	0.284	1.902	1.711	0.018	0.011	9e-04	0.5912	glauconitic ss
50.99	1.802	0.051	0.071	0.378	0.541	0.185	0.234	0.4661	glauconitic ss
51.01	1.902	0.378	0.009	0.004	0.366	0.317	0.213	0.4555	glauconitic ss
51.03	0.244	0.434	0.102	0.074	0.004	9e-04	0.001	0.1228	glauconitic ss
51.05	0.200	0.135	0.091	0.150	5e-04	6e-04	0.061	0.0913	glauconitic ss
51.07	0.302	0.155	0.192	0.340	6e-04	0.007	0.269	0.1807	glauconitic ss
51.09	0.031	0.101	0.040	0.053	0.009	0.012	0.374	0.0884	glauconitic ss

Appendix 13 continued.

Depth (ft)	Column 1	Column 2	Column 3	Column 4	Column 5	Column 6	Column 7	Ave. Perm.	Lithofacies
51.11	0.261	0.045	0.027	0.006	0.183	0.159	0.058	0.1055	glauconitic ss
51.13	0.019	0.002	9e-04	0.003	7e-04	0.002	7e-04	0.0039	glauconitic ss
51.15	0.012	0.002	0.006	0.002	0.002	0.005	0.002	0.0043	glauconitic ss
51.17	0.006	0.007	0.004	0.004	0.002	1e-04	0.001	0.0034	glauconitic ss
51.20	0.001	0.003	0.002	0.002	2e-04	1e-04	1e-04	0.0012	glauconitic ss
51.22	4e-04	5e-04	5e-04	0.001	4e-04	2e-04	3e-04	0.0005	glauconitic ss
51.24	0.001	0.001	7e-04	4e-04	4e-04	4e-04	3e-04	0.0007	glauconitic ss
51.26	0.003	5e-04	1e-04	1e-04	1e-04	1e-04	1e-04	0.0006	glauconitic ss
51.28	2e-04	2e-04	2e-04	7e-04	3e-04	3e-04	5e-04	0.0003	glauconitic ss
51.30	4e-04	9e-04	0.019	0.024	0.003	5e-04	0.002	0.0071	glauconitic ss
51.32	0.002	0.004	0.006	0.010	0.010	0.005	0.007	0.0061	glauconitic ss
51.34	0.215	0.061	0.027	0.024	0.022	0.016	0.119	0.0693	glauconitic ss
51.36	0.083	0.104	0.048	0.160	0.075	0.077	0.059	0.0864	glauconitic ss
51.38	0.022	5e-04	6e-04	8e-04	8e-04	0.002	5e-04	0.0038	glauconitic ss
51.40	4e-04	2e-04	1e-04	2e-04	2e-04	5e-04	3e-04	0.0003	glauconitic ss
51.42	4e-04	2e-04	2e-04	5e-04	7e-04	0.002	0.001	0.0007	glauconitic ss
51.45	1e-04	1e-04	1e-04	3e-04	6e-04	0.001	6e-04	0.0004	glauconitic ss
51.47	1e-04	1e-04	3e-04	2e-04	2e-04	4e-04	4e-04	0.0002	glauconitic ss
51.57	0.028	0.023	0.014	0.006	0.003	0.009	0.005	0.0125	glauconitic ss
51.59	0.014	0.032	0.044	0.010	0.012	0.016	0.011	0.0198	glauconitic ss
51.61	0.035	0.044	0.059	0.038	0.018	0.012	0.011	0.0310	glauconitic ss
51.63	0.057	0.055	0.075	0.066	0.044	1.005	1.510	0.4016	glauconitic ss
51.65	0.085	0.042	0.183	0.051	0.040	0.007	0.002	0.0586	glauconitic ss
51.67	0.026	0.020	0.021	0.052	0.041	0.017	0.019	0.0279	glauconitic ss
51.69	0.023	0.024	0.032	0.051	0.042	0.029	0.020	0.0318	glauconitic ss
51.71	0.021	0.029	0.037	0.052	0.042	0.041	0.020	0.0345	glauconitic ss
51.74	0.021	0.059	0.050	0.052	0.044	0.047	0.031	0.0432	glauconitic ss
51.76	0.011	0.015	0.024	0.047	0.043	0.046	0.031	0.0308	glauconitic ss
51.78	0.040	0.046	0.057	0.062	0.043	0.043	0.078	0.0526	glauconitic ss
51.80	0.026	0.026	0.011	0.011	0.048	0.049	0.060	0.0330	glauconitic ss
51.82	0.029	0.019	0.020	0.011	0.025	0.024	0.015	0.0202	glauconitic ss
51.84	0.013	0.019	0.012	0.008	0.046	0.162	2e-04	0.0370	glauconitic ss
51.86	4e-04	5e-04	4e-04	0.001	6e-04	0.269	2e-04	0.0389	glauconitic ss
51.88	5e-04	4e-04	3e-04	3e-04	5e-04	0.003	2e-04	0.0008	glauconitic ss
51.90	3e-04	2e-04	2e-04	1e-04	1e-04	0.004	3e-04	0.0007	glauconitic ss

Appendix 13 continued.

Depth (ft)	Column 1	Column 2	Column 3	Column 4	Column 5	Column 6	Column 7	Ave. Perm.	Lithofacies
51.92	2e-04	1e-04	1e-04	2e-04	2e-04	0.002	3e-04	0.0004	glauconitic ss
51.94	0.005	0.002	7e-04	8e-04	7e-04	0.002	0.003	0.0020	glauconitic ss
52.01	0.049	0.039	0.014	0.065	0.035	0.019	0.013	0.0332	sandy shale
52.03	0.022	0.005	0.005	0.019	0.020	0.036	0.010	0.0167	sandy shale
52.05	0.009	0.012	0.017	0.022	0.010	0.012	0.067	0.0213	sandy shale
52.07	0.024	0.007	0.030	0.005	0.010	0.018	0.203	0.0425	sandy shale
52.09	0.007	0.006	0.002	0.002	0.003	0.003	0.006	0.0042	sandy shale
52.11	0.002	0.004	0.004	0.004	0.004	0.002	0.003	0.0031	sandy shale
52.13	0.002	0.002	0.004	0.002	0.003	0.002	0.006	0.0027	sandy shale
52.15	0.002	0.002	0.002	0.002	0.002	0.002	0.028	0.0056	sandy shale
52.17	0.002	0.002	0.002	0.003	0.007	0.003	0.051	0.0099	sandy shale
52.19	0.006	0.006	0.004	0.007	0.002	0.004	0.073	0.0145	sandy shale
52.21	0.010	0.010	0.006	0.005	0.004	0.005	0.005	0.0064	sandy shale
52.23	0.014	0.002	0.002	0.002	0.003	0.014	0.007	0.0063	sandy shale
52.26	0.009	0.004	9e-04	0.001	0.001	0.001	0.002	0.0029	sandy shale
52.28	0.002	0.002	0.002	0.003	0.002	0.002	0.003	0.0019	sandy shale
52.30	0.030	0.012	0.025	0.015	0.003	0.003	0.003	0.0132	sandy shale
52.32	0.018	0.073	0.028	0.009	0.007	0.006	0.005	0.0207	sandy shale
52.34	0.006	0.004	9e-04	0.002	0.002	0.006	0.023	0.0062	sandy shale
52.36	0.004	0.003	0.001	0.002	0.002	0.003	0.002	0.0023	sandy shale
52.38	0.002	0.003	0.005	0.007	0.006	0.059	0.002	0.0118	sandy shale
52.40	0.004	0.001	9e-04	0.003	0.008	0.002	0.001	0.0030	sandy shale
52.42	0.001	0.001	0.002	0.001	0.002	0.002	0.001	0.0013	sandy shale
52.44	0.001	0.002	8e-04	0.001	0.002	0.002	0.002	0.0014	sandy shale
52.46	8e-04	9e-04	0.001	0.001	0.001	0.001	0.003	0.0013	sandy shale
52.48	0.002	0.001	0.001	0.001	0.001	0.001	0.003	0.0015	sandy shale
52.51	0.003	0.001	0.001	0.001	0.002	0.002	0.002	0.0018	sandy shale
52.53	0.002	0.001	8e-04	7e-04	0.001	0.002	0.002	0.0014	sandy shale
52.55	0.001	0.001	0.001	8e-04	8e-04	0.001	0.001	0.0010	sandy shale
52.57	0.002	0.001	9e-04	8e-04	9e-04	0.001	0.002	0.0013	sandy shale
52.59	0.007	0.006	0.002	0.001	0.001	9e-04	0.001	0.0027	sandy shale
52.61	0.001	0.001	0.002	0.001	0.001	0.001	0.004	0.0017	sandy shale
52.63	0.004	9e-04	8e-04	0.001	0.001	0.002	0.008	0.0024	sandy shale
52.65	0.002	0.006	0.002	0.002	0.002	0.002	6e-04	0.0022	sandy shale
52.67	0.006	0.005	0.003	0.002	0.001	0.002	8e-04	0.0026	sandy shale
52.69	0.001	0.003	0.003	0.002	0.001	0.001	0.001	0.0017	sandy shale

Appendix 13 continued.

GEOSTATISTICS FOR EACH LITHOFACIES MEASURED IN TOCITO SANDSTONE OUTCROP

GEOSTA-TISTIC	LARGE XBD	MED XBD	INTER-BED	BIOTURB	RIPPLE-LAM	PHOS MDST	GLAUC SS
AVE	4.958	3.243	1.624	0.184	0.725	0.490	0.326
STD	1.617	1.813	1.336	0.333	0.886	0.752	0.456
STDS	1.619	1.815	1.339	0.335	0.893	0.755	0.457
VAR	2.614	3.288	1.786	0.111	0.784	0.565	0.208
VARS	2.623	3.294	1.793	0.112	0.798	0.570	0.209
MAX	8.613	8.954	6.020	1.466	3.000	3.195	2.053
MIN	0.885	0.000	0.000	0.000	0.000	0.000	0.000

Appendix 14. Lithologic data for HOF #2 core. Grain size, mud and cement content, and degree of bioturbation are visual estimates "calibrated" with thin section point-count percentages.

DEPTH	AVE PHI	CLAY	CEMENT	BIOTURB
5.00				5
5.02				5
5.04				5
5.06				5
5.08				5
5.30				5
5.60				5
6.00	3.00	5	25	5
6.02	3.00	5	25	5
6.04	3.00	5	25	5
6.06	2.25	2	25	5
6.08	2.25	2	25	5
6.10	2.25	2	25	5
6.12	2.25	2	25	5
6.15	2.25	2	25	5
6.17	2.25	2	25	5
6.19	2.25	2	25	5
6.21	2.25	2	25	5
6.23	2.25	2	25	5
6.25	2.25	2	25	5
6.27	2.25	2	25	5
6.29	2.25	2	25	5
6.60				5
7.00	2.00	10	5	10
7.25				10
7.50	2.00	1	5	10
8.00	2.50	15	8	10
8.08	2.50	15	8	10
8.50	2.00	15	3	10
8.86	2.00	15	3	10
8.88	2.00	2	3	5
8.90	2.00	2	3	5
8.98	2.00	2	3	5
9.01	1.00	2	3	5

Appendix 14 continued.

DEPTH	AVE PHI	CLAY	CEMENT	BIOTURB
9.05	2.00	2	3	5
9.09	2.00	1	2	5
9.13	2.00	1	2	10
9.17	2.00	1	2	10
9.25	2.00	1	2	10
9.33	2.00	1	2	10
9.37	2.00	1	2	10
9.42	2.25	1	2	10
9.50	2.25	1	2	10
9.58	1.50	1	2	10
9.62	1.50	1	2	10
9.67	1.50	1	2	10
9.75	1.50	1	2	5
9.83	1.50	1	2	5
9.91	1.75	1	2	5
10.00	1.75	1	2	5
10.08	2.00	1	2	5
10.17	2.00	1	2	5
10.25	2.00	1	2	5
10.33	2.00	1	2	5
10.42	2.00	1	2	0
10.50	2.50	15	10	0
10.58	2.00	1	5	0
10.67	2.00	1	2	0
10.75	1.75	1	10	0
10.83	2.00	10	20	
10.91	2.00	10	20	
11.00	2.00	10	20	
11.04	2.00	10	20	
11.08	2.00	10	20	
11.12	2.00	10	20	
11.17	2.00	10	20	
11.21	2.00	10	20	
11.25	2.00	10	20	
11.29	2.00	10	20	

Appendix 14 continued.

DEPTH	AVE PHI	CLAY	CEMENT	BIOTURB
11.33	2.00	10	20	
11.37	2.00	10	20	
11.42	2.00	10	20	
11.50	2.00	2	5	
11.58	2.00	2	5	
11.61	2.00	2	5	
11.70	2.25	15	5	
11.78	2.00	2	3	
11.87				
11.95	2.00	2	3	
11.97	2.00	2	3	
12.06	2.00	1	2	
12.10	2.00	1	2	0
12.15	2.00	1	2	0
12.19	2.00	1	2	0
12.22	2.00	1	2	0
12.30	2.00	1	2	0
12.39	1.50	1	2	0
12.43	2.00	15	10	10
12.47	2.00	15	10	10
12.51	2.00	15	10	10
12.57	2.00	15	10	10
12.70	2.00	15	10	10
12.78	2.00	15	10	10
12.87	2.00	15	10	10
12.95	2.00	15	10	10
13.00	2.00	1	2	0
13.08	2.00	1	2	0
13.17	2.00	1	2	0
13.25	2.00	1	2	0
13.33	2.00	1	2	0
13.42	1.75	1	2	0
13.46	1.75	1	2	0
13.50	1.75	1	2	0
13.58	2.25	3	3	10

Appendix 14 continued.

DEPTH	AVE PHI	CLAY	CEMENT	BIOTURB
13.66	2.25	3	3	10
13.75				10
13.83				10
13.92				10
14.00				10
14.08				10
14.16				10
14.25				10
14.33				10
14.41				10
14.47	2.00	1	2	10
14.50	2.00	1	2	10
14.60	2.00	1	2	10
14.68	1.75	1	2	0
14.77	1.75	1	2	0
14.85	2.00	1	2	0
14.93	2.00	1	2	0
15.02	2.00	1	2	0
15.10	2.00	1	2	0
15.19	2.00	1	2	0
15.27	2.00	1	2	0
15.35	2.00	1	2	0
15.43	2.50	50	10	10
15.52	1.75	2	5	0
15.68	2.00	1	2	0
15.77	2.00	1	2	0
15.82	2.00	1	2	0
15.85	2.00	1	2	0
15.93	2.00	1	2	0
16.02	2.00	8	5	0
16.10	2.00	8	5	0
16.15	4.00	60	1	5
16.17	4.00	60	1	5
16.25	2.00	1	5	0
16.48	2.00	1	5	5

Appendix 14 continued.

DEPTH	AVE PHI	CLAY	CEMENT	BIOTURB
16.50	2.00	1	5	10
16.67	2.00	1	5	10
16.75	2.00	1	23	10
16.92	2.00	1	23	10
17.00	2.00	1	23	10
17.08	2.00	1	23	10
17.17	2.00	1	23	10
17.25	2.00	1	23	10
17.33	2.00	1	23	10
17.42				10
17.50	2.00	1	3.5	10
17.58	2.50	1	25	10
17.62	2.50	60	5	10
17.75	2.25	50	20	0
17.85	1.75	0	1	0
17.92	1.75	0	1	0
18.00	1.75	0	1	0
18.08	2.50	50	25	
18.25	2.50	50	25	
18.42	1.75	1	2	0
18.50	2.00	50	20	10
18.58	2.00	50	20	10
18.66	2.00	50	20	10
18.73	2.00	50	20	10
18.81	1.75	5	5	0
18.90	1.75	5	5	0
18.98	1.50	1	3	0
19.06	1.50	1	3	0
19.15	1.50	1	3	0
19.23	1.50	1	3	0
19.31	2.00	1	3	0
19.40	2.00	1	3	0
19.48	2.00	1	3	0
19.56	2.25	1	2	0
19.65	2.25	1	2	0

Appendix 14 continued.

DEPTH	AVE PHI	CLAY	CEMENT	BIOTURB
19.79	2.00	2	3	0
19.88	1.50	2	15	
19.96	1.50	2	15	
19.98	2.00	1	2	0
20.00	2.00	1	2	0
20.08	2.00	1	2	0
20.17	2.00	1	2	0
20.25	4.00	98	1	15
20.33	4.00	98	1	15
20.40	2.75	2	2	25
20.50	2.75	2	2	5
20.55	2.00	10	5	10
20.60	2.00	10	5	10
20.65	2.00	10	5	10
20.70	2.00	10	5	10
20.80	2.00	60	1	10
20.90	2.00	10	5	10
20.95	2.00	60	1	10
21.00	1.00	0	2	0
21.10	2.00	1	2	0
21.20	1.50	0	2	0
21.30	1.00	0	2	0
21.35	4.00	60	1	0
21.40	1.75	5	3	0
21.50	2.00	5	2	0
21.60	2.00	5	2	0
21.75	2.00	0	1	0
21.79	2.00	0	1	0
21.83	2.00	0	1	0
21.88	2.00	0	1	0
21.92	2.00	0	1	0
21.96	2.00	0	1	0
22.00	2.00	0	1	0
22.04	2.00	0	1	0
22.08	2.00	0	1	0

Appendix 14 continued.

DEPTH	AVE PHI	CLAY	CEMENT	BIOTURB
22.13	2.00	0	1	0
22.17	2.00	0	1	0
22.20	1.25	0	2	0
22.23	1.25	0	2	0
22.25	1.25	0	2	0
22.27	1.25	0	2	0
22.30	1.25	0	2	0
22.35	2.00	1	2	0
22.40	2.00	1	2	0
22.45	1.25	0	2	0
22.50	2.00	1	2	0
22.55	1.25	0	2	0
22.60	2.00	5	5	0
22.65	2.00	5	5	0
22.70	1.50	1	5	0
22.75	2.00	1	2	0
22.80	2.00	1	2	0
22.85	2.00	1	2	0
22.90	2.25	10	10	5
22.95	2.25	10	10	5
23.00	5.00	60	2	5
23.02	2.25	10	10	5
23.05	5.00	60	2	5
23.07	2.25	10	10	5
23.09	2.25	10	10	5
23.11	5.00	60	2	5
23.13	5.00	60	2	5
23.15	2.00	0	2	0
23.17	2.00	0	2	0
23.20	2.00	0	2	0
23.22	2.00	0	2	0
23.24	2.00	0	2	0
23.26	2.00	0	2	0
23.28	2.00	0	2	0
23.30	2.00	0	2	0

Appendix 14 continued.

DEPTH	AVE PHI	CLAY	CEMENT	BIOTURB
23.32	2.00	0	2	0
23.34	2.00	0	2	0
23.36	2.00	0	2	0
23.38	2.00	0	2	0
23.40	2.00	0	2	0
23.42	2.00	0	2	0
23.45	2.00	0	2	0
23.47	2.00	0	2	0
23.49	2.00	0	2	0
23.51	2.00	0	2	0
23.53	2.00	0	2	0
23.55	2.00	0	2	0
23.57	2.00	0	2	0
23.59	2.00	0	2	0
23.61	2.00	0	2	0
23.63	2.00	0	2	0
23.65	2.00	0	2	0
23.67	2.00	0	2	0
23.69	2.00	0	2	0
23.72	2.00	0	2	0
23.74	2.00	0	2	0
23.76	2.00	0	2	0
23.78	2.00	0	2	0
23.80	2.00	0	2	0
23.82	2.00	0	2	0
23.84	2.00	0	2	0
23.86	2.00	0	2	0
23.88	2.00	0	2	0
23.90	2.00	0	2	0
23.92	0.75	0	2	0
23.95	0.75	0	2	0
23.97	0.75	0	2	0
23.99	0.75	0	2	0
24.01	0.75	0	2	0
24.03	2.00	0	2	0

Appendix 14 continued.

DEPTH	AVE PHI	CLAY	CEMENT	BIOTURB
24.05	2.00	0	2	0
24.06	2.00	0	2	0
24.07	2.00	0	2	0
24.09	2.00	0	2	0
24.11	2.00	0	2	0
24.13	2.00	0	2	0
24.15	2.00	0	2	0
24.18	2.00	0	2	0
24.20	2.00	0	2	0
24.22	2.00	0	2	0
24.24	2.00	0	2	0
24.26	2.00	0	2	0
24.28	2.00	0	2	0
24.30	2.00	0	2	0
24.32	2.00	0	2	0
24.34	2.00	0	2	0
24.36	2.00	0	2	0
24.38	2.00	0	2	0
24.40	2.00	0	2	0
24.42	2.00	0	2	0
24.43	2.00	0	2	0
24.45	2.00	0	2	0
24.47	2.00	0	2	0
24.49	2.00	0	2	0
24.51	1.75	0	2	0
24.53	1.75	0	2	0
24.55	1.75	0	2	0
24.57	1.75	0	2	0
24.59	1.75	0	2	0
24.61	2.00	0	2	0
24.63	2.00	0	2	0
24.65	2.00	0	2	0
24.67	2.00	0	2	0
24.69	2.00	0	2	0
24.71	2.00	0	2	0

Appendix 14 continued.

DEPTH	AVE PHI	CLAY	CEMENT	BIOTURB
24.73	2.00	0	2	0
24.75	2.00	0	2	0
24.78	2.00	0	2	0
24.80	2.00	0	2	0
24.82	2.00	0	2	0
24.84	2.00	0	2	0
24.86	2.00	0	2	0
24.88	2.00	0	2	0
24.90	2.00	0	2	0
24.92	2.00	0	2	0
24.94	2.00	0	2	0
24.96	1.25	0	2	0
24.98	1.25	0	2	0
25.00	1.25	0	2	0
25.02	0.75	0	2	0
25.04	0.75	0	2	0
25.06	2.00	0	2	0
25.08	2.00	0	2	0
25.10	2.00	0	2	0
25.12	2.00	0	2	0
25.15	2.00	0	2	0
25.17	2.00	0	2	0
25.19	2.00	0	2	0
25.21	2.00	0	2	0
25.23	2.00	0	2	0
25.25	2.00	0	2	0
25.27	2.00	0	2	0
25.29	2.00	0	2	0
25.31	2.00	0	2	0
25.33	2.00	0	2	0
25.35	2.00	0	2	0
25.37	2.00	0	2	0
25.39	2.00	0	2	0
25.45	2.00	1	15	0
25.47	2.00	1	15	0

Appendix 14 continued.

DEPTH	AVE PHI	CLAY	CEMENT	BIOTURB
25.49	2.00	1	15	0
25.51	2.00	0	2	0
25.53	2.00	0	2	0
25.55	2.00	0	2	0
25.58	2.00	0	2	0
25.60	2.00	0	2	0
25.62	2.00	0	2	0
25.70	2.50	10	15	0
25.72	2.50	10	15	0
25.74	2.50	10	15	0
25.77	2.00	3	5	0
25.79	2.00	3	5	0
25.81	2.00	3	5	0
25.83	2.00	3	5	0
25.85	2.00	3	5	0
26.20	2.00	10	10	0
26.22	1.50	0	5	0
26.24	1.50	0	5	0
26.26	1.50	0	5	0
26.28	1.50	0	5	0
26.30	1.50	0	5	0
26.32	1.50	0	5	0
26.35	2.00	0	2	0
26.37	2.00	0	2	0
26.39	1.75	0	2	0
26.41	1.75	0	2	0
26.43	1.75	0	2	0
26.45	1.75	0	2	0
26.47	1.75	0	2	0
26.49	2.00	0	2	0
26.51	2.00	0	2	0
26.53	2.00	0	2	0
26.55	2.00	0	2	0
26.57	2.00	0	2	0
26.60	2.00	0	2	0

Appendix 14 continued.

DEPTH	AVE PHI	CLAY	CEMENT	BIOTURB
26.62	1.50	0	2	0
26.66	1.50	0	2	0
26.68	2.25	5	5	0
26.70	2.25	5	5	0
26.72	2.25	5	5	0
26.74	2.25	5	5	0
26.78	2.25	0	2	0
26.80	2.25	0	2	0
26.82	2.25	0	2	0
26.84	2.25	0	2	0
26.86	2.25	0	2	0
26.88	2.25	0	2	0
26.91	2.25	0	2	0
26.93	2.25	0	2	0
26.95	2.25	0	2	0
26.97	2.25	0	2	0
26.99	2.25	0	2	0
27.01	2.25	0	2	0
27.03	2.25	0	2	0
27.07	1.50	1	2	0
27.10	1.50	1	2	0
27.12	1.50	1	2	0
27.14	2.00	1	2	0
27.16	2.00	1	2	0
27.18	2.00	1	2	0
27.20	2.00	1	2	0
27.22	2.00	1	2	0
27.25	2.00	1	2	0
27.27	2.00	1	2	0
27.29	2.00	1	2	0
27.31	2.00	1	2	0
27.33	2.00	1	2	0
27.35	2.00	1	2	0
27.37	2.00	1	2	0
27.39	2.00	1	2	0

Appendix 14 continued.

DEPTH	AVE PHI	CLAY	CEMENT	BIOTURB
27.41	2.00	1	2	0
27.43	2.00	1	2	0
27.46	2.00	1	2	0
27.48	2.00	1	2	0
27.50	2.00	1	2	0
27.52	2.00	1	2	0
27.54	2.00	1	2	0
27.56	2.00	1	2	0
27.58	2.00	1	2	0
27.60	2.00	1	2	0
27.62	2.00	1	2	0
27.64	2.00	1	2	0
27.68	1.75	1	2	0
27.70	1.75	1	2	0
27.72	1.75	1	2	0
27.74	1.75	1	2	0
27.76	1.75	1	2	0
27.78	2.00	1	2	0
27.81	2.00	1	2	0
27.83	2.00	1	2	0
27.85	2.00	1	2	0
27.87	2.00	1	2	0
27.89	2.00	1	2	0
27.91	2.00	1	2	0
27.93	2.00	1	2	0
27.95	2.00	1	2	0
27.97	2.00	1	2	0
28.02	2.00	5	5	0
28.04	2.00	1	2	
28.06	2.00	1	2	
28.08	2.00	1	2	
28.10	2.00	1	2	
28.12	2.00	50	10	
28.14	1.75	1	2	5
28.16	1.75	1	2	5

Appendix 14 continued.

DEPTH	AVE PHI	CLAY	CEMENT	BIOTURB
28.18	1.75	1	2	5
28.20	1.75	1	2	5
28.22	1.75	1	2	5
28.24	1.75	1	2	5
28.26	1.75	1	2	5
28.28	1.75	1	2	5
28.30	1.75	1	2	5
28.32	1.50	2	3	10
28.34	1.50	2	3	10
28.36	1.50	2	3	10
28.38	1.50	2	3	10
28.40	1.50	2	3	10
28.46	1.00	10	30	0
28.48	1.00	10	30	0
28.50	1.00	10	30	0
28.52	1.00	10	30	0
28.54	1.75	2	5	0
28.56	1.75	2	5	0
28.58	1.75	2	5	0
28.60	1.75	2	5	0
28.62	1.75	2	5	0
28.64	1.50	0	2	20
28.66	1.50	0	2	20
28.68	1.50	0	2	20
28.70	1.50	0	2	20
28.72	1.50	0	2	20
28.74	1.50	0	2	20
28.76	1.50	0	2	20
28.78	1.50	0	2	20
28.81	1.50	0	2	20
28.83	1.50	0	2	20
28.85	1.50	0	2	20
28.87	1.50	0	2	20
28.89	2.00	0	5	0
28.91	2.00	0	5	0

Appendix 14 continued.

DEPTH	AVE PHI	CLAY	CEMENT	BIOTURB
28.93	1.50	0	2	0
28.95	1.50	0	2	0
28.97	1.50	0	2	0
28.99	2.00	0	5	0
29.01	2.00	0	5	0
29.03	1.50	0	2	0
29.06	1.50	0	2	0
29.08	1.50	0	2	0
29.10	1.50	0	2	0
29.12	1.50	0	2	0
29.14	1.50	0	2	0
29.16	2.00	0	5	0
29.18	2.00	0	5	0
29.20	2.00	0	5	0
29.22	2.00	0	5	0
29.24	1.50	0	2	0
29.32	2.00	0	2	0
29.34	2.00	0	2	0
29.36	2.00	0	2	0
29.38	2.00	0	2	0
29.40	2.00	0	2	0
29.42	2.00	0	2	0
29.44	2.00	0	2	0
29.47	2.00	0	2	0
29.49	2.00	0	2	0
29.51	2.00	0	2	0
29.53	2.00	0	2	0
29.55	2.00	0	2	0
29.57	2.00	0	2	0
29.59	2.00	0	2	0
29.61	2.00	0	2	0
29.63	2.00	0	2	0
29.65	2.00	0	2	0
29.67	2.00	0	2	0
29.69	2.00	0	2	0

Appendix 14 continued.

DEPTH	AVE PHI	CLAY	CEMENT	BIOTURB
29.71	2.00	0	2	0
29.73	2.00	0	2	0
29.77	1.75	8	2	0
29.79	1.75	8	2	0
29.81	1.75	8	2	0
29.83	1.75	8	2	0
29.85	1.75	8	2	0
29.87	1.75	10	22	5
29.89	1.75	10	22	5
29.91	1.75	10	22	5
29.93	1.75	10	22	5
29.95	1.75	10	22	5
29.97	1.75	10	22	5
29.99	1.75	10	22	5
30.01	1.75	10	5	0
30.03	1.75	10	5	0
30.05	1.75	10	5	0
30.07	1.75	10	5	0
30.09	1.75	10	5	0
30.11	1.75	10	5	0
30.13	1.75	10	5	0
30.15	1.75	10	5	0
30.17	1.75	10	5	0
30.19	1.75	10	5	0
30.21	2.00	5	2	0
30.23	2.00	5	2	0
30.25	2.00	5	2	0
30.27	2.00	5	2	0
30.29	2.00	5	2	0
30.31	2.00	5	2	0
30.33	2.00	5	2	0
30.35	2.00	5	2	0
30.37	2.00	5	2	0
30.40	2.00	5	2	0
30.42	2.00	5	2	0

Appendix 14 continued.

DEPTH	AVE PHI	CLAY	CEMENT	BIOTURB
30.44	2.00	5	2	0
30.46	2.00	5	2	0
30.48	2.00	5	2	0
30.50	2.00	5	2	0
30.52	2.00	5	2	0
30.54	2.00	5	2	0
30.56	2.25	0	2	0
30.58	2.25	0	2	0
30.60	2.25	0	2	0
30.62	2.25	0	2	0
30.64	1.75	0	2	0
30.68	2.00	0	2	0
30.70	2.00	0	2	0
30.74	2.00	0	2	0
30.76	2.00	0	2	0
30.78	2.00	0	2	0
30.80	2.00	0	2	0
30.82	2.00	0	2	0
30.84	2.00	0	2	0
30.87	2.00	0	2	0
30.89	2.00	0	2	0
30.91	2.00	0	2	0
30.93	2.00	0	2	0
30.95	2.00	0	2	0
30.97	2.00	0	2	0
30.99	2.00	0	2	0
31.01	2.50	10	10	0
31.05	2.25	1	5	0
31.07	2.25	1	5	0
31.09	2.00	0	15	0
31.11	2.00	0	15	0
31.13	2.00	0	15	0
31.15	2.00	0	15	0
31.17	2.00	0	15	0
31.21	2.00	0	3	0

Appendix 14 continued.

DEPTH	AVE PHI	CLAY	CEMENT	BIOTURB
31.23	2.00	0	3	0
31.25	2.00	0	3	0
31.28	2.00	0	3	0
31.30	2.00	0	3	0
31.32	2.00	0	3	0
31.34	2.00	0	3	0
31.36	2.00	0	3	0
31.38	2.00	0	3	0
31.42	1.50	0	5	0
31.44	1.50	0	5	0
31.48	2.25	10	25	0
31.50	2.00	0	2	0
31.52	2.00	0	2	0
31.54	2.00	0	2	0
31.56	2.00	0	2	0
31.58	2.00	0	2	0
31.60	2.00	0	2	0
31.62	2.00	0	2	0
31.64	2.00	0	2	0
31.66	2.00	0	2	0
31.68	2.00	0	2	0
31.70	2.00	0	2	0
31.72	2.00	0	2	0
31.74	2.00	0	2	0
31.76	2.00	0	2	0
31.78	2.00	0	2	0
31.80	2.00	0	2	0
31.82	2.00	0	2	0
31.84	2.00	0	2	0
31.86	2.00	0	2	0
31.88	2.00	0	2	0
31.91	2.00	0	2	0
31.93	2.00	0	2	0
31.95	2.00	0	2	0
31.97	2.00	0	2	0

Appendix 14 continued.

DEPTH	AVE PHI	CLAY	CEMENT	BIOTURB
31.99	2.00	0	2	0
32.01	2.00	2	3	0
32.03	2.00	2	3	0
32.05	2.00	2	3	0
32.07	2.00	2	3	0
32.09	2.00	2	3	0
32.11	2.00	2	3	0
32.13	2.00	2	3	0
32.16	2.00	2	3	0
32.18	2.00	2	3	0
32.20	2.00	2	3	0
32.22	2.00	2	3	0
32.24	2.00	2	3	0
32.26	2.00	2	3	0
32.28	2.00	2	3	0
32.32	2.00	10	5	5
32.34	2.00	10	5	5
32.36	2.00	10	5	5
32.38	2.00	10	5	5
32.40	2.00	10	5	5
32.42	2.00	10	5	5
32.44	2.00	10	5	5
32.47	2.00	10	5	5
32.49	2.00	10	5	5
32.51	2.00	10	5	5
32.53	2.00	10	5	5
32.55	2.00	10	5	5
32.57	2.00	10	5	5
32.60	2.00	10	5	5
32.62	2.00	10	5	5
32.64	2.00	10	5	5
32.66	2.00	10	5	5
32.68	2.00	10	5	5
32.70	2.00	10	5	5
32.72	2.00	10	5	5

Appendix 14 continued.

DEPTH	AVE PHI	CLAY	CEMENT	BIOTURB
32.74	2.00	10	5	5
32.76	2.00	10	5	5
32.78	2.00	10	5	5
32.80	2.00	10	5	5
32.82	2.00	10	5	5
32.84	2.00	10	5	5
32.86	2.00	10	5	5
32.88	2.00	10	5	5
32.90	2.00	10	5	5
32.92	2.00	10	5	5
32.95	2.00	10	5	5
32.97	2.00	10	5	5
32.99	2.00	10	5	5
33.01	2.00	10	5	5
33.03	2.00	10	5	10
33.05	2.00	10	5	10
33.07	2.00	10	5	10
33.09	2.00	10	5	10
33.11	2.00	10	5	10
33.14	2.00	10	5	10
33.16	2.00	10	5	10
33.18	2.00	10	5	10
33.20	2.00	10	5	10
33.22	2.00	10	5	10
33.24	2.00	10	5	10
33.26	2.00	10	5	10
33.29	2.00	10	5	10
33.31	2.00	10	5	10
33.33	2.00	10	5	10
33.35	2.00	10	5	10
33.37	2.00	10	5	10
33.39	2.00	10	5	10
33.41	2.00	10	5	10
33.43	2.00	10	5	10
33.45	2.00	10	5	10

Appendix 14 continued.

DEPTH	AVE PHI	CLAY	CEMENT	BIOTURB
33.47	2.00	8	3	5
33.49	2.00	8	3	5
33.51	2.00	8	3	0
33.54	2.00	8	3	0
33.56	2.00	8	3	0
33.58	2.00	8	3	0
33.60	2.00	8	3	0
33.62	2.00	8	3	0
33.64	2.00	8	3	0
33.66	2.00	8	3	0
33.68	2.00	8	3	0
33.71	2.00	2	4	5
33.73	2.00	2	4	5
33.75	2.00	2	4	5
33.77	2.00	2	4	5
33.79	2.00	2	4	5
33.81	2.00	2	4	5
33.83	2.00	2	4	5
33.86	2.00	2	4	5
33.88	2.00	2	4	5
33.90	2.00	2	4	5
33.92	2.00	2	4	5
33.94	2.00	2	4	5
33.96	2.00	2	4	5
33.98	2.00	2	4	5
34.00	2.00	2	4	5
34.02	2.00	2	4	5
34.04	1.75	2	3	5
34.06	1.75	2	3	5
34.08	1.75	2	3	5
34.11	1.75	2	3	5
34.13	1.75	2	3	5
34.15	2.25	2	3	5
34.17	2.25	2	3	5
34.19	2.25	2	3	5

Appendix 14 continued.

DEPTH	AVE PHI	CLAY	CEMENT	BIOTURB
34.21	2.25	2	3	5
34.23	2.25	2	3	5
34.25	2.00	2	2	
34.27	2.00	2	2	
34.29	2.00	2	2	
34.31	2.00	2	2	
34.33	2.00	2	2	
34.35	2.00	2	2	
34.37	2.00	2	2	
34.39	2.00	2	2	
34.41	2.00	2	2	
34.43	2.00	2	2	
34.45	2.00	2	2	
34.47	2.00	2	2	
34.49	2.00	2	2	
34.51	2.00	2	2	
34.53	2.00	2	2	
34.55	2.00	2	2	
34.57	2.00	2	2	
34.59	2.00	2	2	
34.61	2.00	2	2	
34.64	2.00	2	2	
34.66	2.00	3	2	
34.68	2.00	3	2	
34.70	2.00	3	2	
34.72	2.00	3	2	
34.74	2.00	3	2	
34.76	2.00	3	2	
34.78	2.00	3	2	
34.80	2.00	3	2	
34.82	2.00	3	2	
34.84	2.00	3	2	
34.86	2.00	3	2	
34.89	2.00	3	2	
34.91	2.00	3	2	

Appendix 14 continued.

DEPTH	AVE PHI	CLAY	CEMENT	BIOTURB
34.93	2.00	3	2	
34.95	2.00	3	2	
34.97	2.00	3	2	
34.99	2.00	3	2	
35.01	2.00	3	2	
35.03	2.00	3	2	
35.05	2.00	3	2	
35.07	2.00	3	2	
35.09	2.00	3	2	
35.11	2.00	3	2	
35.14	2.00	3	2	
35.16	2.00	3	2	
35.18	2.00	3	2	
35.20	2.00	3	2	
35.22	2.00	3	2	
35.24	2.00	3	2	
35.27	2.00	3	2	
35.29	2.00	3	2	
35.31	2.00	3	2	
35.33	2.00	3	2	
35.35	2.00	3	2	
35.37	2.00	3	2	
35.39	2.00	3	2	
35.41	2.00	3	2	
35.43	2.00	3	2	
35.45	2.00	3	2	
35.47	2.00	3	2	
35.49	2.00	3	2	
35.52	2.00	3	2	
35.54	2.00	3	2	
35.56	2.00	3	2	
35.58	2.00	3	2	
35.60	2.00	3	2	
35.62	2.00	3	2	
35.64	2.00	3	2	

Appendix 14 continued.

DEPTH	AVE PHI	CLAY	CEMENT	BIOTURB
35.66	2.00	3	2	
35.68	2.00	3	2	
35.70	2.00	3	2	
35.72	2.00	3	2	
35.74	2.00	3	2	
35.76	2.00	3	2	
35.79	2.00	3	2	
35.81	2.00	3	2	
35.83	2.00	3	2	
35.85	2.00	3	2	
35.87	2.00	3	2	
35.89	2.00	3	2	
35.91	2.00	3	2	
35.93	2.00	3	2	
35.95	2.00	3	2	
35.97	2.00	3	2	
35.99	2.00	3	2	
36.01	2.00	3	2	
36.04	2.00	3	2	
36.06	2.00	3	2	
36.08	2.00	3	2	
36.10	2.00	3	2	
36.12	2.00	3	2	
36.14	2.00	3	2	
36.16	2.00	3	2	
36.18	2.00	3	2	
36.20	2.00	3	2	
36.22	2.00	3	2	
36.24	2.00	3	2	
36.26	2.00	3	2	
36.28	2.00	3	2	
36.31	2.00	3	2	
36.33	2.00	3	2	
36.35	2.00	3	2	
36.37	2.00	3	2	

Appendix 14 continued.

DEPTH	AVE PHI	CLAY	CEMENT	BIOTURB
36.39	2.00	3	2	
36.41	2.00	3	2	
36.43				
36.45	2.00	1	2	
36.47	2.00	1	2	
36.49	2.00	1	2	
36.51	2.00	1	2	
36.53	2.00	1	2	
36.55	2.00	1	2	
36.57	2.00	1	2	
36.60	2.00	1	2	
36.62	2.00	1	2	
36.64	2.00	1	2	
36.66	2.00	1	2	
36.68	2.00	1	2	
36.70	2.00	1	2	
36.72	2.00	1	2	
36.74	2.00	1	2	
36.76	2.00	1	2	
36.78	2.00	1	2	
36.81	2.00	1	2	
36.83	2.00	1	2	
36.85	2.00	1	2	
36.87	2.00	1	2	
36.89	2.00	1	2	
36.91	2.00	1	2	
36.93	2.00	1	2	
36.95	2.00	1	2	
36.97	2.00	1	2	
37.00	2.00	1	2	
37.02	2.00	1	2	
37.04	2.00	1	2	
37.06	2.00	1	2	
37.08	2.00	1	2	
37.10	2.00	1	2	

Appendix 14 continued.

DEPTH	AVE PHI	CLAY	CEMENT	BIOTURB
37.12	2.00	1	2	
37.14	2.00	1	2	
37.16	2.00	1	2	
37.18	2.00	1	2	
37.20	2.00	1	2	
37.22	2.00	1	2	
37.24	2.00	1	2	
37.26	2.00	1	2	
37.28	2.00	1	2	
37.30	2.00	1	2	
37.32	2.00	1	2	
37.35	2.00	1	2	
37.37	2.00	1	2	
37.39	2.00	1	2	
37.41	2.00	1	2	
37.43	2.00	1	2	
37.45	2.00	1	2	
37.47	2.00	1	2	
37.49	2.00	1	2	
37.51	2.00	1	2	
37.53	2.00	1	2	
37.55	2.00	1	2	
37.57	2.00	1	2	
37.59	2.00	1	2	
37.62	2.00	1	2	
37.64	2.00	1	2	
37.66	2.00	1	2	
37.68	2.00	1	2	
37.70	2.00	1	2	
37.72	2.00	1	2	
37.74	2.00	1	2	
37.76	2.00	1	2	
37.78	2.00	1	2	
37.80	2.00	1	2	
37.82	2.00	1	2	

Appendix 14 continued.

DEPTH	AVE PHI	CLAY	CEMENT	BIOTURB
37.84	2.00	1	2	
37.87	2.00	1	2	
37.89	2.00	1	2	
37.91	2.00	1	2	
37.93	2.00	1	2	
37.95	2.00	1	2	
37.97	2.00	1	2	
37.99	2.00	1	2	
38.01	2.00	1	2	
38.03	2.00	1	2	
38.05	2.00	1	2	
38.07	2.00	1	2	
38.09	2.00	1	2	
38.11	2.00	1	2	
38.14	2.00	1	2	
38.16	2.00	1	2	
38.18	2.00	1	2	
38.20	2.00	1	2	
38.22	2.00	1	2	
38.24	2.00	1	2	
38.26	2.00	1	2	
38.28	2.00	1	2	
38.30	2.00	1	2	
38.32	2.00	1	2	
38.34	2.00	1	2	
38.36	2.00	1	2	
38.39	2.00	1	2	
38.41	2.00	1	2	
38.43	2.00	1	2	
38.45	2.00	1	2	
38.47	2.00	1	2	
38.49	2.00	1	2	
38.51	2.00	1	2	
38.53	2.00	1	2	
38.55	2.00	1	2	

Appendix 14 continued.

DEPTH	AVE PHI	CLAY	CEMENT	BIOTURB
38.57	2.00	1	2	
38.59	2.00	1	2	
38.61	2.00	1	2	
38.63	2.00	1	2	
38.66	2.00	1	2	
38.68	2.00	1	2	
38.70	2.00	1	2	
38.72	2.00	1	2	
38.74	2.00	1	2	
38.76	2.00	1	2	
38.78	2.00	1	2	
38.80	2.00	1	2	
38.82	2.00	1	2	
38.84	2.00	1	2	
38.86	2.00	1	2	
38.88	2.00	1	2	
38.91	2.00	1	2	
38.93	2.00	1	2	
38.95	2.00	1	2	
38.97	2.00	1	2	
38.99	2.00	1	2	
39.01	2.00	1	2	
39.03	2.00	1	2	
39.05	2.00	1	2	
39.07	2.00	1	2	
39.09	2.00	1	2	
39.11	2.00	1	2	
39.13	2.00	1	2	
39.15	2.00	1	2	
39.18	2.00	1	2	
39.20	2.00	1	2	
39.22	2.00	1	2	
39.24	2.00	1	2	
39.26	2.00	1	2	
39.28	2.00	1	2	

Appendix 14 continued.

DEPTH	AVE PHI	CLAY	CEMENT	BIOTURB
39.30	2.00	1	2	
39.32	2.00	1	2	
39.34	2.00	1	2	
39.36	2.00	1	2	
39.38	2.00	1	2	
39.40	2.00	1	2	
39.42	2.00	1	2	
39.45	2.00	1	2	
39.47	2.00	1	2	
39.49	2.00	1	2	
39.51	2.00	1	2	
39.53	2.00	1	2	
39.55	2.00	1	2	
39.57	2.00	1	2	
39.59	2.00	1	2	
39.61	2.00	1	2	
39.63	2.00	1	2	
39.65	2.00	1	2	
39.67	2.00	1	2	
39.70	2.00	1	2	
39.72	2.00	1	2	
39.74	2.00	1	2	
39.76	2.00	1	2	
39.78	2.00	1	2	
39.80	2.00	1	2	
39.82	2.00	1	2	
39.84	2.00	1	2	
39.86	2.00	1	2	
39.88	2.00	1	2	
39.90	2.00	1	2	
39.92	2.00	1	2	
39.94	2.00	1	2	
39.97	2.00	1	2	
39.99	2.00	1	2	
40.01	1.75	12	2	

Appendix 14 continued.

DEPTH	AVE PHI	CLAY	CEMENT	BIOTURB
40.03	2.00	10	2	
40.05	2.00	10	2	
40.07	2.00	10	2	
40.09	2.00	10	2	
40.11	2.00	10	2	
40.13	2.00	10	2	
40.15	2.00	10	2	
40.17	2.00	10	2	
40.19	2.00	10	2	
40.21	2.00	10	2	
40.24	2.00	10	2	
40.26	2.00	10	2	
40.28	2.00	10	2	
40.30	2.00	10	2	
40.32	2.00	10	2	
40.34	2.00	10	2	
40.36	2.00	10	2	
40.38	2.00	10	2	
40.40	2.00	10	2	
40.42	2.00	10	2	
40.44	2.00	10	2	
40.46	2.00	10	2	
40.49	2.00	10	2	
40.51	2.00	10	2	
40.53	2.00	10	2	
40.55	2.00	10	2	
40.57	2.00	10	2	
40.59	2.00	10	2	
40.61	2.00	10	2	
40.63	2.00	10	2	
40.65	2.00	10	2	
40.67	2.00	10	2	
40.69	2.00	10	2	
40.71	2.00	10	2	
40.73	2.00	10	2	

Appendix 14 continued.

DEPTH	AVE PHI	CLAY	CEMENT	BIOTURB
40.76	2.00	10	2	
40.78	2.00	10	2	
40.80	2.00	10	2	
40.82	2.00	10	2	
40.83	2.00	10	2	
40.85	2.00	10	2	
40.88	2.00	10	2	
40.90	2.00	10	2	
40.92	2.00	10	2	
40.94	2.00	10	2	
40.96	2.00	10	2	
40.98	2.00	10	2	
41.01	2.00	10	2	
41.03	2.00	10	2	
41.05	2.00	10	2	
41.07	2.00	10	2	
41.09	2.00	10	2	
41.11	2.00	10	2	
41.13	2.00	10	2	
41.15	2.00	10	2	
41.17	2.00	7	2	10
41.19	2.00	7	2	10
41.21	2.00	7	2	10
41.23	2.00	7	2	10
41.26	2.00	15	2	25
41.28	2.00	15	2	25
41.30	2.00	15	2	25
41.32	2.00	15	2	25
41.34	2.00	15	2	25
41.36	2.00	7	2	10
41.38	2.00	7	2	10
41.40	2.00	7	2	10
41.42	2.00	7	2	10
41.44	2.00	7	2	10
41.46	2.00	7	2	10

Appendix 14 continued.

DEPTH	AVE PHI	CLAY	CEMENT	BIOTURB
41.48	2.00	7	2	10
41.50	2.00	7	2	10
41.53	2.00	20	20	70
41.55	2.00	20	20	70
41.57	2.00	20	20	70
41.59	2.00	20	20	70
41.61	2.00	20	20	70
41.63	2.00	20	20	70
41.65	2.00	20	20	70
41.67	2.00	20	20	70
41.69	2.00	20	20	70
41.71	2.00	20	20	70
41.73	2.00	20	20	70
41.75	2.00	20	20	70
41.78	2.00	20	20	70
41.80	2.00	20	20	70
41.82	2.00	20	20	70
41.84	2.00	20	20	70
41.86	2.00	20	20	70
41.88	2.00	20	20	70
41.90	2.00	20	20	70
41.92	2.00	3	2	5
41.94	2.00	3	2	5
41.96	2.00	3	2	0
41.98	2.00	3	2	0
42.00	2.00	3	2	0
42.02	2.00	3	2	0
42.05	2.00	3	2	0
42.07	2.00	3	2	0
42.09	2.00	3	2	0
42.11	2.00	3	2	0
42.13	2.00	3	2	0
42.15	2.00	3	2	0
42.17	2.00	3	2	0
42.19	2.00	3	2	0

Appendix 14 continued.

DEPTH	AVE PHI	CLAY	CEMENT	BIOTURB
42.21	2.00	3	2	0
42.23	2.00	3	2	0
42.25	2.00	3	2	0
42.27	2.00	3	2	0
42.30	2.00	3	2	0
42.32	2.00	3	2	0
42.34	2.00	3	2	0
42.36	2.00	3	2	0
42.38	2.00	3	2	0
42.40	2.00	3	2	0
42.42	2.00	3	2	0
42.44	2.00	3	2	0
42.46	2.00	3	2	0
42.48	2.00	3	2	0
42.50	2.00	3	2	0
42.52	2.00	3	2	5
42.54	2.00	3	2	5
42.56	2.00	3	2	5
42.59	2.00	3	2	5
42.61	2.00	3	2	10
42.63	2.00	3	2	10
42.65	4.00	100	2	30
42.67	2.00	20	10	30
42.69	4.00	100	2	30
42.71	2.00	10	5	10
42.73	2.00	10	5	10
42.75	2.00	10	5	10
42.77	2.00	10	5	10
42.79	2.00	10	5	10
42.81	2.00	10	5	10
42.83	2.00	10	5	10
42.86	2.00	10	5	10
42.88	2.00	10	5	10
42.90	2.00	10	5	10
42.92	2.00	10	5	10

Appendix 14 continued.

DEPTH	AVE PHI	CLAY	CEMENT	BIOTURB
42.94	2.00	10	5	10
42.96	2.00	10	5	10
42.98	2.00	10	5	10
43.00	2.00	10	5	10
43.02	2.00	2	5	5
43.04	2.00	2	5	5
43.06	2.00	2	5	5
43.08	2.00	2	5	5
43.11	2.00	2	5	5
43.13	2.00	2	5	5
43.15	2.00	2	5	5
43.17	2.00	2	5	5
43.19	2.00	2	5	5
43.21	2.00	2	5	5
43.23	2.00	2	5	5
43.25	2.00	2	5	5
43.27	2.00	2	5	5
43.29	2.00	2	5	5
43.31	2.00	2	5	5
43.33	2.00	2	5	5
43.35	2.00	2	5	5
43.38	2.00	2	5	5
43.40	2.00	2	5	5
43.42	2.00	2	5	5
43.44	2.00	2	5	5
43.46	2.00	2	5	5
43.48	2.00	2	5	5
43.50	2.00	2	5	5
43.52	2.00	2	5	5
43.54	2.00	2	5	5
43.56	2.00	2	5	5
43.58	2.00	2	5	5
43.60	2.00	2	5	5
43.62	2.00	2	5	5
43.65	2.00	2	5	5

Appendix 14 continued.

DEPTH	AVE PHI	CLAY	CEMENT	BIOTURB
43.67	2.00	2	5	5
43.69	2.00	2	5	5
43.71	2.00	2	5	5
43.73	2.00	2	5	5
43.75	2.00	2	5	5
43.77	2.00	2	5	5
43.79	2.00	2	5	5
43.81	2.00	2	5	5
43.83	2.00	2	5	5
43.85	2.00	2	5	5
43.87	2.00	2	5	5
43.90	2.00	2	5	5
43.92	2.00	2	5	5
43.94	2.00	2	5	5
43.96	2.00	2	5	5
43.98	2.00	2	5	5
44.00	2.00	2	5	5
44.02	2.00	2	5	5
44.04	2.00	2	5	5
44.06	2.00	2	5	5
44.08	2.00	2	5	5
44.10	2.00	2	5	5
44.12	2.00	2	5	5
44.14	2.00	2	5	5
44.17	2.00	2	5	5
44.19	2.00	2	5	5
44.21	2.00	15	10	50
44.23	2.00	15	10	50
44.25	2.00	15	10	50
44.27	2.00	15	10	50
44.29	2.00	15	10	50
44.31	2.00	15	10	50
44.33	2.00	15	10	50
44.35	2.00	15	10	50
44.37	2.00	15	10	50

Appendix 14 continued.

DEPTH	AVE PHI	CLAY	CEMENT	BIOTURB
44.39	2.00	15	10	50
44.42	2.00	15	10	50
44.44	2.00	15	10	50
44.46	2.00	15	10	50
44.48	2.00	15	10	50
44.50	2.00	15	10	50
44.52	2.00	15	10	50
44.54	2.00	15	10	50
44.56	2.00	15	10	50
44.58	2.00	15	10	50
44.60	2.00	15	10	50
44.62	2.00	15	10	50
44.64	2.00	15	10	50
44.66	2.00	15	10	50
44.69	2.00	15	10	50
44.71	2.00	15	10	50
44.73	2.00	15	10	50
44.75	2.00	15	10	50
44.77	2.00	15	10	50
44.79	2.00	15	10	50
44.81	2.00	15	10	50
44.83	2.00	15	10	50
44.85	2.00	15	10	50
44.87	2.00	2	2	5
44.89	2.00	2	2	5
44.91	2.00	2	2	5
44.94	2.00	2	2	5
44.96	2.00	2	2	5
44.98	2.00	2	2	5
45.00	2.00	2	2	5
45.02	2.00	2	2	5
45.04	2.00	2	2	5
45.06	2.00	2	2	5
45.08	2.00	2	2	5
45.10	2.00	2	2	5

Appendix 14 continued.

DEPTH	AVE PHI	CLAY	CEMENT	BIOTURB
45.12	2.00	2	2	5
45.14	2.00	2	2	5
45.16	2.00	2	2	5
45.18	2.00	2	2	5
45.21	2.00	2	2	5
45.23	2.00	2	2	5
45.25	2.00	2	2	5
45.27	2.00	2	2	5
45.29	2.00	2	2	5
45.31	2.00	2	2	5
45.33	2.00	2	2	5
45.35	2.00	2	2	5
45.37	2.00	2	2	5
45.39	2.00	2	2	5
45.41	2.00	2	2	5
45.43	2.00	2	2	5
45.45	2.00	2	2	5
45.48	2.00	2	2	5
45.50	2.00	2	2	5
45.52	2.00	2	2	5
45.54	2.00	2	2	5
45.56	2.00	2	2	5
45.58	2.00	2	2	5
45.60	2.00	2	2	5
45.62	2.00	2	2	5
45.64	2.00	2	2	5
45.66	2.00	2	2	5
45.68	2.00	2	2	5
45.70	2.00	2	2	5
45.73	2.00	2	2	5
45.75	2.00	2	2	5
45.77	2.00	2	2	5
45.79	2.00	2	2	5
45.81	2.00	2	2	5
45.83	2.00	2	2	5

Appendix 14 continued.

DEPTH	AVE PHI	CLAY	CEMENT	BIOTURB
45.85	2.00	2	2	5
45.87	2.00	2	2	5
45.89	2.00	2	2	5
45.91	2.00	2	2	5
45.93	2.00	2	2	5
45.95	2.00	2	2	5
45.97	2.00	2	2	5
46.00	2.00	2	2	5
46.02	2.00	25	5	75
46.04	2.00	25	5	75
46.06	2.00	25	5	75
46.08	2.00	25	5	75
46.10	2.00	25	5	75
46.12	2.00	25	5	75
46.14	2.00	25	5	75
46.16	2.00	25	5	75
46.18	2.00	25	5	75
46.20	2.00	25	5	75
46.22	2.00	25	5	75
46.25	2.00	25	5	75
46.27	2.00	50	5	75
46.29	2.00	50	5	75
46.31	2.00	50	5	75
46.33	2.00	50	5	75
46.35	2.00	50	5	75
46.37	2.00	50	5	75
46.39	2.00	50	5	75
46.41	2.00	50	5	75
46.43	2.00	50	5	75
46.45	2.00	50	5	75
46.47	2.00	50	5	75
46.49	2.00	50	5	75
46.52	2.00	10	30	70
46.54	2.00	10	30	70
46.56	2.00	10	30	70

Appendix 14 continued.

DEPTH	AVE PHI	CLAY	CEMENT	BIOTURB
46.58	2.00	10	30	70
46.60	2.00	10	30	70
46.62	2.00	10	30	70
46.64	2.00	50	5	80
46.66	2.00	50	5	80
46.68	2.00	50	5	80
46.70	2.00	50	5	80
46.72	2.00	50	5	80
46.74	2.00	50	5	80
46.77	2.00	50	5	80
46.79	2.00	50	5	80
46.81	2.00	50	5	80
46.83	2.00	50	5	80
46.85	2.00	50	5	80
46.87	2.00	50	5	80
46.89	2.00	50	5	80
46.91	2.00	50	5	80
46.93	2.00	50	5	80
46.95	2.00	50	5	80
46.97	2.00	50	5	80
46.99	2.00	50	5	80
47.01	2.00	50	5	80
47.04	2.00	50	5	80
47.06	2.00	50	5	80
47.08	2.00	50	5	80
47.10	2.00	50	5	80
47.12	2.00	30	20	70
47.14	2.00	30	20	70
47.16	2.00	30	20	70
47.18	2.00	30	20	70
47.20	2.00	30	20	70
47.22	2.00	30	20	70
47.24	2.00	30	20	70
47.26	2.00	30	20	70
47.29	2.00	30	20	70

Appendix 14 continued.

DEPTH	AVE PHI	CLAY	CEMENT	BIOTURB
47.31	2.00	30	20	70
47.33	2.00	30	20	70
47.35	2.00	30	20	70
47.37	2.00	10	15	10
47.39	2.00	10	15	10
47.41	2.00	10	15	10
47.43	2.00	10	15	10
47.45	2.00	10	15	10
47.47	2.00	10	15	10
47.49	2.00	10	15	10
47.51	2.00	10	15	10
47.53	2.00	10	15	10
47.56	2.00	10	15	10
47.58	2.00	10	15	10
47.60	2.00	10	15	10
47.62	2.00	15-100	0-30	5
47.64	2.00	15-100	0-30	5
47.66	2.00	5	10	0
47.68	2.00	5	10	0
47.70	2.00	5	10	0
47.72	2.00	5	10	0
47.74	2.00	5	10	0
47.76	2.00	5	10	0
47.78	2.00	5	10	0
47.81	2.00	5	10	0
47.83	2.00	5	10	0
47.85	2.00	5	10	0
47.87	2.00	5	10	0
47.89	2.00	5	10	0
47.91	2.00	5	10	0
47.93	2.00	5	10	0
47.95	2.00	5	10	0
47.97	2.00	5	10	0
47.99	2.00	5	10	0
48.01	2.00	4	10	0

Appendix 14 continued.

DEPTH	AVE PHI	CLAY	CEMENT	BIOTURB
48.03	2.50	75	5	60
48.05	2.50	75	5	60
48.08	2.50	75	5	60
48.10	2.50	75	5	60
48.12	2.50	75	5	60
48.14	2.50	75	5	60
48.16	2.50	75	5	60
48.18	2.50	75	5	60
48.20	2.50	75	5	60
48.22	2.50	75	5	60
48.24	2.50	75	5	60
48.26	2.50	75	5	60
48.28	2.50	75	5	60
48.30	2.50	75	5	60
48.33	2.50	75	5	60
48.35	2.50	75	5	60
48.37	2.50	75	5	60
48.39	2.50	75	5	60
48.41	2.50	75	5	60
48.43	2.50	75	5	60
48.45	2.50	75	5	60
48.47	2.50	75	5	60
48.49	2.50	75	5	60
48.51	1.75	15	5	80
48.53	1.75	15	5	80
48.55	1.75	15	5	80
48.57	1.75	15	5	80
48.60	1.75	15	5	80
48.62	1.75	15	5	80
48.64	1.75	15	5	80
48.66	1.75	15	5	80
48.68	1.75	15	5	80
48.70	1.75	15	5	80
48.72	1.75	15	5	80
48.74	1.75	15	5	80

Appendix 14 continued.

DEPTH	AVE PHI	CLAY	CEMENT	BIOTURB
48.76	1.75	15	5	80
48.78	1.75	15	5	80
48.80	1.75	15	5	80
48.82	1.75	15	5	80
48.84	1.75	15	5	80
48.87	1.75	15	5	80
48.89	1.75	15	5	80
48.91	1.75	15	5	80
48.93	1.75	15	5	80
48.95	1.75	15	5	80
48.97	1.75	15	5	80
48.99	1.75	15	5	80
49.01	1.75	15	5	80
49.03	1.75	15	5	80
49.05	1.75	15	5	80
49.07	1.75	15	5	80
49.09	1.75	15	5	80
49.12	1.75	15	5	80
49.14	1.75	15	5	80
49.16	1.75	15	5	80
49.18	1.75	15	5	80
49.20	1.75	15	5	80
49.22	1.75	10	20	75
49.24	1.75	10	20	75
49.26	1.75	10	20	75
49.28	1.75	10	20	75
49.30	1.75	10	20	75
49.32	1.75	10	20	75
49.34	1.75	10	20	75
49.37	1.75	10	20	75
49.39	1.75	10	20	75
49.41	1.75	10	20	75
49.43	1.75	10	20	75
49.45	1.75	10	20	75
49.47	1.75	10	20	75

Appendix 14 continued.

DEPTH	AVE PHI	CLAY	CEMENT	BIOTURB
49.49	1.75	10	20	75
49.51	1.75	10	20	75
49.53	1.75	10	20	75
49.55	1.75	10	20	75
49.57	1.75	10	20	75
49.59	1.75	10	20	75
49.61	1.75	10	20	75
49.64	1.75	10	20	75
49.66	2.00	50	10	80
49.68	2.00	50	10	80
49.70	2.00	50	10	80
49.72	2.00	50	10	80
49.74	2.00	50	10	80
49.76	2.00	50	10	80
49.78	2.00	50	10	80
49.80	2.00	50	10	80
49.82	2.00	50	10	80
49.84	2.00	50	10	80
49.86	1.75	15	5	25
49.89	1.75	15	5	25
49.91	1.75	15	5	25
49.93	1.75	15	5	25
49.95	1.75	15	5	25
49.97	1.75	15	5	25
49.99	1.75	15	5	25
50.01	1.75	17	5	50
50.03	1.75	15	5	45
50.05	1.75	15	5	45
50.07	1.75	15	5	45
50.09	1.75	15	5	45
50.11	1.75	15	5	45
50.13	1.75	15	5	45
50.16	1.75	5	8	40
50.18	1.75	5	8	40
50.20	1.75	5	8	40

Appendix 14 continued.

DEPTH	AVE PHI	CLAY	CEMENT	BIOTURB
50.22	1.75	5	8	40
50.24	1.75	5	8	40
50.26	1.75	5	8	40
50.28	1.75	5	8	40
50.30	1.75	5	8	40
50.32	1.75	5	8	40
50.34	1.75	5	8	40
50.36	1.75	5	8	40
50.38	1.75	5	8	40
50.41	1.75	5	8	40
50.43	1.75	5	8	40
50.45	1.75	5	8	40
50.47	1.75	5	8	40
50.49	1.75	5	8	40
50.51	1.75	5	8	40
50.53	1.75	5	8	40
50.55	1.75	5	8	40
50.57	1.75	5	8	40
50.59	1.75	5	8	40
50.61	1.75	5	8	40
50.63	1.75	5	8	40
50.65	1.75	5	8	40
50.68	1.75	5	8	40
50.70	2.00	2	15	50
50.72	2.00	2	15	50
50.74	2.00	2	15	50
50.76	2.00	2	15	50
50.78	2.00	2	15	50
50.80	2.00	2	15	50
50.82	2.00	2	15	50
50.84	2.00	2	15	50
50.86	2.00	2	15	50
50.88	2.00	2	15	50
50.90	2.00	2	15	50
50.93	1.75	2	10	50

Appendix 14 continued.

DEPTH	AVE PHI	CLAY	CEMENT	BIOTURB
50.95	1.75	2	10	50
50.97	1.75	2	10	50
50.99	1.75	10	15	50
51.01	1.75	10	15	50
51.03	1.75	5	30	50
51.05	1.75	5	30	50
51.07	1.75	5	30	50
51.09	1.75	5	30	50
51.11	1.75	5	30	50
51.13	1.75	5	30	50
51.15	1.75	5	30	50
51.17	1.75	5	30	50
51.20	1.75	5	30	50
51.22	1.75	5	30	50
51.24	1.75	5	30	50
51.26	1.75	5	30	50
51.28	2.00	15	15	50
51.30	2.00	15	15	50
51.32	2.00	15	15	50
51.34	2.00	2	35	30
51.36	2.00	2	35	30
51.38	2.00	2	35	15
51.40	2.00	2	35	15
51.42	2.00	2	35	15
51.45	2.00	2	35	15
51.47	2.25	40	10	20
51.49	2.25	40	10	20
51.51	2.25	40	10	20
51.53	2.25	40	10	20
51.55	2.25	40	10	20
51.57	2.25	40	10	20
51.59	2.25	40	10	20
51.61	1.75	15	15	20
51.63	1.75	15	15	20
51.65	1.75	15	15	20

Appendix 14 continued.

DEPTH	AVE PHI	CLAY	CEMENT	BIOTURB
51.67	1.75	15	15	20
51.69	1.75	15	15	20
51.71	1.75	15	15	20
51.74	1.75	15	15	20
51.76	2.00	2	35	20
51.78	2.00	2	35	20
51.80	2.00	2	35	20
51.82	2.00	2	35	20
51.84	2.00	2	35	20
51.86	2.00	2	35	20
51.88	2.00	2	35	20
51.90	2.00	2	35	20
51.92				20
51.94				20
51.96				20
51.99				20
52.01	2.25	13	15	50
52.03	2.25	13	15	50
52.05	2.25	13	15	50
52.07	2.25	13	15	50
52.09	2.25	13	15	50
52.11	2.25	13	15	50
52.13	2.25	13	15	50
52.15	2.25	13	15	50
52.17	2.25	13	15	70
52.19	2.25	13	15	70
52.21	2.25	45	15	70
52.23	2.25	45	15	80
52.26	2.25	45	15	80
52.28	2.25	45	15	80
52.30	2.25	45	15	80
52.32	2.25	45	15	80
52.34	2.25	45	15	80
52.36	2.25	45	15	80
52.38	2.25	45	15	80

Appendix 14 continued.

DEPTH	AVE PHI	CLAY	CEMENT	BIOTURB
52.40	2.25	45	15	80
52.42	2.25	45	15	80
52.44	2.25	45	15	80
52.46	2.25	45	15	80
52.48	2.25	45	15	80
52.51	2.25	45	15	80
52.53	2.25	45	15	80
52.55	2.25	45	15	80
52.57	2.25	45	15	80
52.59	2.25	45	15	80
52.61	2.25	45	15	80
52.63	2.25	45	15	80
52.65	2.25	45	15	80
52.67	2.25	45	15	80
52.69	2.25	45	15	80

Appendix 15. Permeability data for subsurface Tocito Sandstone reservoir core. Measurements for the Solar Petr. Navajo Tribal F-151, Pan American Martin Gas Unit C#1, Angel Peak B-37, and Newsom A-3E were made with mechanical field permeameter. Measurements for Pan American Navajo Tribal E-8, H-2, and Gallegos Canyon Unit #250 were conducted by Core Laboratories, Inc., Dallas, TX.

FIELD: HORSESHOE GALLUP

WELL: Solar Petroleum Navajo Tribal F-151

Depth (ft)	'X-axis	Perm. (md)	Ave. Perm. (md)	Porosity (%)
917.040	0.0	4.2296529	2.974405375	
	0.5	2.3968033		
	1.0	2.5680036		
	1.5	2.7031617		
917.250	0.0	2.4794517	2.465085439	
	0.5	2.4507192		
917.420	0.0	7.3367580	5.959599638	
	0.5	6.2251280		
	1.0	6.5586170		
	1.5	3.7178956		
917.830	0.0	2.7031617	3.076454052	
	0.5	3.1815973		
	1.0	2.7031617		
	1.5	3.7178956		
917.920	0.0	3.5952050	3.318695825	
	0.5	4.4004957		
	1.0	3.1262652		
	1.5	2.1528174		
918.080	0.0	4.3353570	2.536516810	
	0.5	1.6590701		
	1.0	1.6721884		
	1.5	2.4794517		
918.170	0.0	2.0781532	1.883021425	
	0.5	1.6878897		
919.500		0.7521349	0.752134900	2.3

Appendix 15 continued.

Depth (ft)	'X-axis	Perm. (md)	Ave. Perm. (md)	Porosity (%)
921.500	0.0	22.1308148	24.512879945	
	0.5	17.6784615		
	1.0	53.3510714		
	1.5	4.8911720		
921.580	1.5	24.2899187	24.289918699	
921.670	1.5	66.3924444	66.392444444	
BURROW	A	27.9220561		
921.400 to 921.700	B	11.2830445		
	C	1.5631326		
	D	34.1057078		
	E	45.4051672		
	F	0.4456682		
922.000	0.0	28.1854717	33.268784563	
	0.5	7.1700135		
	1.0	14.7290975		
	1.5	82.9905556		
922.080	0.0	15.0070050	6.489877139	
	0.5	5.4469870		
	1.0	3.7795420		
	1.5	1.7259746		
922.170	0.0	16.5981111	7.354483620	
	0.5	3.2570759		
	1.0	7.4479210		
	1.5	2.1148265		
922.250	0.0	38.3033333	47.547091141	
	0.5	40.7038147		
	1.0	52.5996479		
	1.5	58.5815686		
922.380	0.0	51.5113793	19.810307709	

Appendix 15 continued.

Depth (ft)	'X-axis	Perm. (md)	Ave. Perm. (md)	Porosity (%)
	0.5	21.1890780		
	1.0	4.4465200		
	1.5	2.0942535		
922.420	0.0	16.6744500	5.659429039	
	0.5	1.7259746		
	1.0	2.4242785		
	1.5	1.8130131		
922.460	0.5	7.7814100	5.891639000	
	1.0	2.8902380		
	1.5	7.0032690		
922.850	0.0	34.3409195	48.131204259	
	0.5	27.0621377		
	1.0	82.9905556		
922.920	0.0	22.1308148	27.751866688	
	0.5	15.9256930		
	1.0	45.1990923		
923.000	0.0	2.4789349	11.255427072	
	0.5	15.5628200		
	1.0	15.7245263		
923.080	0.0	19.1516667	17.444175169	
	0.5	16.6744500		
	1.0	16.5064088		
923.830	0.0	74.6915000	119.990511574	
	0.5	77.8036458		
	1.0	207.4763889		
923.920	0.0	39.8354667	33.847861166	
	0.5	40.3737838		
	1.0	21.3343330		
924.000	0.0	53.5422939	46.301336064	

Appendix 15 continued.

Depth (ft)	'X-axis	Perm. (md)	Ave. Perm. (md)	Porosity (%)
	0.5	42.6808571		
	1.0	42.6808571		
924.040	0.0	4.2797755	3.370832508	
	0.5	2.1148265		
	1.0	3.7178956		
924.080	0.0	32.9763797	22.159945060	
	0.5	31.4490526		
	1.0	2.0544029		
924.500	1.5	18.5109046	18.510904585	17.3
924.540	1.5	13.4507230	13.450723000	
927.000	0.0	179.9795181	233.928517971	
	0.5	121.4495935		
	1.0	207.4763889		
	1.5	426.8085714		
927.080	0.0	271.6054545	275.146795506	
	0.5	248.9716667		
	1.0	304.8632653		
927.170	0.0	96.3761290	231.032088301	
	0.5	129.8982609		
	1.0	466.8218750		
931.208	0.0	173.7011628	80.056648708	
	0.5	49.7943333		
	1.0	16.6744500		
931.250	0.0	1.2762531	10.652413702	
	0.5	14.0065380		
	1.0	16.6744500		
931.290	0.0	2.8346565	7.329916777	
	0.5	2.4455860		
	1.0	16.7095078		

Appendix 15 continued.

Depth (ft)	'X-axis	Perm. (md)	Ave. Perm. (md)	Porosity (%)
931.330	0.0	14.0065380	10.490081767	
	0.5	5.2357773		
	1.0	12.2279300		
940.040	0.0	133.3776786	140.005235060	
	0.5	104.4636364		
	1.0	182.1743902		
940.080	0.0	107.4697842	144.192008152	
	0.5	262.0754386		
	1.0	63.0308017		
940.125	0.0	18.8614899	14.170552458	
	0.5	18.9813215		
	1.0	4.6688460		
940.170	0.0	4.8355905	7.156938906	
	0.5	0.7095333		
	1.0	15.9256930		
942.500	1.5	80.3134409	80.313440860	9.7
942.542	1.5	109.8404412	97.358572861	
	2.5	84.8767045		
943.830	0.0	1.6855157	2.096714549	
	0.5	2.8761640		
	1.0	1.7284639		
943.875	0.0	2.0346378	2.432569320	
	0.5	1.7827168		
	1.0	3.4803533		
943.920	0.0	50.6383051	58.732998024	
	0.5	59.7532000		
	1.0	65.8074890		
943.958	0.0	15.7245263	7.835312105	
	0.5	2.0565155		

Appendix 15 continued.

Depth (ft)	'X-axis	Perm. (md)	Ave. Perm. (md)	Porosity (%)
	1.0	5.7248945		
944.500	1.5	15.7245263	15.724526316	6.6
944.520	1.5	17.8261337	17.826133652	
944.708	1.5	0.8019641	0.801964087	1.0
944.710	1.5	1.4980021	1.498002083	1.0
944.458	1.5	0.8425603	0.842560347	

Appendix 15 continued.

FIELD: CHA CHA GALLUP

WELL: Pan American Navajo Tribal E-8

Depth (ft)	Perm. (md)	Porosity (%)
4834.5	0.12	5.0
4835.5	1.40	10.5
4836.5	167.00	16.9
4837.5	97.00	17.0
4838.5	43.00	15.3
4839.5	26.00	15.4
4840.5	14.00	17.0
4841.5	66.00	13.7
4842.5	3.10	9.9
4843.5	2.10	14.2
4844.5	35.00	16.5
4845.5	4.60	14.1
4846.6	0.03	7.1
4847.5	0.03	2.5

Appendix 15 continued.

FIELD: TOTAH GALLUP

WELL: Pan American Navajo Tribal H-2

Depth (ft)	Perm. (md)	Porosity (%)
5123.5	0.12	4.2
5124.5	0.34	5.6
5125.5	0.14	6.5
5126.5	247.00	15.4
5127.5	277.00	17.3
5128.5	303.00	16.7
5129.5	561.00	12.6
5130.5	81.00	15.2
5131.5	21.00	12.1
5132.5	229.00	16.4
5133.5	94.00	14.7
5134.5	0.06	5.0
5135.5	0.11	6.8
5136.5	0.05	7.0

Appendix 15 continued.

FIELD: GALLEGOS GALLUP

WELL: Pan American Gallegos Canyon #250

Depth (ft)	Perm. (md)	Porosity (%)
5585.5	0.05	4.1
5586.5	0.05	4.6
5587.5	0.10	5.0
5588.5	0.05	5.0
5589.5	0.50	4.5
5590.5	0.30	4.3
5591.5	0.05	5.3
5592.5	0.10	5.4
5593.5	0.60	5.4
5594.5	0.05	5.3
5595.5	0.05	5.0
5596.5	0.05	4.8
5597.5	0.30	4.9
5598.5	0.05	5.2
5599.5	0.40	5.1
5600.5	0.05	5.3
5601.5	0.05	4.5
5602.5	0.05	5.3
5603.5	0.10	4.7
5604.5	0.20	5.8
5605.5	0.10	3.6
5606.5	0.20	6.4
5607.5	0.05	5.1
5608.5	0.05	4.3
5609.5	0.20	3.8
5610.5	0.10	3.3
5611.5	0.10	5.5

Appendix 15 continued.

Depth (ft)	Perm. (md)	Porosity (%)
5612.5	0.05	3.0
5613.5	0.20	6.9
5614.5	0.05	3.8
5615.5	0.20	4.0
5616.5	0.10	3.8
5617.5	0.05	7.0
5618.5	0.05	6.1
5619.5	0.05	6.3
5620.5	0.05	6.7
5621.5	0.05	6.4
5622.5	0.05	6.6
5623.5	0.05	6.4
5624.5	0.10	6.8
5625.5	0.20	7.0
5626.5	0.05	7.9
5627.5	0.05	7.0
5628.5	0.05	7.9
5629.5	0.05	5.8
5630.5	0.05	5.6
5631.5	0.05	6.2
5632.5	0.05	6.4
5633.5	0.10	6.2
5634.5	0.05	6.0
5635.5	0.05	6.3
5636.5	0.05	6.1
5637.5	0.05	5.9
5638.5	0.05	6.8
5639.5	0.05	5.9
5640.5	0.05	6.1

Appendix 15 continued.

Depth (md)	Perm. (md)	Porosity (%)
5641.5	0.05	6.3
5642.5	0.05	7.9
5643.5	0.30	5.9
5644.5	0.10	6.2
5645.5	0.40	9.6
5646.5	0.90	9.0
5647.5	8.00	13.0
5648.5	19.00	11.3
5649.5	35.00	13.6
5650.5	12.00	10.9
5651.5	20.00	11.8
5652.5	5.30	8.0
5653.5	12.00	10.6
5654.5	4.10	9.1
5655.5	22.00	11.9
5656.5	1.20	9.1
5657.5	12.00	9.8
5658.5	18.00	8.6
5659.5	2.90	9.0
5660.5	0.30	7.3
5661.5	0.10	4.9
5662.5	0.05	6.1
5663.5	0.10	7.9
5664.5	0.05	8.6
5665.5	0.05	8.9
5666.5	0.05	9.3
5667.5	0.10	8.9
5668.5	0.05	8.2
5669.5	0.05	8.1

Appendix 15 continued.

Depth (ft)	Perm. (md)	Porosity (%)
5670.5	0.10	6.8
5671.5	0.05	5.7
5672.5	0.05	7.0
5673.5	0.05	7.2
5674.5	0.05	6.6
5675.5	0.05	6.0
5676.5	0.05	8.6
5677.5	0.05	8.4
5678.5	0.05	8.6
5679.5	0.05	6.6
5680.5	0.05	7.8
5681.5	0.05	8.0
5682.5	0.05	7.0
5683.5	0.05	6.6

This thesis is accepted on behalf of the faculty of the Institute by the following committee:

Adviser

November 26, 1993

Date

I release this document to New Mexico Institute of Mining and Technology.

11-26-93

Students Signature Date